NUI MAYNOOTH

Ollscoil na hÉireann Má Nuad

Channelization for Multi-Standard Software-Defined Radio Base Stations

By Álvaro Palomo Navarro

A thesis presented to the

National University of Ireland

in partial fulfilment of the requirements for the degree of

Doctor of Philosophy

Department of Electronic Engineering

National University of Ireland Maynooth

October 2011

Research supervisors: Dr. Rudi Villing and Dr. Ronan Farrell

Head of department: Dr. Seán McLoone

Abstract

As the number of radio standards increase and spectrum resources come under more pressure, it becomes ever less efficient to reserve bands of spectrum for exclusive use by a single radio standard. Therefore, this work focuses on channelization structures compatible with spectrum sharing among multiple wireless standards and dynamic spectrum allocation in particular. A channelizer extracts independent communication channels from a wideband signal, and is one of the most computationally expensive components in a communications receiver. This work specifically focuses on non-uniform channelizers suitable for multi-standard Software-Defined Radio (SDR) base stations in general and public mobile radio base stations in particular.

A comprehensive evaluation of non-uniform channelizers (existing and developed during the course of this work) shows that parallel and recombined variants of the Generalised Discrete Fourier Transform Modulated Filter Bank (GDFT-FB) represent the best trade-off between computational load and flexibility for dynamic spectrum allocation. Nevertheless, for base station applications (with many channels) very high filter orders may be required, making the channelizers difficult to physically implement.

To mitigate this problem, multi-stage filtering techniques are applied to the GDFT-FB. It is shown that these multi-stage designs can significantly reduce the filter orders and number of operations required by the GDFT-FB. An alternative approach, applying frequency response masking techniques to the GDFT-FB prototype filter design, leads to even bigger reductions in the number of coefficients, but computational load is only reduced for oversampled configurations and then not as much as for the multi-stage designs. Both techniques render the implementation of GDFT-FB based non-uniform channelizers more practical.

Finally, channelization solutions for some real-world spectrum sharing use cases are developed before some final physical implementation issues are considered.

Declaration

I hereby declare that this thesis is my own work and has not been submitted in any form for another award at any other university or institute of tertiary education. Information derived from the published or unpublished work of others has been acknowledged in the text and a list of references is given.

_____ _____

Signature Date

“Don’t worry, you will get there in the end.

This is just one of those days that you knew would come.

Don’t ever forget that someone believes in you.

One step at a time!”

Acknowledgements

Some people say that doing a PhD is similar to running a marathon. The most important thing is to concentrate on putting one foot in front of the other, without looking ahead, just keep doing it and finally you will get to the finish line. Well, if a PhD is a marathon, then the people around you during those years are the water points that refresh you and give you energy to keep going.

First, I would like to thank my family, especially my parents and brother. Their support did not start with this PhD, but many years ago. It is thanks to them that this thesis has become a reality. Also to Aisling, for so many things, but especially for going on this journey, full of challenges with me and fuelling it with continuous faith and encouragement. I would especially like to dedicate this to my grandmother Teresa, as I think she would be very proud of this moment.

I would like to thank my supervisor Rudi Villing for his continuous support, encouragement, dedication and patience. Also, I thank my co-supervisor Ronan Farrell, for giving me the opportunity of doing this PhD. Both of them have been very inspirational professionals and sources of learning. I would like to express my gratitude to everyone in the Callan Institute (IMWS when this PhD started) for not only being good colleagues but also good friends. Among them, I would like to thank John Dooley, Magdalena Sánchez, Tomasz Podsiadlik and Justine McCormack for so many great moments inside and outside the lab.

There are many good friends, here in Ireland and Spain, who I would like to thank for their help along these years. I cannot mention them all, as I am sure I would be forgetting someone, but Carol, David, Dani, Pablo, Mario, Kiko, Toni, Rosa, Gustavo, Carla, Ciara, Michael, thanks to all of you.

Finally, I would like to thank the sponsors IRCSET and EADS for the PhD program, in special Jean-Christophe Schiel and François Montaigne for their assistance and support.

Table of contents

List of figures

List of tables

List of notations

$\lfloor a \rfloor$	Largest integer smaller than *a*
$\lceil a \rceil$	Smallest integer larger than *a*
$\mathrm{Im}\{a\}$	Imaginary part of a complex number
$\mathrm{Re}\{a\}$	Real part of a complex number
a	Bold lower case letter represents a vector
A	Bold upper case letter represents a matrix
A/B	Rational sample rate conversion
D	Decimation factor in a channelizer or filter bank
f_{CH}, ω_{CH}	Channel centre frequency in Hertz, in radians
f_{CS}, ω_{CS}	Channel spacing in Hertz, in radians
f_S	Sampling frequency
$h(n)$	Filter impulse response
$H(z)$	Filter transfer function $H(z) = \sum_{n=-\infty}^{\infty} h(n) z^{-n}$
$H(e^{j\omega})$	Filter frequency response $H(e^{j\omega}) = \sum_{n=-\infty}^{\infty} h(n) e^{-j\omega n}$
$\left\|H\left(e^{j\omega}\right)\right\|$	Filter frequency magnitude response
$\bar{H}(\omega)$	Filter zero-phase frequency response $\left\|\bar{H}(\omega)\right\| = \left\|H\left(e^{j\omega}\right)\right\|$
J	Number of standards covered by a non-uniform channelizer
K	Number of channels of a channelizer
L	Interpolation factor
N	Filter order
R	Number of recombined sub-bands in a R-GDFT
W_K	Complex exponential $\exp(j\frac{2\pi}{K})$
X_j	Number of information channels of an specific standard j
δ_p	Filter frequency response passband ripple
δ_s	Filter frequency response stopband ripple
α	Number of real additions per input sample
μ	Number of real multiplications per input sample

ω	Normalized angular frequency, $\omega = 2\pi f / f_S$
ω_p	Filter passband cut-off frequency
ω_s	Filter stopband cut-off frequency
$x(n) * y(n)$	Discrete time domain convolution between two signals $x(n)$ and $y(n)$

List of abbreviations

3GPP	3G Partnership Project
3GPP2	3G Partnership Project 2
ACI	Adjacent Carrier Interference
ADC	Analogue-to-Digital Converter
ASIC	Application-Specific Integrated Circuit
CDFB	Coefficient Decimation Based Filter Bank
C-FRM GDFT	Recursive FRM GDFT-FB
CIC	Cascade Integrator Comb
CMFB	Cosine Modulated Filter Bank
CORDIC	COrdinate Rotation DIgital Computer
CPU	Central Processing Unit
DCSA	Dynamic Contiguous Sub-band Allocation
DCT	Discrete Cosine Transform
DFSA	Dynamic Fragmented Sub-band Allocation
DFT	Discrete Fourier transform
DFT-FB	DFT Modulated Filter bank
DL	Downlink Signal
DSA	Dynamic Spectrum Allocation
DSP	Digital Signal Processing
DST	Discrete Sine Transform
ECC	Electronics Communications Committee
EDGE	Enhanced Data Rates for GSM Evolution
ELT	Extended Lapped Transform
EMFB	Exponential Modulated Filter Bank
ERC	European Radiocommunications Committee
ERO	European Radiocommunications Office
ETSI	European Telecommunications Standard Institute
FDD	Frequency Duplex Division
FDMA	Frequency Division Multiple Access
FFT	Fast Fourier Transform

FIR	Finite Impulse Response
FPCC	Farrow Per-Channel Channelizer
FPGA	Field-Gate Programmable Array
FRM	Frequency Response Masking
FRM GDFT-FB	Frequency Response Masking GDFT-FB
FRM-FB	FRM-based Filter Bank
FSA	Fixed Sub-band Allocation
GDFT-FB	Generalised DFT Modulated Filter Bank
GPP	General Purpose Processor
GPRS	General Packet Radio Service
GPU	Graphic Processor Unit
GSM	Global System for Mobile Communications
H-GDFT	Hybrid GDFT-FB
HSPA	High Speed Packed Access
HTQMFB	Hybrid Tree Quadrature Mirror Filter Bank
I/Q	In-phase/Quadrature
IF	Intermediate Frequency
IIR	Infinite Impulse Response
ISI	Inter-Symbol Interference
ISM	Industrial, Scientific and Medical
ITU	International Telecommunication Union
LTE	Long Term Evolution
MDFT-FB	Modified DFT Modulated Filter Bank
M-FRM GDFT	Multi-stage FRM GDFT-FB
M-GDFT	Multi-stage GDFT-FB
NCMA	Normalized Constant Modulus Algorithm
NPR	Near Perfect Reconstruction
OFDM	Orthogonal Frequency-Division Multiplexing
OFDMA	Orthogonal Frequency-Division Multiplexing Access
OTA	Over-The-Air
PAMR	Public Access Mobile Radio
P-CDFB	Parallel CDFB
PC-FRM GDFT	Parallel C-FRM GDFT
P-FRM	Parallel FRM-FB

P-FRM GDFT	Parallel FRM GDFT-FB
P-GDFT	Parallel GDFT-FB
PH-GDFT	Parallel H-GDFT
PM-FRM GDFT	Parallel M-FRM GDFT
PM-GDFT	Parallel M-GDFT
PMR	Professional Mobile Radio
PR	Perfect Reconstruction
PSK	Phase Shift Keying
QAM	Quadrature Amplitude Modulation
QMF	Quadrature Mirror Filter
RC-FRM GDFT	Recombined C-FRM GDFT
RF	Radio Frequency
R-FRM GDFT	Recombined FRM GDFT-FB
R-GDFT	Recombined GDFT-FB
RH-GDFT	Recombined H-GDFT
RM-FRM GDFT	Recombined M-FRM GDFT
RM-GDFT	Recombined M-GDFT
SDR	Software-Defined Radio
SMFB	Sine Modulated Filter Bank
SRC	Sample Rate Conversion
TDMA	Time Division Multiple Access
TEDS	TETRA Enhanced Services
TETRA	TErrestrial Trunked RAdio
TQMFB	Tree Quadrature Mirror Filter Bank
UL	Uplink Signal
UMTS	Universal Mobile Telecommunications System
VDSL	Very-High-Bitrate Digital Subscriber Line
WiMAX	Worldwide Interoperability for Microwave Access

List of publications

- A. Palomo Navarro, R. Villing, R. Farrell, "Practical Non-Uniform Channelization for Multi-standard Base Stations," *ZTE Comms. Journal. Special topic: Digital Front-End and Software Radio Frequency in Wireless Communication and Broadcasting*, *ZTE Communications Special Topics in Advances in Digital Front-End and Software RF Processing and Advances in Mobile Data Communications*, Vol. 9, No. 4, December 2011.

- A. Palomo Navarro, T. Keenan, R. Villing, R. Farrell, "Non-uniform channelization methods for next generation SDR PMR base stations," in *Computers and Communications (ISCC), 2011 IEEE Symposium on*, 2011, pp. 620-625.

- A. Palomo Navarro, R. Villing, R. Farrell, "Overlapped polyphase DFT modulated filter banks applied to TETRA/TEDS SDR base station channelization," presented at *the Royal Irish Academy Communication and Radio Science Colloquium*, 2010.

- L. Gao, A. Palomo Navarro, R. Villing, R. Farrell, "Opportunities and challenges for SDR in next generation TETRA systems," presented at the *CISDR* 2008 *Workshop*, Maynooth, Ireland, 2008.

- A. Palomo Navarro, R.Villing, R. Farrell, "Software Defined Radio Architectures Evaluation," presented at the *Proceedings of the SDR* '08 *Technical Conference and product Exposition*, Washington DC, 2008.

Chapter 1

Introduction

Channelization is the extraction of independent communication channels from a wideband signal, performed in the receiver of a communications device. Channelization is achieved by filtering, to isolate the channels of interest, and down-conversion, to prepare the channels for subsequent baseband processing.

In wireless communications, and more specifically mobile networks, the Radio Frequency (RF) interface is formed by two types of devices: base stations and mobile stations. The physical RF channels employed to transmit information from base stations to mobile stations are termed Downlink (DL) channels. On the other hand, the physical channels used to transmit information from mobile stations to base stations are termed Uplink (UL) channels. For a mobile station, channelization generally means extracting a single information channel from the DL signal. At the base station side, however, channelization normally implies the extraction of multiple channels from the UL signal, where different channels originate from different mobile stations. Consequently, the channelizer (and in general the complete physical layer of the receiver) must be designed in accordance to the single-channel or multi-channel extraction requirements

The significant cost of base stations and the regulatory limitation on electromagnetic emissions has encouraged mobile communication operators to deploy multi-standard base stations which support several mobile communications standards. To date, the spectrum allocation for different mobile communication standards has typically been based on a coarse grained frequency division. That is, different radio standards are allocated independent and non-overlapping frequency bands which are reserved for their exclusive use. This approach simplifies the radio design because each standard operates in effective isolation from the others. Therefore, different UL and DL frequency bands are employed by for the communications between base stations and

mobile stations depending on the communication standard. Base stations which implement this coarse grained frequency division approach to multi-standard support usually employ a different channelization structure per UL signal/standard as shown in Figure 1.1a. For this reason, each channelizer filters and down-converts just a channel type whose characteristics depend on the corresponding standard. In general, these channelizers have been implemented using an independent processing chain for every channel (per-channel approach) or by using uniform modulated filter banks.

Unfortunately, however, coarse grained frequency division does not represent optimum use of the available spectrum because bands reserved for exclusive use by a standard may be under-utilised some of the time. Rather than reserve a frequency band for exclusive use by a single radio standard, a more efficient alternative is to allow multi-standard sharing of such a frequency band. In this case, the frequency band is no longer reserved for exclusive use by a single standard but is instead shared among the multiple radio standards. This may be achieved by Dynamic Spectrum Allocation (DSA) of the channels within the frequency band among the radio standards. If, as is typically the case for heterogeneous radio standards, these channels are not uniform in their bandwidth or centre frequencies, then DSA becomes more challenging than for uniform channels. The possibility of dynamic shared spectrum has been considered for both private and commercial mobile communication standards. One example is the Terrestrial Trunked Radio (TETRA) professional communications standard and its high-speed evolution, TETRA Enhance Data Service (TEDS). Another example, in the commercial communications field, is the reuse or *re-farming* of the Global System for Mobile Communications (GSM) 900 and 1800 MHz frequency bands with third and fourth generation mobile communication standard channels such as the Universal Mobile Telecommunications Standard (UMTS) [1-2].

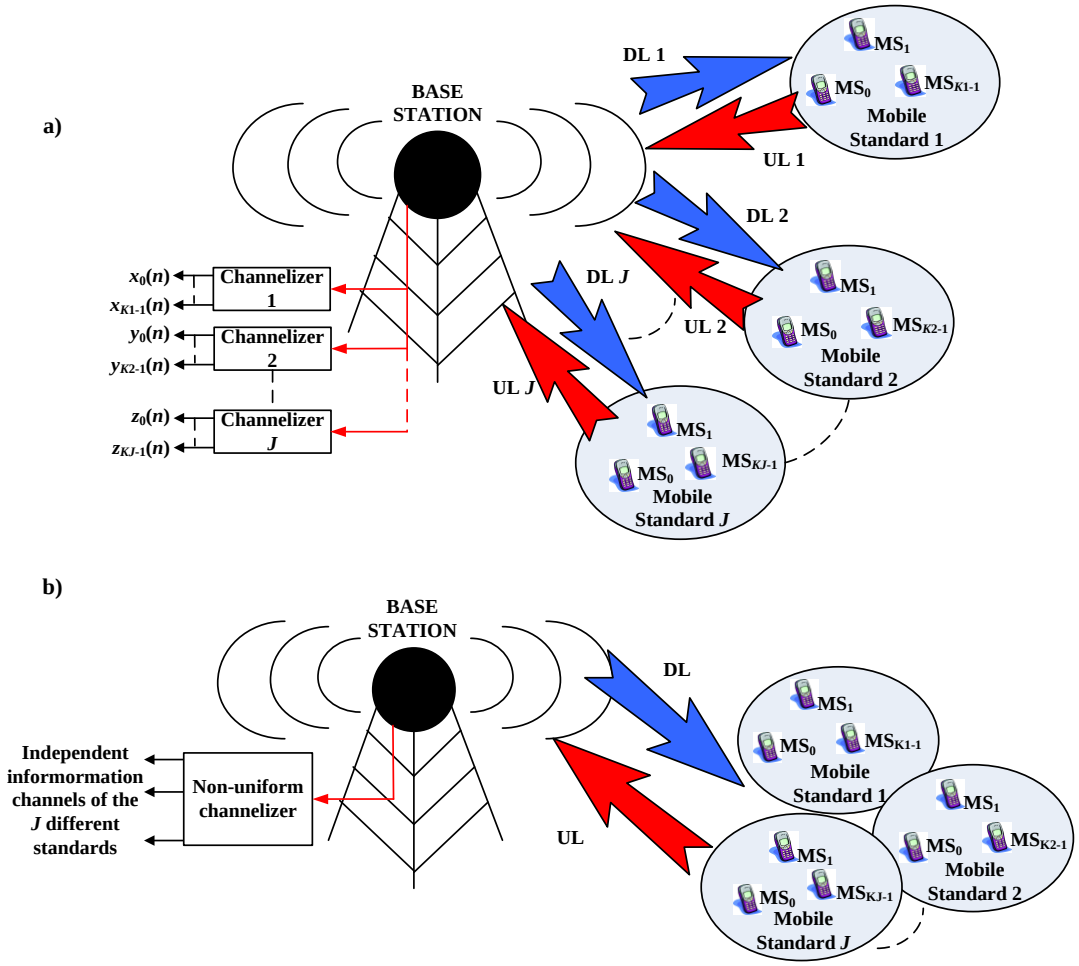

Figure 1.1 Multi-standard base station, a) where an independent UL and DL is used for each standard and b) with DSA applied.

The DSA solution to the radio spectrum under-utilisation requires changes to the mobile communication RF interface. In contrast to Figure 1.1a, the physical channels of the multiple standards which now share a frequency band will be multiplexed onto a single DL or UL signal as shown in Figure 1.1b. Among these channels, the ones belonging to the different standards could possibly have different bandwidths and consequently different centre frequency allocation requirements. In channelization terms, the extraction of these *non-uniform* types of channels at the base station requires a non-uniform channelization method capable to filter them at the required centre frequencies. In addition, the non-uniform channelizer needs to reconfigurable in case the allocation and number of non-uniform channels varies within the UL frequency band. Hence, channel bandwidth flexibility and reconfigurability are two of the most desirable characteristics of a non-uniform channelizer.

Software-Defined Radio (SDR) proposes a radio architecture where the analogue to digital (and digital to analogue) conversion is performed as close as possible to the antenna. In SDR most of the radio components, now in the digital domain, are implemented in a reconfigurable platform. This reconfigurability makes SDR particularly suitable for working with multi-standard systems and for providing an upgrade path to future standards. In an SDR base station digital conversion is applied to the wideband UL, comprising all the mobile stations channels, immediately after the RF front-end. Following this, multi-rate Digital Signal Processing (DSP) techniques are used to filter and shift to baseband all the independent information channels.

The physical implementation of the digital part of an SDR receiver is generally implemented in a generic reconfigurable hardware platform. This type of hardware provides the reconfigurability required by the non-uniform channelizer, however in terms of performance, it represents a less optimized option in comparison with a circuit designed for a specific application. In addition, among all the DSP operations performed in the SDR receiver, channelization is the most computationally expensive [3]. For this reason, this thesis focuses on the study and implementation of efficient channelization techniques, specifically non-uniform techniques, to be applied to multi-standard SDR base stations.

1.1 Research motivation

The objective of this thesis was to determine, from the base station perspective, how best to implement an efficient non-uniform channelization system suitable for multi-standard DSA using real world radio standards. This is a challenging problem because of the large number of channels managed by a base station together with the strict filtering constraints required by some standards.

Although the literature describes a number of different non-uniform channelization methods, these do not, in general, appear to have been evaluated against real world standards. A common shortcoming is that existing methods are generally designed for systems where the transmitter and receiver present

symmetric structures that perform complementary actions, like the analysis and synthesis parts of a filter bank. However, in the case of base stations using filter bank structures, this symmetry can not be exploited because the wideband UL signal received at the base station is in fact an aggregate of single carrier signals transmitted by mobile devices experiencing a variety of channel effects (see Figure 1.1a). As a consequence, there is no single synthesis part of the filter bank. Many of the non-uniform channelization structures proposed in literature do not consider this limitation.

Finally, there does not appear to be a comparative evaluation or benchmark of the different non-uniform channelization methods in the literature. It is therefore unclear how an SDR designer should choose a non-uniform channelization method for implementation. For this reason, a comprehensive evaluation of the different methods applied to standardised use cases is justified.

1.2 Thesis layout

Chapters 1–3 present relevant background material while the author's contributions are detailed in chapters 4–8.

Chapter 2 provides an overview of SDR and why it is suitable for a new generation of SDR base stations. The particular use case of a TETRA and TEDS multi-standard base station is also introduced in this chapter as a suitable platform for evaluating the multi-standard channelization problem.

Chapter 3 covers multirate DSP theory applied to uniform channelization methods. Efficient per-channel and uniform modulated filter banks approaches to channelization are examined. These methods serve as the basis of many of the non-uniform channelization techniques discussed in following chapters.

Chapter 4 evaluates the performance and limitations of existing non-uniform channelization techniques when applied to a DSA, in particular to the Dynamic Fragmented Sub-band Allocation (DFSA) use case. For each method, the computational load, DFSA flexibility, easy upgrade, reconfigurability, previous Sample Rate Conversion (SRC) and baseband SRC are examined. Thereafter,

each of the methods is benchmarked against three different TETRA V&D and TEDS use cases. The results show that the Generalized Discrete Fourier Transform Modulated Filter Bank (GDFT-FB) structures, parallel and recombined, provide the best trade off between computational load and the rest of parameters previously enumerated for non-uniform baseband channelization.

Chapter 5 seeks to overcome the principal design limitation of the GDFT-FB, namely, the large filter orders that are required. Multi-stage filtering has been successfully used to divide the working load of a filter into several stages, each of which is much smaller, easier to design, and easier to implement than the original single large filter. The multi-stage concept is applied to the GDFT-FB in two different ways: in the first of these, a frequency response masking (FRM) filter inserted before the filter bank permits a relaxed prototype filter specification for the filter bank; in the second technique, a half-band filter is applied to every output of the filter bank and, again, this permits a relaxed prototype filter specification for the filter bank. In both cases, the result is a useful reduction in the number of filter coefficients and computational load relative to the basic GDFT-FB implementation.

Chapter 6 uses the FRM technique to implement the prototype filter in a modulated filter bank more efficiently. In previous work FRM had been applied to the cosine modulated filter bank (CMFB) and here this is extended to the GDFT-FB. Several variants of the FRM technique are considered, including the full FRM structure and the positive branch structure (narrowband FRM), critically decimated and oversampled designs, and both even and odd sub-band stacking schemes. Again the results show a reduction (relative to the basic GDFT-FB) in the number of coefficients for all the proposed configurations, and a reduction in the number of operations in some of the cases. The combination of multi-stage techniques with the FRM GDFT-FB is also shown to achieve further reductions.

Chapter 7 examines the generalisation and applicability of the channelization techniques evaluated in the thesis. To do so, two real world base station examples involving 3G and 4G standards are considered: first, providing 4G communications to Professional Mobile Radio (PMR) communication systems

using WiMAX or LTE channels; and second, the re-farming of the GSM 900 and 1800 MHz bands with UMTS and LTE channels. As part of this, specific consideration is given to certain hardware implementation issues, further filter optimisation (e.g. approximately linear phase IIR filters), and interaction with the baseband processing components such as equalization.

Chapter 8 concludes the work and suggests a basis for future work that could be developed.

1.3 Novel contributions

The contributions of this thesis to the fields of mobile communications, multirate digital signal processing and SDR are:

- The specific study of DFSA schemes applied to SDR multi-standard base stations from the channelization point of view.
- The evaluation of the uniform per-channel channelization and uniform complex modulated filter banks (DFT-FB and EMFB) channelization for complex input signals and a large number of channels.
- A comprehensive evaluation of non-uniform channelization techniques applied to multi-standard base stations employing DFSA. The results of this evaluation show that GDFT-FB based non-uniform channelizers offer the best trade-off between DFSA capabilities and computational load for this particular use case.
- The application of two different multi-stage filtering techniques to GDFT-FBs. When used as either uniform or non-uniform channelizers, a reduction in the filter orders and computational load is achieved. In addition, an easier filter design process is achieved for some of the non-uniform GDFT-FB channelizers due to the application of the multi-stage techniques.
- The application of the full FRM and narrowband FRM techniques to GDFT-FBs to obtain lower order prototype filters. Consequently,

reductions in the computational load and benefits in the non-uniform GDFT-FB based channelizers are also achieved.

- The demonstration of the suitability of the proposed non-uniform channelization techniques to current (at the time of writing) mobile communications trends, such as the provision of 4G channels to PMR communications and the "re-farming" of the GSM frequency bands.

- The demonstration that it is possible to apply IIR filters with approximate linear phase response to the techniques previously presented in order to achieve more efficient implementations. This option would be possible as long as the phase linearity requirements allow a certain level of non-linearity in the system phase response.

- The demonstration that the reduced filter orders and computational load achieved with the techniques proposed in this thesis can facilitate the physical implementation of the channelizers. Among the benefits, the reduction of the fixed-point quantization and round-off errors, the option to use assisting design tools and the optimization with other baseband digital signal processing modules.

1.4 Chapter conclusions

The design of next generation multi-standard SDR base stations using DSA techniques has several challenges. From the point of view of the uplink signal channelization, filtering techniques which can manage several channel bandwidths and centre frequencies simultaneously would be required. Considering this particular problem, this thesis focuses on the multirate digital signal processing techniques which can allow these channelization requirements to become possible to implement on a reconfigurable platform. In Chapter 2, the different DSA schemes and the required reconfigurable requirements are studied more in detail.

Chapter 2

Dynamic Spectrum Allocation and Software-Defined Radio

2.1 Introduction

The dramatic rate at which new mobile communication standards are appearing in the telecommunications world requires a new perspective on frequency spectrum management. Following on from Chapter 1, the concept of DSA and its different implementation possibilities is explored in more detail as a solution to maximize frequency spectrum utilization. Channel allocations based on DSA can be concretely applied to real world communications standards such as TETRA and TEDS which can co-exist in the same frequency band. Therefore, these two standards are used throughout the remainder of the thesis as the basis for use cases which can be used to evaluate the techniques reviewed and proposed in this thesis.

DSA techniques affect not only the way in which spectrum resources are managed, but also the components that form the mobile network RF interface, e.g. base stations and mobile stations. Consequently, an increased level of flexibility and reconfigurability is required to deal with a range of bandwidths and centre frequencies. To efficiently achieve these two capabilities, in this chapter the possibility of employing SDR technology as an alternative to hardware-based designs on base stations is reviewed. Within the different parts of a SDR receiver structure, special attention is given to the previously introduced concept of channelization. More concretely, the channelizer implementation on a SDR base station and its demanding computational requirements.

2.2 Fixed spectrum allocation and dynamic spectrum allocation

Wireless communications (include mobile communications) employ electromagnetic waves to transmit information between a transmitter and a receiver. At the transmitter, the digital or analogue information is modulated onto a carrier signal at a specific radio frequency which is transmitted through the wireless channel [4]. On the receiver side, the signal at the specific carrier frequency is filtered, down-converted and demodulated so that the information can be extracted. The range of carrier frequencies employed in wireless communication is generally denoted as electromagnetic spectrum or frequency spectrum. These frequencies vary from few kilohertz, for some navigation services, to several hundreds of gigahertz, for satellite and radiolink communications [5]. In general, for each general type of service, one or more communication standards are in use. For example mobile communications is governed by standards which include TETRA and TEDS for PMR communications, and GSM and UMTS for commercial mobile communications.

To date, spectrum allocation has typically been based on the coarse grained frequency division multiplexing of radio standards. That is, each radio standard is allocated an independent and non-overlapping frequency band which is reserved for its exclusive use [5]. Some of these bands may be internationally reserved for certain services. Examples include the FM radio broadcast band; the open 2.4 GHz Industrial, Scientific and Medical (ISM) band used by communications standards such as Wi-Fi, Bluetooth and Zigbee; the 380 MHz band used in Europe for Professional Mobile Radio Communications (PMR); and the GSM 900 MHz band. Spectrum that is not internationally reserved is regulated and assigned by the radiocommunications agencies of different countries or worldwide regions (Japan-Asia, EE.UU.-America, Europe-Africa), under the general supervision of the International Telecommunication Union (ITU) [6]. This fixed spectrum allocation simplifies the radio design (and is often a necessity for analogue communications schemes) but it does not represent optimum use of the available spectrum because bands reserved for exclusive use may be under-utilised some of the time.

For mobile communications in particular, cellular networks represent an effort to maximize the utilization of the frequency bands given to each standard [7]. Its basis is the division of RF coverage area into sub-areas known as *cells*. The essential principle is that a set of *S* adjacent cells (known as a cluster) use different sub-sets of carrier frequencies from the frequency band allocated to the standard. Therefore, interference between cells in the cluster is avoided. In addition, the same sub-set of frequencies can be reused again by a cell in another cluster separated by more than a distance *D*, where *D* is known as the *reuse distance*. In general, *S* determines the number of frequency sub-sets and it is known as *spatial reuse factor*. In the multi-standard base station model shown in Figure 1.1a, each DL and UL signal would use one of the frequency sub-sets associated with its corresponding standard.

Although the cellular concept was first introduced in the 1970's for analogue mobile networks it is still used by current digital mobile communications [8]. However, with the advent of multi-antenna technology, the latest 4G standards, such as Long Term Evolution (LTE), are expected to reduce the spatial reuse factor to S=1. With S=1, each cell can avail of the whole frequency band for transmission [9]. Nevertheless, while cellular deployment solves the problem of maximizing the capacity of a single standard in a given frequency band it does not seek to maximize the utilization of the entire frequency spectrum. Rather than reserving a frequency band for exclusive use by a single radio standard, a more efficient alternative is to allow the frequency band to be shared by several standards [10]. As introduced in Chapter 1, with PMR standards this idea has been studied for TETRA and TEDS [1]. With commercial standards, reuse of the GSM 900 MHz frequency band by various standards has been considered, specifically UMTS, its evolution, High Speed Packet Access (HSPA), and the fourth generation LTE [2].

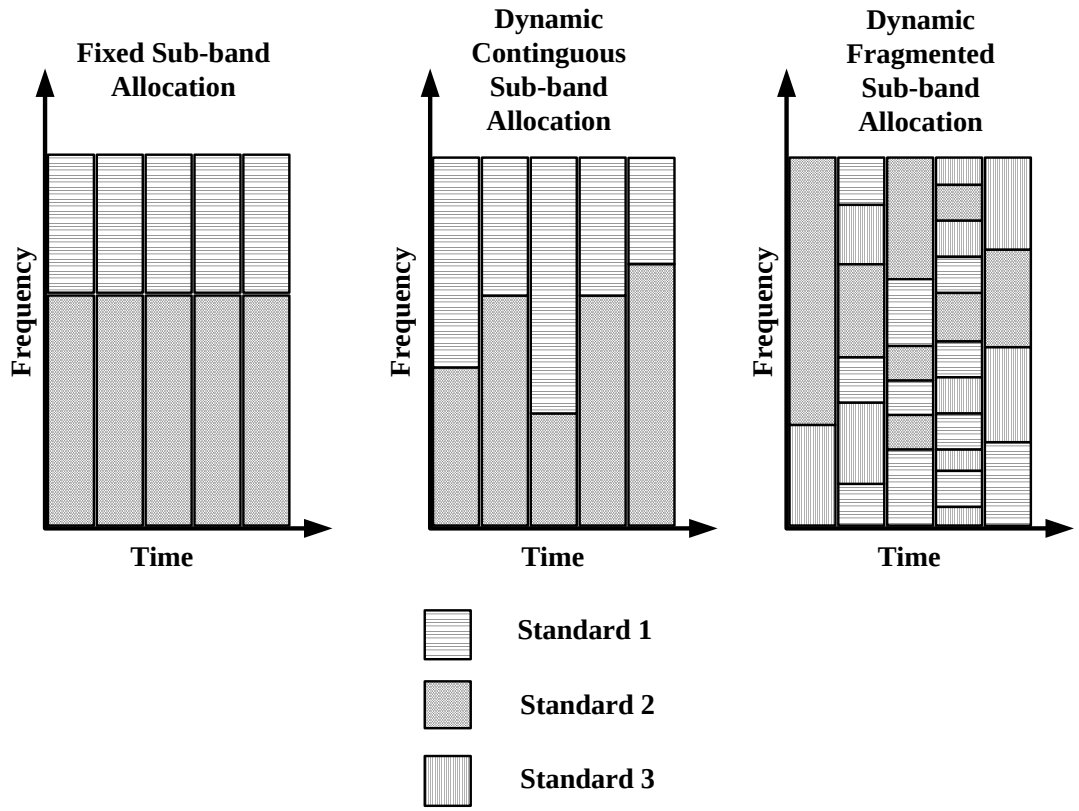

Figure 2.1 Fixed vs. dynamic spectrum allocation techniques [10].

Frequency band sharing between several standards can be achieved by either fixed or dynamic allocation of the standard channels into sub-bands [10], as depicted in Figure 2.1. Each one of the three schemes in Figure 2.1 represents a possible allocation scheme for the common UL or DL signal depicted in Figure 1.1b. If Fixed Sub-band Allocation (FSA) is used, the bandwidth provided for each standard within the shared frequency band is constant. This sharing scheme represents the least flexible (but simplest to implement) option. If one of the standards does not make use of the whole bandwidth provided, the other standard can not take these unused frequencies to allocate more channels and therefore increase its capacity. Therefore, one of the bands may be under-utilised.

In contrast, DSA schemes show better ability to maximize the frequency band capacity. The Dynamic Contiguous Sub-band Allocation (DCSA) scheme provides adjacent frequency sub-bands to each one of the standards without constraining the dividing frequency. Consequently, if a standard does not require its complete sub-band then the adjacent ones can reuse it by expanding their

boundaries. However, the limitations and complexity of this scheme increase when more than two standards are intended to be allocated in the shared band.

Dynamic fragmented sub-band allocation (DFSA) defines the most flexible scheme. In DFSA, each standard is given different bandwidth *fragments* within the shared frequency band depending on their traffic needs. The bandwidth of these fragments can range from a single channel to the whole frequency band (if, for example, only one of the standards needed to allocate channels at that specific instant).

In general, there are different examples where the DSA implementation is necessary, such as:

- Composite reconfigurable wireless networks, in which frequency bands are shared by multiple heterogeneous licensed wireless standards, such as GSM, UMTS, WLAN and Digital TV [10].

- Cognitive radio, which seeks the reuse of unused frequency "white spaces" in the frequency bands used by the licensed services. These white spaces can be used by un-licensed services, with the permission of the licensed ones, as long as they do not cause any interference with the primary channels [11-15].

- Spectrum access scheduling, where, unlike the two previous technologies, heterogeneous services share the spectrum by time division multiplexing instead of by frequency division [16].

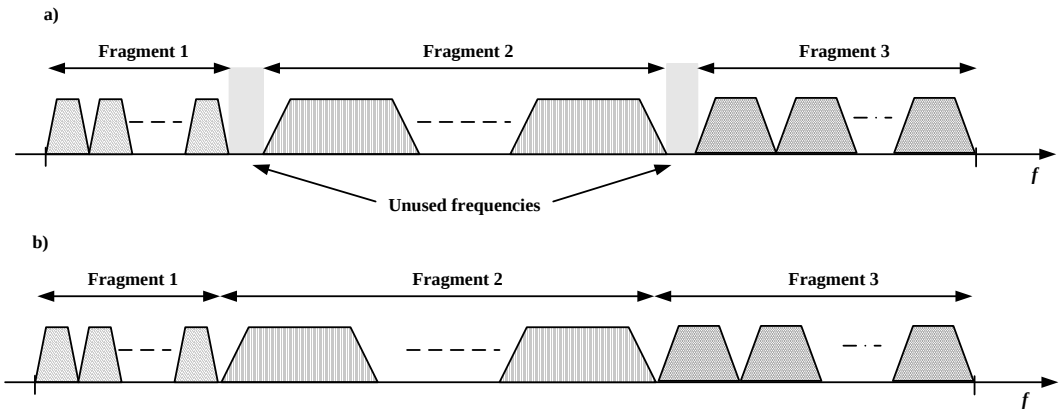

Figure 2.2 Multi-standard DFSA channels allocation variants. a) Standard specific allocation, b) grid-constrained and unconstrained allocation.

Although DFSA is the most desirable of the three options presented in Figure 2.1 in terms of flexibility and utilization, it is more challenging to implement than the other two options. From the perspective of a multi-standard base station, there are two main challenges. First, it requires a more complex DSA algorithm to control the frequency band distribution among the different standards. Second, non-uniform filtering techniques are usually required to filter and down-convert the channels of interest from each standard sharing the UL signal. To understand the requirement for and challenges of non-uniform filtering it is worth considering a few ways in which channel centre frequencies may be allocated to multiple standards occupying multiple frequency fragments (as shown in Figure 2.2): standard specific allocation, grid-constrained allocation, or unconstrained allocation.

To maintain maximum compatibility with deployed equipment, channel centre frequencies in each fragment must satisfy the rules for the standard allocated to that fragment. When the rules used by adjacent fragments are not compatible with one another, the upper edge of the highest frequency channel in the lower fragment and the lower edge of the lowest frequency channel in the adjacent fragment may be separated by an unusable white space as in Figure 2.2a. Similarly, when seeking to allocate a fragment for one or more channels, the fragment bandwidth may have to be larger than otherwise required because of unusable white space. Therefore, although this scheme provides backward compatibility, it does not maximize spectrum utilization.

Grid-constrained allocation and unconstrained allocation are essentially variants of the same scheme (Figure 2.2b). In unconstrained allocation, channel centre frequencies may be chosen freely and there is no need for unusable white space between standards just to comply with a centre frequency allocation rule. It does however place reconfigurability demands on the receiver which may be difficult to meet. A useful compromise, therefore, is grid-constrained allocation in which the possible centre frequencies are limited to a grid of discrete possibilities, but the spacing on this grid can be smaller than the normal channel spacing in any one standard. This scheme allows the size of unusable white space to be minimized while constraining the reconfigurability demands placed on the receiver.

A DFSA channelizer must be able to support one or more of the centre frequency allocation schemes just described. In addition, the channelizer must be able to dynamically adapt to the current channel allocation pattern at every instant. For both challenges, channelizer complexity increases with the number of standards sharing the frequency band.

It should be clear that achieving better frequency spectrum utilisation by employing multiplexed frequency spectrum poses a major technology challenge. From the radio transmission point of view, especially when considering the base stations, new flexible non-uniform channelization techniques are required.

2.3 Multi-standard PMR base stations

TETRA is a wireless digital telecommunication standard developed to provide reliable and robust digital communications to Professional Mobile Radio (PMR) and Public Access Mobile Radio (PAMR) applications [17-18]. As its name specifies, TETRA is a “trunked” system oriented to allow a large number of user groups to share the same radio resources [19]. The objective is to provide interoperability between different government heath and safety corps such as ambulances, police, fire brigade and army. In contrast with commercial mobile communication standards, PMR communication systems provide enhanced communication capabilities such as very fast call set up, increased information

security and encryption, direct-mode to allow two mobile stations communicate without a base station, and one-to-many and many-to-many communications mode [20]. In addition, PMR standards are generally allocated lower frequency bands than the commercial standards, so the free-space attenuation produced by the wireless channel over the transmitted signals is smaller.

TETRA is a European Telecommunication Standard Institute (ETSI) standard that in its first version was mainly oriented towards voice and limited data transmission, similar to GSM in the public communications sector. The first version of TETRA, commonly known as TETRA Voice & Data (TETRA V&D), was presented in 1996. Apart from ETSI, the TETRA MoU, also known as TETRA Association, has worked actively in promoting the use of TETRA and working on its improvements [21].

Progressive improvements of the first version of TETRA following the increasing demand of higher data rates led to the creation of the second release of TETRA that was publicly announced in 2005 [22]. TETRA release 2, provided new capabilities over release 1 similar to those by the General Packet Radio Service (GPRS) or Enhanced Data Rates for GSM Evolution (EDGE) for GSM. From these new capabilities, the TETRA Enhanced Data Service (TEDS) is perhaps most significant [1, 22-24].

TEDS was designed to maintain compatibility with TETRA V&D by using the same control channels, whilst at the same time providing increased RF channel bandwidths and data rates. Higher data rates are achieved by introducing new modulation schemes and bandwidths in contrast with TETRA V&D which relied on a single bandwidth and phase modulation scheme. TEDS can choose between several Phase-Shift Keying (PSK) and Quadrature Amplitude Modulation (QAM) schemes. Additionally, the TETRA V&D fixed bandwidth of 25 kHz is increased in TEDS to 50, 100, or 150 kHz. These new capabilities lead to data rates up to 691.2 kbits/sec in comparison with the maximum 36 kbits/sec of TETRA V&D.

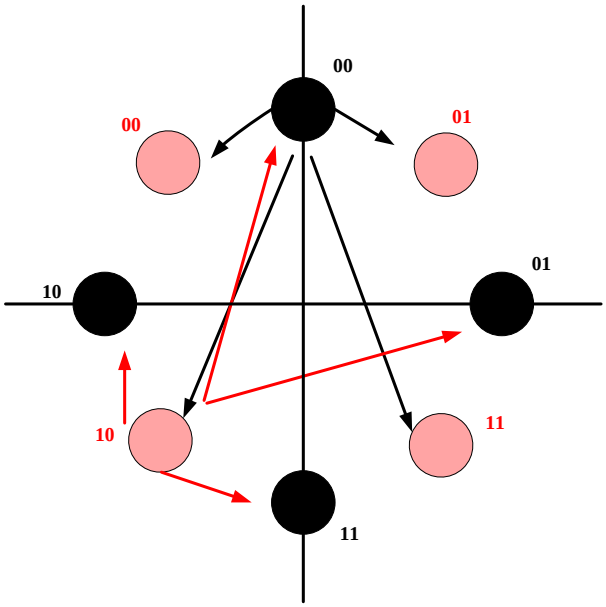

Figure 2.3 π/4-DQPSK modulation scheme constellation.

2.3.1 TETRA V&D and TEDS modulation schemes

TETRA V&D was designed to use only one modulation scheme, π/4 DQPSK, with a data rate of 36 kbits/sec. This modulation scheme shifts the phase of the RF carrier in steps of ±π/4 or ±3π/4 radians representing the phase difference between the current symbol and the previous one. It can be seen as two overlapped QPSK constellations, one shifted π/4 with respect to the other. The first symbol is mapped to the corresponding point on the in-phase constellation; the second one is mapped using the shifted constellation; and the process continues in this way mapping alternate symbols to the in-phase and shifted constellation. Figure 2.3 shows the modulation symbol constellation and the possible transitions that can occur [17]. For example, if the current symbol is '00' in the constellation in black, the black arrows show the only transitions allowed are to the symbols of the shifted constellation. The same situation happens when the '10' symbol of the constellation in red is considered to be the current one.

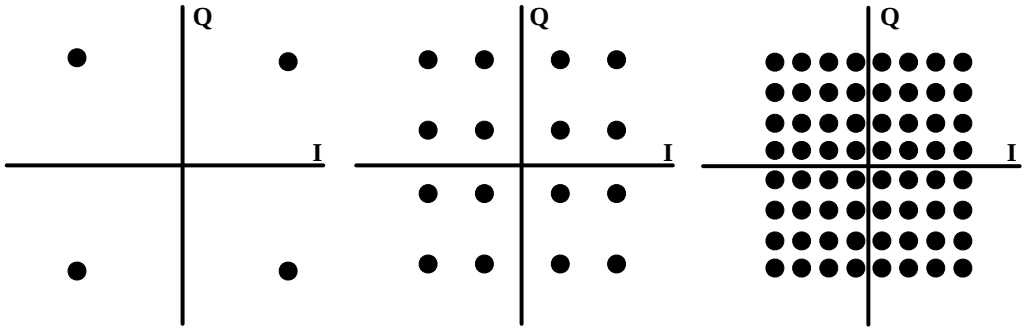

Figure 2.4 4-QAM, 16-QAM and 64-QAM modulation schemes constellations.

There are two main benefits of this modulation scheme. First, encoding the phase difference between one symbol and the previous one provides the advantage of using a non-coherent receiver where it is not necessary to estimate the carrier phase to carry out the demodulation correctly. Second, considering the possible transitions that can take place between two symbols it can be observed that none of them pass through the centre of the constellation. In other words, the amplitude of the carrier signal will never reach zero and this improves its performance when a noisy channel is present.

With the introduction of TEDS, additional modulation schemes were added to the TETRA standard. The use of DQPSK modulation scheme was restricted to 25 kHz channels, whereas the QAM modulation schemes could take advantage of the improvements introduced in TEDS and use channels of up to 150 kHz.

On the phase modulation side, π/4-DQPSK was kept to maintain interoperability with the previous TETRA V&D systems and π/8-DQPSK was added to provide data rates of up to 54 kbits/sec. Its principle is the same as depicted in Figure 2.3 for π/4-DQPSK but in this case the two constellations are formed by 8 possible points, so three bits are embedded into every symbol instead of two, which provides the higher data rate. As a drawback, π/8-DQPSK is more sensitive to errors because if one wrong symbol is received the error affects to three bits instead of two.

Table 2.1 Multi-carrier TEDS QAM channels.

Bandwidth	Number of sub-carriers	Total symbol rate
25 kHz	8	19.2 ksymbols/sec
50 kHz	16	38.4 ksymbols/sec
100 kHz	32	76.8 ksymbols/sec
150 kHz	48	115.2 ksymbols/sec

On the other hand, the QAM modulation schemes (Figure 2.4) respectively use 2, 3, or 4 information bits encoded in each one of the symbols of the constellation. For signal spaces with a large number of symbols (e.g. 16 or 64 symbols) QAM schemes are more robust to noise than PSK schemes [25]. In TEDS each channel is divided into a number of frequency-division multiplexed sub-carriers, each carrying a complex signal using the QAM modulation. The sub-carrier approach is used because the low symbol rate in each one of them gives the modulated transmission inherent resistance to time dispersion thereby avoiding the need for an adaptive equalizer in the receiver. In this way, a sub-carrier approach with 8 sub-carriers per 25 kHz is used, leading to 8, 16, 32, and 48 sub-carriers in 25 kHz, 50 kHz, 100 kHz, and 150 kHz carriers respectively.

The modulation symbol rate in each sub-carrier is 2,400 symbols/sec and the spacing between them is 2.7 kHz. The characteristics of the different TEDS QAM channels are given in Table 2.1.

According to the TEDS standard specification [17], the sub-carrier centre frequencies for the baseband channel (centred at DC) are determined by

$$f_k = \frac{\left(0.5625 - \left(\frac{K_T}{2} - k\right)1.125\right)}{T}, \quad \text{for } k = 0,1,...,K_T - 1 \tag{2.1}$$

where K_T represents the number of sub-carriers (which depends on the TEDS channel), f_k represents the sub-carrier centre frequency and T denotes the symbol duration (T=1/2400 s). An example for the centre frequencies of a TEDS 25 kHz channels is shown in Table 2.2.

Table 2.2 Centre frequencies for TEDS 25 kHz channel sub-carriers relative to DC.

Sub-carrier (*k*)	Centre frequency (kHz)
0	-9.45
1	-6.75
2	-4.05
3	-1.35
4	1.35
5	4.05
6	6.75
7	9.45

2.3.2 TETRA V&D and TEDS radio transmission and reception

TETRA V&D and TEDS use the same air interface based on a mixture of Frequency Division Multiple Access (FDMA) and Time Division Multiple Access (TDMA). Each TETRA carrier is divided into 4 timeslots of 14.167 ms and each one is assigned to a different user. Multislot communications are also possible in order to provide higher data rates. Each time slot is associated with a pair of RF frequencies separated by a fixed offset for Frequency Duplex Division (FDD), i.e. one frequency for the UL and the other for the DL. In Europe, the European Radiocommunications Committee (ERC) reserves the frequency band between 380 and 400 MHz for the TETRA safety and security service [26]. In this range UL frequencies are allocated between 380 and 385 MHz while DL frequencies lie between 390 and 395 MHz. There is always a fixed separation of 5MHz between the carriers containing the UL and DL slots assigned to a user. [26] also considers other frequency bands that European countries can adopt to implement TETRA communication systems.

The channel spectrum allocation of TETRA, and all other PMR standards in general, is defined by the Electronics Communications Committee (ECC) and the European Radiocommunications Office (ERO). For these systems, in [27] it is specified that the allocation of the different radio channels in the UL and DL bands needs to be compliant with the following expression

$$f_{CH}(n) = Band\_edge + (n - 0.5) \times Channel\_spacing \qquad (2.2)$$

where f_{CH} is the centre frequency, *n* the number of channel and *Band_edge* the lower edge frequency of the multiplexed frequency band. Therefore, for each possible channel spacing (25, 50, 100 or 150 kHz), the available spectrum is divided into frequency sub-bands equal to the channel spacing (starting from *Band_edge*) and channels are allocated within the 5 MHz DL and UL bands.

2.3.3 TETRA V&D and TEDS joint implementation

At the time of writing, TETRA device manufacturers are still seeking solutions for an efficient joint implementation of TEDS and TETRA V&D in base stations and mobile stations. The upgrade of an existing TETRA V&D system is of particular interest. The primary issue of technical debate is whether the new TEDS channels should be allocated in the frequency bands that already exist for the TETRA V&D channels (using fixed or dynamic spectrum allocation), or instead new frequency bands should be specifically reserved for its specific allocation (410-430 MHz or 450-470 MHz) [1, 28-30]. Clearly the latter scheme does not provide the most efficient spectrum utilization.

For equipment manufacturers a direct consequence of a separate frequency band implementation is that base stations and mobile stations must be upgraded to cover the additional spectrum. The main constraint in this upgrade is that the most common antenna used in TETRA base stations is limited to an RF bandwidth of 32 MHz which would not allow the use of the band between 410 and 430 MHz to accommodate TEDS channels in addition to the 380-400 MHz band already used for TETRA V&D.

Therefore, [1] concludes that while a separate band solution would be suitable for future equipment generations, it is not suitable for existing networks. For existing networks, the single band option is the most cost effective and practical solution for TETRA V&D networks that need to be upgraded to TEDS. The only possibility for adding extra spectrum to the existing band would be the use of the frequencies between 385-390 MHz and 395-400 MHz in the countries where they are not already used by the North Atlantic Treaty Organization (NATO).

Backward compatibility can be maintained by keeping the current TETRA control channel, signalling, roaming, and protocols that are currently used by TETRA V&D. In this way the current base station can be reused and existing mobile stations do not become obsolete. However, the necessary hardware upgrade required by the base station poses an important economic factor.

The significant complexity and cost of the hardware transceivers produced by the addition of just one TEDS channel encourages the search for alternatives [31]. The primary alternative explored in this work is an SDR solution based on DFSA and non-uniform channelization. This option can represent a lower upgrade cost and provides greater flexibility than a hardware based approach to implement DFSA for TETRA V&D and TEDS channels in the 380-400 MHz band. In addition, possible future upgrades might not need any hardware replacement, just SDR reconfiguration.

2.4 SDR as a DSA enabling technology

Better spectrum utilization based on DSA techniques requires the implementation of supporting technology in the base station to become a reality. Greater flexibility in spectrum allocation also requires greater flexibility in the structures employed to allocate and channelize the channels from the shared frequency band.

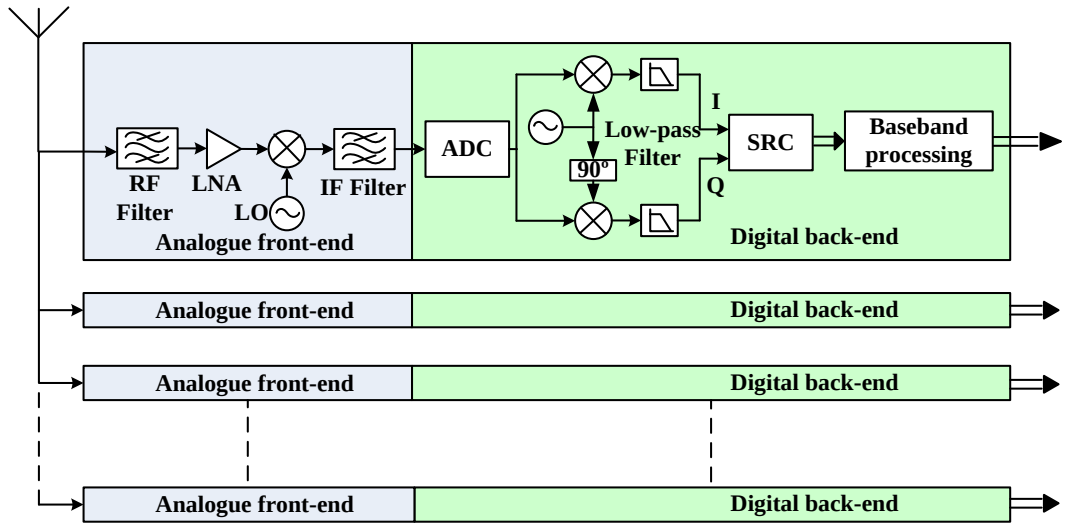

Figure 2.5 Hardware based base station receiver.

Traditionally, the structure of a base station receiver is composed of the parallel connection of dedicated circuitry for each channel. Figure 2.5 shows this structure and how each channel is independently filtered and down-converted from the received RF signal. In each branch the analogue front-end is in responsible for filtering of the channel of interest from the other channels in the UL signal and down-converting it. Subsequently, the digital back-end performs equalization, timing recovery, demodulation, and other information extraction operations. The circuits are specifically designed for a certain type of communication channel. If the base station supports more than one mobile communication standard, more than one type of receiver structure is employed for as many channels as each standard requires.

The suitability of the structure in Figure 2.5 for DSA schemes varies depending on whether FSA, DCSA or DFSA channel allocation is considered (see Figure 2.1). For FSA, the hardware based per-channel receiver is a reasonable solution since neither the number of channels nor their centre frequencies and bandwidths vary in the FSA scheme.

However, when DCSA or DFSA schemes are considered, the use of dedicated hardware circuits for each channel is more complex (and less efficient). For DCSA, the number of channels allocated to each standard can vary at each time instant. If the channels of different standards have different characteristics (as is usually the case) then, for each standard, there will need to be enough standard-specific hardware circuits to handle the maximum number of channels that can be allocated to that standard. Depending on where the frequency boundary between standards lies at any moment in time, some hardware circuits of one or other standard will be unused leading to inefficiency.

DFSA is less efficient again to implement in hardware because circuits covering the entire frequency band are required for all standards (if full flexibility is to be offered). Furthermore, if grid-constrained or unconstrained centre frequency allocation is permitted, the hardware circuits will require the ability to reconfigure their centre frequencies.

A certain level of reconfigurability for the DCSA and DFSA cases can be achieved by implementing *software controlled hardware* [32]. This approach allows certain parameters of the configuration of each branch to be reconfigured within a sub-set of possibilities previously programmed (e.g. the frequencies of the analogue and digital mixers or the demodulation scheme at the digital back-end). However, once designed, these parameter sets can usually not be updated, for example, to handle new communications standards. More software-oriented solutions can be considered to achieve higher levels of reconfigurability, and therefore, may more efficiently support DSA schemes. Among the more software oriented solutions, SDR is the most flexible candidate solution.

2.4.1 What is SDR?

Communication systems reconfigurability became a topic of interest to the U.S. Army in the late 70's due to the lack of interoperability among the different standards that were used by the different armed forces. Improved interoperability became a major necessity for field operations where the communication between forces was crucial and, therefore, the SPEAKeasy project was created in 1992 to create reconfigurable radio devices that would facilitate these communications [33-34].

In that same year, the term software radio was introduced in [35]. Furthermore, the ideal model for a software radio was presented together with the enabling technologies that could make it applicable to commercial communications. Specifically, a software radio was defined as a wireless communication device which could be reprogrammed to allow communications using different modulation schemes and frequencies without altering or replacing hardware. This reconfiguration could possibly be done using Over-The-Air (OTA) download.

According to [36], software radio reflects the convergence of two dynamically developing technological forces of this period: digital radio and software technology. Digital radio facilitated the wireless revolution that gave birth to the mobile phone mass market whilst software technology, over the same period, both facilitated and rode the Internet wave.

In the literature the terms software radio and SDR have mainly been considered synonyms, and therefore interchangeable. Some authors have distinguished between them, but with different ideas of the scope of both terms [37-38]. In this thesis, software radio and SDR are considered to represent the same principle. In particular, the SDR description given by the Wireless Innovation Forum (formerly known as the SDR Forum and the principal international organization promoting SDR evolution) is

> *SDRs provide software control of a variety of modulation techniques, wideband or narrowband operations, communications security functions (such as hopping), and waveform requirements of current and evolving standards over a broad frequency range. The frequency bands covered may still by constrained at the front-end requiring a switch in the antenna system.* [32]

The lack of reconfigurability and upgradability typically inherent in hardware-based structures (like the one in Figure 2.5) has led some authors to propose SDR as a candidate for the next generation of multi-standard commercial mobile communication devices [36, 39-42]. One of the main objectives of SDR is to permit the implementation of all these different standards on a general purpose reconfigurable hardware platform. Reconfigurability in this case means anything from updating the parameters of a specific function or adding a totally new one without the necessity of acquiring a new device. These advantages do not only affect to the end users. Networks operators, manufacturers and regulators would also benefit from this reconfigurability [43].

2.4.2 SDR and ideal SDR

In a wireless communications device, SDR is typically understood to encompass all the baseband digital processing operations (modulation/demodulation, coding, channelization, equalization, timing recovery, etc) whereas the RF functions are performed by an analogue front-end component.

In contrast, *ideal* SDR increases the scope of digital reconfigurability. The Wireless Innovation Forum establishes the differences between SDR and ideal SDR as

> *ideal SDRs provide dramatic improvement over an SDR by eliminating the analogue amplification or heterodyne mixing prior to digital-analogue conversion. Programmability extends to the entire system with analogue conversion only at the antenna, speaker and microphones[32]*

As Figure 2.6 shows, the signal is digitally converted as close as possible to the antenna with all radio functionality implemented using DSP and only a minimal essential amount of analogue hardware used. In this scheme the radio is able to transmit and receive extremely large bandwidths. In the receiver scenario, this would allow the radio to digitise the entire RF band with DSP used for all receiver functionality including tuning, filtering and demodulation. In such a radio device, it would be possible to receive signals on multiple frequencies simultaneously with each individual signal using different bandwidths and modulation schemes.

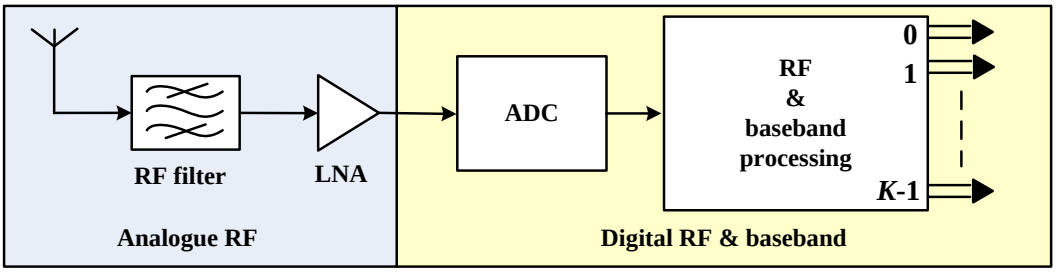

Figure 2.6 Ideal SDR receiver implementation.

Likewise, in the transmitter scenario, DSP software is used to generate a wideband signal capable of transmitting anywhere in the RF band. It would be possible to simultaneously modulate multiple signals using different frequencies, bandwidths and modulation schemes. Effectively the analogue RF-front end of the ideal software radio would act as a physical gateway to the electromagnetic spectrum with all radio functionality implemented by DSP software.

2.4.3 SDR physical implementation limitations

Attempting to physically implement SDR based devices has uncovered important limitations in each of the stages differentiated in Figure 2.6. In general, the classic approach to build SDR systems has divided the system into three stages: analogue front-end, digital front-end, and digital back-end, as depicted in Figure 2.7 [40, 44-45]. The aim of the analogue general-purpose front-end is to act as an interface between the antenna and DSP hardware. This should be a multi-standard front-end which permits the reception and transmission of arbitrary frequencies and bandwidths. In the next stage, the digital front-end groups the Analogue-to-Digital Converter (ADC) and channelizer prior to the independent channel processing carried out by the digital back-end. These three different tasks may be performed in different hardware platforms if needed.

From the antenna to the final information bits of every channel, the level of reconfigurability required by the three stages depicted in Figure 2.4 can vary. This reconfigurability level has direct impact in the type of hardware platform that can be employed, the performance and the optimization. In [44] some of the options considered for the physical implementation of the three stages are:

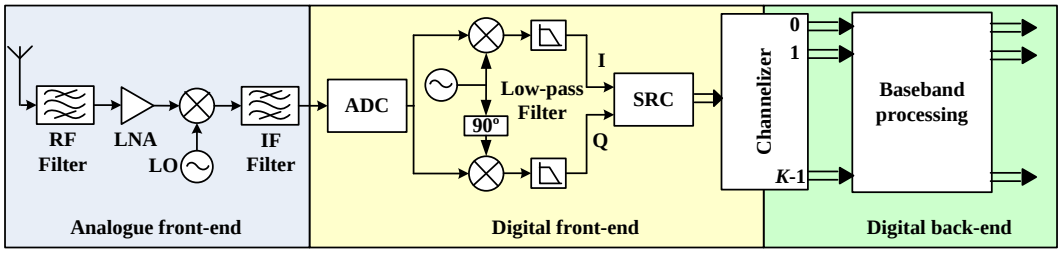

Figure 2.7 Practical SDR receiver implementation.

1. Analogue front-end. Dedicated hardware platforms such as Application Specific Integrated Circuits (ASIC) can be particularly designed to receive and transmit a wideband frequency band and perform the corresponding down-conversion or up-conversion to/from the intermediate frequency (for the heterodyne transceiver case in Figure 2.7). For direct conversion the signal is down-converted to or up-converted directly from baseband. Due to

their application specific designs, the power consumption and performance of ASICS can be highly optimized.

2. At the digital front-end, depending on the channels allocation in the wideband received signal a certain level of reconfiguration is required for the independent channels separation to be performed by the channelizer. These digital processing operations are carried out at a high sample rate given by the ADC, which can be in some cases reduced by an intermediate SRC between ADC and channelizer. Consequently, efficient DSP algorithms are required for their implementation. Field-Programmable Gate Arrays (FPGA) and programmable DSP processors generally include efficient signal processing modules which might be desirable for these types of tasks. In addition they can provide the required level of reconfiguration for the digital front-end operations.
3. The digital back-end encompasses all the baseband digital operations required for all the different implemented standards. Consequently a high level of reconfigurability is required. General Purpose Processors (GPP), e.g. Central Processing Units (CPU), are one possibility to achieve the reconfigurability requirements but their lack of specific DSP capabilities in comparison with FPGAs or DSP processors makes them less efficient signal processing tasks.

To maximize reconfigurability processing tasks should be progressively translated from the analogue front-end to the digital front-end as the technology advances. Eventually, a completely digital reconfigurable system may be achieved where the analogue to digital conversion is performed right next to the antenna as shown in Figure 2.6.

2.4.3.1 Analogue and digital front-ends

Even in the early software radio literature, the practical implementation of a digital RF front-end has been recognised as a significant challenge [44, 46-48].

The ADC is a key component in SDR technology since its speed determines the maximum frequency of the multi-channel received signal which can be possibly processed by the digital front-end. In order to achieve the desired ADC performance different implementation techniques have been proposed [49-52].

These techniques include bandpass sampling which combines the digitization of an RF signal at a lower sample rate with its direct down-conversion, all in one operation [53-57]. The continuous evolution of these techniques has lead to the recent appearance of direct RF-sampling ADCs which can perform at frequencies beyond 2.7 GHz at up to 3.6 GSPS, bringing the ideal SDR concept closer to the reality [58].

Some research work has also been carried out to maximize the flexibility of SRC structures employed in SDR, such as the one allocated between the ADC and the channelizer [59-60]. These methods propose SCR methods where the interpolation or decimation factor can be adapted depending on the communication standard requirements. More important, they can perform rational sample rate conversion which might be desirable for matching the sample rate with an integer number of the symbol rate of for a particular standard channel.

Finally, channelization forms the interface between the wideband multichannel digital signal (centred at intermediate frequency or DC) and the processing of independent baseband channels. Its allocation either on the digital front-end side or on the digital back-end of the SDR receiver has been discussed as a trade-off between flexibility and performance [61]. However, the high working sample rate is the main factor that leads to its allocation in the digital front-end part. Depending on the application, the number of channels can vary from one in the case of a mobile station to hundreds in the case of a base station. Base station channelization poses one of the main challenges in SDR implementations and is addressed in more detail in the next section and remainder of this work.

2.4.3.2 Digital back-end: SDR architectures

The digital back-end encompasses the set of functions that form the baseband processing of the independent channels from the different standards. The output of the baseband processing functions is generally known as *waveform*. To implement these waveforms different SDR software architectures have been developed. These can be divided into open source architectures, such as OSSIE, GNU Radio or IRIS [37, 62-64] and licensed architectures, such as the Scari

Software Suite from the Canadian Research Centre (CRC) or Spectra CX from Zeligsoft and PrismTech [65-66].

Due to their free access nature, open source SDR software architectures have gathered almost all (if not all) of the interest from academic research community [67-83]. GNU Radio is a software application for building and deploying SDR systems under a GNU General Public License. It was initially developed by the Massachusetts Institute of Technology (MIT) under the Spectrum Ware project [84] but it has undergone substantial development since then. OSSIE (Open Source SCA Implementation: Embedded) is an SDR implementation of the Joint Tactical Radio System (JTRS) Software Communications Architecture (SCA) [85]. It was developed by Virginia Tech University for educational use as well as for research applications using SDR in 2004. Finally, IRIS (Implementing Radio In Software) was developed by Trinity College Dublin [64]. It implements a component framework designed to run on a GPP. In general, these software architectures employ efficient programming languages such as C++ to implement the digital signal processing blocks, and script languages such as Python (GNURadio) or XML (OSSIE and IRIS) to describe the module interconnections and configuration parameters [86-87].

SDR software architectures intend to provide the highest level of reconfigurability for radio waveforms implementation. For this reason they have usually been targeted at GPP platforms. However, the lack of specific signal processing functions in GPPs, in comparison with other less flexible platforms as dedicated DSP hardware or FPGAs, makes the real-time signal processing required for wireless communications standards difficult [76-77, 84]. In addition, latency between the RF hardware and the GPP appears as another important challenge to allow real-time communications processing [78-80].

Researchers have also implemented the software architectures on FPGAs [81], cell processors [82] and Graphics Processor Units (GPU) [83]. Although real time processing of a small number of channels has been demonstrated this is still not sufficient for the case of a base station where a large number of channels must be handled.

2.4.4 An SDR multi-standard base station implementation: the channelization challenge

Similar to a hardware radio designs, SDR designs are also constrained by their specific target application. In the case of mobile communications, the design of the base stations and mobile stations will be constrained by different factors. For example, power consumption is a big issue for mobile stations since they have limited power supplied by a battery. Therefore, reducing the power consumption to maximize the battery life is a major priority. On the other hand, the SDR receiver architecture given in Figure 2.7 can be simplified in the case of a mobile station since only a single channel needs to be received.. As a result, the channelization and baseband processing costs are reduced.

In contrast to mobile stations, base stations are not strictly limited in their power consumption, although currently the tendency is to move towards "greener" implementations [88]. However, the channelization operation of a multi-standard base station which must handle a large number of channels from different standards is a computationally expensive operation to perform. For example, Table 2.3 shows the computational load in millions of instructions per second (MIPS) for the transmitter and receiver structure of one UMTS channel in a UMTS SDR [3]. In this example channelization was performed on a per-channel basis. From the table it can be seen that channelization represents the biggest computational load of the physical layer implementation. When applied to a base station which must handle a large number of channels, the total computational load necessary presents perhaps the most challenging DSP issue.

The challenge increases in a multi-standard base station. In this case, not only there is a large number of channels to be channelized, but also these channels may have different characteristics. Channelization complexity increases even more when DSA schemes are used (see Figure 1.1b), particularly DFSA schemes. In this case, the down-conversion and filtering of the different non-uniform channels need to be considered for a wide range of possible centre frequencies within the wideband multi-channel signal. Hence, non-uniform channelization applied to multi-standard SDR base stations to provide DFSA

represents an additional challenge within the already difficult channelization task.

Table 2.3 Signal processing load for one UMTS channel reproduced from [3].

Function	Partition	Tx/Rx	MIPS
Channelization	IF	Rx	3,000
Path searcher	Chip rate	Rx	1,500
Access detection	Chip rate	Rx	650
Rake receiver	Chip rate	Rx	650
Maximal ratio combining	Chip rate	Rx	24
Channel estimation	Symbol rate	Rx	12
AGC, AFC	Symbol rate	Rx	10
Deinterleaving rate matching	Symbol rate	Rx	12
Turbo decoding	Symbol rate	Rx	52
Channelization	IF	Tx	3,000
Transmitter	Chip rate	Tx	900
Interleaving	Symbol rate	Tx	12
Turbo encoding	Symbol rate	Tx	15
TOTAL			9,837

Although channelization in SDR base stations has been considered by different researchers, their work has mainly focused on implementations for a single communication standard or multiple standards with FSA schemes [89-93]. There has been some work on the non-uniform channelization field, but this has generally not been applied to concrete base stations and dynamic fragmented spectrum access. In the following chapters an overview and evaluation of these techniques will be done, together with the proposition of new ones, to improve the overall performance and capabilities.

2.5 Chapter conclusions

DSA schemes present a possible solution to maximizing spectrum utilization by dynamic sharing between different radio standards. DFSA, in particular, offers the best spectrum utilization. The implementation of DSA schemes would find an application in current real-world standards. For example, in the common frequency band implementation of TETRA V&D and TEDS base stations. However, the implementation of the DSA signal processing operations for multiple standards in a mobile communications device imply advances in current technology, specially for the DFSA option.

When the suitability of the classic hardware-based design for a base station receiver is considered for DSA, in particular DFSA, the results show that type of design is no longer an optimum and efficient solution. As a more efficient possibility, the implementation of the DSA compliant base station using software-based designs, specifically SDR, is considered because of its better flexibility. For SDR the channelizer is concluded to be a key element in the DSA support. However, it also represents a challenging task because of the high computational load it requires in comparison with the rest of the signal processing operations. Generic reconfigurable hardware platforms (e.g. CPU, FPGA, GPU) offer more flexible implementation options than ASIC designs. However, their generic scope makes them less efficient for particular DSP operations than optimized ASICs. Therefore, channelizers implemented on generic reconfigurable hardware platforms require efficient designs which minimize their computational load.

Chapter 3

Uniform Wideband Channelization

3.1 Introduction

In the previous chapter, channelization was identified as a computationally demanding operation in SDR implementations. In particular, channelization applied to SDR multi-standard base stations was considered the most challenging case based on two factors: the large number of channels and the different types of them.

Focusing on the first factor, in this chapter different wideband signal uniform channelization techniques for base stations are reviewed. These are mainly based on the per-channel approach (where each channel is filtered and down-converted independently), and on uniform complex modulated filter banks (where a single set of mixing and filtering resources is used to process all the communication channels). In addition, these structures represent the background information for the different non-uniform wideband channelization techniques that will be presented in the next chapter.

3.2 Wideband complex baseband signal channelization

As seen in Chapter 2, in an SDR base station receiver the digital front-end groups the channelization and SRC tasks [40, 44]. More specifically, channelization is composed of the down-conversion and filtering of every communication channel.

In general, mobile communication standards employ quadrature digital modulation techniques to maximize the signal capacity [4, 94]. Using quadrature

techniques, two different real-valued signals are modulated on two orthogonal components using the same carrier frequency. The orthogonality between them prevents the two signals from distorting each other even when using the same carrier frequency. The advantage is that the amount of information sent using a certain signal bandwidth is doubled compared to when only one real signal gets used. The two orthogonal signals are commonly termed In-phase and Quadrature (I/Q) components.

In general, communication signals with I/Q components are called complex-valued signals, in contrast with real-valued signals which have just a single real component. In complex signals, the I/Q components form the real and imaginary parts of the complex signal samples respectively. This complex-valued notation is useful because it simplifies some of the signal processing operations performed with such signals. Consequently, the complex representation of I/Q signals and their operations is generally known as *complex signal processing* [95]. As an example, Figure 3.1 shows the equivalence between the real implementation of a complex signal frequency modulation of the input signal

$$x(n) = x_I(n) + jx_Q(n) \tag{3.1}$$

using real-valued operations (as it is generally implemented in reality) and its equivalence using complex signal processing notation. Both operations are equivalent to each other, however the second one provides a simpler notation.

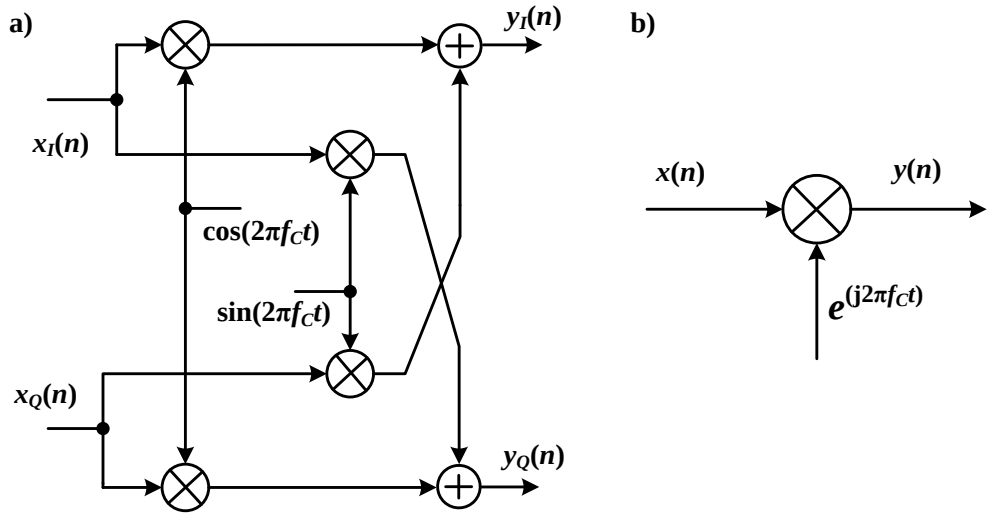

Figure 3.1 Frequency modulation expressed using a) real-valued signals considering the I/Q components separately, b) complex signal processing.

From the frequency domain perspective, the baseband and bandpass spectrum of a real-valued and a complex-valued signal differ [96]. The frequency response of a real-valued signal is strictly conjugate symmetric, with its real part symmetric and the imaginary part anti-symmetric. Consequently, its magnitude response is symmetric with respect to zero frequency and the phase response anti-symmetric. On the other hand, the spectrum of a complex-valued signal does not show any type of symmetry. Figure 3.2 depicts the difference between the baseband and bandpass spectrum of both type of signals.

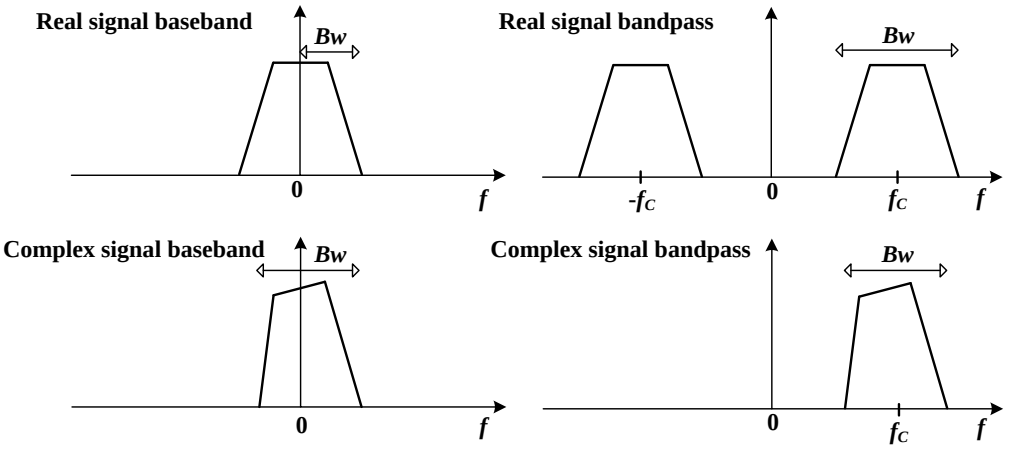

Figure 3.2 Real signal spectrum and complex signal spectrum.

In the digital front-end of an SDR base station receiver, Figure 2.7, the wideband digital signal of bandwidth B_W is passed to the channelizer from the ADC. Depending on the receiver configuration, the signal can be shifted directly from RF to DC prior to the ADC, or it can be centred provisionally in an Intermediate Frequency (IF), digitally converted by the ADC, and finally shifted to DC. The first configuration is known as *direct conversion receiver* whereas the second is knows as *superheterodyne receiver* (see Figure 2.7) [44]. The main difference between both structures is the use of two ADCs by the direct conversion receiver for only one ADC by the superheterodyne receiver. From the analogue point of view, the use of two ADCs in the case of direct conversion (one for the in-phase component and one for the quadrature component) provides at least twice the bandwidth available in comparison to the superheterodyne case. It also avoids the need to use an anti-mirror filter needed in a superheterodyne receiver to suppress the undesired signal replica produced by the multiplication of the interest channel with a real cosine or sine signal. As a drawback, direct conversion receivers require the use of algorithms to suppress the imbalance between the I/Q components, and this ultimately makes superheterodyne receivers more attractive for some applications, such as base stations [44].

Eventually the signal delivered to the channelizer is a digital baseband complex-valued I/Q signal of bandwidth B_W containing the different UL information channels. Within this wideband digital signal, the information channels are allocated at centre frequencies between $-B_W/2$ and $B_W/2$. To reduce the high sample rate of the signal obtained from the ADC, and intermediate SRC can be applied to reduce the sample rate up to $f_S = B_{W,}$ considering the Nyquist sampling criterion [25]. Thereafter, the channelizer module is in charge of the individual channel down-conversion from their centre frequency (f_{CH}) to DC and filtering. Finally, once the channel of interest has been separated from the adjacent channels, further sample rate reduction (or *downsampling*) can be performed up to $f_S=B_{CH}$, where B_{CH} represents the individual channel bandwidth. The relationship between the channelizer input and one of the channelizer outputs is shown in Figure 3.3.

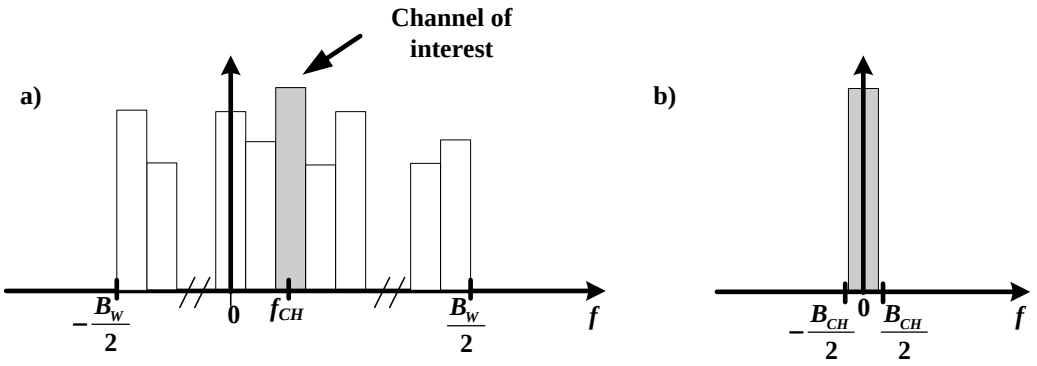

Figure 3.3 a) Channelizer wideband multi-channel input signal, b) one of the channelizer outputs with one of the information channels after its down-conversion to DC, filtering and downsampling.

In base stations, the channelization of the different UL information channels has traditionally been done with a *per-channel* approach where a dedicated signal processing chain is applied to each channel. However, this does not result in an efficient option when these are a large number of channels. As an alternative to the per-channel design, filter banks designs share part of the signal processing between all the different channels leading to greater efficiency.

3.3 Per-channel channelization

The channelizer structure for the per-channel approach is based on the implementation of a parallel and independent digital signal processing chain for every transmitted and received channel. After the analogue front-end and ADC, the wideband digital signal is delivered to every parallel processing chain to carry out the down-conversion and filtering of every channel independently. Figure 3.4 shows this configuration.

The digital wideband signal delivered from the analogue to the digital front-end contains all the communication channels centred at both sides of the DC frequency. Following, every parallel signal processing chain demodulates the channel of interested from its centre frequency to DC and applies a lowpass filter, *H(z)*, prior to the final downsampling to reduce the sample rate.

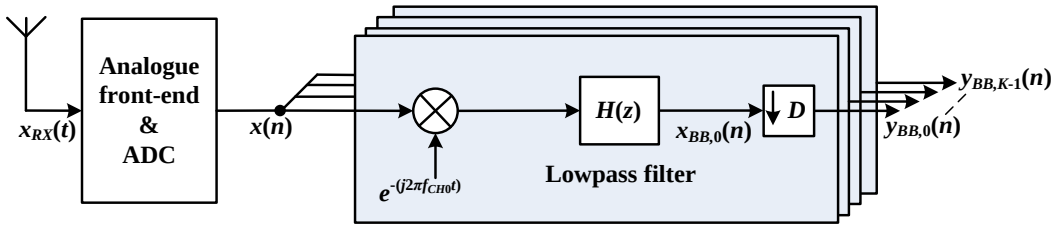

Figure 3.4 Channelizer using per-channel approach to filter and down-convert the different channels of the UL signal.

At the channelizer, the order of the down-conversion and filtering operations can be swapped [91]. Therefore two possibilities can be considered: digital down-conversion followed by lowpass filtering, or complex bandpass filtering followed by digital down-conversion.

The first option, down-conversion and lowpass filtering (Figure 3.4), is given by

$$x_{BB,k}(n) = h(n) * \left(x(n) e^{-(j2\pi f_{CHk} n)} \right) \quad \text{for } k = 0, ..., K-1 \tag{3.2}$$

where K is the total number of channels. It is followed by the downsampling operation

$$y_{BB,k}(n) = x_{BB,k}(nD) \quad \text{for } k = 0, ..., K-1 \tag{3.3}$$

In the frequency domain, the overall operation can be expressed as

$$X_{BB,k}(n) = H(z) X(z e^{j\omega_{CHk}}) \quad \text{for } k = 0, ..., K-1 \tag{3.4}$$

and

$$Y_{BB,k}(z) = \frac{1}{D} \sum_{i=0}^{D-1} X_{BB,k}(z^{1/D} W_D^i) \quad \text{for } k = 0, ..., K-1 \tag{3.5}$$

where $W_D^k = e^{j\frac{2\pi k}{D}}$.

Most commonly, when all the channels belong to a same standard, the centre frequencies match a multiple of the channel spacing defined for the particular

system. Each one of the channels is allocated at a frequency that is an integer multiple of the channel spacing from the DC frequency as

$$f_{CH} = \pm m f_{CS} \quad \text{for } m = 0,...,(K-1)/2 \tag{3.6}$$

where f_{CS} represent the channel spacing.

Generally in communication systems Finite Impulse Response (FIR) filters are preferred to Infinite Impulse Response (IIR) filters because it is easy to achieve an exact linear phase and stable response [97]. In addition, when a FIR filter is designed to have linear phase, its impulse response is symmetric or anti-symmetric as

$$h(n) = \begin{cases} h(N-n) & \text{for symmetric impulse responses} \\ -h(N-n) & \text{for antysymmectric impulse responses} \end{cases} \tag{3.7}$$

where N is the filter order. Hence, effectively only (N+1)/2 coefficients contribute to the frequency response of the filter, whereas the other half just provide the linear phase property. Therefore, only half of the coefficient multiplications have to be computed. Despite their impulse response symmetry advantage, FIR filters generally require much higher orders than IIR filters.

A FIR filter is generally designed using the windowing method or optimized methods, such as equiripple or least-squares [98-100]. Optimized methods provide better solutions to FIR filter implementations since they allow more control over the filter design parameters and optimize the response for a given filter order N. In particular, the equiripple filter design is generally preferred for communication applications [101]. Its passband ripple is constant in the entire band and does not exhibit a higher peak next to the pass-band cut-off frequency like in the window or least-squares methods. This is important for communication systems channels since the value of the pass-band ripple will have an influence in the Inter-Symbol Interference (ISI) in the time domain, whereas the stopband ripple will determine the Adjacent Channel Interference (ACI) in the frequency domain [98]. Moreover it is possible to choose the values of the pass-band and stop-band ripples independently of each other.

Generally in all FIR filter designs, the order of the filter is directly proportional to the ratio between the transition band and the sampling rate for which the filter is designed [98-99]. To approximate the order of a FIR filter, the following equation can be used [102]

$$N \approx \frac{-20\log_{10}\left(\sqrt{\delta_p \delta_s}\right) - 13}{14.6\left[\left(\omega_s - \omega_p\right)/2\pi\right]} \tag{3.8}$$

As it can be observed, the filter order is a function of the passband ripple (δ_p), stopband attenuation (δ_s) and normalised transition band width (ω_s - ω_p), where

$$\omega = 2\pi f / f_S \tag{3.9}$$

Consequently, for a given set of values for δ_p, δ_s, f_p and f_s, the sample frequency f_S will determine the normalized transition band and therefore the filter order. Taking these factors into account, the reduction of the sample rate f_S appears to be the best solution to reduce the computational load of a FIR filter.

To calculate the computational load of the per-channel approach first the digital down-conversion is considered. Both the digital signal *x(n)* and the mixing signal are complex signals, so digital down-conversion implies complex multiplication. This operation requires four real-valued multiplications and two real-valued additions. However, for FIR filters only half of the multiplications need to be performed. Thereafter, lowpass filtering requires the multiplication of real-valued filter coefficients with the complex-valued multi-channel signal centred at DC. In total the number of real multiplications, μ, and real additions, α, required per input sample for each channel is given by

$$\mu_{PC} = N + 5 \tag{3.10}$$

$$\alpha_{PC} = 4(N + 1) \tag{3.11}$$

where N is the order of the real coefficient FIR lowpass filter.

These operations will all be carried out at the high sample rate of the multi-carrier signal at the input of the channelizer. This makes the per-channel option very inefficient for a base station which must channelize a large number of channels.

It is possible to change the order of the down-sampling and filtering leading to bandpass filtering instead of lowpass filtering. This changes the filter coefficients from real to complex. Therefore, both the filtering and down-conversion require complex multiplications. Compared to the down-conversion followed by lowpass filtering, a computational overhead is introduced in the bandpass filters by the fact that double amount of real multiplications and additions are required. Therefore, there is no reason why this method would be preferable to the first one.

3.3.1 The CORDIC algorithm

Multiplications are more intensive operations than additions or register shifts in a DSP device. For this reason, structures which do not required multiplications are always preferred by designers. The COrdinate Rotation DIgital Computer (CORDIC) algorithm [103-104] it is itself a set of shift-add algorithms that can be implemented to carry out trigonometric functions in DSP devices. It was originally designed to convert complex numbers from polar to cartesian coordinates without using multiplies. If the conventional digital complex down-conversion is considered, as shown in Figure 3.1, a cosine and a sine functions are used. In this case, the amplitude values of the cosine and sine functions are usually stored in a read-only memory (ROM) table. For high resolution implementations (n bits) the size of the table increases exponentially with a size of approximately $2^n \times n$ bits, leading to large chip area, high power consumption and lower speed [105]. The application of the CORDIC algorithm provides both a reduction in the size of the ROM table ($\approx n \times n$ bits required) and a multiply-free implementation. In addition, despite a higher complexity design than the straight-forward conventional version, some DSP device manufacturers provide CORDIC implementations ready to use by DSP designers [106].

3.4 Multirate efficient filter implementation

Equations (3.10) and (3.11) show that the length of the lowpass filter represents the main contribution to the number of operations. The different solutions proposed to decrease the computational complexity of the per-channel approach are based on two principle ideas: reduction of the number of multiplications to be carried out and reduction of the sample rate that the filtering operation is performed at.

Multirate filtering techniques based on Cascade Integrator Comb (CIC) filters, polyphase FIR filter partitions, half-band filters and Frequency Response Masking (FRM) [97, 107-108] represent four possible solutions to reduce the sample rate of the wideband multi-channel signal by a factor up to *D* before the filtering of the signal of interest. This factor is mainly determined by the oversampling ratio between the wideband signals sample rate and the bandwidth of the signal of interest.

$$D \leq \frac{f_S}{B_W} \tag{3.12}$$

3.4.1 Cascade Integrator Comb (CIC) filters

CIC filters, also known as *slink* filters [109], represent a multiply-free way to carry out the filtering and decimation of the individual signals [98]. However, CIC filters are determined by only three integer parameters which results in a limited range of filtering characteristics. According to [98, 110], the CIC frequency response is given by

$$H(z) = \left(\sum_{n=0}^{D_{CIC}-1} z^{-n} \right)^R = \left(\frac{1 - z^{-D_{CIC}}}{1 - z^{-1}} \right)^R \tag{3.13}$$

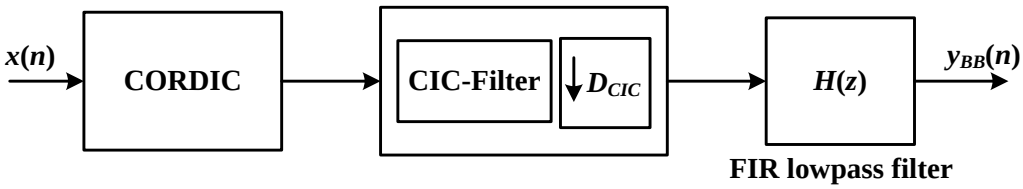

Figure 3.5 Per-channel approach option using CORDIC algorithm, CIC filter + downsampler and final lowpass filter.

In equation (3.13) D_{CIC} represents the down-sampling factor whereas R represents the number of stages of the CIC filter. Generally, the filters are formed by 3-to-5 cascade stages. The more the stages there are the narrower the width of the main lobe of the final frequency response and the smaller the magnitude of the secondary lobes.

In addition, the downsampling value D_{CIC} needs to be chosen so that the bandwidth of the channel of interest (B_{CH}) is approximately less than or equal to 25% of the output sample rate. This restriction arises because the non-constant pass-band gain of the CIC filter frequency response distorts the baseband spectrum. Unless the channel spacing between the signals is large, the CIC passband will include some of the channels adjacent to the channel of interest. For this reason a final lowpass filter is necessary in order to eliminate these undesired frequency components as in Figure 3.5. As an advantage, this last lowpass filter will work at a lower sample rate which will reduce its order and the number of operations per second. In addition, the FIR filter can be designed so that its passband frequency response is the inverse that the CIC filter one. As a result, the distortion introduced by the non-constant CIC passband response is cancelled [98].

3.4.2 Noble identities and polyphase filter decomposition

The previously described method permits more efficient filtering designs, but it has important design limitations. CIC filters designs are very constrained and the filter parameters such as transition band width and passband roll-off are difficult to control.

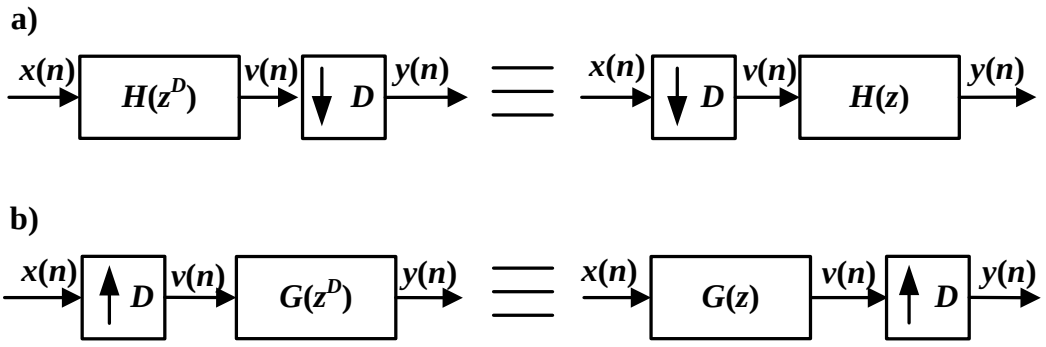

Figure 3.6 Noble identities. a) Noble identity I applied to decimation (downsampling + filtering), b) noble identity II applied to interpolation (upsampling + filtering).

Another multirate signal processing possibility is the polyphase decomposition of a digital filter [97, 107, 111]. This method can be applied to interpolation and decimation filters in order to carry out the convolution operations at the lower sample rate, reducing the number of operations per second that need to be performed. Before describing the polyphase decomposition, it is convenient to present two important properties of the multirate systems known as the *noble identities* which can be applied to interpolators and decimators, as shown in Figure 3.6.

A decimator's function is to reduce the sample rate of a given signal by a factor *D*. To do so, decimation is divided into two operations: filtering and downsampling (Figure 3.6a). The filter employed is generally called an *anti-aliasing* filter. Its function is to limit the bandwidth of the input signal to π/D rad to avoid the overlapping or *aliasing* of the output signal with its shifted replicas, or *aliases*, generated during the downsampling operation [107]. Therefore, the input signal $x(n)$ is first filtered by the anti-aliasing filter $H(z)$

$$v(n) = h(n) * x(n) \leftrightarrow V(z) = H(z)X(z) \tag{3.14}$$

obtaining the bandwidth limited signal $v(n)$, and later downsampled

$$y(n) = v(nD) \leftrightarrow Y(z) = \frac{1}{D}\sum_{k=0}^{D-1} V_k(z^{\frac{1}{D}} e^{-j2\pi k/D}) \tag{3.15}$$

to obtain the output signal $y(n)$. If the anti-aliasing filter impulse response is the result of its upsampling by the same factor D, noble identity I can be applied to change the order of the filtering and downsampling operations (Figure 3.6a). Consequently, the filtering operations can be performed at the lower sample rate of the system output.

In contrast with decimation, interpolation increases the sample rate of the input signal by a factor D. It is decomposed into upsampling and *anti-image* filtering [107]. In *zero insertion interpolators*, the increase in the sample rate of the input signal $x(n)$ is achieved by introducing D-1 zeros between two consecutive samples, as

$$v(n) = \begin{cases} x(n/D), & n = 0, \pm D, \pm 2D, \ldots \\ 0, & \text{otherwise} \end{cases} \leftrightarrow V(z) = X(z^D) \tag{3.16}$$

obtaining $v(n)$ with the increased sample rate. After, the anti-image filter limits the output signal bandwidth to π/D rad, separating the lowpass version of the input signal $x(n)$ from its bandpass images obtained during the upsampling operations as

$$y(n) = g(n) * v(n) \leftrightarrow Y(z) = G(z)V(z) \tag{3.17}$$

Like the decimation case, if the anti-image filter impulse response is the result of its upsampling by the same factor D, noble identity II can be applied to change the order of the upsampling and filtering operations (Figure 3.6b). Consequently the filter works at the lower sample rate of the system input.

The basis of the polyphase decomposition is the grouping of filter coefficients that are multiplied by the same delay. In this way, time and operations are saved. Consider a 2-fold polyphase representation of a analysis filter given by

$$\begin{aligned} H(z) &= \sum_{n=-\infty}^{\infty} h(n)z^{-n} = \sum_{n=-\infty}^{\infty} h(2n)z^{-2n} + \sum_{n=-\infty}^{\infty} h(2n+1)z^{-(2n+1)} \\ &= \underbrace{\sum_{n=-\infty}^{\infty} h(2n)z^{-2n}}_{E_0(z^2)} + z^{-1} \underbrace{\sum_{n=-\infty}^{\infty} h(2n+1)z^{-2n}}_{E_1(z^2)} \end{aligned} \tag{3.18}$$

In this case the $H(z)$ filter coefficients can be grouped into 2 polyphase components $E_0(z)$ and $E_1(z)$.

The general D-fold decomposition form groups the analysis filter coefficients $H(z)$ into D polyphase components according to

$$H(z) = \sum_{n=-\infty}^{\infty} h(n) z^{-n} = \sum_{p=0}^{D-1} z^{-p} E_p(z^D) \tag{3.19}$$

where $E_p(z)$ are called polyphase components and the coefficients $e_p(n)$ are obtained by

$$e_p(n) = h(nD + p), \qquad 0 \le p \le D-1 \tag{3.20}$$

$$E_p(z) = \sum_{n=-\infty}^{\infty} h(nD + p) z^{-n} \tag{3.21}$$

The polyphase decomposition represented by (3.19) is commonly known as *type 1*. It is necessary to describe a *type 2* polyphase decomposition since it will be used later when the uniform modulated filter banks are presented. It is given by

$$H(z) = \sum_{p=0}^{D-1} z^{-(D-1-p)} R_p(z^D) \tag{3.22}$$

$E_p(z)$ and $R_p(z)$ are known as type 1 and type 2 polyphase components respectively. $E_p(z)$ and $R_p(z)$ are related to each other by

$$R_p(z) = \begin{cases} E_0(z), & \text{for } p = 0 \\ E_{D-p}(z), & \text{for } p = 1, \ldots, D-1 \end{cases} \tag{3.23}$$

So the coefficients $r_p(n)$ are obtained by

$$r_p(n) = h(nM - p), \qquad 0 \le p \le D-1 \tag{3.24}$$

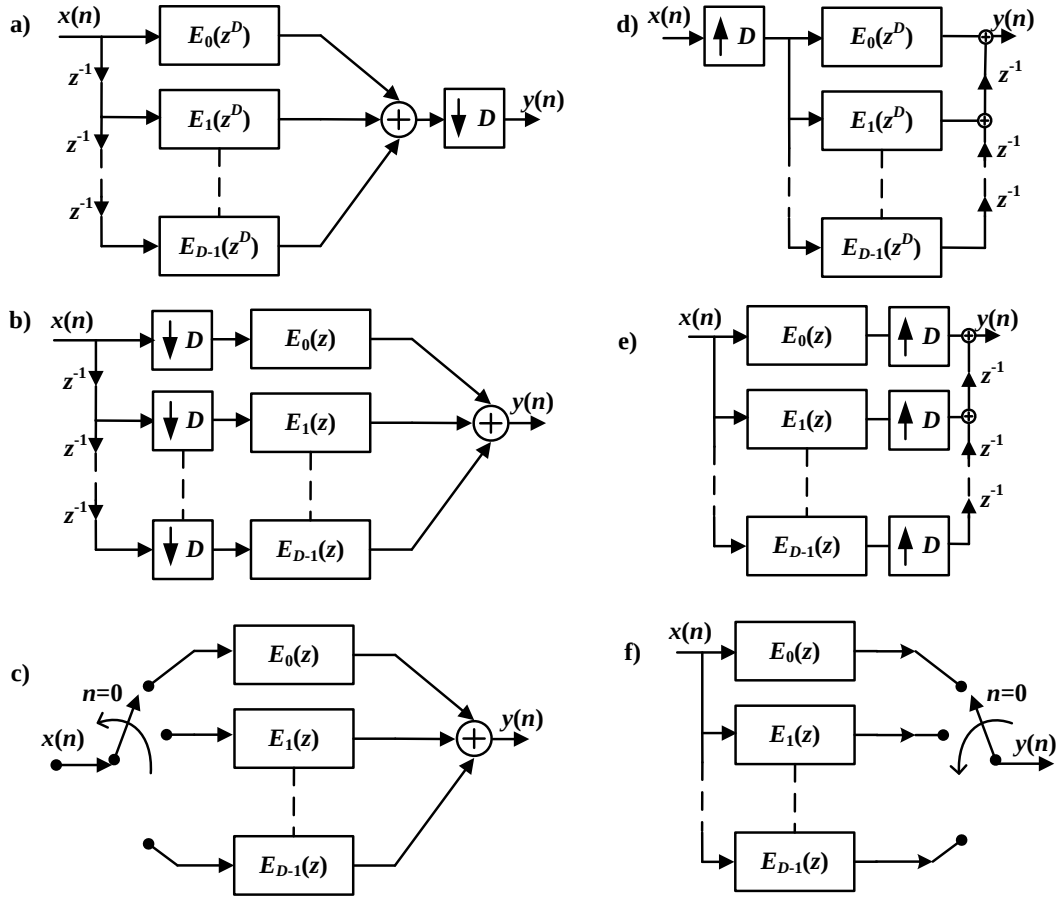

Figure 3.7 Polyphase decomposition applied to interpolation and decimation filters.

Using the noble identities and polyphase decomposition more efficient implementations of the decimation and interpolation filters can be obtained. Figure 3.7a and Figure 3.7b show how noble identity I applied to the type 1 polyphase decomposition of a decimation filter can reduce the filtering rate by inserting the downsampling operation prior to the polyphase filter components. Similarly, Figure 3.7d and Figure 3.7e show how the application of noble identity II to an interpolation filter can achieve the same type of filter rate reduction.

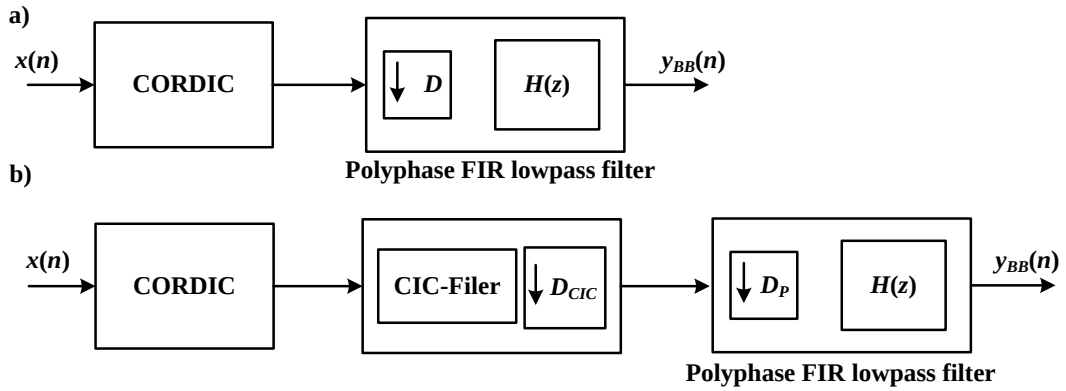

Figure 3.8 Performance improvement options by using CORDIC algorithm and a) polyphase FIR filter, b) CIC filter plus polyphase FIR filter.

Commutators are commonly used to replace delay chains and SRC parts. Figure 3.7c shows the delay chain and downsamplers replaced by a rotating counter clockwise commutator which delivers one sample to one polyphase at each input sample rate instant. In this way, the filtering rate is D times smaller than the system input sample rate. The initial position for the instant n=0 is indicated in Figure 3.7f. The same method is applied to the interpolation filter by inserting another rotating counter clockwise commutator which collects the D outputs from the polyphase branches per input signal unit of time of the.

If type 2 polyphase decomposition is used, the main difference from Figure 3.7 is that clockwise commutators for both interpolation and decimation filters have an initial position at the instant n=0 at the R_{D-1} polyphase branch.

The application of the polyphase decomposition to the per-channel processing chain is depicted in Figure 3.8a. Because the polyphase implementation is used, the decimator is allocated prior the lowpass filter and the number of real multiplications and additions per input per channel is reduced to

$$\mu_{PC} = \frac{N+1}{D} + 4 \tag{3.25}$$

$$\alpha_{PC} = \frac{2N}{D} + 2 \tag{3.26}$$

Table 3.1 Number of real multiplications per input sample (μ) for different per-channel approaches.

	Direct approach	CIC + FIR per-channel approach	Polyphase per-channel approach	CIC + polyphase FIR per-channel approach
Filter	$(N+1)K$	$\frac{(N+1)}{D}K$	$\frac{2(N+1)}{D}K$	$\frac{2(N+1)}{D_{CIC}D}K$
Digital Down Conversion	$4K$	–	–	–
Total	$(N+5)K$	$\frac{(N+1)}{D}K$	$\frac{2(N+1)}{D}K$	$\frac{2(N+1)}{D_{CIC}D}K$

It is important to remark that even though the sample rate is decreased in the polyphase implementation the FIR filter still needs to be designed using the input signal sample rate f_S, so the number of coefficients will be the same as for a non-polyphase implementation.

CIC and polyphase filters can be combined [98] by replacing the lowpass FIR filter in Figure 3.5 with a polyphase FIR filter that performs a second downsampling by D_P, so the decimation factor D is obtained after two decimation operations in cascade as

$$D = D_{CIC}D_P \tag{3.27}$$

This structure is shown in Figure 3.8b exhibits advantages over the structures in Figure 3.5 and Figure 3.8a. From the first one, it allows a bigger downsampling factor prior to the FIR filter which reduces sample rate that the FIR performs. From the second one, the prior downsampling carried out after the CIC filter reduces the sample rate at the input to the polyphase FIR filter, which allows the order of the necessary FIR filter to be reduced by approximately a factor D_{CIC}. As a drawback, the limited range of CIC filters might make the use of the structure in Figure 3.8b unsuitable for some applications. Table 3.1 presents the number of real multiplications per input complex sample necessary for the

approaches presented in Figure 3.4, Figure 3.5 and Figure 3.8, with *K* representing the number of channels filtered and down-converted. For the structures using CIC filters, all the multiplications correspond to the FIR filter cascaded with the CIC filter.

According to the results, the structure in Figure 3.8a (when sufficiently flexible for the application), requires fewer multiplies than the polyphase decomposition structure. This is due to the capacity of the lowpass filter after the CIC filter to exploit the symmetry in its impulse response which can not be done in the polyphase filter of the second case. However, the one in Figure 3.8b provides the advantages that only one filter has to be designed and a much bigger design flexibility and control over the filter mask. When the application allows the use of CIC filters, its combination together with the polyphase partition provides the best results.

3.4.3 Half-band filters

Half-band filters are generally employed by multirate structures, interpolators or decimators, with a SRC factor equal to 2 to perform as anti-image or anti-aliasing filters respectively [98, 100, 112]. This selection is generally based on their frequency response. FIR half-band filters allocate the -6 dB cut-off point at the frequency $\pi/2$ rad providing a symmetric transition band width from this point to both sides of the spectrum.

The other principal property of half-band filters, which makes them an important component in multirate designs, is that in their impulse response all the even coefficients are equal to zero with the exception of the one centred at the origin. This property, plus the typical symmetric impulse response of linear phase FIR filters, makes them very efficient in comparison with other filter designs. In particular, only roughly one fourth of the multiplications need to be computed. Both the impulse response and magnitude frequency response of a half-band filter are shown in Figure 3.9a.

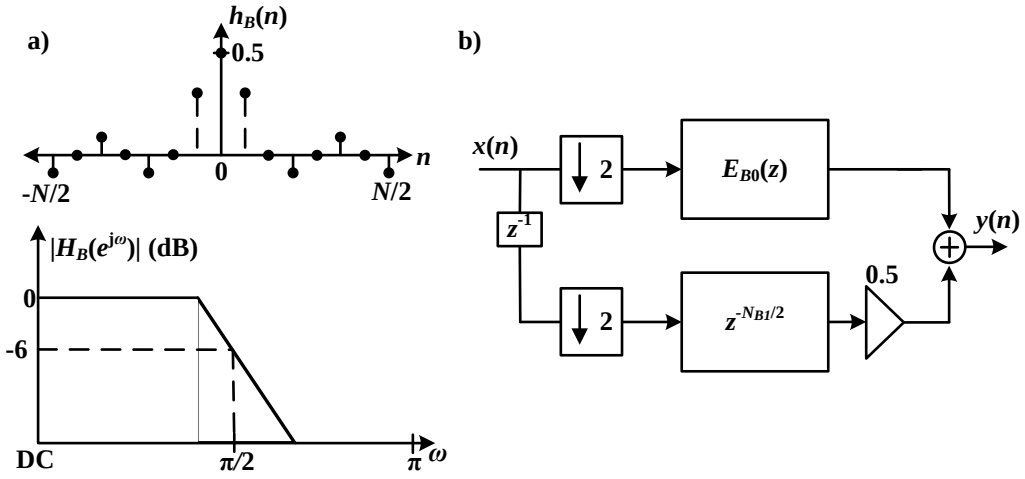

Figure 3.9 Half-band filter a) impulse and frequency response, b) efficient polyphase implementation of half-band filter as a decimator.

As with any other FIR filter, half-band filters can be implemented using a 2-fold polyphase decomposition. The polyphase decomposition of the half-band filter is given by

$$H_B(z) = \sum_{n=-\infty}^{\infty} h_B(n) z^{-n} = \sum_{p=0}^{1} z^{-p} E_{Bp}(z^2) \tag{3.28}$$

where $E_{B0}(z)$ groups the non-zero odd coefficients, and $E_{B1}(z)$ groups all the zero coefficients plus the middle coefficient equal to 0.5. Due to their particular impulse response, one of the polyphase branches is purely formed by a delay group equal to the order of each polyphase component (N_{B0} and N_{B1}) divided by two and a multiplier corresponding to the coefficient centred at the origin. Figure 3.9b shows the polyphase structure of a half-band filter used as decimator after applying the nobel identity I from Figure 3.6a.

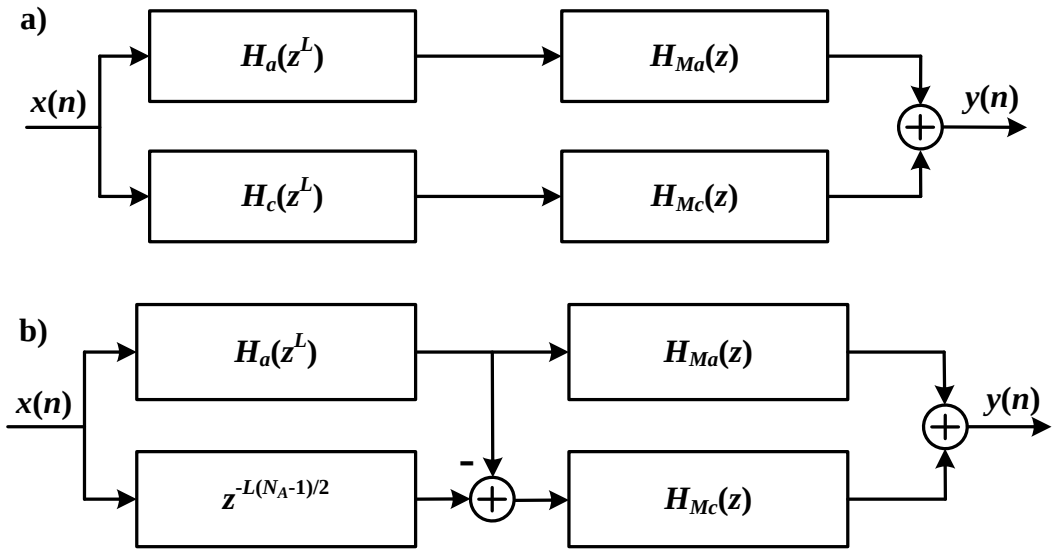

Figure 3.10 Frequency response masking. a) Direct implementation, b) efficient implementation.

3.4.4 Frequency Response Masking (FRM)

The FRM technique was proposed in [108] as a solution for reducing the design complexity of FIR filters with very sharp transition bands. Instead of employing a single FIR filter with stringent specifications, the FRM parallel structure is formed by two branches with two FIR filters in each (Figure 3.10a). These two branches are generally known as *positive* (top) and *complementary* (bottom) branches. The filters in both branches have more relaxed filtering requirements than the direct implementation FIR filter; consequently, the filters in the FRM structure require fewer coefficients and smaller number of multiplications. The combination of the outputs from the two FRM branches results in the desired sharp frequency response. Figure 3.11a shows the filtering process in both the positive and complementary branches and how their addition concludes in the desired filtering specification.

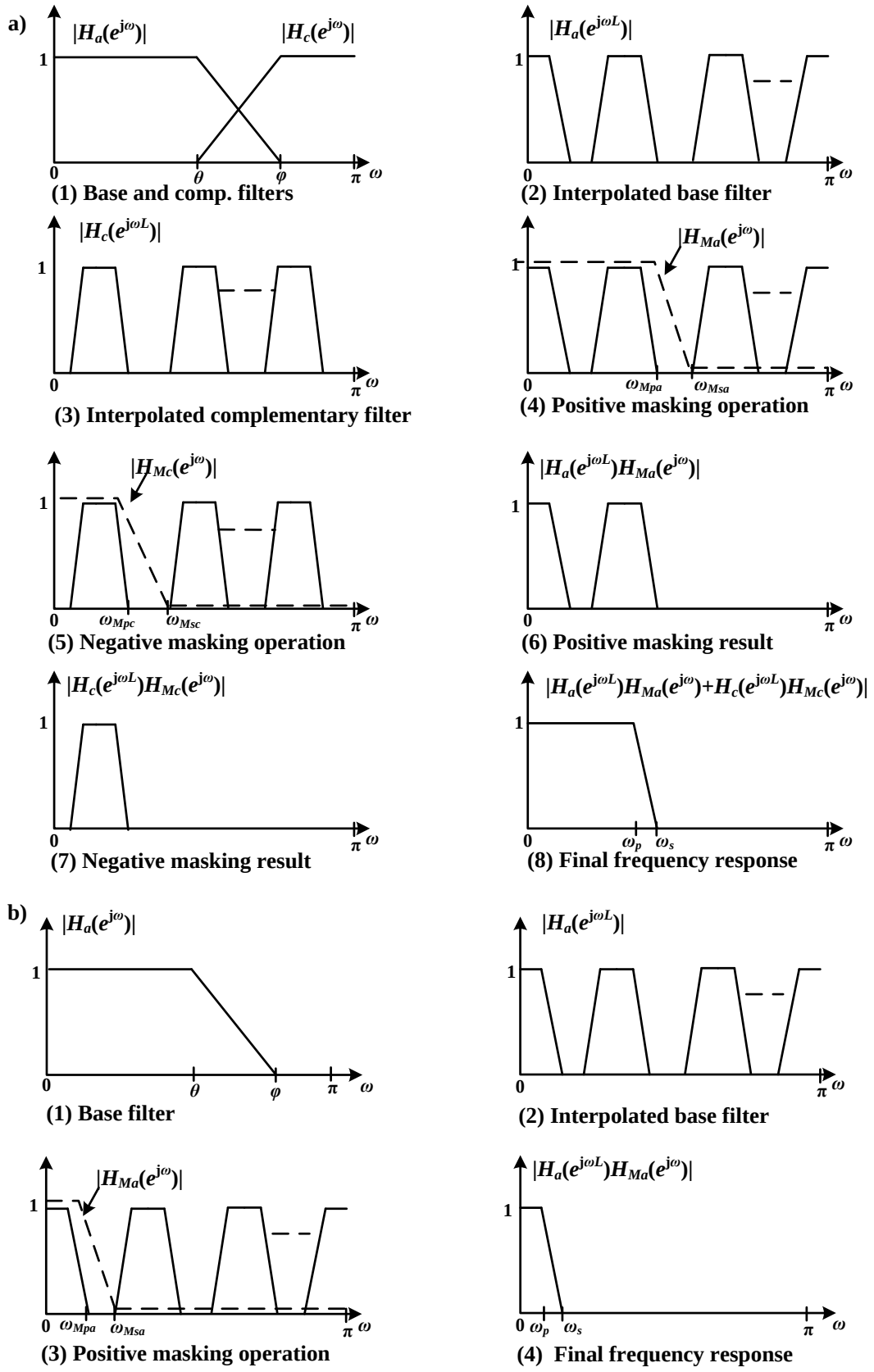

Figure 3.11 FRM operations. a) Full FRM, b) narrowband FRM [113].

The *base*, $H_a(z)$, and *complementary*, $H_c(z)$, filters, as the name of the second expresses, have complementary frequency responses as shown in Figure 3.11a(1) [114]. When both of them are interpolated by a factor L (by adding L-1 zeros between their coefficients), the passband and transition band widths in their frequency responses get reduced by the same factor. In addition, bandpass and highpass replicas of the interpolated frequency responses appear at frequencies which are a multiple of $2\pi/L$ rad. The function of the *masking* filters, $H_{Ma}(z)$ and $H_{Mc}(z)$, is to filter the interpolated frequency responses of both base and complementary filters so only some of the replicas are kept. Finally, the addition of the two interpolated and masked frequency responses provide the desired filtering specifications.

The transfer function of the Figure 3.10a structure is given by

$$H(z) = H_a(z^L)H_{Ma}(z) + H_c(z^L)H_{Mc}(z) \tag{3.29}$$

where $H_a(z)$ and $H_c(z)$ are the base and complementary filters, whereas $H_{Ma}(z)$ and $H_{Mc}(z)$ are the positive and complementary masking filters.

The complementary relationship between the filters $H_a(z)$ and $H_c(z)$ can be expressed as

$$H_c(z) = z^{-(N_A/2)} - H_a(z) \tag{3.30}$$

where N_A is the order of the base filter. Therefore, the complementary filter can be obtained by subtracting the $H_a(z)$ output from a delayed version of the input signal. This leads to the efficient implementation shown in Figure 3.10b.

In certain applications where a very narrow filter passband is desired, the interpolation and masking operations of the positive FRM branch are sufficient [108]. This special case is generally known as *narrowband* FRM in contrast with the *full* FRM case. Consequently the transition band is purely given by the first image of the interpolated base filter frequency response (Figure 3.11b). Now (3.29) is reduced to

$$H(z) = H_a(z^L)H_{Ma}(z) \tag{3.31}$$

Table 3.2 FRM filters specifications calculation.

	Full FRM (Case 1)	Full FRM (Case 2)	Narrowband FRM
Base filter	$\theta = \omega_p L - 2m\pi$ $\phi = \omega_s L - 2m\pi$	$\theta = 2m\pi - \omega_s L$ $\phi = 2m\pi - \omega_p L$	$\theta = \omega_p L$ $\phi = \omega_s L$
Masking filter $H_{Ma}(z)$	$\omega_{Mpa} = \dfrac{2m\pi + \theta}{L}$ $\omega_{Msa} = \dfrac{2(m+1)\pi - \phi}{L}$	$\omega_{Mpa} = \dfrac{2(m-1)\pi + \phi}{L}$ $\omega_{Msa} = \dfrac{2m\pi - \theta}{L}$	$\omega_{Mpa} = \omega_p$ $\omega_{Msa} = \dfrac{2\pi}{L} - \omega_s$
Masking filter $H_{Mc}(z)$	$\omega_{Mpc} = \dfrac{2m\pi - \theta}{L}$ $\omega_{Msc} = \dfrac{2m\pi + \phi}{L}$	$\omega_{Mpc} = \dfrac{2m\pi - \phi}{L}$ $\omega_{Msc} = \dfrac{2m\pi + \theta}{L}$	---

The different passband and stopband of the base and masking filters can be calculated according to Table 3.2 once the desired passband (ω_p) and stopband (ω_s) cut-off frequencies are given. As seen in Table 3.2, for the full FRM two different design *cases* are given. The difference between the case 1 and case 2 is that in the first the final filter transition band is given by one of the base filter interpolated replicas, whereas in the second this is done by one of the complementary filter replicas. For the narrowband FRM, since only the positive branch is used, there is only one design method.

For the case 1 and case 2 the value of m is given by

$$\begin{aligned} &\text{Case 1: } m = \left\lfloor \omega_p L / 2\pi \right\rfloor \\ &\text{Case 2: } m = \left\lceil \omega_s L / 2\pi \right\rceil \end{aligned} \tag{3.32}$$

where $\left\lfloor \omega_p L / 2\pi \right\rfloor$ denotes the largest integer smaller than $\omega_p L / 2\pi$, and $\left\lceil \omega_s L / 2\pi \right\rceil$ denotes the smallest integer bigger than $\omega_s L / 2\pi$.

From Figure 3.11 and Table 3.1 it is clear that all the filters employed in the filtering process have larger transition bands than the final frequency response obtained. Consequently, as seen in (3.8), all of them have a lower filter order than the direct implementation using a single filter from Figure 3.4. Hence, the smaller the final transition band required, the bigger the benefit that applying the

FRM technique can provide due to the ease of filter design provided. Depending on the specific case, the combination of all the coefficients of the four filters involved (or two in the case of narrowband FRM), can also lead to a smaller total number of multiplications in comparison with a single filter design.

As a drawback, when FRM is used no signal downsampling can be performed before the FRM filtering structure output, as in Figure 3.4, in contrast with designs using CIC filters or FIR polyphase filters. This means that all the filtering operations are carried out at the wideband input signal sample rate. Despite the ease with which the different filters may be designed, if the total number of coefficients is bigger than in the single filter case, the computational load will be bigger too.

3.5 Filter bank based channelizers

Using the per-channel channelization approach the complexity of the implementation grows linearly with the number of channels. This can represent a high computational load in systems like base stations where a large number of channels are channelized from the UL signals.

Observing the SDR base station receiver structure from Figure 2.7, the channelizer is implemented as part of the digital front-end on a DSP reconfigurable hardware platform. Therefore, it is reasonable to think that all the independent branches of the per-channel approach can also share some of the processing tasks since they are all embedded into the same hardware. Consequently, the total computational load can be reduced.

Filter banks, also known as transmultiplexers when applied to communications, are a solution to the linear growth in computational load when the number of channels to be supported increases. When applied to system such as base stations, uniform modulated filter banks effectively perform the filtering and down-conversion operations of all the channels by sharing the processing operations between them [97]. In addition, they use the polyphase

decomposition of the channelization filters to reduce the sample rates that the operations are perform at.

3.5.1 Filter bank and transmultiplexer basis

The basic structure of a filter bank is depicted in Figure 3.12a. In general, it is divided into three main blocks: the analysis bank, which carries out the decomposition of the fullband signal into *K* different sub-band components; the middle sub-band signal processing, which is specific to the application that the filter bank is used for (i.e. sub-band equalization, echo cancellation, etc.); and the synthesis bank, which is in charge of resynthesising the fullband signal back from the *K* sub-components.

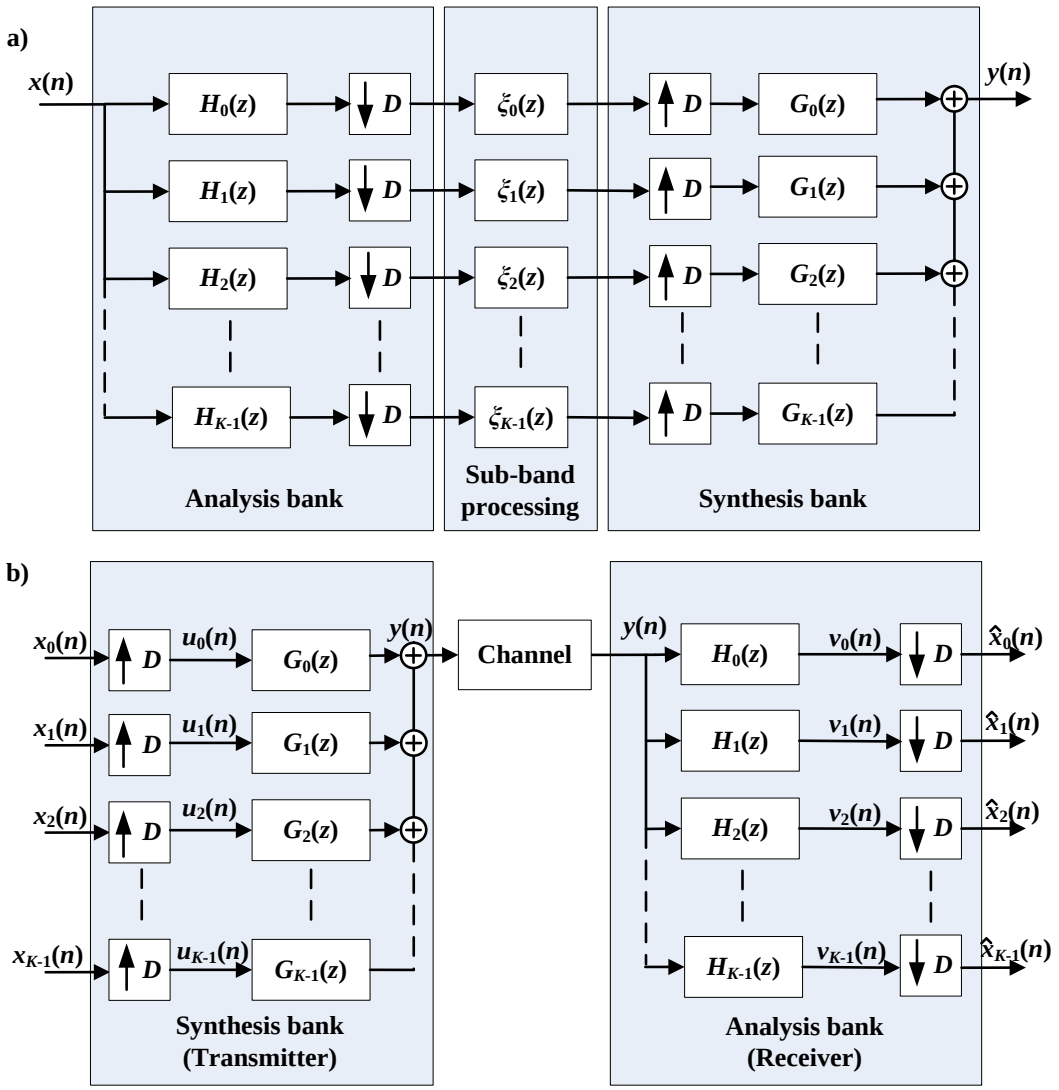

Figure 3.12 General structure of a) filter bank, b) transmultiplexer.

Transmultiplexers represent a variation of filter banks applied to communications systems (Figure 3.12b). In this case, the synthesis bank is used in the transmitter side to multiplex a set of K narrowband signals ($x_0 \ldots x_{K-1}$) into a wideband signal by shifting the channels along the frequency spectrum.

First, the individual communication signals, which use the same sample rate f_S, are upsampled by a factor D to obtain a D-fold compression of their spectrum. Then, the interpolation filters, $G_k(z)$, extract one of the images per channel in order to add them together in the FDM signal. In Figure 3.13(b), (d) and (f) the shadowed images represent the ones extracted by the interpolation filters $G_0(z)$, $G_1(z)$ and $G_2(z)$. These filters will generally have the same frequency response, but shifted to a centre frequency multiple of $2\pi/K$ in order to choose the correct spectrum image. As a consequence, ideally, the addition of all the images of the different channels to form the FDM signal does not cause any overlap among them.

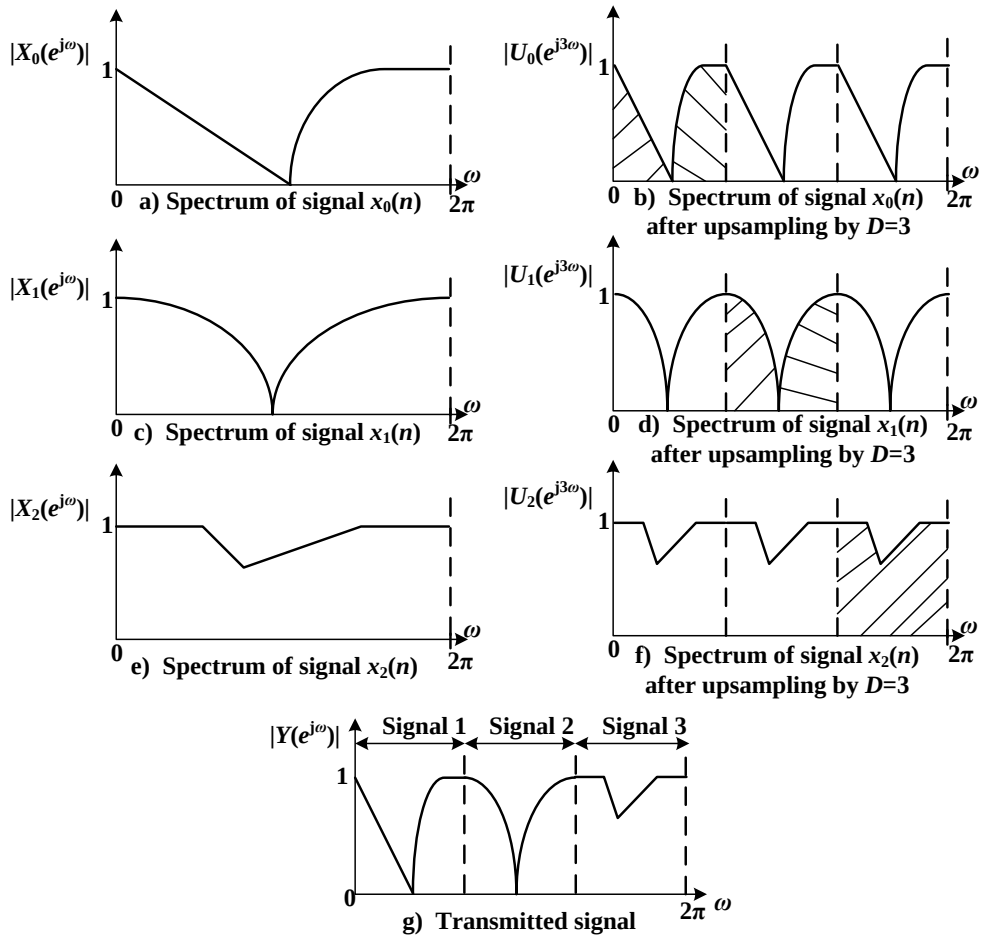

Figure 3.13 Transmultiplexer transmitter operations.

On the receiver side, the analysis bank is applied to the wideband input signal to filter and down-convert the K individual channels. It is composed of a collection of decimation filters, $H_k(z)$, followed by a set of down-samplers. As in the synthesis bank, the analysis filter $H_0(z)$ is a lowpass filter whereas the other filters are bandpass type. All of them have the same frequency response, centred at the same frequencies multiples of $2\pi/K$ as in the transmitter side.

If $D=K$ the filter bank or transmultiplexer is described as *critically decimated*. On the contrary, if D is smaller than K the system is known as an *oversampled* or *non-critically decimated* filter bank or transmultiplexer.

The structure depicted in Figure 3.12 is also known as *parallel structure* and it is very similar to the per-channel approach addressed in the first section of this chapter. Therefore, the parallel structure shares the same low efficiency and the proportional computational load increase with the per-channel structure when the number of channels tends to grow. In addition, every independent filter $G_k(z)$ and $H_k(z)$ needs to be designed separately taking into account their specifications such as passband and stopband cut-off frequencies or passband and stopband ripples.

3.5.2 Design issues: perfect reconstruction and oversampling

In applications where filter banks are employed (Figure 3.12a), considering that the signal processing between the analysis and synthesis banks should not produce any change over the sub-band signals ($\xi = 1$), ideally the overall aim in the design of the filter bank would be to have an output signal equal to the input signal up to a certain delay as

$$y(n) = x(n-d) \tag{3.33}$$

The achievement of this fact is knows as *perfect reconstruction*. In addition, if a certain amount of distortion is accepted, it is known as *near perfect reconstruction* [107].

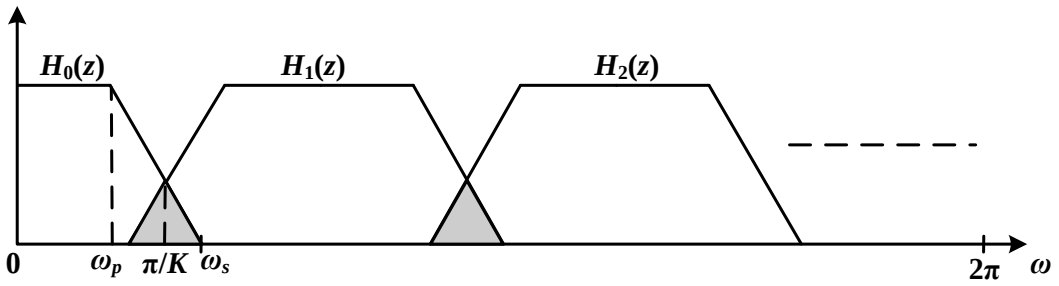

Figure 3.14 Frequency response of the non-zero transition band lowpass filter and bandpass modulated filters.

The same concept is also applied to transmultiplexers where ideally it is desired that the relation between the transmitted and received signals is also nothing more than a delay if it assumed that the channel does not introduce any effect on the signal.

$$\hat{x}_k(n) = x_k(n-d), \quad k = 0,1,...,K-1 \tag{3.34}$$

In reality, filter banks and transmultiplexers suffer three kinds of distortions: sub-band cross talk, amplitude distortion and phase distortion [107]. Sub-band cross talk is produced by the fact that the frequency response of the analysis and synthesis filters have a non-zero transition band and non-zero stopband gain as it can be seen in Figure 3.14. In the analysis bank, this means that the signals are not perfectly band limited which leads to aliasing when the downsampling operation is carried out. In the synthesis bank, the same effect is produced by imaging when the upsampling operation is performed. These effects can be reduced by designing the analysis and synthesis filters with sharp transition bands which minimizes the overlapped region between adjacent filters and increases the attenuation in the stopbands. Unfortunately, this solution leads to high order filters, which makes the filter bank or transmultiplexer less efficient.

On the other hand amplitude and phase distortions are produced by the characteristics of the overall filter bank frequency response. It can be defined as

$$T(z) = \frac{1}{K}\sum_{k=0}^{K-1} H_k(z)G_k(z) \tag{3.35}$$

where $T(z)$ represents the overall transfer function. If $\left|T(e^{j\omega})\right|$ is not constant it means that the filter bank or transmultiplexer introduces amplitude distortion. Also, if $T(e^{j\omega})$ has nonlinear phase response, it means that the system introduces phase distortion. The first can be minimized by reducing the passband ripple of the filters' frequency response; whereas the latter can be cancelled by using FIR filters since they can ensure a linear frequency response. This solution entails a reduction of the efficiency since in order to achieve a smaller passband ripple the order of the filter must be increased. Also, linear phase FIR filters implementation requires more operations than other types of filters, such as IIR filters, which have potential for instability and do not have perfect linear phase response.

In filter bank applications, such as sub-band coding [115] or sub-band speech processing [116], and transmultiplexer implementations, such as Very High Bit-Rate Digital Subscriber Sines (VDSL) modems [117-118] or Orthogonal Frequency Division Multiplexing (OFDM) systems [119], both the analysis and synthesis banks are considered to be part of the same signal processing chain. In the transmultiplexer case it means that the transmitter uses a synthesis bank to transmit the multi-channel signal and the receiver employs an analysis bank to receive and recover every channel from the multi-channel signal (as in Figure 3.12b). For these cases, different methods to get perfect reconstruction have been proposed [107, 120-122]. In all of them, the cancellation of the undesired effects is achieved by certain relationships between the frequency responses of the filters $H(z)$ and $G(z)$. These relationships lead to more relaxed filter designs and even to the use of IIR filters in some cases, which permits more efficient implementations.

Oversampled transmultiplexers introduce a redundancy by increasing the number of samples per channel, and the output sample rate as a result. This fact, despite looking like a drawback, provides noticeable benefits when perfect reconstruction is sought. First, it reduces aliasing distortion by preventing the cross-talk components produced by the non-zero transition band of the filters from aliasing back into the band of the decimated signal [97, 123-127]. Second, it increases the design freedom for perfect reconstruction analysis and synthesis

filters for modulated filter banks and reduces the noise produced by the sub-band cross talk.

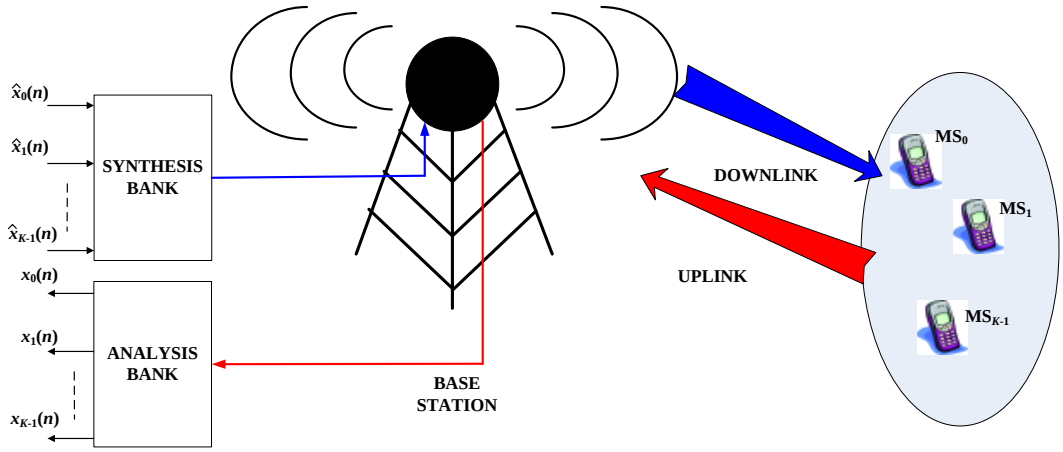

Figure 3.15 Transmultiplexer applied to asymmetric mobile communication scenario between base station and mobile stations.

For the case of a base station, the perfect reconstruction solution based on the relationships between analysis and synthesis filters is not viable since both analysis and synthesis banks act independently forming an *asymmetric* design (Figure 3.15). As shown in Figure 3.15 the transmitter part of the base station generates a wideband multi-channel DL signal in which every channel is destined for a different end user or mobile station. This mobile station will probably have a receiver architecture designed to select only one of those channels like in the per-channel approach in Section 3.3. On the other hand, the receiver part of the base station will receive a wideband multi-channel UL signal composed of individual channels transmitted by individual mobile stations. Consequently, sharp filters and oversampled filter bank designs are the two main design factors which can minimize aliasing effects in the base station channelizer.

3.5.3 Complex uniform modulated filter banks

Considering that all the information channels in Figure 3.12 share the same properties, bandwidth and sample rate, it makes sense to think that the frequency response of the independent analysis and synthesis filters can also share the same specifications. The only difference between them is the centre frequency at

which they are allocated. This kind of transmultiplexer or filter bank is called *uniform* because all the K channels are evenly distributed along the spectrum. The channel centre frequencies are separated from each other by

$$f_{CS} = \frac{f_S}{K} \tag{3.36}$$

where f_{CS} is the channel spacing and f_S is the sample rate at the input of the analysis bank or at the output of the synthesis bank.

Consequently, the different bandpass filters of the analysis ($H_1(z)\ldots H_{K-1}(z)$) and synthesis ($G_1(z)\ldots G_{K-1}(z)$) banks can be obtained by the modulation of the lowpass $H_0(z)$ and $G_0(z)$ filters. Therefore these filter banks are called *uniform modulated filter banks*, and $H_0(z)$ and $G_0(z)$ are called *prototype filters*. Furthermore, the properties of the polyphase filter decomposition can be applied to the uniform modulated transmultiplexers to dramatically reduce the number of operations and allow an efficient management of large numbers of channels.

In general, uniform modulated filter banks (and transmultiplexers) can be classified as real or complex modulated. When applied to communications, the real modulation is generally used for wired communication applications such as VDSL [118]. These communications use real baseband modulation techniques which make the use of real modulated filter banks the main implementation option. However, in wireless communications (and mobile communications among) complex baseband signals are used to achieve a better spectrum usage, as seen in Section 0. Therefore, these systems require the use of complex modulated filter banks or transmultiplexers to carry out the wideband multi-channel signal channelization [96]. Complex uniform modulated filter banks can be further classified in two main groups: DFT Modulated Filter Banks (DFT-FB) and Exponentially Modulated Filter Banks (EMFB).

3.5.3.1 DFT modulated filter banks (DFT-FB)

DFT-FBs are based on the complex modulation of the K-1 bandpass filters from the lowpass prototype filter using the DFT algorithm [97-98, 107]. As with other modulated filter banks, design simplicity is obtained because only the lowpass

prototype filter must be designed; the remaining bandpass filters automatically inherit the same properties after their modulation from lowpass prototype. In comparison with the filter bank structure in Figure 3.12, DFT-FBs only require the implementation of one filter and one DFT matrix. Furthermore, the use of the Fast Fourier Transform (FFT) algorithm in certain circumstances can reduce the computational burden even more.

DFT-FBs have been widely proposed to be used in communications as a transmultiplexer for complex signals [89, 91-93, 128-135]. In the receiver side of the base station, the analysis bank is composed by uniformly spaced filters with an even-type stacking arrangement. Even-type means that there is a lowpass filter centred at DC as shown in Figure 3.16. Considering a critically decimated ($D=K$) filter bank design, the centre frequencies of the different K filters are given by

$$\omega_{CHk} = \frac{2\pi k}{K} = \frac{2\pi k}{D}, \quad k = 0,1,...,K-1 \tag{3.37}$$

This function is applied to the modulation of the different bandpass filters as

$$h_k(n) = h(n)W_K^{kn}, \quad \text{for } k = 1,2,...,K-1 \tag{3.38}$$

where $h(n)$ is the lowpass prototype and

$$W_K = e^{j(2\pi/K)} \tag{3.39}$$

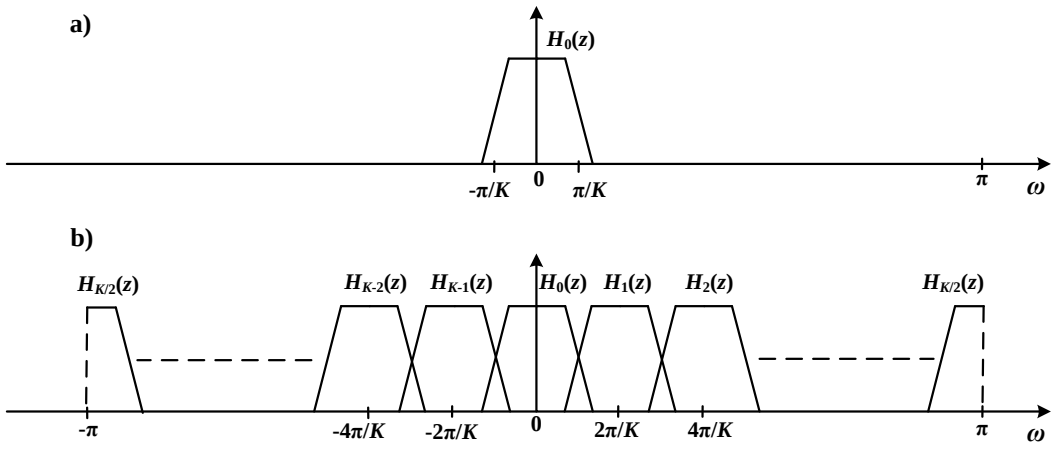

Figure 3.16 DFT-FB a) lowpass prototype filter, b) bandpass filters frequency allocation.

Considering the polyphase type 1 decomposition of the lowpass prototype filter $h(n)$, every polyphase component is obtained by

$$h(n) = \sum_{p=0}^{K-1} e_p(n) = \sum_{p=0}^{K-1} h(nK+p), \quad p = 0,1,...,K-1 \tag{3.40}$$

In the frequency domain,

$$H(z) = \sum_{p=0}^{K-1} E_p(z^K) z^{-p} = \sum_{n=-\infty}^{\infty} h(nK+p) z^{-n} \tag{3.41}$$

Applying (3.38) into (3.40) yields

$$\begin{aligned} e_{k,p}(n) &= h(nK+p) W_K^{k(nK-p)} \\ &= h(nK+p) W_K^{-kp} \end{aligned} \tag{3.42}$$

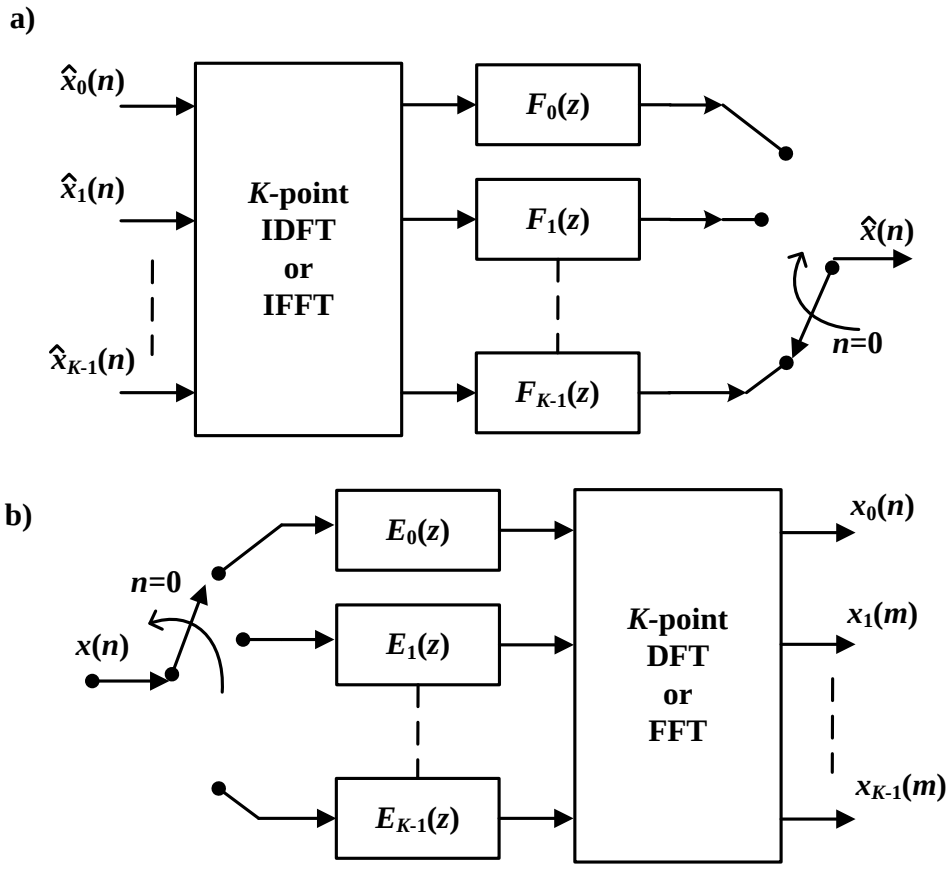

Figure 3.17 Polyphase DFT modulated transmultiplexer a) transmitter, b) receiver.

Consequently, the polyphase components of the bandpass filters obtained from the lowpass prototype can be expressed as

$$e_{k,p} = e_p W_K^{-kp}, \quad \text{for } p,k = 0,1,...,K-1 \tag{3.43}$$

or in the frequency domain

$$H_k(z) = \sum_{p=0}^{K-1} E_p(z^K) z^{-p} W_K^{-kp}, \quad p,k = 0,...,K-1 \tag{3.44}$$

where W_K^{-kp} factor is the DFT matrix whose indices are the polyphase branch number *p* and the transmultiplexer channel *k*. The computational load is shared between all the analysis filters and so the total computation is decreased by a factor of *K*. In addition, another *K* saving factor is achieved by using the polyphase decomposition itself which allows downsampling to take place prior to filtering.

Using the same methodology, on the transmitter side the synthesis bank carries out the filtering and allocation of the channels on the spectrum in frequencies also determined by equation (3.37). If a type 2 polyphase decomposition is applied this time to the synthesis filters, from the synthesis prototype filter $g(n)$ the polyphase branches of the bandpass filters are obtained by

$$f_{k,p}(n) = g_k(nK - p), \quad \text{for } p,k = 0,1,...,K-1 \tag{3.45}$$

where

$$g_k(n) = g(n) W_K^{kn}, \quad \text{for } k = 0,1,...,K-1 \tag{3.46}$$

and $g_k(n)$ represents the different bandpass modulated synthesis filters.

Analogously to the analysis bank,

$$G_k(z) = \sum_{p=0}^{K-1} F_p(z^K) z^{-p} W_K^{kp}, \quad p,k = 0,...,K-1 \tag{3.47}$$

where the modulation factor W_k^{kp} represents the inverse DFT (IDFT).

This modulation operation using the DFT algorithm (or IDFT) requires K^2 complex multiplications since both the DFT coefficients and the input signal samples are complex numbers. Therefore, the computational load DFT algorithm increases quickly with the number of channels managed.

A reduction in the number of the DFT operations can be achieved by choosing *D* and *K* as a power-of-two, in which case an FFT algorithm (radix-2 or split-radix) can be used instead [136-137]. On one hand, for the radix-2 algorithm, the most efficient implementation requires 3 real multiplications and 3 real additions per complex multiplication between a complex-valued input sample and a factor W_K^i [138]. On the other hand, the split-radix provides the minimum amount of operations as well as the minimum number of real multiplications [137]. The computational load of both FFT algorithms is presented in Table 3.3. Although the split-radix algorithm provides the lowest computational load, the radix-2 algorithm is more commonly implemented in DSP devices like FPGAs [139].

In the prototype filter implementation, every polyphase component is formed by $(N+1)/K$ real-valued coefficients, where *N* is the order of the prototype filter. Considering the complex-valued input samples, every polyphase component requires $2(N+1)/K$ real multiplications and $2((N+1)/K-1)$ real additions. Therefore, the number of real multiplications and real additions per complex input sample for the analysis or synthesis bank in a critically decimated DFT-FB are

$$\mu_{DFT-FB,RADIX-2} = \frac{2(N+1)+\frac{3K}{2}(\log_2(K)-5)+8}{K} \tag{3.48}$$

$$\alpha_{DFT-FB,RADIX-2} = \frac{2(N+1-K)+\frac{7K}{2}(\log_2(K)-5)+8}{K} \tag{3.49}$$

Table 3.3 *K*-point FFT algorithms computational load [137].

FFT algorithm	Real multiplications per input sample (μ)	Real additions per input sample (α)
Radix-2	$\frac{3K}{2}(\log_2(K)-5)+8$	$\frac{7K}{2}\left(\log_2\left(K\right)-5\right)+8$
Split-radix	$K\log_2(K)-3K+4$	$3K\log_2(K)-3K+4$

when the radix-2 algorithm is used, whereas the for the split-radix case they are given by

$$\mu_{DFT-FB,SPLIT-RADIX} = \frac{2(N+1)+K\log_2(K)-3K+4}{K} \tag{3.50}$$

$$\alpha_{DFT-FB,SPLIT-RADIX} = \frac{2(N+1-K)+3K\log_2(K)-3K+4}{K} \tag{3.51}$$

Despite their simplicity and efficiency, DFT-FBs have difficulty in achieving perfect reconstruction or near perfect reconstruction [107]. To address this issue, a variation of the DFT-FB known as Modified DFT-FB (MDFT-FB) has been proposed [140-144]. The difference relies on the separate processing of the real and imaginary parts of the complex input signals. Therefore, perfect reconstruction and near perfect reconstruction can be achieved in both filter bank and transmultiplexer applications, such as filtered OFDM [145]. However, as discussed in previous sections perfect reconstruction is not useful in mobile communications where mobile stations and base stations use asymmetric channelization structures. In addition, MDFT-FBs require extra computation and resources in comparison with DFT-FBs to process the same amount of channels. This overhead makes them less attractive for base station application.

3.5.3.2 Exponential modulated filter banks (EMFB)

The difficulty of DFT-FBs to achieve perfect reconstruction or near perfect reconstruction, especially when the system is designed as critically decimated, has led to other options to implement complex modulated filter banks apart from MDFT-FBs. EMFBs are an alternative structure based on the parallel connection of a Cosine Modulated Filter Bank (CMFB) and a Sine Modulated Filter Bank

(SMFB) [96, 146-149]. Both CMFB and SMFB are real modulated filter banks, which imply that all the multiplications and additions in the EMFB are real-valued unlike in the DFT-FB. The structured of an EMFB applied as a transmultiplexer is shown in Figure 3.18.

Uniform CMFBs and SMFBs, unlike DFT-FBs, employ real modulation methods to derive the bandpass filter from the lowpass prototype [107, 121]. To achieve this filter modulation, Discrete Cosine Transforms (DCT) and Discrete Sine Transforms (DST) are used respectively [150]. In general, the DCT-IV and DST-IV are chosen [107, 148, 151].

For a CMFB the different analysis and synthesis filters are obtained by the modulation of the lowpass prototype filter using the DCT as

$$h_k^c(n) = 2h(n)\cos\left[\frac{(2k+1)\pi}{2K}\left(n-\frac{N}{2}\right)+(-1)^k\frac{\pi}{4}\right] \tag{3.52}$$

$$g_k^c(n) = 2g(n)\cos\left[\frac{(2k+1)\pi}{2K}\left(n-\frac{N}{2}\right)-(-1)^k\frac{\pi}{4}\right] \tag{3.53}$$

For the SMFB, the same method is used but this time using the DST as

$$h_k^s(n) = 2h(n)\sin\left[\frac{(2k+1)\pi}{2K}\left(n-\frac{N}{2}\right)+(-1)^k\frac{\pi}{4}\right] \tag{3.54}$$

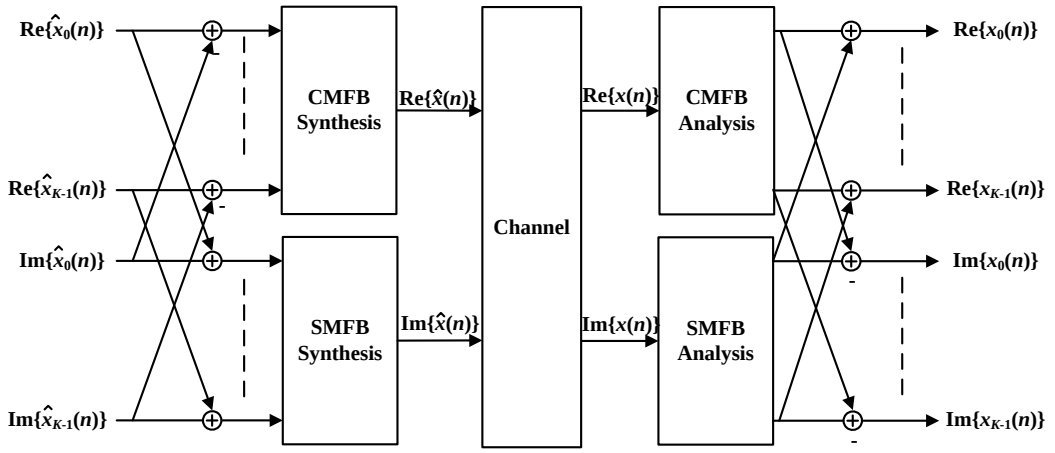

Figure 3.18 Exponentially modulated filter bank used as transmultiplexer.

$$g_k^s(n) = 2g(n)\sin\left[\frac{(2k+1)\pi}{2K}\left(n-\frac{N}{2}\right)-(-1)^k\frac{\pi}{4}\right] \tag{3.55}$$

where k indicates the channel under interest, K the total number of channels and N is the order of the lowpass prototype filter. This length is usually chosen to be equal to N=2mK-1 (where m is a positive integer number) for perfect reconstruction purposes [107].

As in the DFT-FB case, if the EMFB critically decimated case is considered ($D = K$), the K different channels are uniformly allocated in centre frequencies also given by (3.37).

For the CMFB part design, if the constraint that the length of the prototype filter is L=2mK is established, the polyphase components of the prototype filter can be represented as

$$E_p^c(z) = \sum_{n=0}^{2m-1} h(mK+p)z^{-n} \tag{3.56}$$

whereas the polyphase components of the other derived bandpass filters are obtained as

$$E_{k,p}^c(z) = \sum_{n=0}^{2m-1} 2h(mK+p)c_{k,(mK+p)}z^{-n} \tag{3.57}$$

where

$$c_{k,n} = \cos\left[\frac{(2k+1)\pi}{2K}\left(n-\frac{L}{2}\right)+(-1)^k\frac{\pi}{4}\right] \tag{3.58}$$

For the specific filter length L=2mK, the cosine function presents a periodic property which can be exploited by applying it to (3.57).

$$\cos\left\{\frac{(2k+1)\pi}{2K}\left[(n+2mK)-\frac{L}{2}\right]+(-1)^k\frac{\pi}{4}\right\}= \\ =(-1)^m\cos\left[\frac{(2k+1)\pi}{2K}\left(n-\frac{L}{2}\right)+(-1)^k\frac{\pi}{4}\right] \tag{3.59}$$

After rearranging the terms according to [152], the polyphase components of the prototype filter and bandpass analysis filters are expressed as

$$E_p^c(z)=\sum_{n=0}^{m-1}h(2nK+p)z^{-n},\quad p=0,1,...,2K\text{-}1 \tag{3.60}$$

and

$$E_{k,p}^c(z)=2c_{k,p}E_p^c(-z^2)+2c_{k,(p+K)}z^{-1}E_{(p+K)}^c(-z^2),\quad p=0,1,...,K-1 \tag{3.61}$$

Now, the prototype filter is divided in $2K$ polyphase components. For the derived bandpass filters their polyphase components are grouped in two terms. The first one makes reference to the first K polyphase components of the prototype filter, whereas the second makes reference to the last K components.

Using equation (3.19) the different analysis filters can be expressed as

$$H_k^c(z)=\sum_{p=0}^{K-1}E_{p,k}^c(z^K)z^{-p} \tag{3.62}$$

Therefore, the whole analysis bank can be expressed using a matrix notation as

$$\begin{pmatrix}H_0^c(z)\\H_1^c(z)\\\vdots\\H_{K-1}^c(z)\end{pmatrix}=\begin{pmatrix}\mathbf{C_{1A}} & \mathbf{C_{2A}}\end{pmatrix}\begin{pmatrix}E_0^c(-z^{2K})\\z^{-1}E_1^c(-z^{2K})\\\vdots\\z^{-(2K-1)}E_{2K-1}^c(-z^{2K})\end{pmatrix} \tag{3.63}$$

with $\mathbf{C_{1A}}$ and $\mathbf{C_{2A}}$ being K x K matrices with the DCT-IV coefficients in the form

$$\mathbf{C_{1A}}=\sqrt{K}(-1)^i\mathbf{C^{IV}}(\mathbf{I}-(-1)^m\mathbf{J}) \tag{3.64}$$

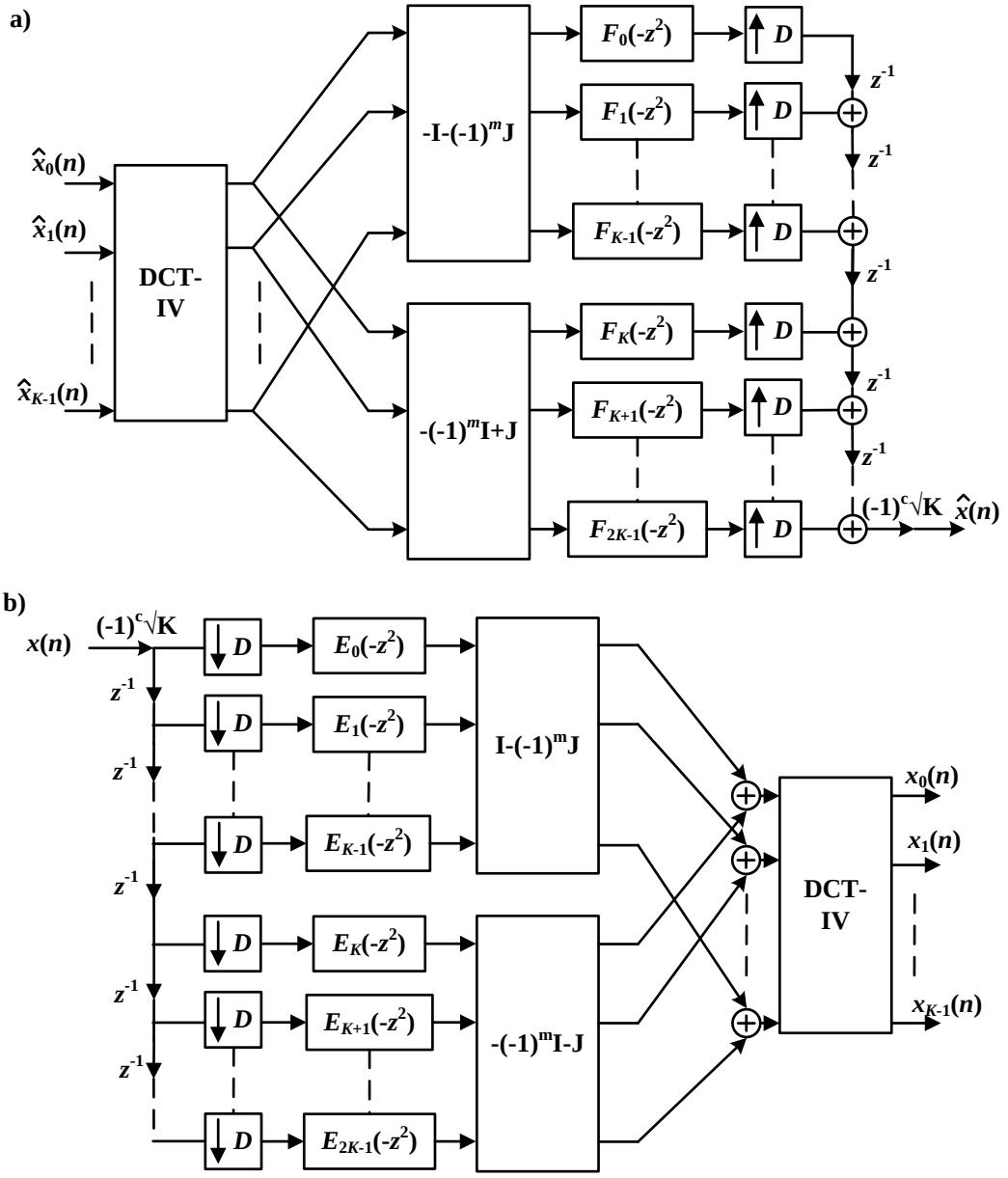

Figure 3.19 Cosine modulated filter bank a) synthesis bank, b) analysis bank.

$$\mathbf{C_{2A}} = \sqrt{K}(-1)^i \mathbf{C^{IV}}((-1)^m \mathbf{I} - \mathbf{J}) \tag{3.65}$$

where the $\mathbf{C^{IV}}$ matrix is given by (3.66) as

$$\left\{\mathbf{C^{IV}}\right\}_{k,n} = \sqrt{\frac{2}{K}} \cos\left[\frac{2k+1}{2K}\left(n+\frac{1}{2}\right)\pi\right] \tag{3.66}$$

and

$$i = \lfloor m/2 \rfloor \tag{3.67}$$

Previously in (3.64), (3.65) and (3.66) **I** represents a K x K identity matrix, **J** is a K x K reversal matrix.

For the SMFB the same methodology from (3.56) to (3.66) can be applied, but this time considering the DST-IV. Finally, an equivalent structure for the SMFB to the one shown in Figure 3.19 is achieved.

In the same way that for the FFT algorithm, there are different implementations for the DCT-IV and DST-IV. Among them, the one presented in [153] provides the best computational load with

$$\mu_{DCT,DST} = \frac{K}{2}\log_2(K) + K \tag{3.68}$$

real multiplications and

$$\alpha_{DCT,DST} = \frac{3K}{2}\log_2 K \tag{3.69}$$

real additions to compute a real-valued K-length sequence.

For the prototype filter, the length L=2mK condition needs to be met (N=2mK-1). In this case, the lowpass prototype is divided within 2K polyphase components of 2m coefficients each. Since the complex input samples get divided into their real in-phase and quadrature components, all the multiplications and additions carried out in the polyphase components and modulation transforms are real-valued. The total number of real multiplications and additions of an EMFB for every complex input sample for a critically decimated case is

$$\mu_{EMFB} = \frac{2(N+1) + K\log_2 K + 2K}{K} \tag{3.70}$$

and

$$\alpha_{EMFB} = \frac{2N + 3K\log_2 K + 2K}{K} \tag{3.71}$$

3.6 Computational load analysis for per-channel and complex modulated filter bank channelizers

This section focuses on the comparison of the uniform channelization approaches under the base station context. As a difference to [89, 91] where only the per-channel approach and DFT modulated transmultiplexers were considered, here EMFBs are also included.

The filter bank structures taken into account for evaluation are the polyphase DFT-FB, both radix-2 and split-radix cases, and the polyphase EMFB. For the per-channel approach, the structure in Figure 3.8b is chosen as the most efficient candidate considering that the design allows the use of CIC filters (which do not use multipliers); otherwise, the polyphase FIR option from Figure 3.8a would need to be used. The number of real multiplications of the three channelizers for a number of channels K is given in Table 3.4.

For the four cases, to be compliant with the EMFB requirements, the length of the prototype filter is considered to be $L=2mK$ ($N=2mK-1$). The input signals are considered to be complex-valued I/Q samples and the channelizers work in critically decimated conditions where $D=K$.

For the CIC downsampling, due to the limitation between channel bandwidth and sample rate explained before, the decimation factor is chosen to be

$$D_{CIC} = D/4 \tag{3.72}$$

Together with the decimation factor of the cascaded polyphase filter, the total decimation is given by

$$D = D_{CIC} D_P \tag{3.73}$$

Table 3.4 Number of multiplications per complex input sample for every channelization structure.

Uniform channelizer structure	Multiplications per input sample (μ)
CIC + Polyphase FIR Per-Channel Approach	$\frac{2(N+1)}{D_{CIC}D}K$
DFT Modulated Filter Banks with radix-2 algorithm	$\frac{2(N+1)+\frac{3K}{2}(\log_2(K)-5)+8}{K}$
DFT Modulated Filter Banks with split-radix algorithm	$\frac{2(N+1)+K\log_2(K)-3K+4}{K}$
Exponential Modulated Filter Banks	$\frac{2(N+1)+K\log_2 K+2K}{K}$

The comparison is based on the number of multiplications per channel required when the number of channels increases. To make it independent of the filter order, the number of multiplications is normalized with respect to *m*. In Figure 3.20, the computational load of the four different structures is presented. The number of multiplications per channel in the per-channel approach increases linearly with the number of channels employed. For a given fixed frequency band, the bigger the number of channels the narrower the transition band required for the filters, therefore, the bigger the filter order and the number of operations per channel. For the filter bank based methods, the number of multiplications remains approximately constant. This is because modulated filter banks share the computational load between all the channels. The results show the more efficient performance of the filter bank based approaches, especially when the number of channels to be managed increases.

Focusing only on the filter bank methods, Figure 3.21 shows how the number of multiplications per channel increases with the number of channels *K*. Here it can be seen that the computational load does not increase linearly as it seemed the per-channel approach, but more slowly. It is worth noting that the DFT-FB requires fewer multiplications than the EMFB for all values of *K*. Whether the radix-2 or split-radix algorithm performs better for the DFT-FB case depends on the number of channels. In conclusion, unless perfect reconstruction or near

perfect reconstruction is required, DFT-FBs provide more efficient implementations in comparison with EMFBs.

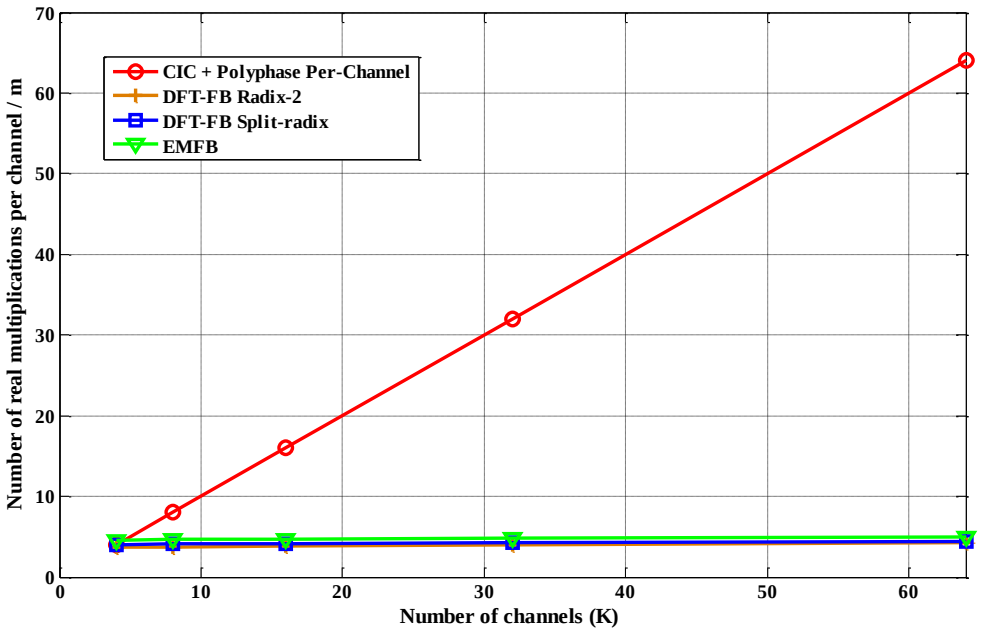

Figure 3.20 Computational comparison of uniform channelization methods.

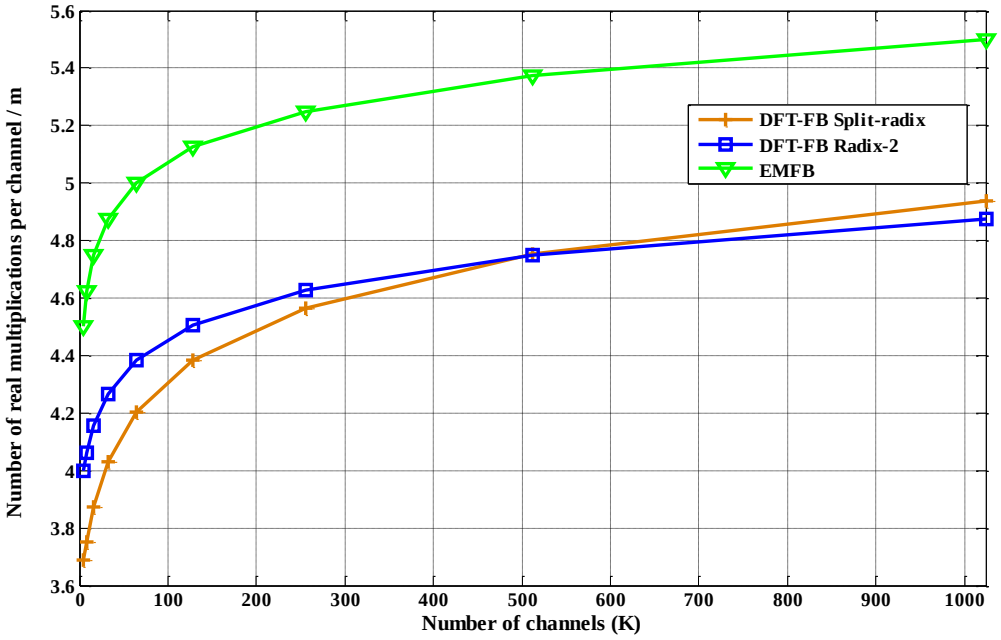

Figure 3.21 Computational comparison for uniform modulated filter banks based channelizers.

Apart from the polyphase implementation, other alternative structures have been proposed for DFT-FBs and EMFBs. For the DFT-FBs, designs based on *Weyl-Heinsenberg* frames and *Weighted Overlap-Add* structures are used to achieve perfect reconstruction in oversampled DFT-FB designs [97, 123, 125, 154-159]. For the EMFBs, alternatives to the polyphase filters included the fast Extended Lapped Transform (ELT) and the lattice structure [96, 107, 121, 148, 151, 160]. Both structures also provide extra advantages in comparison with polyphase EMFB when perfect reconstruction is intended.

3.7 Chapter conclusions

In this chapter the fundamentals of wideband digital uniform channelization were reviewed. First, the complex baseband channelizer input signal was analysed using complex digital signal processing. Thereafter, the classical per-channel approach was presented together with different multirate filter designs to reduce its complexity. Filter banks and transmultiplexers were then presented as an alternative to simplify and efficiently perform the uniform channelization task when a large number of channels must be managed. Their main advantage over per-channel designs is that the filtering operations are shared among the different channels when they are implemented as modulated filter banks. Because wireless communications uses complex quadrature signals (for bandwidth efficiency), two forms of complex modulated filter banks were studied: DFT-FBs and EMFBs.

It was shown that the computational load of uniform per-channel channelizers is higher than filter bank channelizers, particularly for a large numbers of channels. Among the filter bank channelization structures, it was shown that DFT-FBs have a lower computational load than EMFBs.

Chapter 4

Non-Uniform Wideband Channelization

4.1 Introduction

The channelization of wideband signals containing channels from different standards requires the use of non-uniform channelization techniques. The uniform channelization structures described in Chapter 3 represent efficient options when only one type of communication channel is considered. Unfortunately, they can not provide the capabilities that multi-standard SDR base stations require (see Chapter 2). However, these uniform channelization structures provide the basis for non-uniform channelization techniques which can achieve these multi-standard needs.

A number of non-uniform channelization techniques have been proposed that are mainly oriented to SDR devices [128, 161-165]. The different design methods and structures of these solutions can make it very difficult for a designer to determine which one is the most appropriate solution for a specific implementation. Some publications have tried to deal with this problem by evaluating a sub-set of these non-uniform channelization techniques [166-167]. Nevertheless, these evaluations do not provide a full vision of the capabilities of the non-uniform channelizers since in general they do not address the two main factors in multi-standard SDR base stations: DFSA flexibility and management of large number of channels.

In this chapter, non-uniform channelization issue is examined from the perspective of the multi-channel SDR base station presented in Chapter 2. Therefore, the non-uniform structure needs to be compliant with three different

requirements: a large number of channels in the received UL signal, support for simultaneous multi-standards and flexible channel allocation required for DFSA.

First, the key parameters to be considered for these structures are reviewed, followed by a description of the different methods. Secondly, the different methods are evaluated based on the SDR base station key points given previously: large number of channels, multi-standard and DFSA. Finally, the evaluation is completed by applying the different methods to a real world use case with the TETRA V&D and TEDS standards.

4.2 Evaluation metrics for non-uniform channelizers

In order to establish a basis for evaluation of the non-uniform channelizers, several key points or *metrics* which characterize the channelizer performance are considered. On one hand, some of these metrics depict the performance of the channelizer within the SDR wideband receiver system from Figure 2.7. In it, the channelizer is allocated at the end of the digital front-end right after the ADC and before the independent baseband processing of the independent channels. Therefore, the interaction of the channelizer with the ADC and later baseband processing is studied. On the other hand, the independent performance of the non-uniform channelizer is determined by factors like computational load, DSA flexibility or easy upgrade.

Therefore, the factors considered in the performance evaluation of a non-uniform channelizer are:

1. **Computational load:** The computational load of a channelizing structure is influenced by the previous points. It represents the main consideration when a design is intended to be implemented in a DSP device such as a CPU or FPGA. Even though the computational capacity of these programmable devices increases regularly, an efficient implementation is still desired since processing of a large number of channels can quickly become impractical.

2. **DFSA flexibility:** Probably the most desirable property of the base station channelization system is the capacity to filter and down-convert channels distributed over the shared frequency band using DFSA. Flexibility refers to the capacity of a non-uniform channelizer to tune its filters to any desired bandwidth at any centre frequency in the digitized spectrum band.

3. **Easy upgrade:** Multi-standard base stations might be designed to be compliant with a set of second, third and fourth generation communications standards, but in the future new communication system additions could be performed. Depending on the type of structure, future centre frequencies, bandwidths and filtering characteristics will require bigger or smaller changes in the channelizer structure.

4. **Reconfigurability:** Changes in the DFSA configuration in the channelizer input signal could require some level of reconfigurability in the channelizer. For example, filter re-design or paths cancellation. Preferably, reconfiguration processes which require significant computational load, such as filter designs and optimization, should be done in the offline mode before the channelizer starts operating.

5. **Previous sample rate conversion:** In the SDR receiver chain, at the digital front-end the wideband received signal is first digitized by the ADC and then passed to the channelizer as a baseband complex signal. Depending on the type of non-uniform channelizer, the input signal sample rate needs to be compliant with certain requirements. Therefore, integer or fractional SRC blocks could be necessary between the ADC and channelizer. Fractional SRC can be efficiently performed by fractional delay filters; however, this has the disadvantage that a large error is introduced in the higher frequency components [168].

6. **Baseband sample rate conversion:** Post-processing of the independent channels after the channelization typically covers SRC, equalization, time recovery and symbol demodulation [25]. In general, the function of this SRC module is to adapt the signal sample rate of every channelizer output

to provide an integer number of samples-per-symbol. This is a requirement for the processing of timing recovery and symbol demodulation operations. Therefore if the channelizer can provide appropriate sample rates for baseband processing then it can save the use of an SRC module in every channelizer output.

4.3 Non-uniform channelization methods

In the multirate signal processing literature, there can be found different non-uniform channelizers that try to deal with a multi-standard solution in the most efficient way in order to be applied to SDR technologies. This section intends to present a description of these structures and their applications by paying special attention to the points described in Section 4.2. As a result, a comparison can be established based on the benefits, drawbacks and constraints of the different methods.

The non-uniform channelizers covered here are based on the uniform channelization methods presented in Chapter 3. However, they are adapted to deal with a multi-standard input signal using DFSA. For example, the structure first presented in Section 4.3.1 is based on the per-approach described in Section 3.3. Secondly, the tree quadrature mirror filter bank is based on the efficient half-band filters introduced in Section 3.4.3. After these methods, non-uniform structures based on a more flexible version of the DFT-FB in Section 3.5.3.1 are presented. Finally, two other methods based on the FRM technique, Section 3.4.4, to implement efficient FIR filters are reviewed.

4.3.1 Farrow Per-Channel Channelizer (FPCC)

Traditionally, the channelization task has been performed in a per-channel approach using dedicated circuitry. As in Figure 3.4, in every branch a single channel is frequency shifted to DC and lowpass filtered before its sample rate is converted to an adequate value for the rest of the demodulating stages. These three operations are specifically designed for a channel centre frequency and bandwidth, therefore the processing of any other type of channels with different

centre frequency, bandwidth and/or requiring a different SRC is not possible, leading to a very inflexible structure.

In order to break the constraints imposed by the per-channel structure in Figure 3.4, a non-uniform per-branch channelizer has been proposed [165, 169-171]. By introducing adaptive rational SRC and filtering in every channelizer branch, in the form of Farrow-based filters, different types of channel can be down-converted using the same processing blocks. Consequently, the same processing branch can be employed to channelize different centre frequencies and bandwidths. If the non-uniform channelizer is required to be upgraded to support a new communication standard, only the coefficients of the Farrow filters have to be updated. In contrast, the per-channel structure in Figure 3.4 would require the implementation of new processing branches in parallel specifically designed for the new standard.

Farrow-filters were presented as a method to synthesize a fractional controllable delay or carry out an arbitrary sample rate conversion by using polynomial-based interpolation [172-173]. This is especially useful when applied to irrational SRC factors [174]. However, as with other fractional delay filtering methods, they introduce a distortion in the higher frequency components close to the Nyquist frequency [168]. A Farrow filter is formed internally by a set of linear phase sub-filters $S_P(z)$, which form a global transfer function equal to

$$\hat{H}(z,\tau)=\sum_{i=0}^{P}\tau^{i}S_{i}(z),\quad |\tau|\le 0.5 \tag{4.1}$$

where τ represents the fractional delay value necessary for the rational SRC and P is the polynomial order. Figure 4.1a shows the structure of a Farrow filter. When the sub-filters $S_P(z)$ are linear phase FIR filters, the Farrow filter is commonly referred as *modified* Farrow filter [175]. More concretely, a type of modified Farrow structure, known as *transposed* Farrow structure, is generally preferred to be used on the receiver side since it offers better aliasing component attenuation when decimation is performed [176]. The structure for the modified and transposed Farrow is the same as in Figure 4.1a, the only difference between

them is that the calculation of the fractional delay values (τ) changes. For the transposed Farrow filter the values of τ are given by

$$\left[n_{in}+\tau(n_{in})\right]T_{in} = n_{out}T_{out} \Leftrightarrow \tau(n_{in}) = n_{out}\frac{T_{in}}{T_{out}} - n_{in} \tag{4.2}$$

where n_{in} and n_{out} are the input/output sample index, B/A is the rational SRC factor and $T_{out} = T_{in}\dfrac{B}{A}$

For modified and transposed Farrow filters, a relationship can be established between the Farrow structure sub-filters and the polyphase components of an FIR filter [176]. A Farrow filter is equivalent to the FIR filter which performs the bandwidth filtering operations in a rational SRC with factor A/B of Figure 4.1b. The FIR filter $H_F(z)$ is considered to be formed by a number B of polyphase components, $G_b(z)$, as

$$H_F(z) = \sum_{b=0}^{B-1} z^{-b} G_b(z^B) \tag{4.3}$$

$$G_b(z) = \sum_{n=0}^{N_P} g_b(n) z^{nB} \tag{4.4}$$

where N_P is the order of every polyphase component.

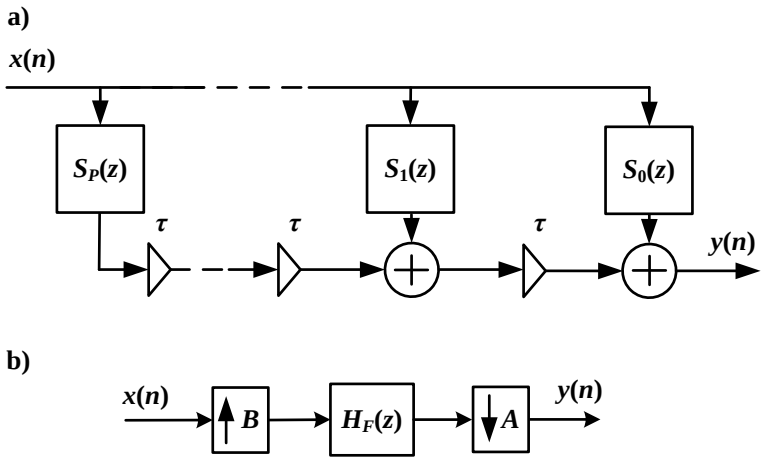

Figure 4.1 Farrow filter structure. a) Implementation using sub-filters. b) Equivalent FIR filter model.

The relationship between the polyphase components of the FIR filter, $G_b(z)$, and the Farrow sub-filters, $S_p(z)$, is given by the matrix

$$\begin{bmatrix} s_0 \\ s_1 \\ \vdots \\ s_P \end{bmatrix} = \begin{bmatrix} g_0 \\ g_1 \\ \vdots \\ g_{B-1} \end{bmatrix} \begin{bmatrix} 1 & (2\tau_0 - 1) & \cdots & (2\tau_0 - 1)^P \\ 1 & (2\tau_1 - 1) & \cdots & (2\tau_1 - 1)^P \\ \vdots & \vdots & \cdots & \vdots \\ 1 & (2\tau_{B-1} - 1) & \cdots & (2\tau_{B-1} - 1)^P \end{bmatrix}^{-1} \tag{4.5}$$

where $\mathbf{s_p}$ represent row vectors with the Farrow sub-filters, and $\mathbf{g_b}$ are row vectors with the FIR polyphase filter components.

Therefore, a modified or transposed Farrow filter can be designed from a linear phase FIR polyphase filter. The difference is that the Farrow filter is formed by $P+1$ sub-filters of order N_P , in contrast with the equivalent FIR filter which is formed by B polyphase component of order N_p. In general, the number of sub-filters is smaller than the interpolation factor B, therefore the Farrow filter requires less coefficients than its equivalent FIR filter. In addition, the SRC factor A/B and filter bandwidth can be varied with just changing the values of τ without altering the filter coefficients.

In Figure 4.2 the equivalent receiver for the two non-uniform channelizers using Farrow filters are depicted using the equivalent FIR filter models [165, 169-171]. In both non-uniform channelizers of Figure 4.2, a set of J different communication standards is supported. Therefore, the Farrow filter of each one of the K branches forming the channelizer can adopt J different configurations. This means, different values of the SRC factors A and B as

$$\hat{A}_k, \hat{B}_k \in (A_1, B_1, A_2, B_2, ..., A_J, B_J) \quad \text{for } k = 0,1,...,K-1 \tag{4.6}$$

In the non-uniform channelizer of Figure 4.2a, known as a *multimode channelizer* in the original literature, each of the K branches in the receiver is designed to extract each of the input signal channels by down-converting using a variable frequency mixer, and filtering using the Farrow filter. Each Farrow filter is formed by the filter $H_F(z)$ and the variable rational SRC given by (4.6). As a consequence, any branch can extract from the multi-channel input signal

any of the J types of channel. The Farrow filter is followed by a fixed integer decimation factor D_F common to all the branches. This option is beneficial when the number of channels is large (and consequently the required decimation factor A_j / B_j) since it allows the fractional decimation factor given by the Farrow filter to remain small. However, it increases the implementation size since one more filter operation is added per branch. In Figure 4.2b, known as *Farrow based multimode channelizer*, the fixed filter decimation formed by the filter $F(z)$ and the downsampler D_F is removed. Therefore, the Farrow filter is responsible for the complete SRC in each of the branches. This reduces the system complexity but can increase the number of operations per second performed by the Farrow filter depending on the necessary values of A_j and B_j.

Since any branch can channelize any of the J different information channel types, the total number of branches in parallel is chosen based on the prediction of the maximum number of channels that would need to be simultaneously channelized. This generally matches the scenario where the whole frequency band is occupied by channels of the standard with the smallest bandwidth.

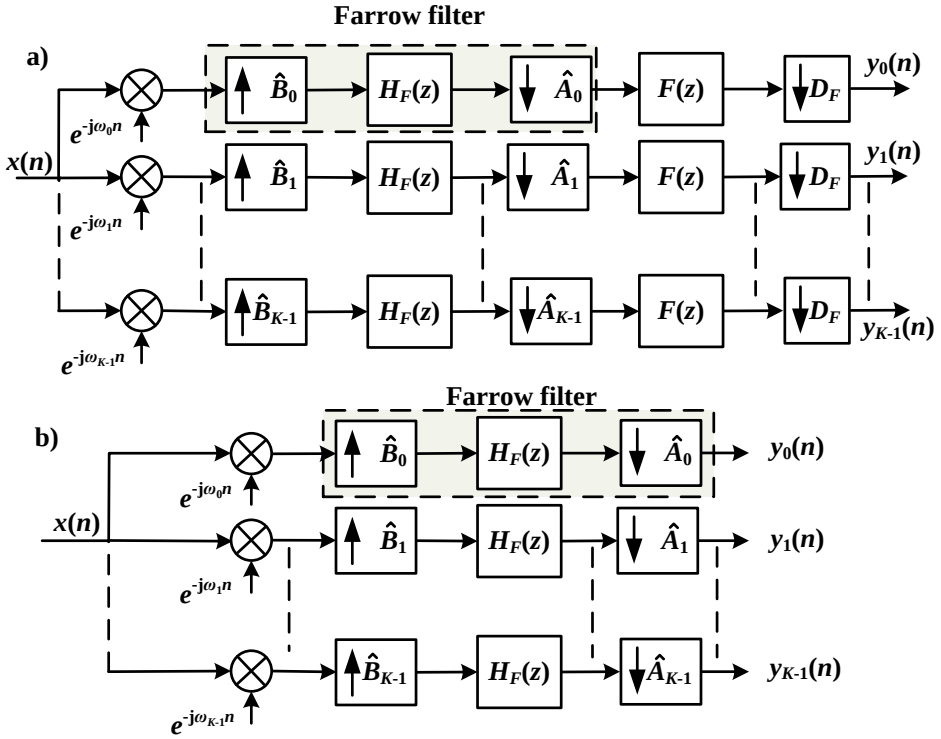

Figure 4.2 Non-uniform equivalent models of a channelizer using Farrow structures a) with only adaptive fractional decimation, b) with adaptive fractional decimation followed by fixed integer decimation.

For both multimode channelizers, the SRC factors are chosen according to the required output sampling periods of the different type of channels, T_j, where it is needed to satisfy

$$T_0 \frac{A_0}{B_0} = T_1 \frac{A_1}{B_1} = \ldots = T_{J-1} \frac{A_{J-1}}{B_{J-1}} = T_S \tag{4.7}$$

for the case in Figure 4.2b where T_S is the input sampling period. For the case in Figure 4.2a

$$T_0 \frac{A_0}{B_0} = T_1 \frac{A_1}{B_1} = \ldots = T_{J-1} \frac{A_{J-1}}{B_{J-1}} = T_S D_F \tag{4.8}$$

In most situations, the different values of A_j/B_j will be rational, that is the main reason why the Farrow-filter is necessary. Due to the flexibility provided by the values of A_j and B_j, a wide range of SRC between input and output sample rate can be carried out. This can eliminate the necessity for SRC modules before and after the channelizer. However, due to the oversampling usually applied by the ADC to the digital signal, a prior decimation of the signal is recommended to reduce the number of operations per second. Then the value of A_j/B_j can be adapted to obtain directly an integer number of samples per symbol at the outputs and avoiding the SRC before the baseband processing of every channel.

Changes in the DFSA configuration of the multi-channel input signal will require some reconfigurability of the multimode transmultiplexers to adapt themselves to the new down-conversion and filtering requirements. For both multimode transmultiplexer in Figure 4.1, the reconfiguration process starts by the selection of the total necessary number of branches. Following, for each branch, the frequency mixers are tuned to the desired channel centred frequency and the rational SRC factor of the Farrow filter chosen from (4.6). Finally, the set of values for the fractional delay τ need to be loaded into the Farrow filter for the specific A/B sample rate factor according to (4.2). These values do not need to be recalculated every time the SRC factor is changed, they can be stored in a look-up table and loaded when needed. In addition, the coefficients of the Farrow sub-filters $S_p(z)$ do not require any action.

If the channelizers need to be upgraded to support a new standard, the Farrow based multimode channelizer in Figure 4.2b requires two actions. First, the update of the SRC factors set in (4.6) with a new value which is compliant with (4.7). Second, the calculation of the fractional delay values for the new SRC factor according to (4.2). For the multimode channelizer in Figure 4.2a, apart from the actions already mentioned for the Farrow based multimode channelizer, it requires the re-design of the low-pass decimation filter $F(z)$.

From the scalability and computational load point of view, its implementation is highly constrained by the number of channels that will be handled. As in the uniform per-channel channelizer in Chapter 3, the multimode channelizers do not share any computational load among the different branches. Therefore, the computational load grows linearly with the number of channels. In addition, the bigger the number of channels, the higher the sampling rate of the channelizer input signal will be after the ADC and SRC. This will increase the sample rate that the frequency mixers and Farrow filters work at.

4.3.2 Tree Quadrature Mirror Filter Bank (TQMFB)

As for the uniform channelizers, apart from the per-channel approach, filter banks represent the main alternative to non-uniform channelization. Also, again the main difference between them is that the filter bank's part of the signal processing load is shared by all the channels instead of being independently carried out by every branch. As a consequence, this usually means a reduction in the number of operations, but a more limited flexibility due to required similarities between channels. Non-uniform filter banks have had special importance in the digital speech processing field where the spectral bands with different bandwidth need to be subtracted and processed. The wavelet transform has historically been one of the methods to carry out this digital speech processing [107, 177]. Its implementation is based on the use in cascade of Quadrature Mirror Filter Banks (QMFB).

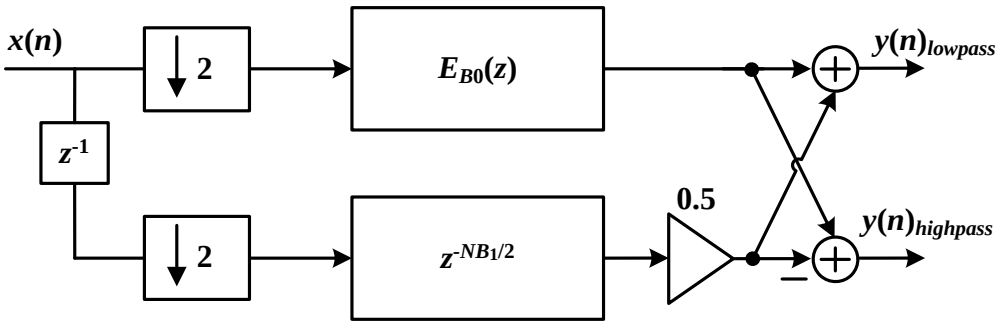

Figure 4.3 Efficient QMFB implementation.

A QMFB is composed by a complementary lowpass and highpass half-band filter [107]. Lowpass half-band filters were reviewed in Chapter 3 as an efficient multirate filter implementation when a factor-of-2 upsampling or downsampling is required. Like the lowpass version, highpass half-band filters have a symmetric impulse response and their odd coefficients, with the exception of the one placed on $n = 0$, are zero. In the frequency domain, they have the same symmetric transition band centred on $\pi/2$ as the lowpass filter. This fact means that the lowpass and highpass filters are magnitude complementary [112]. Due to the complementary characteristic between both filters, the highpass filter can be derived from the lowpass one as

$$H_{B,HP}(z) = H_{B,LP}(-z) \tag{4.9}$$

Consequently, both lowpass and highpass half-band filters share the same polyphase components

$$H_{B,LP} = E_0(z^2) + z^{-1}E_1(z^2) \tag{4.10}$$

$$H_{B,HP}(z) = E_0(z^2) - z^{-1}E_1(z^2) \tag{4.11}$$

From the efficient polyphase half-band decimation structure in Figure 3.9, the implementation of the QMFB is shown in Figure 4.3.

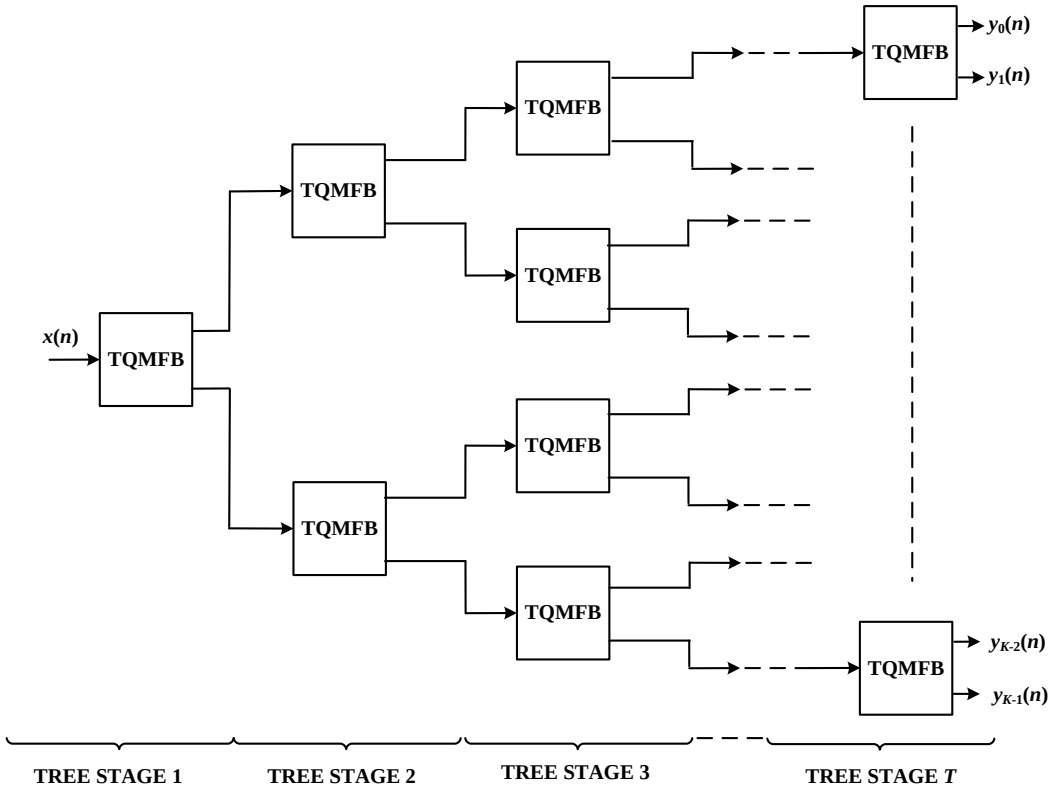

Figure 4.4 TQMFB channelizer.

Like in the wavelet transform, non-uniform channelizers which employ several QMFBs connected in cascade. More specifically, they use tree structures where every node of the tree is formed by a QMFB as in Figure 4.4, generally denoted as tree QMFB (TQMFB) [107, 162, 164, 178-179]. At the non-uniform TQMFB channelizer, the single wide band signal is split into two sub-bands, each of which is decimated. Subsequently, each sub-band is again split into two and decimated. In this way a progressive bandwidth and data rate halving is achieved in every branch of the tree. All the branches of the tree that are allocated in the same stage (considering that the TQMFB is formed by T stages as in Figure 4.4) will have the same bandwidth and the same sample rate. Depending on what channel bandwidth and sample rate are intended to be extracted, they will be extracted of a certain stage of the tree.

Despite their simplicity and easy scalability, TQMFBs have limitations to their functionality. In a TQMFB there is a dependency between the channel spacing obtained at every tree stage and the sample rate of the input signal. These channel spacings are equal to half the sample rate that the filters work at and

they are related to each other depending on the stage by a power-of-two. For example, let the sampling frequency of the input wide band signal at the receiver be f_S, and f_{CS1}, f_{CS2} and f_{CS3} represent the channel spacing at stages 1, 2 and 3 respectively. Employing the proposed architecture, f_{CS1}, f_{CS2} and f_{CS3} are obtained as

$$f_{CSt} = f_S / 2^t, \quad \text{for } t = 1, 2, 3 \tag{4.12}$$

where t represents the stage from which the outputs are being taken. For example, the TETRA V&D standard requires the channel spacing to be equal to 25 kHz. If an input signal containing 256 TETRA V&D channels is fed to the channelizer input, according to (4.12), the sampling frequency of this multi-channel signal would need to be equal to 6.4 MHz and the number of stages $t = 8$. For the rest of the intermediate stages ($t = 1, 2, \ldots, 7$) the channel spacings obtained would be power of two multiples of 25 kHz. Due to this constraint, the TQMFB is only suitable for multi-standard applications where channel spacings are a power-of-two multiple of each other. As a direct consequence, the same power-of-two limitation applies to the bandwidths of the different channels.

According to (4.12), the sample rate of the input channelizer signal delivered by the ADC has to be adapted according to the required channel spacings. This means that the SRC between the ADC and the channelizer is necessary. Similarly, the channelizer outputs have a sample rate equal to the channel spacing of the stage at which they are extracted. This means that another SRC per outputs is generally required unless the channel spacing matches a valid sample rate for the baseband processing.

Depending on the DFSA configuration in the input signal, the TQMFB reconfiguration is based on the extraction of the channels of each standard from the correct outputs of the correct tree stage. Since the whole set of braches in each stage is used, some branches of the tree can be eliminated to save their part of the computation. If the TQMFB is upgraded to support a new standard, the TQMFB does not need to be modified unless the channel spacing of the new standard is smaller or bigger than any of the standards already supported. In that

case, extra stages would need to be added at the end or the beginning of the TQMFB respectively. Due to the lowpass-highpass relationship of the filters in each QMFB, the TQMFB employs an even-stacked channel allocation as the DFT-FB in Figure 3.16.

The computational load and system delay of the TQMFB is proportional to the number of stages. The reduction of the computing overhead generated by a large number of stages has been proposed by generating a Hybrid TQMFB (HTQMFB) structure that combines the TQMFB with a uniform DFT-FB [180]. In the HTQMFB, as shown in Figure 4.5, the main idea is to divide the channelization structure into a uniform channelization front-end and a non-uniform channelization back-end. The front-end is formed by a uniform DFT analysis bank that splits the wideband input signal into a number of uniform sub-bands. After this, each one of the sub-bands is non-uniformly decomposed by a TQMFB back-end in order to recover all the individual channels.

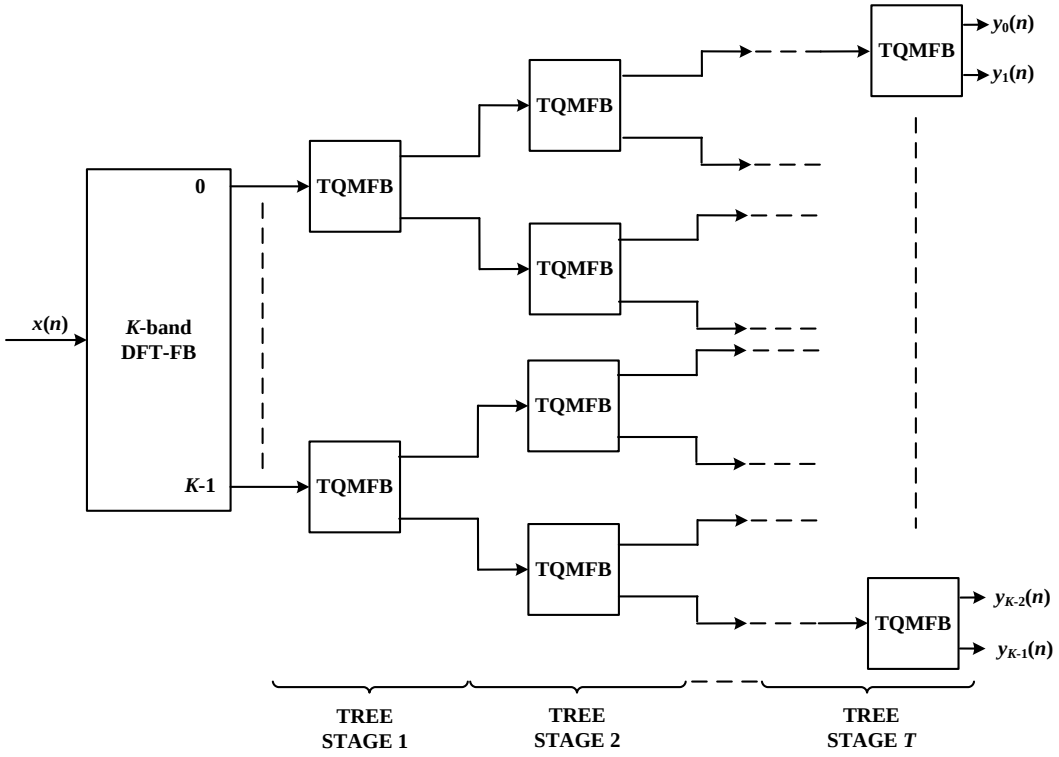

Figure 4.5 Hybrid TQMFB channelizer structure.

Other research works have focused on overcoming the power-of-two constraint related to the fixed channel spacings obtained in each of the stages of the TQMFB [167, 181-183]. Even though more flexibility is achieved, the new channel spacing capabilities are also very tied to the specific DFSA configuration and in general they imply an increase in the computational load and complexity of the channelizer.

4.3.3 Parallel Generalized DFT-FB (P-GDFT)

Within the non-uniform channelizers based on filter banks, like the QMFB, some of them take advantage of the low complexity and high efficiency of uniform modulated filter banks. Uniform modulated filter banks were introduced in Chapter 3 as a efficient solution to real world multicarrier communications such as OFDM or VDSL [96, 98]. Generally, in wireless digital communications, baseband signal processing is carried out using complex valued signals. For this reason, complex modulated filter banks such as DFT-FB or EMFB are employed. Between them, DFT-FBs were shown in Section 3.6 to require a smaller number of operations in comparison with EMFB.

Both types DFT-FB and EMFB can be obtained from a more general uniform modulated filter bank known as Generalized DFT-FB (GDFT-FB) [97]. For some applications, GDFT-FBs are preferred to DFT-FBs since they allow more flexible channel stacking and extra phase shifts that could be useful for certain applications. GDFT-FBs support even and odd channel stacking (as shown in Figure 4.6) whereas DFT-FBs only support even stacking.

Similar to DFT-FBs, GDFT-FBs implement different bandpass filters $H_k(z)$ obtained by the GDFT modulation of the lowpass prototype filter $H(z)$. This modulation can be expressed as

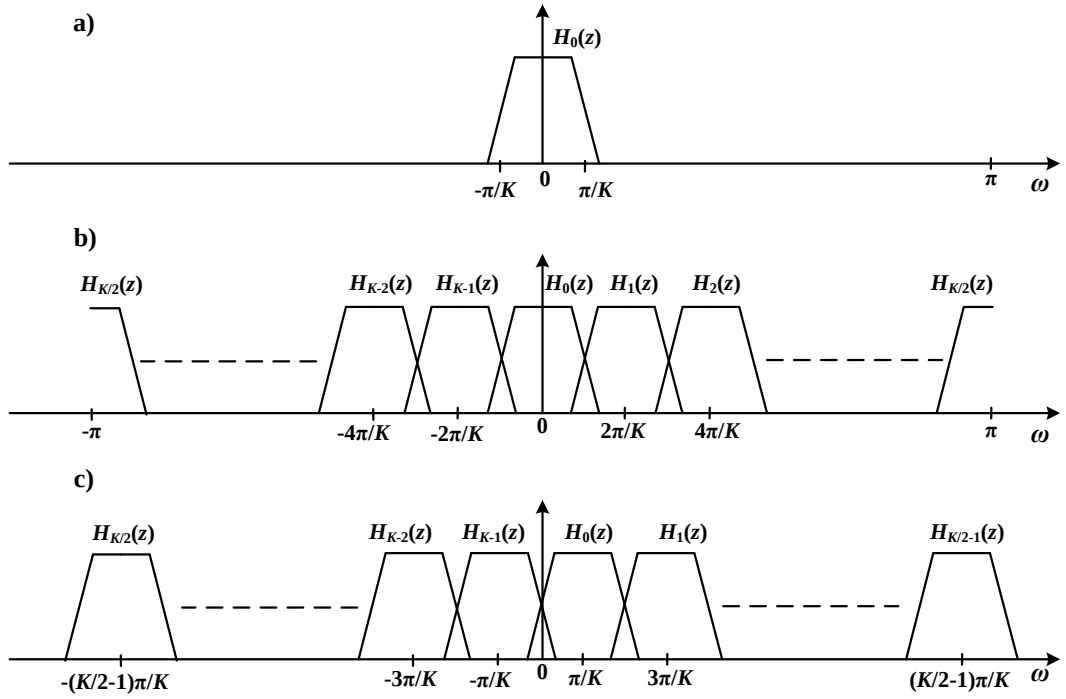

Figure 4.6 GDFT-FB a) prototype filter, b) even-stacked sub-band allocation similar to DFT-FB, c) odd-stacked sub-band allocation.

$$H_k(z) = W_K^{-(k+k_0)n_0} H(zW_K^{(k+k_0)}) \tag{4.13}$$

where K represents the number of channels of the analysis bank and $W_K = e^{j\frac{2\pi}{K}}$. The parameters k_0 and n_0 determine respectively the way the sub-bands get stacked in the spectrum and their phase. If k_0=0 and n_0=0 the channel spectrum allocation is characterised as *even-stacked* where the first channel is centred at DC (Figure 4.6b). In this case the GDFT-FB structure simply reduces to the classic DFT-FB. In contrast, if k_0=1/2 an *odd-stacked* configuration is achieved where no channels are centred at DC. Instead, all channels are shifted a distance equal to half of the channel spacing (Figure 4.6c).

In both even and odd stacked cases, the channel spacing is equal to

$$\omega_{CS} = \frac{2\pi}{K} \text{ rad} \tag{4.14}$$

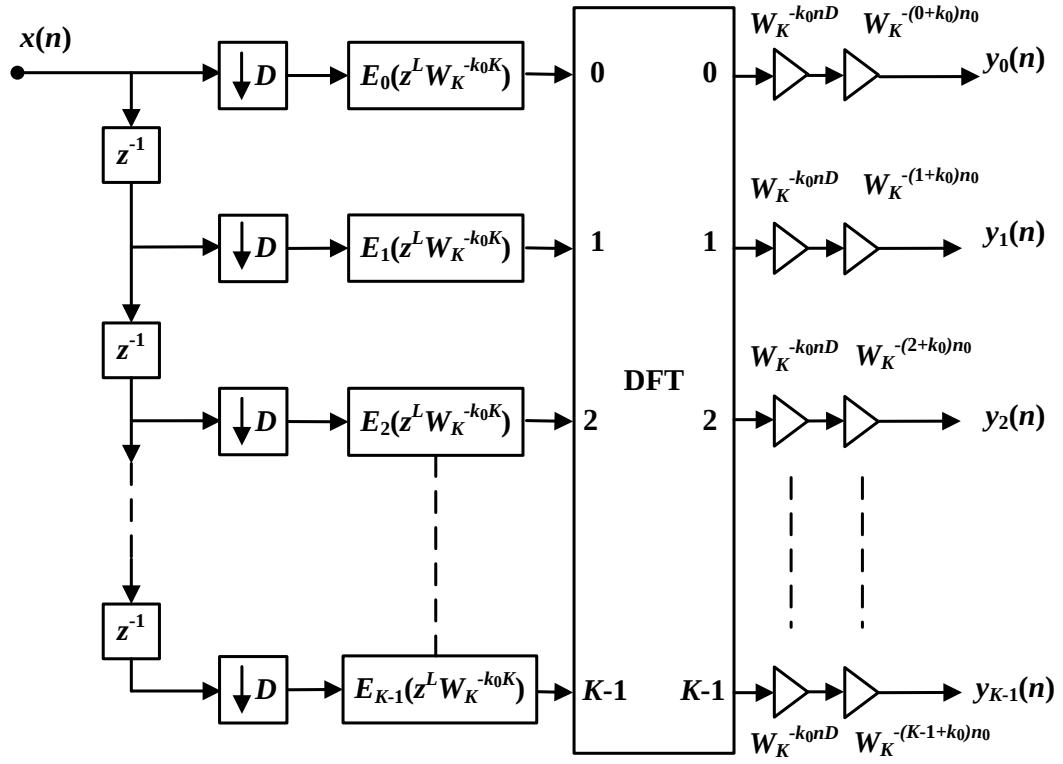

Figure 4.7 Generalized DFT analysis bank.

Due to the application of the noble identities to the K^{th} filter polyphase components, like for DFT-FBs in Section 3.5.3.1, a decimation factor D can be applied prior to the filtering operation to reduce the number of operations. As with other modulated filter banks, the GDFT-FB can take advantage of the prototype filter polyphase decomposition and noble identities [107] to form the efficient implementation depicted in Figure 4.7. In this implementation,

$$H(z) = \sum_{p=0}^{K-1} z^{-p} E_p(z^K) \tag{4.15}$$

$$H_k(z) = W_K^{-(k+k_0)n_0} \sum_{p=0}^{K-1} z^{-i} W_K^{-kp} W_K^{-k_0 p} E_p(z^K \cdot W_K^{-k_0 K}) \tag{4.16}$$

The complex exponentials $W_K^{-k_0 K}$ and $W_K^{-k_0 p}$ can be directly hard coded into the polyphase components of the filter bank, while W_K^{-kp} represents the DFT algorithm. Additionally, after the DFT, a factor $W_K^{-k_0 nD}$ needs to be applied in

order to shift the outputs $y_k(n)$ to DC. Finally $W_K^{-(k+k_0)n_0}$ is applied to the outputs for phase correction purposes in case that $n_0 \neq 0$.

Depending on the value of the decimation factor D, the filter bank can be classified as critically decimated ($K=D$) or oversampled ($K=L_{DFT}D$) where L_{DFT} represents the *oversampling factor*. The benefits of oversampled filter banks in terms of reduced aliasing were presented in Section 3.5.2. The cost of an oversampled filter bank is the additional computational load resulting from the filter bank running at a sample rate which is a factor L_{DFT} higher [128, 184-185].

From the computational load of the critically decimated even-stacked DFT-FB, (3.48) and (3.49), the computational load of a GDFT-FB can be expressed as

$$\mu_{GDFT-FB,EVEN} = \frac{L_{DFT}}{K}\left[2\left(N+1\right)+\frac{3K}{2}\left(\log_2\left(K\right)-5\right)+8\right] \tag{4.17}$$

$$\alpha_{GDFT-FB,EVEN} = \frac{L_{DFT}}{K}\left[2\left(N+1-K\right)+\frac{7K}{2}\left(\log_2\left(K\right)-5\right)+8\right] \tag{4.18}$$

for the even-stacked case, and

$$\mu_{GDFT-FB,ODD} = \frac{L_{DFT}}{K}\left[4\left(N+1\right)+\frac{3K}{2}\left(\log_2\left(K\right)-5\right)+8+4K\right] \tag{4.19}$$

$$\alpha_{GDFT-FB,ODD} = \frac{L_{DFT}}{K}\left[4\left(N+1-\frac{K}{2}\right)+\frac{7K}{2}\left(\log_2\left(K\right)-5\right)+8+2K\right] \tag{4.20}$$

for the odd-stacked case, where K is the number of sub-bands and N is the prototype filter order. In all the expressions, the first element corresponds to the polyphase FIR prototype filter and the second to the FFT Radix-2 algorithm (Table 3.3).

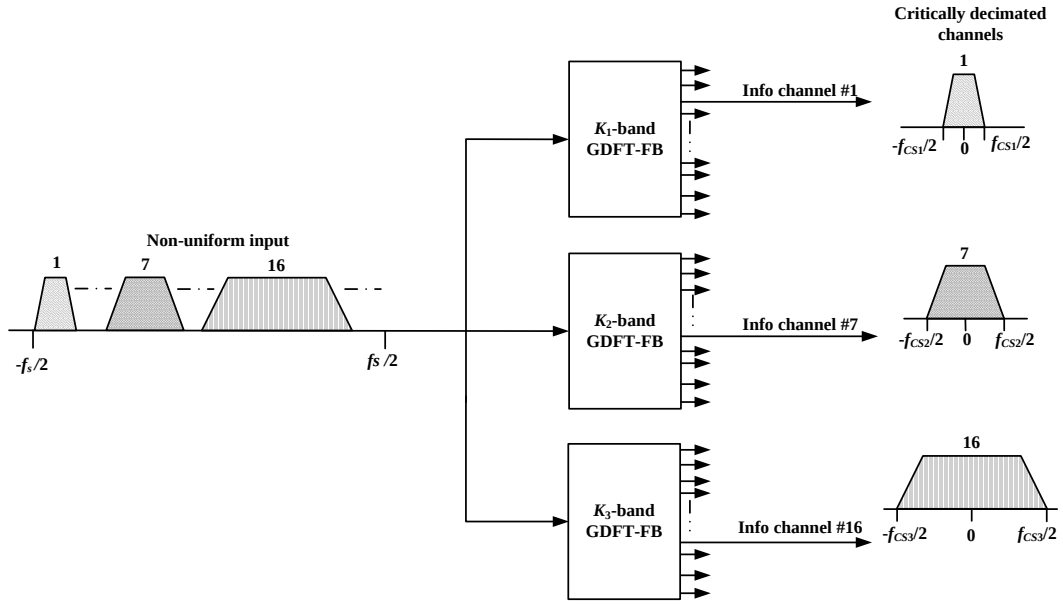

Figure 4.8 P-GDFT channelization structure.

To achieve DFSA, the parallel GDFT-FB (P-GDFT) was proposed in [186] as a non-uniform channelizer for base stations, shown in Figure 4.8. The channelizer processes the wideband signal through a number of different critically decimated odd-stacked GDFT-FBs operating in parallel. Here each filter bank implements a uniform division of the frequency band for a specific channel spacing and all filter banks overlap in frequency. They all receive a common input signal from the ADC and intermediate SRC. To achieve the correct channel spacing in all parallel GDFT-FBs, in compliance with (4.14), the common input signal sample rate must meet

$$f_S = K_j f_{CSj}, \quad j = 1, 2, ..., J \tag{4.21}$$

where J is the number of standards supported, and K_j and f_{CSj} are the number of sub-bands and the channel spacing in each GDFT-FB respectively. In case (4.21) can not be met by all J standards, alternatively independent SRC could be applied before the required GDFT-FBs.

The digitized wideband signal with a sample rate of f_S, is fed into J parallel filter banks. Narrow band channels are extracted by selecting appropriate outputs from each of the filter banks. Any legal combination of channels can be specified by choosing the appropriate filter banks and channel numbers.

Changes in the input signal DFSA configuration do not require redesign or re-optimization of the channelizer structure. Only the choice of the GDFT-FBs outputs needs to be adapted. In the case of an upgrade that introduces a new standard, a new GDFT-FB may need to be designed and introduced in parallel with the rest if its channel spacing specifications are not met by any of the existing ones.

Because every GDFT-FB is applied independently, the decision to design each one as critically decimated or oversampled is based only on the filtering necessities of the corresponding standard. If the filtering requirements are met, a critically decimated option is preferred because it has a smaller number of operations per second. For a critically decimated GDFT-FB, the output sample rate is equal to the channel spacing given by (4.21). These output sample rates may not match the required symbol rate for a given standard, so an intermediate SRC between each channelizer output and the independent baseband channel processing would be required.

Although the P-GDFT structure is simple to implement and offers flexible reconfiguration it can have a high ratio of unused sub-band outputs depending on the input signal DFSA configuration. Since all the sub-bands in each GDFT-FB share the overall input signal computation, the processing of these null sub-bands can not be avoided, thus the computational load remains constant no matter what the channel allocation is.

4.3.4 Recombined GDFT-FB (R-GDFT)

Non-uniform channelization using recombined oversampled filter banks, R-GDFTs among them, have been proposed in [128, 161, 187-189]. The essential idea of an R-GDFT non-uniform channelizer is to first analyse a signal into uniformly spaced narrow sub-bands and then recombine groups of adjacent sub-bands to form wider bandwidth sub-bands. In contrast with the P-GDFT, the necessity to recombine some of the adjacent GDFT-FB sub-bands requires the minimization of the aliasing effects. Therefore, oversampling GDFT-FB designs are chosen for the R-GDFT.

The bandwidth of each of the uniformly spaced GDFT-FB sub-bands is known as the *granularity band*. Depending on the design criteria, this granularity band can be chosen as the bandwidth occupied by the minimum guard band required [128], the bandwidth of the narrowest type of channel [185], or some trade-off in between [190]. This decision, together with the total bandwidth covered by the input signal, will determine number of sub-bands of the GDFT-FB and its complexity. In particular, if the granularity band is chosen to match a narrow guard band and the channelizer receives a signal with a large bandwidth, the size of the filter bank can become impractical to implement. However, the size of the granularity band with respect to the total bandwidth also determines the centre frequency freedom for channel down-conversion. The larger the number of granularity bands, the greater the flexibility in choosing different centre frequencies for the channel filters.

If an odd-stacked GDFT-FB channel configuration is considered, the possible channel centre frequencies are given by

$$\left.\begin{array}{l} \omega_{CH} = \dfrac{2\pi R}{K}\left(n+\dfrac{1}{2}\right), \quad \text{for } R \text{ odd} \\ \omega_{CH} = \dfrac{2\pi R}{K} n, \quad \text{for } R \text{ even} \end{array}\right\} \; n = 0,1,2,...,K-1 \tag{4.22}$$

In (4.22) K represents the number of sub-bands that the frequency band is divided into and R is the number of sub-bands necessary to recombine a specific type of narrowband channel (Figure 4.9). The recombined channels can be allocated at any normalized centre frequency defined by (4.22) as long as all the sub-bands to be recombined are available. Unlike the P-GDFT where each type of channel can only be centred at a multiple of its channel spacing, the centre frequency freedom increases in the R-GDFT case. If the granularity band bandwidth is a fraction of the channel spacing or a particular type of channel, the constrained of centre frequencies at multiples of the channel spacing does not apply anymore. In compliance with (4.22), the smaller the granularity band the larger the number of sub-bands K, and therefore the wider the centre frequencies possibilities.

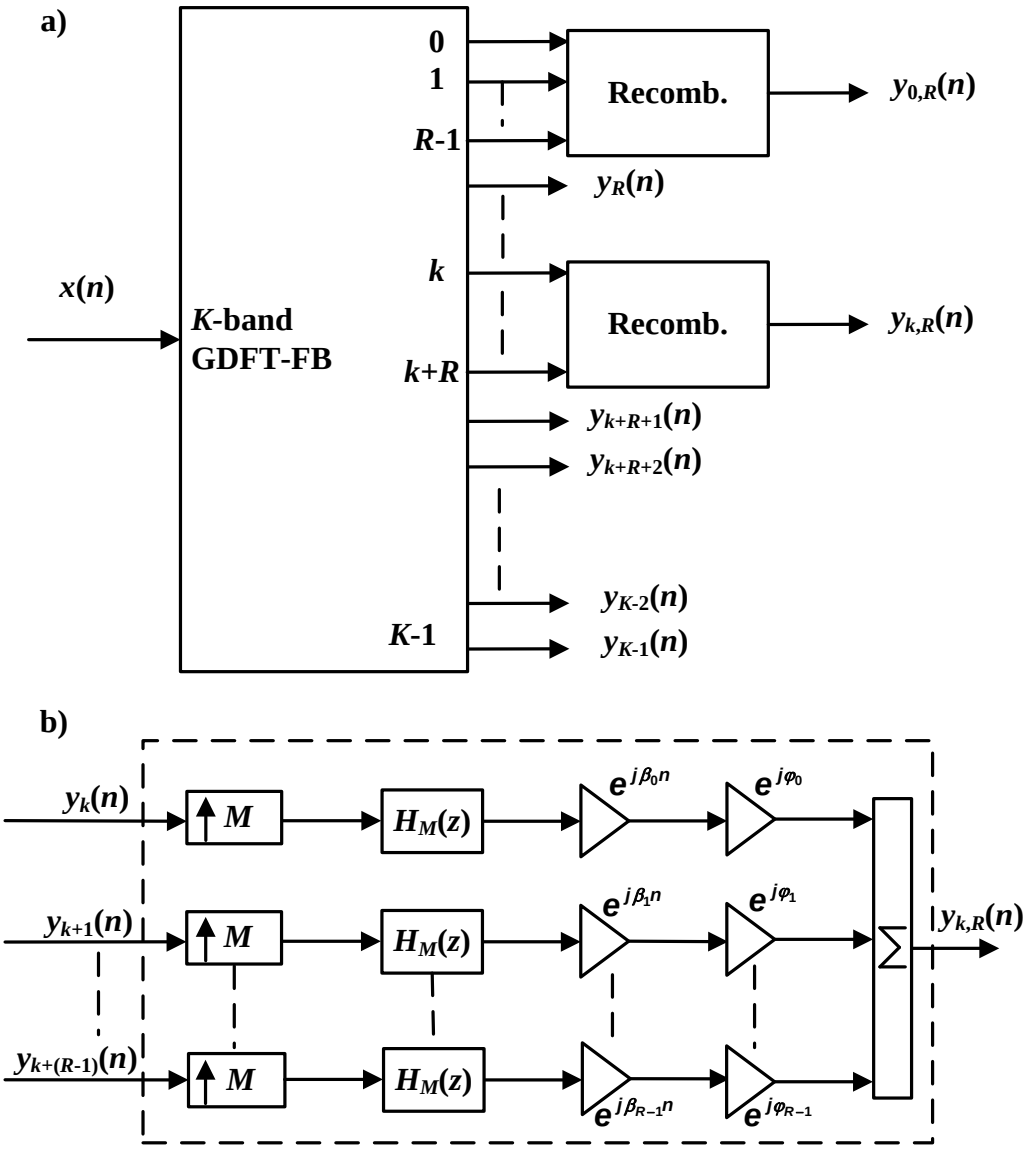

Figure 4.9 R-GDFT channelizer a) structure, b) detail on the recombination structure.

The reconfiguration required when the input signal DFSA varies involves only the reallocation of the recombination structures. To support new standards, the GDFT-FB remains the same unless the new standard channels require a smaller granularity band or a wider range of centre frequencies. In this case, the GDFT-FB and recombination structures have to be updated. Otherwise, only a new recombination structure needs to be introduced by adapting the interpolators and frequency mixers to the new requirements.

Recombination is carried out by the structure shown in Figure 4.9b. Every recombined signal denoted by $y_{k,R}(n)$ is formed by R adjacent sub-bands allocated from the k^{th} output of the GDFT-FB onwards as

$$Y_{k,R}(z) = \sum_{r=0}^{R-1} e^{j\varphi_r} Y_{k+r}(z^M) H_M(ze^{-j\beta_r}) \tag{4.23}$$

Therefore, recombination is achieved by interpolating each of the R sub-bands by a factor M, frequency shifting by β_r to the correct centre frequency, and phase correction φ_r in order to finally add these shifted in-phase channels together. In addition, to keep the frequency response passband ripple within the filtering specifications limits and minimize amplitude distortion of the recombined channels, a magnitude complementary prototype filter is required [114]. Depending on the type of communication standard, a certain degree of non-linearity in the phase response and non-flatness in the passband of the recombined channels could be accepted. Consequently, the perfect in-phase sub-band addition and magnitude complementary conditions could be relaxed or suppressed.

Since the GDFT-FB outputs are already oversampled by a factor L_{DFT}, the interpolation factor can be chosen as

$$M \le R/L_{DFT} \tag{4.24}$$

For $M=R/L_{DFT}$, the frequency and phase shifts are obtained respectively as

$$\beta_r = \pi + \frac{\pi}{R}(2r+1) \quad \text{for } r = 0,...,R-1 \tag{4.25}$$

$$\varphi_r = -(\frac{MN}{2D} + \frac{N_M}{2})\beta_r \quad \text{for } r = 0,...,R-1 \tag{4.26}$$

Another difference with the P-GDFT is that the R-GDFT computational load changes according to the number of channels that need to be recombined and the number of sub-bands required for each one. The recombination part can be done

using different methods from simple upsamplers, mixers and adders [185, 191] to synthesis filter banks [128, 190]. The method used in Figure 4.9b has the advantage that the interpolation factor *M* can be replaced with a rational value and provide an output sample rate at a multiple of the symbol rate.

4.3.5 FRM based non-uniform channelizers

FRM was presented in Chapter 3 as another multirate solution to implement efficient filter structures. In addition, two non-uniform channelizers based on FRM have also been proposed as FRM-based Filter Banks (FRM-FB) [192-194] and the Coefficient Decimation-based Filter Banks (CDFB) [163, 195].

Figure 3.10a showed how the FRM structure is formed by four different filters: one base filter, one complementary filter and two masking filters. However, the relationship between the base and complementary filters allow a design where only the base filter and the masking filters are required (Figure 3.10b). Depending if the entire FRM structure was used, full FRM, or just its positive branch, narrowband FRM, the different steps to achieve the required filter frequency response were depicted in Figure 3.11.

In a FRM-FB (Figure 4.10), the base and complementary filters are designed so that their images provide the required passband and transition band specifications. After their interpolation by a factor *L*, the frequency responses formed by the lowpass filter and the bandpass images are obtained as shown before in Figure 3.11. Then a real lowpass filter, a real highpass filter, and *L*-2 complex bandpass filters have to be designed to filter all the individual channels. For the FRM-FB, the interpolation factor is chosen as

$$L = \frac{K}{2} \tag{4.27}$$

where *K* is the maximum number of channels of that might be allocated in the frequency band. This configuration allows channelizing input signals where the channel spacing is equal to

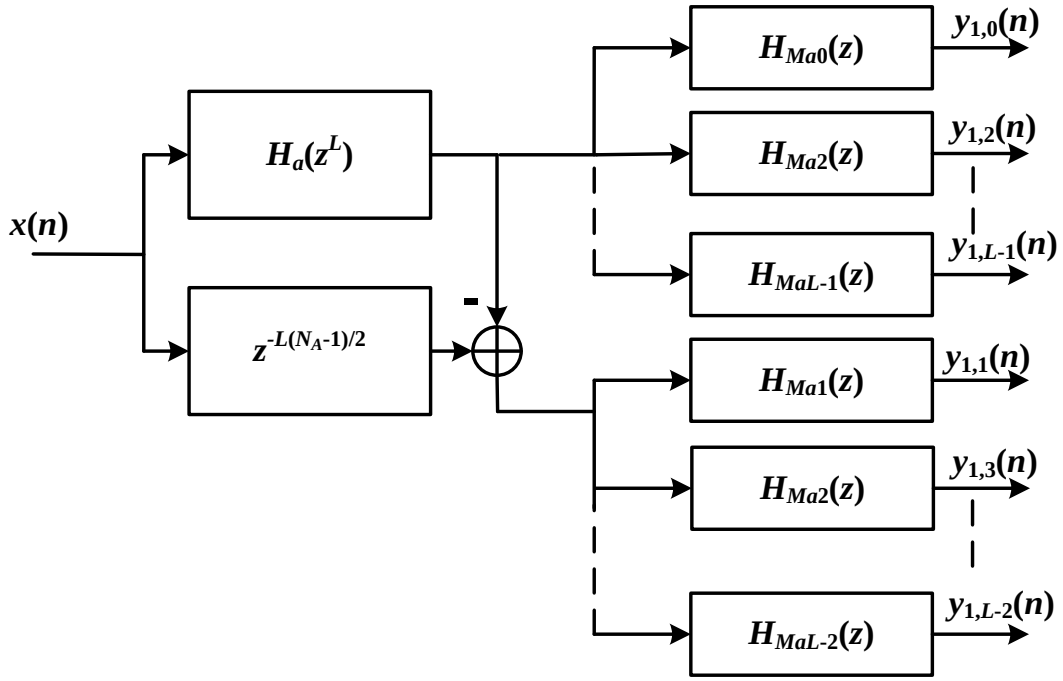

Figure 4.10 FRM-FB structure.

$$f_{CS} = \frac{2\pi}{K} \tag{4.28}$$

Also, although not shown in Figure 4.10, a set of complex mixers are necessary afterwards to centre each channel at baseband.

For FRM-FB, the multi-standard (or non-uniform channelization) implementation relies on the idea of using the same base filter coefficients but with different interpolation factors (*L)* to create the necessary frequency responses for the different *J* standards. Considering that there are *J* different passband and stopband filtering specifications to be met using the same base filter but different interpolation factors, it is necessary to achieve the following identities

$$\omega_{p1}L_1 - \lfloor \omega_{p1}L_1 \rfloor = \omega_{p2}L_2 - \lfloor \omega_{p2}L_2 \rfloor = \ldots = \omega_{pJ}L_J - \lfloor \omega_{pJ}L_J \rfloor \tag{4.29}$$

$$\omega_{s1}L_1 - \lfloor \omega_{s1}L_1 \rfloor = \omega_{s2}L_2 - \lfloor \omega_{s2}L_2 \rfloor = \ldots = \omega_{sJ}L_J - \lfloor \omega_{sJ}L_J \rfloor \tag{4.30}$$

These requirements represent the first difficulty for this method, since for values of $J > 2$, it is difficult to find values of L that satisfy the expressions unless the

necessary passband and stopband cut-off frequencies are multiples of each other. This non-uniform channelizer is designed to switch between different standard configurations in time. However, its design does not permit down-converting channels from a DFSA frequency band since only one type can be down-converted at a time. To address this, several FRM-FB structures must be allocated in parallel so that each one down-converts a different type of channel. The result is equivalent to replace each GDFT-FB in Figure 4.8 by an FRM-FB. The new structure is denoted as Parallel FRM-FB (P-FRM).

For different DFSA configurations of the input signal, as in the P-GDFT case, the individual channels are obtained by selecting the appropriate P-FRM outputs. However, in this case computational load can be saved by not computing the operations of those masking filters which are not used to extract an information channel. To achieve this, the receiver needs to be aware of the current channel allocation scheme in the channelizer input signal. Despite of the saving in the computing of the branches not used, the rest of the filters still work at a much higher sample rate than in the P-GDFT since no decimation is carried out prior to filtering.

As an alternative to FRM-FB, the CDFB is another way of achieving non-uniform filter banks based on the FRM. The difference between an FRM-FB and a CDFB is that in the FRM-FB the base filter is interpolated as in the classic FRM implementation whereas in the CDFB it is decimated by removing every D_C^{th} coefficient.

Due to the filter coefficients decimation, the passband and the transition band of the frequency response of the base filter remain the same size, but copies of the response are created at frequency multiples of $2\pi/D_C$. The decimation is carried out by substituting every D_C-1 coefficients of the filter impulse response $h_a(n)$ with zero. This operation is represented by

$$h'_a(n) = h_a(n)c_D(n) \tag{4.31}$$

where

$$c_D(n) = 1 \quad \text{for} \quad n = mD_C; m = 0,1,2,etc \ \text{ and } c_D(n) = 0 \tag{4.32}$$

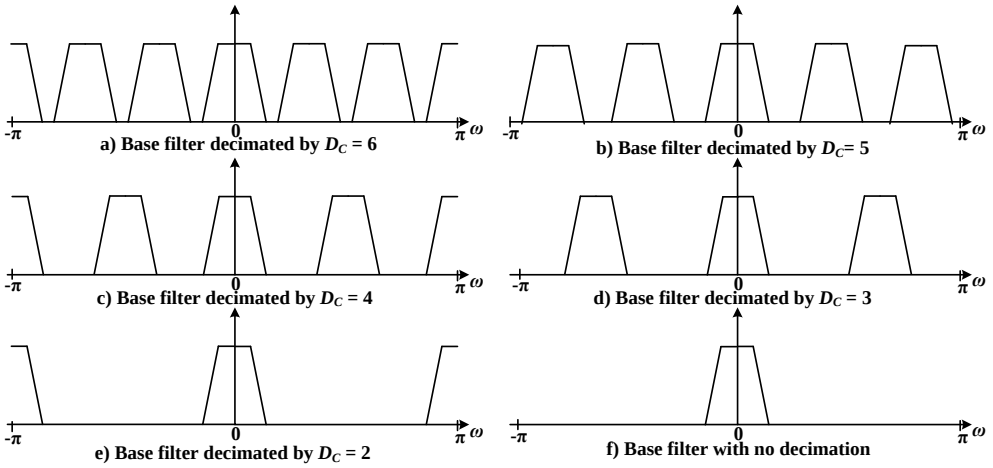

Figure 4.11 CDFB for different values of D_C.

Figure 4.11 shows the CDFB example for values of D_C from one to six. Between Figure 4.11f and the rest of the figures, it can be seen how the passband and transition band of the base filter have not changed. However, as a result of the coefficient decimation, copies at frequencies multiples of $2\pi/D_C$ have appeared. Therefore, the decimated base filter can extract the channels from the input signal which match the centre frequencies of its copies, as in (4.28) for FRM-FB. Later, a set of masking filters, like the ones applied in Figure 4.10 for the FRM-FB, need to be applied for each channel followed by complex mixer to shift the channel to DC.

Despite of the coefficient decimation, which permits calculating only the D_C^{th} part of the base filter coefficients, for cases like in Figure 4.11a where the base filter copies are required to be very close to each other the CDFB presents disadvantages versus the FRM-FB. In order to separate the different channels, the masking filters will require very sharp transition bands and therefore high orders in contrast with the FRM-FB where they require more relaxed specifications. In addition, it is important to note that the decimation operation produces a degradation of the passband and stopband ripples of the decimated versions of the base filter compared to the original frequency response. For this reason, the original base filter needs to be over-designed in order to satisfy the channelization specification with the specifications for the different values of D_C. Consequently, the system will experience an increase in the number of operations [196].

A second possibility for extracting the channels of the CDFB without using masking filters was proposed in [166, 195]. Using the example from Figure 4.11, this alternative method consists on the extraction of the channels by subtracting the different versions of the decimated base filter for different decimation factors (i.e. subtracting Figure 4.11f to Figure 4.11e to obtain the channel centred at π rad). However, this method can only be applied to real baseband signals and not to complex baseband signals due to all the filtering operations being real-valued.

Similar to the FRM-FB, to support DFSA, a number of CDFBs have to be run in parallel (P-CDFB) as in Figure 4.8, each one designed for a specific standard.

Other common issues to the FRM-FB and CDFB are:

- All the operations in FRM-FB or CDFB are carried out at the sample rate of the wideband input signal provided from the ADC or intermediate SRC, in contrast to other systems like modulated filter banks which work at a much lower sample rate. After obtaining the individual outputs, independent SRC can be applied to reduce this sample rate before baseband processing.

- In both cases, as for the P-GDFT, the upgrade of the system for a new standard is done by designing and adding a new FRM structure and then this is added in parallel with the rest.

- Both FMR-FB and CDFB implement an even-stacked filter allocation by default. If odd-stacked filter allocations are required, a frequency shift of the base filter is required. However, this implies that the base filter will have complex coefficients instead of real coefficients, increasing the number of operations.

4.4 Evaluation

The evaluation of the different non-uniform channelizers is divided into two parts. First, the comparison of the performance of the non-uniform channelizers based on the metrics described in Section 4.2, except for the computational load, is carried out. Second, the computational load of the multiple non-uniform channelizers is examined in detail. To support the computational load evaluation three use cases based on the TETRA V&D and TEDS standards are used.

4.4.1 Metrics

In Section 4.3 each non-uniform channelizer has been independently reviewed from its basic signal processing operations to its performance based on the metrics described in Section 4.2.

In order to establish a quick comparison between all non-uniform channelizers, the results obtained for each one of them independently are summarized in Table 4.1 with the exception of the computational load. This will be examined in the next section with more detail due to its importance in the channelizer performance. Considering the rest of evaluation metrics, some of the non-uniform channelizers can be grouped together since they have shown similar capabilities for all of them. Therefore, P-FRM and P-CDFB are grouped into the FRM based category; and TQMFB and HTQMFB are grouped into the TQMFB based one.

In the table, for each type of non-uniform channelizer, each metric is evaluated using the scale: very good (+++), good (++), acceptable (+) and bad (-). These grades are given relatively to the channelizer/s which perform better for a specific metric, giving it/them the (+++) mark. The rest are given marks between (++) and (-) when their performance approaches more or less to the best one respectively. Methods with the same performance in a specific metric are given the same mark.

Table 4.1 Non-uniform methods capabilities comparison.

	FPCC	P-FRM P-CDFB	TQMFB HTQMFB	P-GDFT	R-GDFT
DSFA flexibility	+++	+	-	+	++
Upgrade	+++	+	++	+	++
Reconfigurability	++	+++	+++	+++	++
ADC SRC	+++	++	++	++	++
Baseband SRC	+++	++	++	++	+++

Starting by the DFSA flexibility, the FPCC provides the wider range of the centre frequencies and bandwidths due to its per-channel configuration nature. Next, the R-GDFT also provides a high level of reconfigurability due to the division of the frequency band into granularity bands according to (4.22). For FRM based channelizers and P-GDFT, the possible centre frequencies for each of the J standards are limited to frequencies multiple of $2\pi/K_j$, where K_j is the number of channelizer outputs for each of the standard. Finally, the lowest performance is provided by the TQMFB because not only the centre frequencies for each standard are limited by multiples of $2\pi/K_j$, but also by a power-of-two relationship between standards. In addition, all the filter bank based methods can provide even or odd-stacked filters allocation, except for the TQMFB, which can only provide even-stacked.

For easy upgrade, if the bandwidth of the new standard is equal to the bandwidth of any the standards already supported, no changes are required in any of the channelizers in terms of filtering. Otherwise, different changes are required in each of the cases. For the FPCC, changes only require the recalculation of the fractional delay parameters according to (4.2) for the new SRC factor and an update of the centre frequency of the complex mixers. No action is required for the filters. For TQMFB based channelizers the changes consist on the addition of new stages in the QMFB tree, whereas for the R-GDFTs only the recombination structures are adapted if bigger channel bandwidths need to be supported. Finally, for all the parallel non-uniform channelizers (P-GDFT, P-FRM and P-CDFB) the addition of a new uniform channelizer in the parallel structure would be required. For all of them, the centre frequencies of the new

standard could be supported depending on the constraints expressed in the previous paragraph for each channelizer.

In terms of reconfigurability as a response to variations in the input signal DFSA configuration, the parallel channelizers (P-GDFT, P-FRM and P-CDFB) and the TQMFB channelizers provide the most efficient solution. The changes only imply extracting the independent channels from the correct outputs of the parallel structure or TQMFB. For the FPCC, the reconfigurability implies the recalculation of the amount of braches required and the set up of the complex mixer centre frequency and fractional delay values for every branch. In the R-GDFT, the recombination structures inputs have to be reconnected to the correct GDFT-FB outputs to recombine the necessary sets of sub-bands.

Finally, for the SRC, both after the ADC and before the baseband processing, the FPCC is the only channelizer which can save the necessity to apply them since it has no restrictions for the input sample rate and can apply any fractional SRC to obtain the desired output rate. Within the rest of channelizers, only the R-GDFT can avoid the use of the baseband SRC by adapting the interpolation factor in the recombination structure. For the rest, SRC prior and after the channelizer is required to be compliant with the input and output sample rates needed.

It is clear that, according to the metrics evaluated, the FPCC method appears the best overall as a result of the superior flexibility provided by a per-channel approach compared to a filter bank. The next one in terms of overall performance is the R-GDFT, which apart from the FPCC, offers the best results within the filter bank based group. Following, the parallel based approaches which find more limitations in terms of upgrade and flexibility. Finally, the TQMFB base designs which have their biggest limitation in the relationships between the tree stages.

Despite of the results in Table 4.1, the addition of the computational load to the overall comparison ultimately determines which non-uniform channelizer is the mot suitable for a specific application. In Section 4.4.2 the comparison analysis is completed with the calculation of the computational load for the different methods.

4.4.2 Computational load

Computational load is maybe the most important factor in determining whether a channelizer is practical or not for a certain application. In general for all of the non-uniform channelizers, the computational load is determined by five main parameters: the maximum number of channels (K), the number of information channels actually used (X, with $X \leq K$), the orders of the FIR filters required (N), the number of communication standards supported (J), and the sample rate (f_S). More in particular, the computational load of the FPCC gets also affected by the number of Farrow sub-filters (P) and the interpolation factors (B). For the TQMFB and HTQMFB, the number of QMFB stages (T) represents an important factor as well. In the case of R-GDFT, the number of recombined sub-bands (R) and interpolation factor (M) of the recombination structures also need to be taken into account.

Considering that the multi-channel input signal is composed of complex I/Q samples, Table 4.2 contains the number of real multiplications required per input sample for each non-uniform channelizer for an even-stacked filter allocation. In Appendix A, the number of real multiplications for the odd-stacked filter allocation is given in Table A.1. The number of real additions per input sample for the even and odd-stacked cases is given in Table A.2 and Table A.3 respectively.

To ensure a perfect linear phase response and establish an objective comparison between the methods, floating-point FIR Remez equiripple filter designs obtained using MATLAB's *fdatool* are used in all cases. To approximate the order of the different FIR filters (3.8) is employed. This expression showed that the sample rate of a filter input signal is a major factor in determining its order. This is a key issue since the different channelization methods require different input sample rates from the SRC after the ADC. For the structures formed with GDFT-FBs or TQMFBs, sample rates which are a power-of-two multiple of the channel spacing between sub-bands are required. For the GDFT-FB this condition allows the use of FFT algorithms. For the TQMFB, the condition is established by the power-of-two multiple relationship between the channel spacings at each stage and the input signal sample rate.

Table 4.2 Non-uniform methods number of real multiplications per input sample for even-stacked sub-band allocation.

Non-uniform channelizer	Real multiplications per input sample (μ)
FPCC	$\sum_{j=1}^{J} X_j \left[(N_P + 1)(P + 2) + P + 7 \right]$
TQMFB	$\frac{N_{QMF} + 1}{4} T$
HTQMFB	$\frac{2(N_{DFT} + 1) + \frac{3K}{2}\left(\log_2(K) - 5\right) + 8}{K} + \frac{N_{QMF} + 1}{4} T$
P-FRM	$2\sum_{j=1}^{J}\left(\frac{N_{Aj} + 1}{2} + \frac{N_{Mj} + 1}{2}\right) + 4\sum_{j=1}^{J}\left[\left(X_j - 1\right)\frac{N_{Mj} + 1}{2} + 4X_j\right]$
P-CDFB	$2\sum_{j=1}^{J}\left(\frac{N_{Aj} + 1}{2X_j} + \frac{N_{Mj} + 1}{2}\right) + 4\sum_{j=1}^{J}\left[\left(X_j - 1\right)\frac{N_{Mj} + 1}{2} + 4X_j\right]$
P-GDFT	$\sum_{j=1}^{J} L_{DFTj}\left[\frac{2\left(N_{DFTj} + 1\right) + \frac{3K_j}{2}\left(\log_2\left(K_j\right) - 5\right) + 8}{K_j}\right]$
R-GDFT (GDFT-FB part)	$L_{DFT}\left[\frac{2\left(N_{DFT} + 1\right) + \frac{3K}{2}\left(\log_2\left(K\right) - 5\right) + 8}{K}\right]$
R-GDFT (Recomb. structure)	$\sum_{j=1}^{J} \frac{L_{DFT}}{K}\left[X_j\left(M_j \times R_j\left(2\frac{N_{Ij} + 1}{2} + 4 + \frac{4}{M_j}\right)\right)\right]$

For FRM-FB and CDFB the input sample rate needs to be a multiple of the channel bandwidths. Subsequently, the different interpolation and decimation factors (L and D_C) are determined by this relationship between the input sample rate and bandwidths. Finally, in the FPCC, the required value of f_S is dependent on the fractional SRC values required for the different standards.

Table 4.3 Relationships between prototype filters.

Non-uniform channelizer	Prototype filters relationships
FPCC	$N_P = \frac{N_S}{\max(B_j)}$
TQMFB/HTQMFB	$N_{QMF} = N_S$
P-FRM	$N_{Aj} = \frac{N_j}{(K_j - 1)}$, $N_{Mj} = N_j \frac{\omega_{sj} - \omega_{pj}}{BW_j}$
P-CDFB	$N_{Aj} = 1.2 \times N_j$, $N_{Mj} = N_j$
P-GDFT	$N_{DFTj} = N_j$
R-GDFT	$N_{DFT} = N_S$

For the rest of the filter design parameters, the selection of the passband and stopband ripples and transition band width is dependent on the channelizer type of structure and the communication standards implemented. For channelizers where a single filter can process more than one type of channel, the values of the ripple and transition band values need to comply with the most stringent of the requirements from the standards involved. This filter design applies to: FPCC, TQMFB, HTQMFB and R-GDFT structures. On the other hand, for the parallel structures such as P-FRM, P-CDFB and P-GDFT, different filter parameters are needed for each branch in accordance with the channel specifications for the branch.

In order compare methods fairly, it is necessary to relate the filter order of all channelizers. To do so, two kinds of prototype filters are defined. First, a filter $H_S(z)$ with order N_S that gathers the most stringent characteristics among the J standards implemented (transition band width and ripples). Second, a set of J filters, $H_j(z)$, that implements the necessary filtering mask specifications for every standard. These prototype filters are required for the non-uniform channelizers employing parallel structures. For both $H_S(z)$ and $H_j(z)$ the same sample frequency is considered. As usual, the filter order will scale with f_S if all the other parameters are constant.

Table 4.4 TETRA V&D and TEDS channels filter design specifications.

Channel	Filters design specifications
TETRA V&D (25 kHz) /TEDS 25 kHz	$f_p = 11.5$ kHz, $f_s = 13.5$ kHz, $\delta_p = 0.1$ dB, $\delta_s = 55$ dB
TEDS 50 kHz	$f_p = 22.8$ kHz, $f_s = 27.2$ kHz, $\delta_p = 0.1$ dB, $\delta_s = 55$ dB
TEDS 100 kHz	$f_p = 44.4$ kHz, $f_s = 55.6$ kHz, $\delta_p = 0.1$ dB, $\delta_s = 55$ dB
TEDS 150 kHz	$f_p = 70.5$ kHz, $f_s = 77$ kHz, $\delta_p = 0.1$ dB, $\delta_s = 55$ dB

The relationship between the orders of the prototype filters $H_S(z)$ and $H_j(z)$, and the orders of the filters used in each non-uniform channelizer employed to calculate their computational load (Table 4.2, Table A.1, Table A.2 ,Table A.3), is given in Table 4.3.

4.4.3 Analysis use cases

The simple observation of the computational load equations given in Table 4.2 and Appendix A for the different non-uniform channelizers does not give a clear interpretation of the differences among them. For this reason, use cases are employed to obtain a more understandable comparison method.

To do so, the TETRA V&D and TEDS standards presented in Chapter 3 are employed. For them, the prototype filter orders are calculated using (3.8) according to the TETRAV&D and TEDS filtering requirements expressed in Table 4.4. For both, the values of the pass band ripple and stop band ripple are the same, δ_p= 0.1 dB and δ_s= 55 dB respectively. The transition band width is directly related to the standards channel guard bands. The MATLAB implementation of Kaiser's equation (3.8) for estimating the FIR filter orders is included in Appendix B.

4.4.3.1 Use case 1

In the first use case TETRA V&D, TEDS 50 kHz and TEDS 100 kHz are allocated in the TETRA frequency band from 380 MHz and 400 MHz (Section 2.3). In this use case channels are allocated in accordance with the constraints

imposed by the ECC an ERO for PMR communications in (2.2) (see Chapter 2) [197].

TETRA V&D, TEDS 50 kHz and TEDS 100 kHz share the property that their bandwidths and channel spacings are a power-of-two multiple of the smallest one. This makes them suitable for all the different channelization methods described in this chapter. Furthermore, TETRA V&D and TEDS use FDD such that channels are allocated within 5 MHz DL and UL bands. In this use case, it is considered that the base stations avails of the entire 5 MHz frequency band for DL and UL (spatial reuse factor equal to 1).

Within the use case, three different channel allocation configurations were examined:

- Configuration 1: 50% of the band occupied by TEDS V&D (25 kHz), 25% of the band occupied by TEDS 50 kHz and 25% of the band occupied by TEDS 100 kHz (X_1=100 channels, X_2=26 channels, X_3=12 channels).
- Configuration 2: 25% of the band occupied by TEDS V&D, 50% of the band occupied by TEDS 50 kHz and 25% of the band occupied by TEDS 100 kHz (X_1=52 channels, X_2=50 channels, X_3=12 channels).
- Configuration 3: 25% of the band occupied by TEDS V&D, 25% of the band occupied by TEDS 50 kHz and 50% of the band occupied by TEDS 100 kHz (X_1=50 channels, X_2=25 channels, X_3=25 channels).

The channels of one of the standards occupy most part of the frequency band (50 %) in each configuration, while the other two standards share the rest by occupying approximately 25 % of the frequency band each. In the first configuration, the predominant standard is TETRA V&D; in the second configuration TEDS 50 kHz; and in the third configuration TEDS 100 kHz. Because of the increase in the bandwidth of the predominant channels in each configuration, the overall number of channels gets progressively reduced between configurations. This fact affects positively to the channelization methods which can avoid computing certain filters depending on the configuration (FPCC, P-CDFB and P-FRM), and negatively to the R-GDFT since a bigger number of sub-bands need to be recombined.

In the multi-channel input signal, an odd-stacked channel allocation is considered (with no channel centred at DC). All the non-uniform channelization methods evaluated were able to handle this use case with the exception of the TQMFB which can only manage even-stacked configurations. However, its computational load is included for comparison purposes. The design parameters used for each one of them are given in Table A.4 in Appendix A. It is important to remark that for this use case, the FPCC was able to deliver an integer number of samples per symbol (10 samples/symbol) to the baseband processing part of the receiver without any intermediate SRC. This would imply a reduction in the baseband processing after the channelizer for the FPCC case.

From Table 4.4 it is seen how TETRA V&D has the most stringent filter requirements, whereas the requirements are more relaxed for TEDS 50kHz and TEDS 100kHz. According to Table A.4, for all channelizers except for P-FRM and P-CDFB the input sample rate is f_S = 6.4 MHz; therefore the order for the prototype filters $H_S(z)$ and $H_j(z)$ (j = 1,2,3) are N_S = 8085, N_1 = 8085, N_2 = 3584 and N_3 = 1444. For P-FRM and P-CDFB the input sample rate is f_S= 5 MHz to comply with (4.28), and the filter orders (obtained by linear scaling) are N_S = 6317, N_1 = 6317, N_2 = 2800 and N_3 = 1129. From these generic filter orders, the corresponding orders for the specific cases are calculated according to the Table 4.3 relationships.

The computational load results for use case 1 are shown in Figure 4.12. In the bar diagrams it can be observed how the P-CDFB requires a significantly bigger number of operations in comparison with any other of the methods. This is produced by the requirements of filtering channels which are very close to each other in the frequency band, as it was explained in Section 4.3.5. On the other hand, the P-FRM requires fewer operations than the P-CDFB but still more than other methods like HTQMFB and the GDFT-FB. In both cases, the high computational load is also caused by the high rate at which the filtering operations are performed.

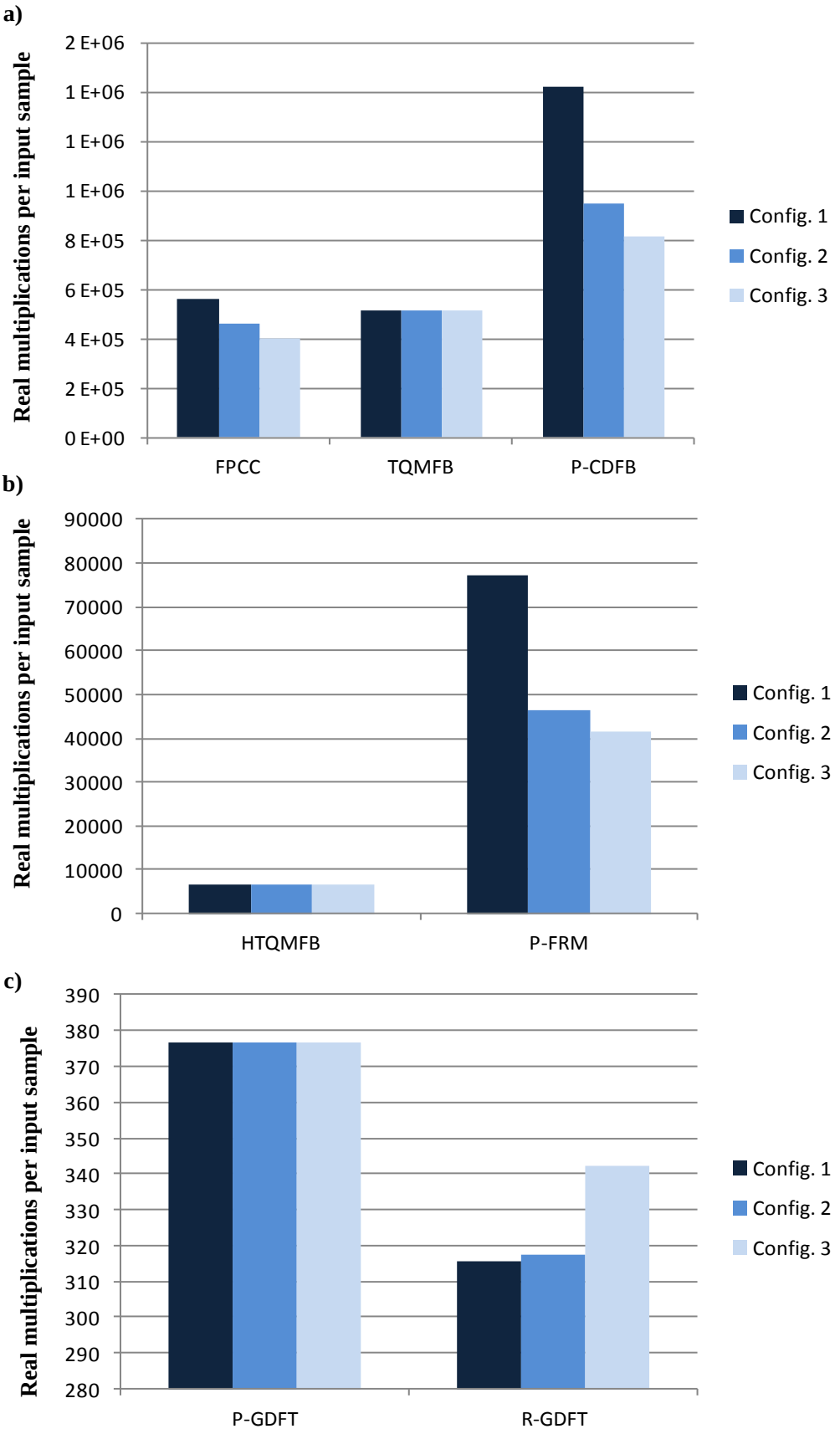

Figure 4.12 Use case 1 computational load results.

The FPCC requires the second highest computational load of all the methods. This is produced by the large number of parallel branches employed and the high sample rate that the operations are carried out at. For the configurations 2 and 3, the presence of more channels with bigger bandwidths reduces the amount of branches required, and therefore the amount of operations of the FPCC, requiring fewer operations than the TQMFB for those cases.

For the TQMFB, the big difference between the input sample rate and the smallest bandwidth required implies the implementation of a large number of stages. Consequently the computational load is high. Since many of these stages are not actually used for extracting channels, they all can be replaced by a GDFT-FB in the HTQMFB. Figure 4.12b shows the important savings in the number of operations between the TQMFB and the HTQMFB. The HTQMFB even provides smaller computational loads than the P-FRM.

The most efficient performance is obtained in Figure 4.12c for the P-GDFT and R-GDFT. These two methods require significantly less operations than any other non-uniform channelizer considered in this chapter. As described in Section 4.3, the computational load of the P-GDFT remains constant whereas the computational load of the R-GDFT increases with the number of channels requiring sub-band recombination. For the three use cases considered in use case 1, the R-GDFT is more efficient than the P-GDFT. However, if a total frequency band occupation with channels requiring recombination, TEDS 50 kHz and TEDS 100 kHz, can make the P-GDFT more efficient than the R-GDFT. Figure 4.13 shows how when the frequency band is fully occupied by TEDS 100 kHz channels, the P-GDFT requires less number of operations than the R-GDFT.

Therefore, the most efficient performance, between P-GDFT and R-GDFT, depends on the application use case and the DFSA configuration.

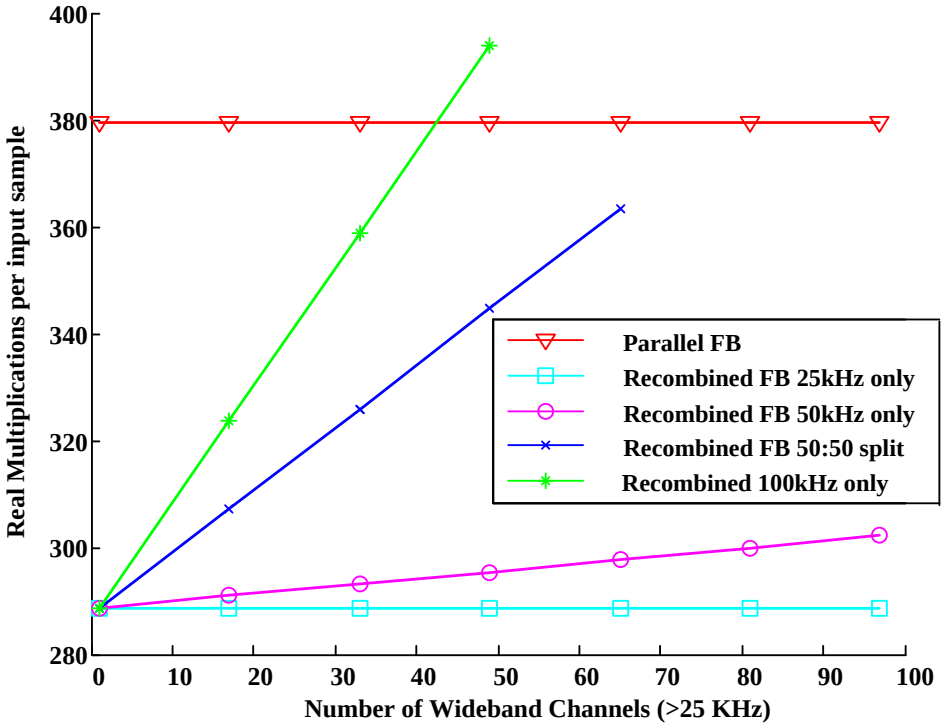

Figure 4.13 Computational computation comparison between P-GDFT and R-GDFT.

4.4.3.2 Use case 2

In this use case, the multi-channel TETRA UL frequency band is shared by TETRA V&D, TEDS 50 kHz and TEDS 150 kHz (TETRA 100 kHz channels are not considered now). Here, the power-of-two relationship between all channel bandwidths is lost, but all channel bandwidths are still a multiple of the smallest one. The channel allocation is performed in accordance with the ECC constraints as in use case 1.

Unlike use case 1, not all the non-uniform channelization methods are compliant with the restrictions imposed here. More specifically, TQMFB based structures do not allow an efficient management of spectrum sub-bands when a power-of-two ratio does not exist between the channel bandwidths. Consequently TQMFB methods are not considered for this use case. For the rest of the methods, Table A.4 summarizes the configuration parameters applied.

Again, for an odd-stacked case, three different channel allocation configurations will be tested:

- Configuration 1: 50% of the band occupied by TEDS V&D, 25% of the band occupied by TEDS 50 kHz, and 25% of the band occupied by TEDS 150 kHz (X_1=100 channels, X_2=26 channels, X_3=8 channels).
- Configuration 2: 25% of the band occupied by TEDS V&D, 50% of the band occupied by TEDS 50 kHz, and 25% of the band occupied by TEDS 150 kHz (X_1=50 channels, X_2=51 channels, X_3=8 channels).
- Configuration 3: 25% of the band occupied by TEDS V&D, 25% of the band occupied by TEDS 50 kHz and 50% of the band occupied by TEDS 150 kHz (X_1=50 channels, X_2=24 channels, X_3=17 channels).

The filter orders, N_S, N_1 and N_2 remain the same as in use case 1. To achieve the correct channel spacing for the 150 kHz channels, the input sample rate needs to be adapted for the P-FRM, P-CDFB and P-GDFT as expressed in Table A.. For $H_3(z)$ the order is N_3 = 3732 for f_S = 9.6 MHz , N_3 = 2488 for f_S = 6.4 MHz and N_3 = 1983 for f_S = 5.1 MHz.

Figure 4.14 shows the computational load results for use case 2. In comparison with Figure 4.12, the relative performance between all the non-uniform channelizers remains the same. The worst performance is obtained for the P-CDFB, followed by the FPCC. The best performance is again given by the P-GDFT and the R-GDFT. From Figure 4.14c it is noticeable that the introduction of the TEDS 150 kHz channels produce a computation increase in both P-GDFT and R-GDFT in comparison with use case 1 (Figure 4.12). Between them, the difference in the number of multiplications per input sample is bigger in use case 2 than in use case 1, which reveals that the R-GDFT would be more efficient for every input signal DFSA configuration than the P-GDFT, unlike Figure 4.13.

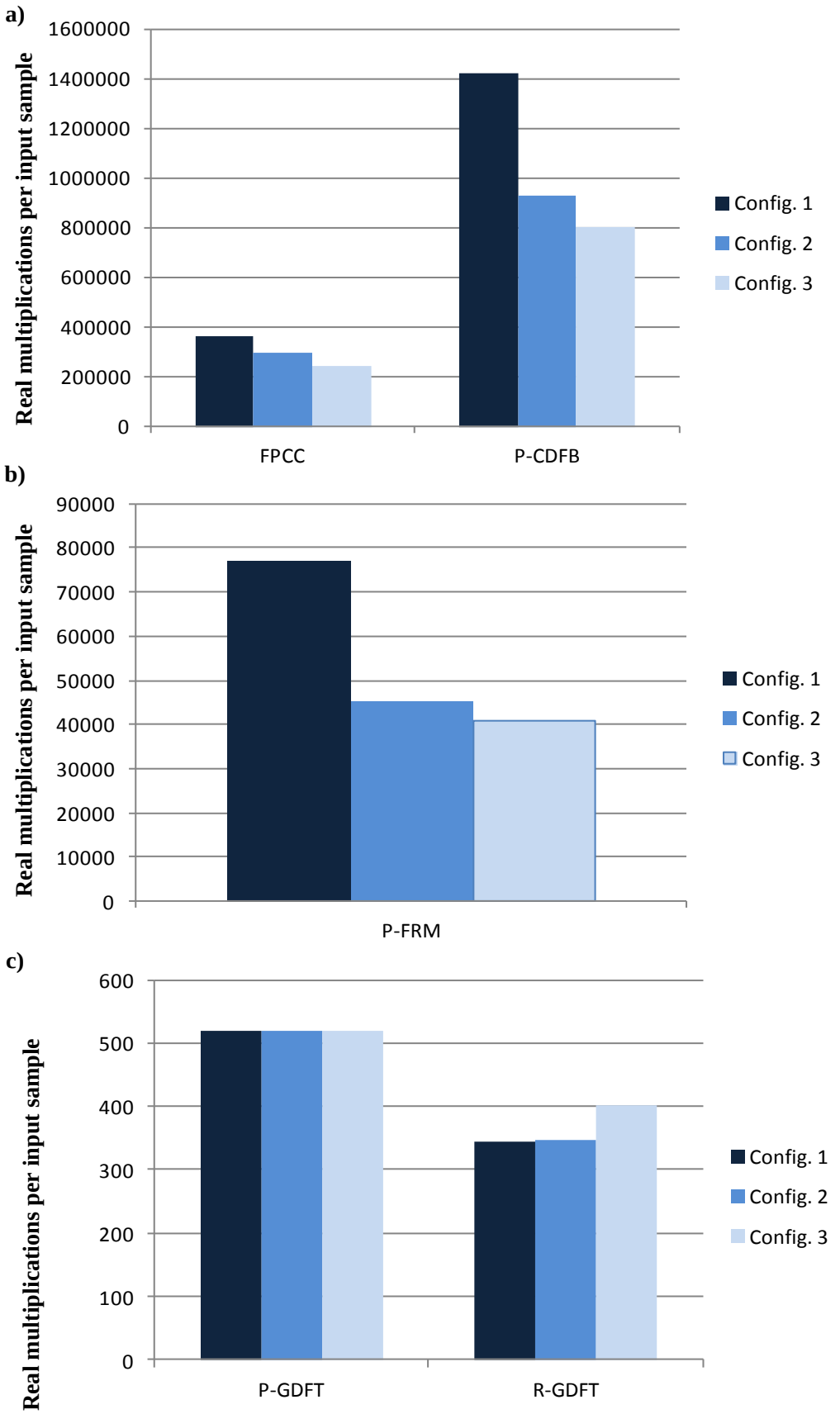

Figure 4.14 Use case 2 computational load results.

4.4.3.3 Use case 3

In use case 3 the multi-channel frequency band is shared by TETRA V&D (25 kHz), TEDS 50 kHz and TEDS 150 kHz as in use case 2. However, unlike use case 2, the channels are not allocated according to the ECC constraints. Instead, the channels can be allocated at any centre frequency multiple 12.5 MHz for the TETRA V&D channels or any frequency multiple of 25 kHz for the TEDS 50 kHz and TEDS 150 kHz, from the lower frequency band edge (as long as they do not go over the lower or upper band edges).

From the methods under study, only the FPCC and the R-GDFT support the required channel allocation. In the FPCC, since every channel is processed by an independent branch, any centre frequency can be chosen for any of the channels as long as its bandwidth does not overlap with another one.

For the R-GDFT, the possible centre frequencies are given by (4.22). In use case 1 and 2, since all the bandwidths were multiples of the smallest one (25 kHz), the granularity band was chosen equal to this. As a consequence, any of the channels could have been allocated at any frequency multiple of 25 kHz for even number of recombined sub-bands, or offset by 12.5 MHz for an odd number of recombined sub-bands. For use case 3, the configuration from use case 1 and use case 2 allow the desired centre frequencies for the TEDS 50 kHz and TEDS 100 kHz channels. However, if more flexibility was required, for example centre frequencies at multiples of 12.5 kHz for these two types of TEDS channels, smaller granularity bands and larger amount of sub-bands would be required.

For this use case the computational load result for the FPCC and R-GDFT are the same since the types and number of channels in every configuration are the same. The only difference is the freedom in the centre frequencies election. For the case that a higher centre frequency freedom was required, and the size of the R-GDFT increased as a result, from the computational results of previous use cases it can be seen that the difference in computation between the FPCC and the R-GDFT is around our orders of magnitude. Therefore, the R-GDFT would still be more efficient than the FPCC.

Table 4.5 Comparison use cases generalisation table.

Non-uniform channelizer	Use cases supported			Computational load
	Use case 1	Use case 2	Use case 3	
FPCC	Y	Y	Y	-
TQMFB	Y	N	N	-
HTQMFB	Y	N	N	++
P-FRM	Y	Y	N	+
P-CDFB	Y	Y	N	-
P-GDFT	Y	Y	N	+++
R-GDFT	Y	Y	Y	+++

4.4.4 Generalising the results

Even though TETRA V&D and TEDS channels were employed in the previous three use cases, the results can be generalised for other standards. The first use case established the situation where all the managed bandwidths are power-of-two multiples of the smallest one and the channel allocation was governed by (2.2). Therefore the channels could only be allocated at centre frequencies separated from the lowest frequency band edge by (i+0.5) (i as a positive integer) times their bandwidth.

In use case 2, the first condition was relaxed so that channels could have any bandwidth that it is not limited to power-of-two multiples. In the TETRA V&D and TEDS case the bandwidths are all multiples of 25 kHz, but this is not a necessary condition. The channel allocation rules in use case 2 match those in use case 1.

Finally, in use case 3, the channel allocation rules were relaxed so that channels of the different standards could be allocated at any centre frequency as long as they did not overlap with other channels.

Table 4.5 summarizes the information from the three previous use cases. In it, the suitability of each non-uniform channelizer for each generalised use case is acknowledged (Y) or denied (N). In addition, using the same scale which was

applied to Table 4.1, the computational load of each channelizer is evaluated based on the results in Figure 4.12 and Figure 4.14.

4.5 Chapter conclusions

In this chapter a critical evaluation of different non-uniform channelizers proposed by other researchers and some novel ones proposed by the author (e.g. P-GDFT) is carried out for the specific multi-standard SDR base station application from Chapter 2. Unlike other comparison studies purely based on the reconfigurability of the non-uniform channelizers, this evaluation provides a new approach based on two factors: a wider set of metrics, which defines the channelizer capabilities with more accuracy, and the specific application of the channelizers to real-world use cases.

In a similar way to Chapter 2 for the uniform channelizers, in this chapter the non-uniform channelizers are classified into two groups: the per-channel based channelizers (i.e. FPCC) and the filter bank based channelizers (i.e. TQMFB, P-GDFT, P-FRM, etc.). Among all of them, FPCCs provide the highest level of DFSA flexibility but, similarly to the results obtained in Chapter 2 for the uniform case, their computational load is high when a large number of channels may be handled. This high load is mainly produced by the independent processing operations carried out in each of the branches. Unlike the FPCCs, filter banks based non-uniform channelizers share the computational load among the different channels. Therefore, TQMFBs and HTQMFBs have a lower computational load than FPCCs, especially HTQMFBs, but they have very constrained capabilities in terms of channel centre frequencies and bandwidths. These constraints can be relaxed using FRM based methods (e.g. FRM-FB and CDFB) but the high sample rate of their filtering operations results in high computational loads, especially for the P-CDFB.

GDFT-FB based methods (P-GDFT and R-GDFT) have present the smallest computational loads. Moreover, R-GDFT showed the smallest computational load in most of the configurations and the greatest flexibility for allocating the channel centre frequencies. Therefore, among the set of non-uniform

channelizers, R-GDFTs are the most suitable solution for a multi-standard SDR base station, followed by the P-GDFT. Nevertheless, for all the methods considered the FIR filter designs were found to require very high filter orders (e.g. around 8000 coefficients for the theoretical TETRA V&D prototype filter). A fixed-point implementation of a filter with such a large order would require a very large number of bits to represent the values obtained in the multiplications and additions implied in the filtering operation. Therefore, such high orders make the physical implementation of these channelizers not realistic, no matter what their computational load or flexibility is. Therefore, the reduction of the filter order of the GDFT-FB based non-uniform channelizers stands as a key factor for their practical design and application.

Chapter 5

Multi-Stage Filtering Techniques Applied to GDFT-FB

5.1 Introduction

The evaluation in Chapter 4 showed that GDFT-FB based non-uniform channelizers have the best performance (as measured by computational load) while still offering DFSA flexibility. When the number of channels is large, however, they still present some implementation difficulties, most notably in the requirements for high order filters. In DSP literature, multi-stage filtering has been used to divide the work load of a filter into several stages, particularly when high filter orders are needed. Using this approach, the number of filter coefficients in every stage is smaller than in the single-stage case yielding filters which are more practical to implement. Consequently, in this chapter two multi-stage filtering techniques were applied to non-uniform GDFT-FBs: first a combination of the FRM technique and GDFT-FBs, and second a combination of GDFT-FBs with half-band filters.

There were two main objectives of this work. First, the filter orders should be reduced to make filter implementations practical in real systems. Second, it was desirable that the computational load could be reduced (or at least not increased).

5.2 Multi-stage narrowband filters

For communications applications, FIR filters are generally chosen for their linear phase response. As seen in Chapter 2, in a linear phase FIR filter of length

N+1 (order N) a symmetric or anti-symmetric relationship between the filter coefficients is required [99]. Therefore, only (N+1)/2 coefficients are freely assignable. This limitation means that perfect linear phase FIR filter designs with stringent transition band and stopband specifications, as in Chapter 4, require a large number of coefficients. As an alternative, for applications where non-perfect linear phase response is allowed (and therefore the symmetric coefficient property is not required) a minimum-phase FIR or IIR filter design can provide a more optimum solution with a reduced number of filter coefficients.

Nevertheless, when a linear phase response is required, multi-stage filtering [112] is a useful technique that can be applied to FIR filter design to reduce the total number of filter coefficients. Multi-stage filtering uses multirate signal processing techniques to implement sharp transition band filters by cascading several filters with more relaxed specifications instead. This technique can be applied to systems with the same sample rate at the input and the output, or to systems used to perform sample rate conversions, i.e. interpolators and decimators, typically those that have large sample rate conversion factors.

As an example, Figure 5.1a shows the implementation of a narrowband filter formed by a decimator structure, followed by a *kernel* filter and finally an interpolation structure [112]. The decrease in the sample rate resulting from the decimator makes the number of coefficients required by the kernel filter smaller. The interpolator recovers the initial sample rate. A polyphase implementation of both decimation and interpolation filters, plus the strategic position of the kernel filter between them, allows the system to perform its operations at the lowest sample rate. Consequently the number of operations per second is less than for a single stage case. The necessity of applying a decimation factor of at least 2, limits this multistage application to filter designs where the filter passband cut-off frequency is smaller than a quarter of the input sample rate [112].

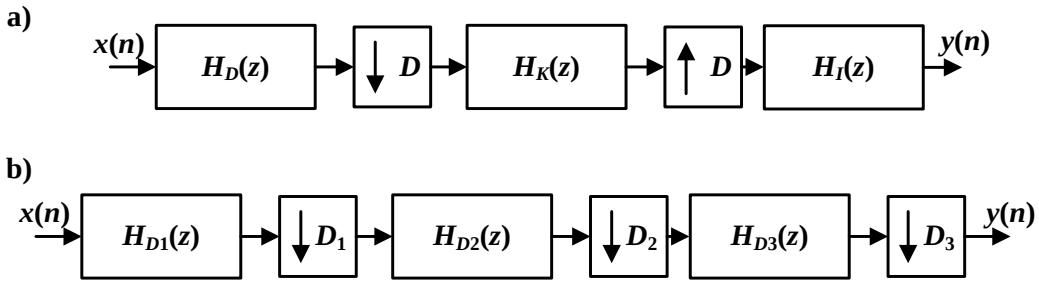

Figure 5.1 3-stage filtering example applied to a) Narrowband filter with same input and output sample rate, b) D-band Decimator with $D=D_1 \cdot D_2 \cdot D_3$.

In the other example, Figure 5.1b, the multi-stage approach is used to implement a decimator structure. Instead of using a single anti-alias filter with a sharp cut-off frequency around π/D rad, a sequence of several decimators is used instead. The downsampling factors are chosen to produce the same final sample rate conversion, that is $D=D_1 \cdot D_2 \cdot D_3$. By using a polyphase implementation for every filter, a progressive reduction in the operation rate is achieved for each one of them.

In both examples, a single original filter is factorized into multiple component filters which, when cascaded, reproduce the original filter magnitude and phase response. Component filters have specifications that are more relaxed than the original filter. Therefore, the number of coefficients in each one is smaller (often much smaller) than the original filter and their design is simplified. The total computational load is often reduced relative to the original filter because of the sample rate reductions in the multi-stage structure.

The FRM technique described in Chapter 3 and employed in some non-uniform channelizers in Chapter 4 represents another example of cascaded filtering. As shown in Chapter3, FRM can be used to achieve sharp transition bands with fewer filter coefficients. However, in a FRM structure the sample rate remains constant unlike multi-stage filtering structures formed from interpolators and decimators. This was the main reason why in Chapter 4 the non-uniform channelizer designs based on the FRM technique showed a very high number of operations per second in comparison with other methods.

Apart from their application to a single narrowband filter design, multi-stage filtering techniques can be applied to filter banks to reduce the filter orders. In the specific case of uniform modulated filter banks, such as GDFT-FBs, the addition of a second filtering stage can help relax the specifications of the prototype filter, consequently reducing the number of coefficients necessary. In the following sections two examples of multi-stage filtering applied to uniform GDFT-FBs are presented. By reducing the high filter of the uniform GDFT-FBs with narrowband specifications and a large number of channels, more efficient implementations of the P-GDFT and R-GDFT non-uniform channelizers described in Chapter 4 can be achieved. In filter bank literature the term multi-stage typically refers to a structure in which multiple filter bank stages are cascaded to form a complete filter bank [180, 198]. In contrast, the approaches presented here apply the multi-stage technique to the prototype filter of just one filter bank.

5.3 Hybrid GDFT-FB (H-GDFT) design

The results obtained in Chapter 4 for the FRM based non-uniform channelizers (FRM-FB and CDFB) showed that one of the main contributions to their rather high computational load is the high sample rate used throughout the channelizer. In FRM based channelizers, both the base and masking filters work at the same high sample rate as the input multi-channel signal. When a wide frequency band with a large number of channels is to be channelized, this operation at the input sample rate is a significant disadvantage relative to channelizers that perform decimation of the input signal before the filtering operations.

Furthermore, for the FRM-FB non-uniform channelizer (Figure 4.10) a separate bandpass filter is necessary to extract each channel from the positive and complementary filter branches. When the channelizer is designed to work with a large number of channels, this implementation is inefficient because all the bandpass masking filters working in parallel contribute to the computational load.

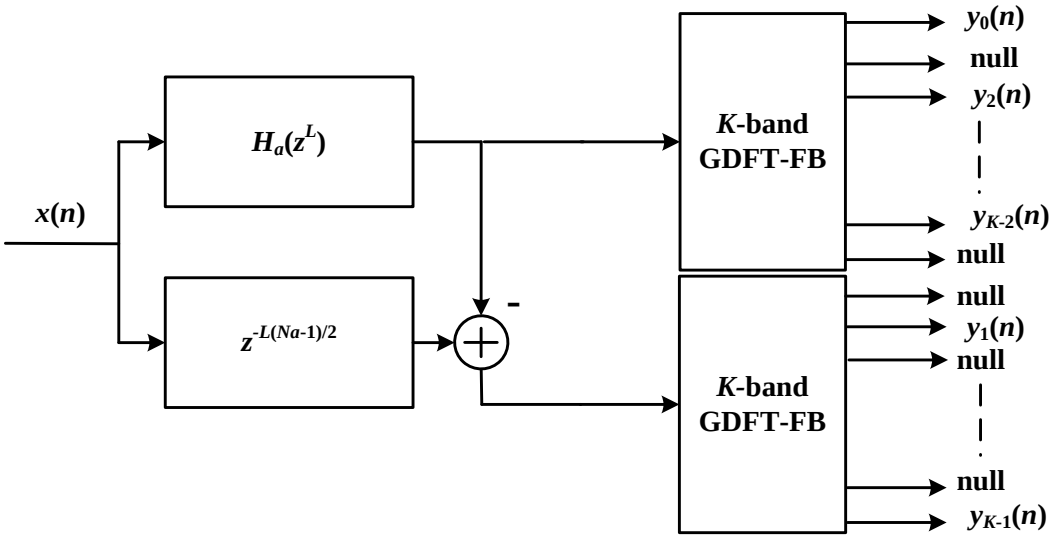

Figure 5.2 H-GDFT structure.

The performance of the FRM-FB can be improved by replacing the masking filters by two GDFT-FBs. As shown in Figure 5.2, each set of masking filters in the positive and complementary branches is replaced by a GDFT-FB with identical size. In contrast with the bandpass filters in the FRM-FB, these two modulated filter banks have the advantages of just requiring one single prototype filter and working at the lower sample rate provided by the decimation operations inside them. This new hybrid design will be called the Hybrid GDFT-FB (H-GDFT).

In the H-GDFT, as in the FRM-FB, the interpolated versions of the base filter and complementary filter extract half of the wideband input signal channels, even and odd channels respectively. In order to obtain the same filtering specifications for the base and complementary filters images, both of them require the same bandpass and transition band widths. To achieve this, the base filter must be designed with symmetric transition band centred at $\pi/2$ rad, or in other words, as a half-band filter (Figure 5.3a). Half-band filters were presented in Chapter 3 as efficient FIR filter implementations which are specially suited for interpolation or decimation by a factor of 2. Because they have a symmetric impulse response in which every second coefficient is equal to zero, only approximately a fourth of their multiplications have to be computed. From the frequency response perspective, the -6 dB frequency occurs exactly at $\pi/2$ rad.

This makes them useful for R-GDFTs since the magnitude-complementary property required by the R-GDFT prototype filter is easily achieved.

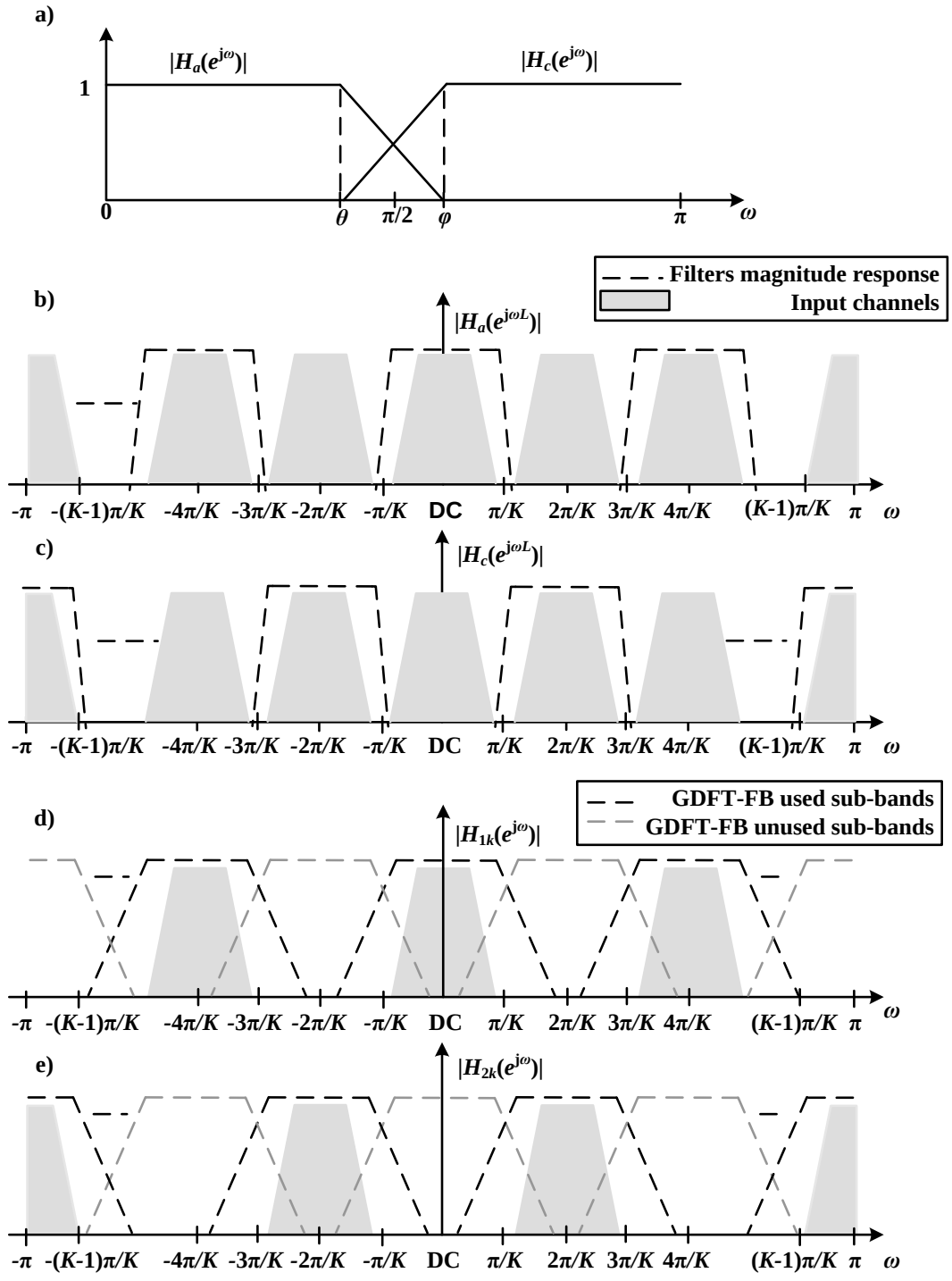

Figure 5.3 H-GDFT filtering operations. a) Base filter design. b) First stage, interpolated base filter response, c) interpolated complementary filter response. d) Second stage, GDFT-FB filtering of every second channel from the base filter outputs, e) and complementary filters outputs.

The interpolation factor of the base half-band filter is determined by the number of sub-bands of the GDFT-FBs according to

$$L = \frac{K}{2} \tag{5.1}$$

where K is the number of sub-bands in the GDFT-FBs. Therefore, the base filter passband and stopband specifications are given by

$$\theta = \omega_{pass} L \tag{5.2}$$

$$\phi = \omega_{stop} L \tag{5.3}$$

The initial mashing performed by the base and complementary filters yields two multi-channel signals each of which contains a null for every second channel. This benefits the prototype filter design of the filter banks in two ways. First, they can be critically decimated due to the reduced aliasing effect from the adjacent bands. Second, the transition band constraints of the prototype filter can be relaxed leading to a reduction of its order. Since the desired sharp transition band is given by the base filter, the GDFT-FBs prototype filter can be designed with a less sharp transition band between π/K and $2\pi/K$ rad.

Figure 5.3b to Figure 5.3e show the two-stage filtering operation. The first stage is the same as in the FRM-FB, with the base filter and its complementary version properly designed to filter the different channels using their frequency modulated images obtained after interpolation. Secondly, the GDFT-FBs are applied separately to the positive and complementary branches to extract the information.

To ensure that the base filter images are centred exactly at the same centre frequencies as the GDFT-FBs sub-bands, the input sample rate of the multi-channel signal needs to comply with (5.4)

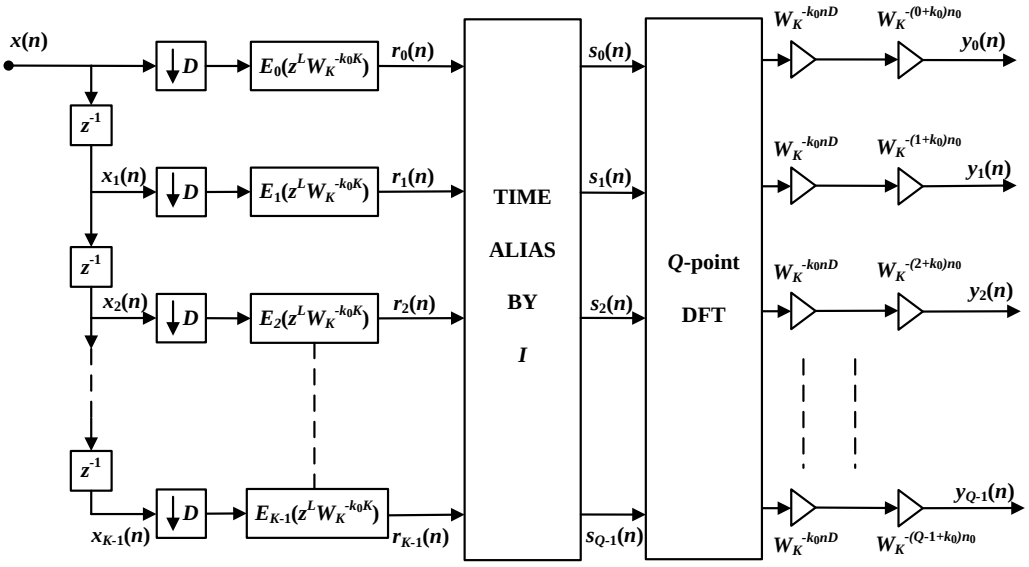

Figure 5.4 GDFT-FB with DFT reduction.

$$f_S = K \times f_{CS} \tag{5.4}$$

where f_{CS} represents the desired sub-band channel spacing.

Considering that half of the total number of sub-bands are null (unused) in each GDFT-FB, further reductions in channelizer computation can be achieved. If only every I-th sub-band of a GDFT-FB is employed to receive information, K-point DFT or FFT operation can be replaced by an (K/I)-point DFT or FFT [89]. The only condition that has to be met is that K is a multiple of I as

$$K = Q \times I \tag{5.5}$$

Since only Q of the output sub-bands are needed, then only Q of the DFT input samples have to be computed. Figure 5.4 shows a GDFT-FB design where the $s_i(n)$ signals are created as *time aliased* versions of a number I of $r_i(n)$ signals [89, 199]. The time aliased signal is obtained according to

$$s_i(m) = \sum_{i=0}^{I-1} r_{q+Qi}(m) \quad 0 \le q \le Q-1 \tag{5.6}$$

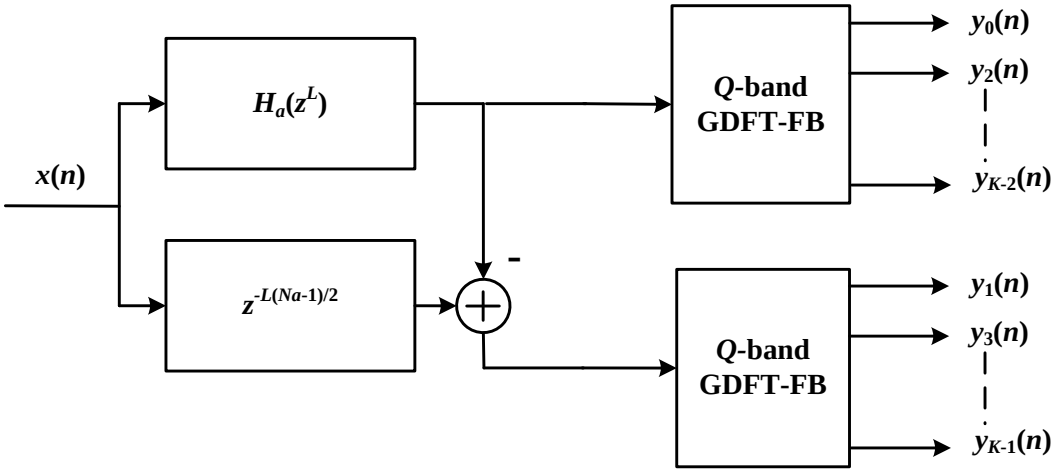

Figure 5.5 H-GDFT implementation with DFT reduction techniques.

As a result only the sub-bands containing actual information channels are processed by the DFT (or FFT).

In the particular case of the H-GDFT, $I = 2$ since only every second sub-band is effectively used. Therefore, the K-point DFT operations in each one of the GDFT-FBs is replaced by a $K/2$-point (or Q-point) DFT. Consequently, from Figure 5.2, part of the computation of the null sub-bands is saved leading to the more efficient implementation in Figure 5.5.

The number of operations for the new hybrid implementation considering multiplications and additions for every complex input sample is given by

$$\mu_{H-GDFT,EVEN} = \left(\frac{N_A+1}{2}\right) + 2\frac{L_{DFT}}{K}\left[2(N+1) + \frac{3K}{4}\left(\log_2\left(\frac{K}{2}\right) - 5\right) + 8\right] \quad (5.7)$$

and

$$\alpha_{H-GDFT,EVEN} = N_A + 2\frac{L_{DFT}}{K}\left[2(N+1-K) + \frac{7K}{4}\left(\log_2\left(\frac{K}{2}\right) - 5\right) + 8\right] \quad (5.8)$$

respectively. These equations represent an even stacked channel configuration, where N_A is the order of the FRM base filter.

For the odd stacked case, both the base filter and the filter bank prototype have complex-valued coefficients due to their bandpass properties. Therefore, as happened with the single-stage GDFT-FB, an increase in the number of operations is experienced relative to the even-stacked case. The number of real multiplications and additions are given by

$$\mu_{H-GDFT,ODD} = 2\left(\frac{N_A+1}{2}\right) + 2\frac{L_{DFT}}{K}\left[4(N+1) + \frac{3K}{4}\left(\log_2\left(\frac{K}{2}\right)-5\right)+8+2K\right] \quad (5.9)$$

$$\alpha_{H-GDFT,ODD} = (2N_A+1) + 2\frac{L_{DFT}}{K}\left[4\left(N+1-\frac{K}{2}\right) + \frac{7K}{4}\left(\log_2\left(\frac{K}{2}\right)-5\right)+8+K\right] \quad (5.10)$$

For the H-GDFT, the GDFT-FBs can be chosen to be critically decimated ($L_{DFT} = 1$) or oversampled ($L_{DFT} > 1$) depending on the designer requirements. For the critically decimated case, the absence of immediate adjacent channels for every information channel reduces the ACI effects and the effects of aliasing after decimation.

When applied to non-uniform channelizer, several critically decimated H-GDFT could be used in parallel as the P-GDFT (Figure 4.8), denoted as PH-GDFT. Another option is to use an oversampled H-GDFT to implement an R-GDFT (Figure 4.9), RH-GDFT, due to the necessity to minimize the aliasing effects.

5.4 Multi-stage GDFT-FB (M-GDFT)

A second novel technique for reducing the filter orders of the GDFT-FB can be realized using multi-stage techniques with a progressive SRC as in Figure 5.1b [189]. There are various ways in which the multi-stage factorization could be applied to the prototype filter. However, the use of half-band filters is attractive because of same impulse and frequency response properties which were described in the previous section for the H-GDFT.

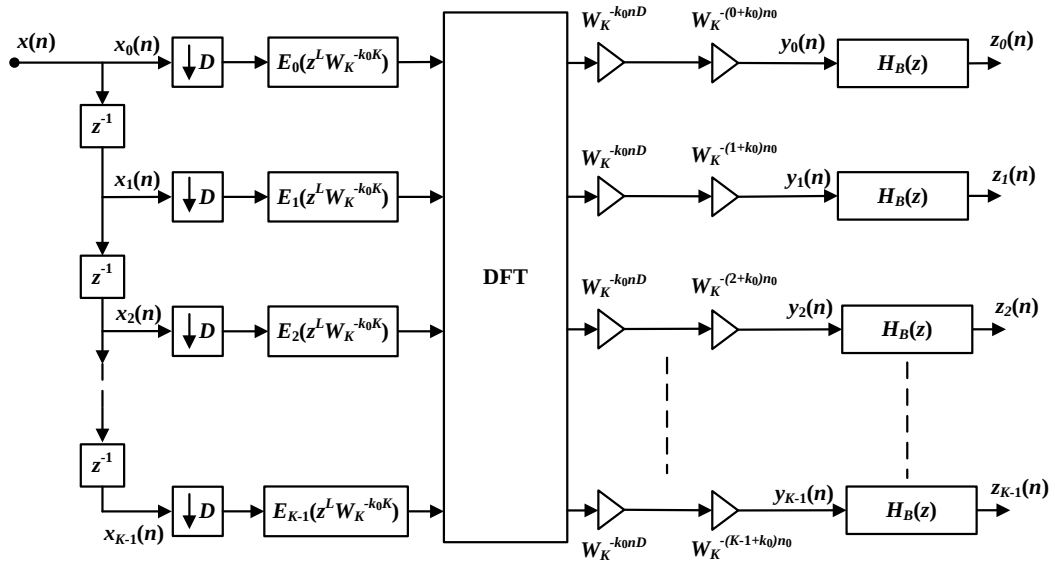

Figure 5.6 M-GDFT where a half-band filter is added after every sub-band output.

For the M-GDFT, but not for the H-GDFT, further advantages can be achieved by implementing half-band filters using their polyphase decomposition (Figure 3.9). This allows the downsampling operation to be performed before the filtering and, because of the zero valued coefficients, allows one of the polyphase branches to be formed from a pure delay followed by the middle filter coefficient [98].

For the M-GDFT, the specification of the prototype filter $H(z)$ (and hence its polyphase components) is relaxed and a half-band filter $H_B(z)$ is subsequently applied to every sub-band output to achieve the original filtering specifications. This design is shown in Figure 5.6.

In the original single-stage design, the prototype filter transition band is rather narrow and centred at π/K. In the revised multi-stage design the prototype filter transition band is shifted so that it starts at π/K and its width is increased such that it extends to $2\pi/K$, thereby including frequency components from adjacent channels. The subsequent half-band filter added to each sub-band output reproduces the original sharp transition band and also eliminates the undesired frequency components from the adjacent channels passed by the relaxed prototype filter. This filtering process is depicted in Figure 5.7.

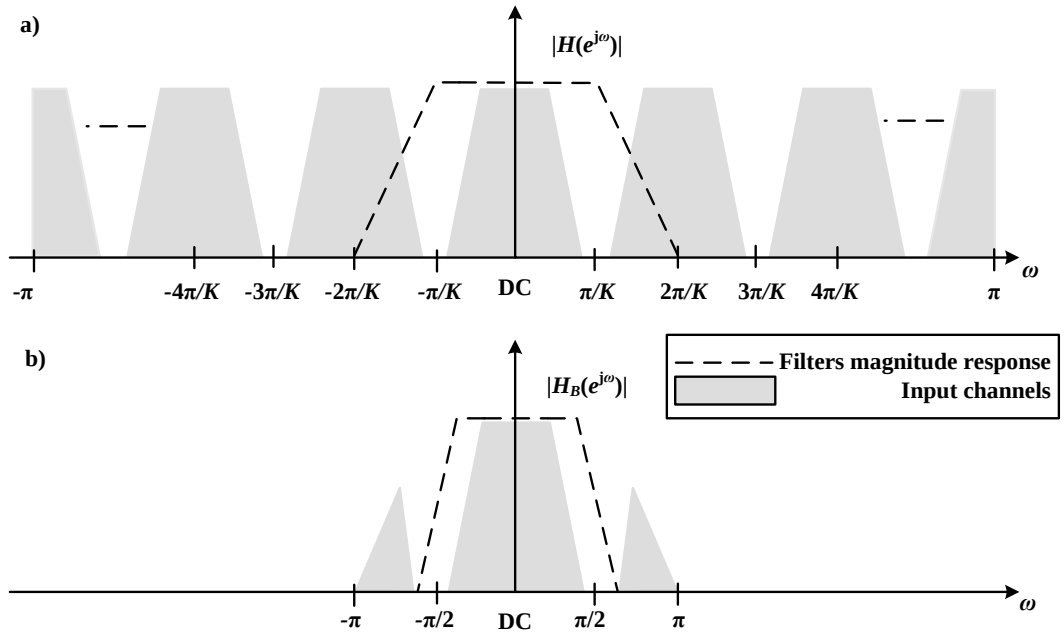

Figure 5.7 M-GDFT filtering operations applied to one of the information channels. a) First, example of the GDFT-FB filtering the channel centred at DC with relaxed transition band. b) Half-band filter performing the sharp filtering of the channel and eliminating the frequency components from adjacent channels.

In order to apply the half-band filters at the GDFT-FB sub-bands output, the filter bank can not be configured as critically decimated, but must instead be oversampled by 2 (K=2D). There are two reasons for this: first, oversampling prevents the undesired adjacent channel frequencies from aliasing with the channel of interest; second, the specific oversampling by a factor of 2 is required to allow the use of half-band filters.

Due to the more relaxed filtering specifications shown in Figure 5.7a, the M-GDFT prototype requires fewer coefficients than in the single-stage design. However, the addition of the half-band filters add extra computational load to the channelizer. For the M-GDFT, the number of real multiplications and additions per complex input for the channelizer is now determined by

$$\mu_{M-GDFT,EVEN} = \frac{L_{DFT}}{K}\left[2\left(N+1\right)+\frac{3K}{2}\left(\log_2\left(K\right)-5\right)+8+2X\,\frac{\left(N_B+1\right)}{8}\right] \quad (5.11)$$

$$\alpha_{M-GDFT,EVEN} = \frac{L_{DFT}}{K}\left[2\left(N+1-K\right)+\frac{7K}{2}\left(\log_2(K)-5\right)+8+2X\,\frac{N_B}{4}\right] \quad (5.12)$$

for the even channel stacked case, where N_B is the order of the half-band filter, K is the number of GDFT-FB sub-bands and X is the number of information channels. When all the GDFT-FB outputs are used to channelize information channels, then $X=K$. However, if some of the sub-bands are not used as information channels, they are nulls, then there is no added benefit in applying the half-band filters to them and $X<K$.

For the odd-stacked sub-band case, the number of real multiplications and additions per input sample is given by

$$\mu_{M-GDFT,ODD} = \frac{L_{DFT}}{K}\left[4(N+1)+\frac{3K}{2}\left(\log_2(K)-5\right)+8+4K+2X\frac{(N_B+1)}{8}\right] \quad (5.13)$$

and

$$\alpha_{M-GDFT,ODD} = \frac{L_{DFT}}{K}\left[4\left(N+1-\frac{K}{2}\right)+\frac{7K}{2}(\log_2(K)-5)+8+2K+2X\frac{N_B}{4}\right] \quad (5.14)$$

5.5 Application to non-uniform channelizers

Both the P-GDFT and R-GDFT non-uniform channelizers were described in Chapter 4 as approaches to implement multi-standard DFSA schemes based on GDFT-FBs. Each of them exhibited different trade-offs between the non-uniform channels frequency allocation flexibility and their computational load. Nevertheless, they shared a limitation in common: their prototype filters were of high order when channelizing a large number of channels.

Since both P-GDFT and R-GDFT are based on the uniform GDFT-FB, both can benefit from the coefficients reduction that the H-GDFT and M-GDFT can provide. This in turn may lead to a reduction in the total computational load of the non-uniform channelizers and, consequently, a more feasible implementation.

The application of either of the two multi-stage techniques to the GDFT-based non-uniform channelizers is achieved by replacing the GDFT-FB component by

with the chosen multi-stage GDFT-FB. For the P-GDFT, this operation is carried out for each of the parallel GDFT-FBs. On the other hand, for the R-GDFT only the filter bank providing the set of granularity frequency bands has to be updated.

5.5.1 Computational load comparison

To evaluate the coefficient reduction advantages of the multi-stage designs, the same TETRA V&D and TEDS design examples used in Chapter 4 use case 1 for the P-GDFT and R-GDFT channelizers were applied. Filtering requirements for the TETRA V&D and TEDS channels used the specifications from Table 4.4 and (3.8) was used to calculate the different filter orders.

For the multi-stage designs, the filter orders for the GDFT-FBs forming the P-GDFT and R-GDFT are shown in Table 5.1 together with numbers for the single-stage GDFT-FBs for comparison. Although the multi-stage designs are composed of two filtering stages instead of one, their filters are designed with either a much larger transition band (base filter and prototype filters) or smaller sample rate (half-band filters). In both cases, the result is a reduction in the overall required filter orders.

Comparing Figure 5.3 and Figure 5.7 it can be seen that there is a duality between the filtering operations of the H-GDFT and M-GDFT. In both cases, the prototype filter for the GDFT-FBs has the same passband and transition band requirements. Similarly, the interpolated base filter of the H-GDFT and the half-band filters of the M-GDFT have the same order. Consequently, the filter orders required by the H-GDFT and M-GDFT are identical as shown in Table 5.1.

Table 5.1 Filter orders calculated for the P-GDFT and R-GDFT non-uniform channelizers using multi-stage GDFT-FB designs for use case 1.

		Uniform filter bank structure		
	Sub-band bandwidth	GDFT-FB	H-GDFT	M-GDFT
P-GDFT	25 kHz	*N=8085*	N_A=64 N=1294	N=1294 N_B=64
	50 kHz	*N=3584*	N_A=595 N=58	N=595 N_B=58
	100 kHz	*N=1444*	N_A=46 N=291	N=291 N_B=46
R-GDFT	25 kHz	*N=8085*	N_A=64 N=1294	N=1294 N_B=64

Table 5.1 also shows that savings between 76.7% and 83.2% of the number of non-zero coefficients are achieved for the different TETRA V&D and TEDS channel types by using the H-GDFT and the M-GDFT. This can have an important impact on the physical implementation of the digital filters since far fewer coefficient values need to be stored requiring and fewer resources are therefore required.

Apart from the benefits in terms of filter design and implementation, reducing the number of coefficients can also lead to a reduction in the computational load of the non-uniform channelizers in many cases. Table 5.2 shows, as a percentage in comparison with the single-stage methods, the number of coefficients, real multiplications and real additions required to implement both the critically decimated P-GDFT and oversampled R-GDFT channelizers for the TETRAV&D and TEDS use case 1 from Section 4.4.3.1. As in use case 1, the operations are calculated for the odd-stacked sub-band allocations in the filter banks.

Table 5.2 Number of coefficients and computational load of the multi-stage GDFT-FB based non-uniform channelizers for use case 1 in comparison with the P-GDFT and R-GDFT[1].

Non-uniform channelizer	Number of coefficients (%)	μ (%)	α (%)
PM-GDFT (oversampled)	16.7	73.5	92.3
PH-GDFT (crit. sampled)	16.7	86.9	128.6
RM-GDFT (oversampled)	16	35.3	45
RH-GDFT (oversampled)	16	84.2	125.9

[1] Note: For the R-GDFT structures, the numbers presented represent only the GDFT-FB part of the channelizer. The recombination structure used to recombine the TEDS 50 and 100 kHz channels is the same for both single-stage and multi-stage cases and is not included for that reason.

Observing the number of coefficients, for both structures around 84 % of the total non-zero coefficients is saved with respect to the single-stage implementations of the non-uniform channelizers. This is a direct consequence of the reduction in the individual uniform filter banks as shown in Table 5.1. For the critically decimated P-GDFT channelizer, computational savings are achieved for both the PH-GDFT and PM-GDFT. For the later, this happens even though it is implemented as oversampled due to its design constraints. Finally, for the oversampled R-GDFT non-uniform channelizer, a reduction in the number of real multiplications per input sample is also achieved for both RM-GDFT and RH-GDFT designs. For the number of additions, both RH-GDFT and PH-GDFT require a larger number of additions in comparison to the single-stage cases.

The performance of the two non-uniform channelizers can be compared in terms of their total number of real multiplications per sample for the different DFSA configurations, as in [161]. The three configurations implemented in Chapter 4 for use case 1 (Section 4.4.3.1) were used to compare the single-stage channelizers with the multi-stage designs. The results obtained are shown in

Figure 5.8. As expected, the P-GDFT channelizers show a constant computational load independent of the channel allocation pattern. On the other hand, the computational load of the R-GDFT structures varies depending on the number of recombined channels and their type. For the three DFSA configurations considered, in accordance with the results from Table 5.2, the multi-stage structures require fewer real multiplications than the single-stage designs. In general, the structures using M-GDFT required the lowest computational load.

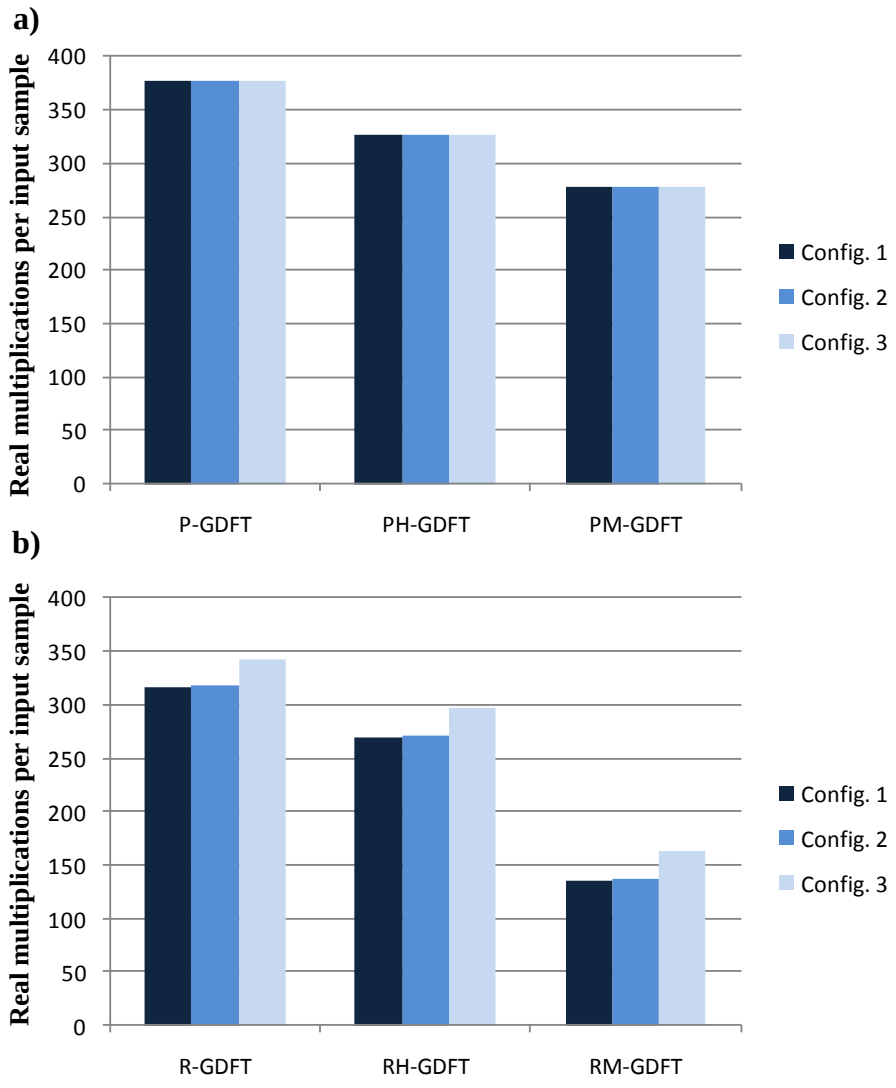

Figure 5.8 Use case 1 computational load comparison for a) parallel versions of GDFT-FB, H-GDFT and M-GDFT, b) recombined versions of GDFT-FB, H-GDFT and M-GDFT.

5.5.2 Filter design example

The filter orders from Table 5.1 are theoretical values calculated according to (3.8). In practical implementations [191], the actual filter orders may be higher because of the deterioration in the filter's frequency response caused by effects such as ACI and aliasing [184]. Aliasing increments with the number of channels and therefore additional overdesign of the filters is required.

As an example, an oversampled (L_{DFT} = 2) channelizer for eight TETRA V&D 25 kHz channels was designed using the single-stage GDFT-FB, multi-stage GDFT-FB and hybrid GDFT-FB. The theoretical order for the single-stage prototype filter was 253, whereas for the multi-stage and hybrid designs the prototype filter order was 42 and the half-band, or base, filter order was 64. All filters were designed as FIR Remez equiripple filters using MATLAB's fdatool using floating-point precision. Again in here, the specifications from Table 4.4 were used. These include maximum passband and stopband ripples equal to δ_p=0.1 dB and δ_s=55 dB respectively.

For these theoretical values the magnitude response of the single-stage GDFT-FB has less than 55 dB of attenuation in the stopband and more than the permitted maximum passband ripple. Due to aliasing, for the multi-stage designs, the cascade of the two filters produces decay in the stopband that provides the desired attenuation in most of the stopband, however in the passband the maximum ripple is also exceeded. To achieve the required specifications, the ideal prototype filters must be overdesigned to compensate for the aliasing effect. This will usually lead to filter orders that are larger than the theoretical predictions, particularly in the single-stage case.

The required specifications were met when the order of the single-stage GDFT-FB prototype filter order was increased from 253 to 280. For the H-GDFT and M-GDFT, the order of the GDFT-FB prototype filter was increased from 42 to 52, and the half-band and base filter order from 64 to 70. In total, the single-stage needed 37 coefficients more compared to 16 needed by the two filters of the multi-stage structures. Figure 5.9a shows the complete the

magnitude response of the three designs, whereas Figure 5.9b focuses on the passband ripple.

From Figure 5.9 it is clear that both H-GDFT and M-GDFT have almost identical magnitude responses when the same filter orders and filter design methods are used. In the stopband, both show decay in the attenuation ripple that reduces the ACI in comparison with the almost constant ripple of the single-stage design. For the M-GDFT and H-GDFT, despite that equiripple filter designs are used for all the filters, the cascading of several filters has the effect that the overall frequency response does not present a uniform ripple in the passband.

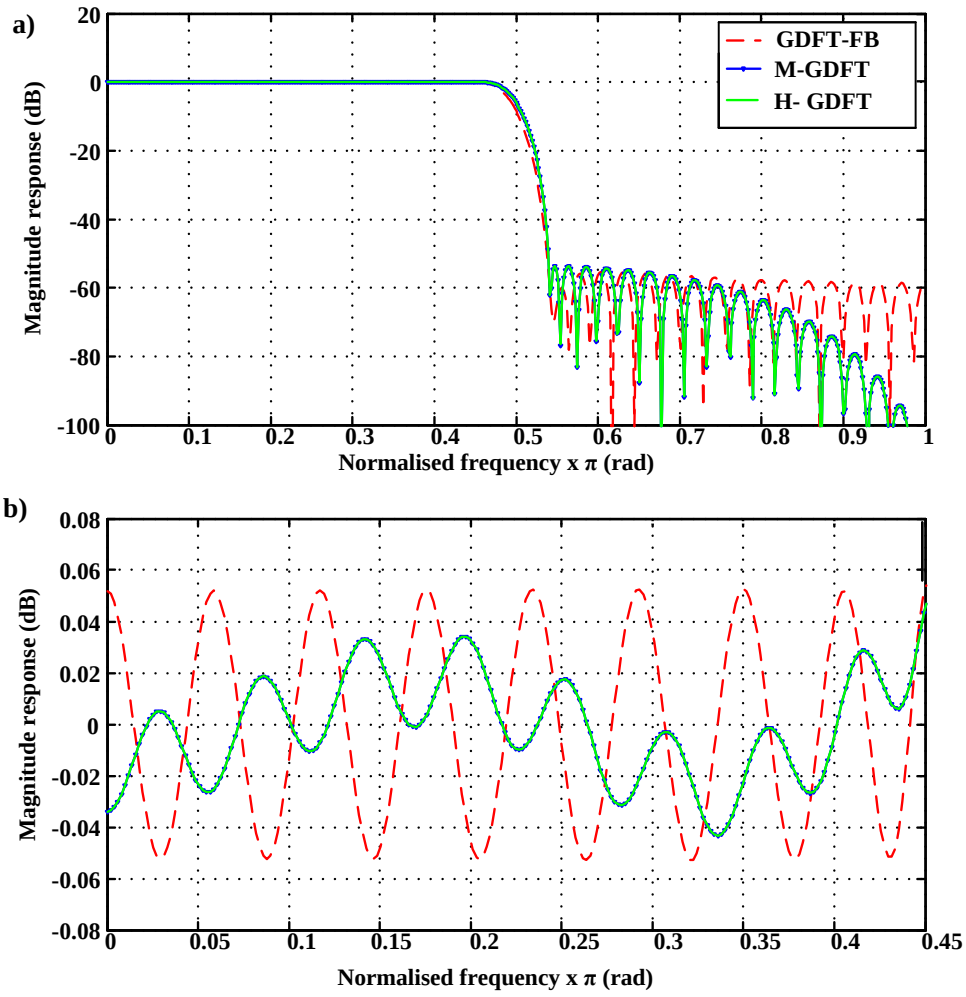

Figure 5.9 GDFT-FB, M-GDFT and H-GDFT a) output magnitude response for an 8-channels TETRA V&D channelizer, b) passband ripple detail.

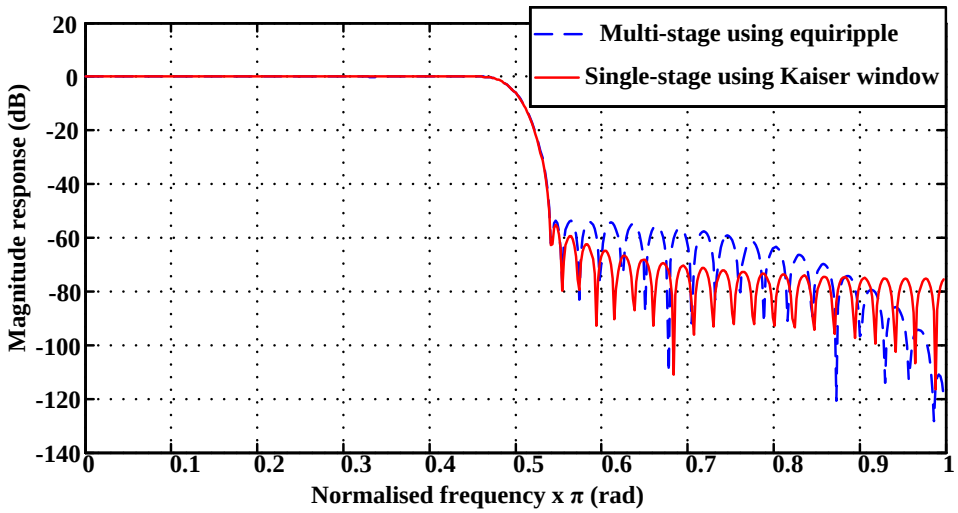

Figure 5.10 Magnitude response comparison between multi-stage method using optimal equiripple filter design and single-stage using Kaiser-window design

Despite the equiripple filter design method provides an optimized approach to the required specifications using a certain filter order, when used as filter bank prototype filters they do not always provide the best option against aliasing and ACI [200]. An alternative option is the employment of Kaiser-window filters [99]. Although Kaiser filters need more coefficients than optimized equiripple filters, they present a decay in their stopband that minimizes the aliasing effects when applied into filter banks [100, 200]. Figure 5.10 shows the comparison between the previous 8-chanel TETRA V&D M-GDFT design employing equiripple filter design and a single-stage GDFT-FB employing a Kaiser-window design.

To obtain the required specifications the Kaiser prototype filter requires an order of 328. This is higher than the single-stage GDFT-FB equiripple design, but provides a decay in the stopband. Figure 5.10 shows that in the Kaiser GDFT-FB case, the attenuation of the stopband increases faster in the closest frequencies to the passband than for the M-GDFT equiripple design. For the M-GDFT-FB equiripple design, the attenuation in the stopband increases more slowly but continuously throughout, thus reaching bigger values than the Kaiser window design. In conclusion, the multi-stage designs group the advantages of the reduced orders given by optimized equiripple filter designs and the reduced aliasing effects given by a decay in the stopband attenuation, as for Kaiser

prototype filters. Even higher decays in the stopband could be achieved by using Kaiser prototype filters in the M-GDFT and H-GDFT, however more coefficients would be required.

5.5.3 Recombination structure implications

In Section 4.3.4 several different issues related to the filter design and the structure employed for sub-band recombination in the R-GDCFT were discussed. First, there is the necessity of designing the prototype filter as a magnitude complementary *K*-band filter [114]. This means that the lowpass prototype filter and the other *K-1* modulated passband filters must comply with

$$\sum_{k=0}^{K-1}\left|H_k(e^{j\omega})\right| = 1 \quad 0 < \omega < 2\pi \tag{5.15}$$

This requirement ensures that no amplitude distortion is introduced in the recombined channels when they are recombined from several granularity sub-bands. Since all the passband filters in the GDFT-FB are obtained from the modulation of the prototype filter, the magnitude complementary design only affects the lowpass prototype. Therefore, the -6 dB cut-off point of the prototype filter frequency response needs to be placed at π/K rad frequency, where K is the number of sub-bands.

Generally the design of a magnitude complementary filter requires optimization of its coefficients to achieve the correct -6 dB cut-off point [161]. In addition, this property is highly constrained by the filter order; a variation in the filter order may necessitate re-optimization. Therefore, for high order single-stage GDFT-FB to achieve the complementary property a large number of coefficients are required must be optimized. For the H-GDFT or the M-GDFT using half-band filters at as the base filter or at the sub-band outputs respectively, such as optimization is not required. For the H-GDFT, the base half-band filter keeps the magnitude complementary property after being interpolated, therefore the output transition band allocates the -6 dB cut-off point exactly at $\pi/(2*L)$. For the M-GDFT, the half-band filter design places the -6 dB cut-off point automatically at the $\pi/2$ rad frequency of the sub-bands frequency response. This makes

M-GDFT and H-GDFT better candidates than single-stage GDFT-FB for optimizing the R-GDFT design.

The recombination structure employed in R-GDFTs (see Figure 4.9b) applies a phase shift to each of the *R* sub-bands to be recombined which must take account of the filter orders used. Therefore, these phase shifts may be modified when using a M-GDFT. In contrast, the frequency shifts required for the recombination remain the same as for the single-stage case since the sub-band allocation does not vary. Both of them are given for the RM-GDFT case by

$$\varphi_r = -\left[M\left(\frac{N}{2D} + \frac{N_B}{2} \right) + \frac{N_M}{2} \right] \beta_r \quad \text{for } r = 0,...,R-1 \tag{5.16}$$

and

$$\beta_r = \pi + \frac{\pi}{R}(2r+1) \quad \text{for } r = 0,...,R-1 \tag{5.17}$$

For the RH-GDFT the phase shift is given by

$$\varphi_r = -\left[M\left(\frac{LN_A + N}{2D} \right) + \frac{N_M}{2} \right] \beta_r \quad \text{for } r = 0,...,R-1 \tag{5.18}$$

As a design example, the 8-band channelizer from Section 5.5.2 was used to separate an input signal composed of one TEDS 100 kHz channel, one TEDS 50 kHz channel and two TETRA 25 kHz channels as shown in Figure 5.11. Each channel is created from random binary digital signals mapped on π/4-DQPSK constellations at the same symbol rates than the TETRA V&D, TEDS 50 kHz and TEDS 100 kHz channels respectively. Then the four channels are interpolated, frequency shifted and added together to form the input signal represented in Figure 5.11.

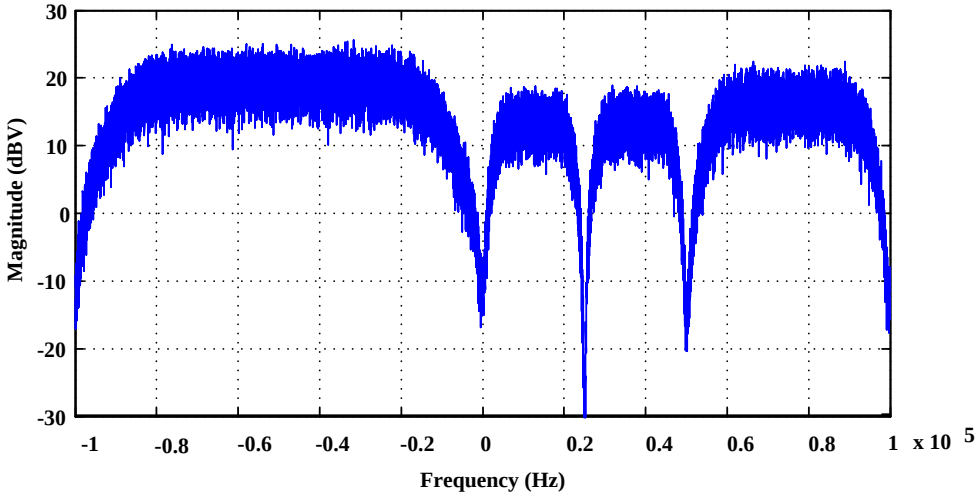

Figure 5.11 Multi-channel input signal for channelization.

After the RM-GDFT sub-band extraction and recombination, the four different channels extracted were as shown in Figure 5.12. Each channel was extracted correctly.

In addition, the recombined output magnitude responses were examined and Figure 5.13 shows that the 0.1 dB passband ripple limit was not exceeded.

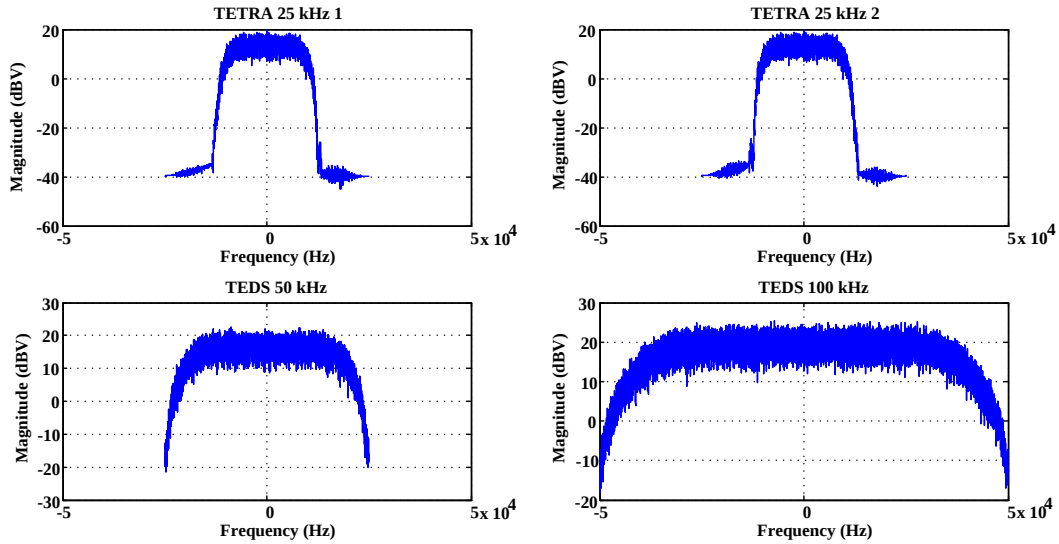

Figure 5.12 RM-GDFT channelizer output signals for input in Figure 5.11.

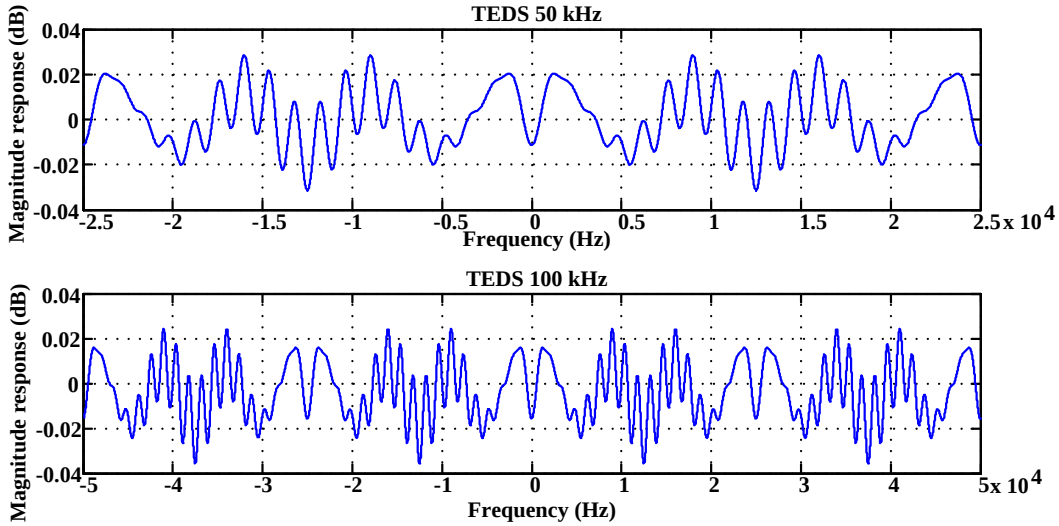

Figure 5.13 RM-GDFT channel output magnitude responses.

5.6 Chapter conclusions

In this chapter two new multi-stage techniques were applied to uniform GDFT-FBs with the objective of reducing their filter orders, and consequently, their computational load and practical implementation complexity. Both of the techniques presented, H-GDFT and M-GDFT, showed a reduction in the number of filter coefficients and the computational load with respect to the single-stage GDFT-FB design. In addition, the filter response of both H-GDFT and M-GDFT was demonstrated to achieve improved stopband attenuation in comparison with the GDFT-FB due to the decay produced by the filters cascading.

When applied to parallel and recombined structures (PH-GDFT, RH-GDFT, PM-GDFT, RM-GDFT) the multi-stage techniques were shown to achieve better results, with up to 84% fewer filter coefficients and up to 65% lower computational load. In addition, because of the use of half-band filters, the RH-GDFT and RM-GDFT offer a more straightforward means for achieving the required magnitude complementary property of the prototype filter than the single-stage R-GDFT version.

Chapter 6

FRM Applied to GDFT-FB

6.1 Introduction

In Chapter 5 a hybrid technique using FRM, H-GDFT, was applied to the GDFT-FB. In this previous approach the multichannel input is first filtered by an interpolated base and complementary filter to create multichannel intermediate signals containing only even numbered or odd numbered channels respectively. These even/odd multichannel signals are then supplied as inputs to a pair of GDFT-FBs whose filtering requirements are relaxed (relative to a single stage design) because occupied channels are now separated by twice the original channel spacing. It was, however, shown that the H-GDFT technique was outperformed by the M-GDFT (which uses an oversampled GDFT-FB and half-band filters on every output). Therefore in this chapter a new alternative application of the FRM technique to GDFT-FBs is evaluated. Specifically, the FRM technique is directly used to implement the GDFT-FB prototype filter thereby reducing the number of filter coefficients that are required by a single stage GDFT-FB. Thereafter, multi-stage techniques may be applied to reduce the number of filters coefficients and, desirably, the computational load still further.

Previous researchers have applied the FRM technique to prototype filter implementation in real modulated filter banks, CMFBS [113, 201-207]. Its usage has provided a reduction in the number of non-zero coefficients needed by the filters and often, but not in all the cases, a reduction in the number of operations (in those case because the objective was mainly the reduction of parameters optimization for perfect reconstruction instead of the computational load). However, FRM has not been applied to complex valued signals and in particular it has not been applied to complex modulated filter banks.

In this chapter the procedure and benefits of the direct FRM which is optimized for use in uniform filter banks is introduced. Thereafter this optimized FRM is applied to the even-stacked GDFT-FB. Subsequently it is shown that this can be further optimized by using the narrowband variant of the optimized FRM structure. Optimized full and narrowband techniques are then applied to the odd-stacked GDFT-FB before introducing a final optimization for oversampled GDFT-FBs based on the noble identities. After this, the computational load of the single-stage GDFT-FBs, multi-stage GDFT-FBs (H-GDFT and M-GDFT), and FRM GDFT-FBs developed in this chapter is compared using one of the TETRA V&D and TEDS use cases. Finally, two additional optimizations are considered: the recursive application of the FRM technique to the FRM filters themselves; and multi-stage techniques (as considered in Chapter 5). The chapter concludes with a brief analysis of how the (uniform) FRM GDFT-FBs can be incorporated into a non-uniform channelizer and any special considerations that arise.

6.2 Special class of FRM

The FRM is formed by four filters as shown in Figure 3.10a: a base filter $H_a(z)$, a complementary filter $H_c(z)$ and two masking filters $H_{Ma}(z)$, *and* $H_{Mc}(z)$. The transfer function of the overall filter is given by

$$H(z) = H_a(z^L)H_{Ma}(z) + H_c(z^L)H_{Mc}(z) \tag{6.1}$$

In the initial structure proposed in [108], the passband and stopband requirements of the base filter could be chosen freely. From the base filter, the complementary filter could be created as given by (3.30) yielding the more efficient structure shown in Figure 3.10b.

However, a special class of FRM filter can be created by constraining the base filter transition band to include the normalized frequency $\pi/2$ [208], as in Figure 6.1a. This condition enables a design which is an analogue of the lowpass and highpass half-band filters employed in the QMFB and the H-GDFT.

Accordingly, the relationship between base and complementary filter can expressed as

$$H_c(z) = H_a(-z) \tag{6.2}$$

Consequently, another efficient implementation can be achieved since both filters share the same polyphase components

$$H_a(z) = H_{a0}(z^2) + z^{-1}H_{a1}(z^2) \tag{6.3}$$

$$H_c(z) = H_{c0}(z^2) + z^{-1}H_{c1}(z^2) = H_{a0}(z^2) - z^{-1}H_{a1}(z^2) \tag{6.4}$$

When (6.4) is applied to (6.1), the structure in Figure 6.1b is obtained.

Apart from the constrained base filter transition band, another noteworthy difference between the traditional FRM implementation in [108] and the special class of FRM proposed in [208] is the order of the base and complementary filters. In traditional FRM, the base filter is designed as a FIR linear phase filter with even order and symmetric impulse response. Therefore, when (3.30) or (6.2) are applied to form the complementary filter, it will have the same properties as the base filter. The masking filters are designed as linear phase FIR filters and can be even or odd ordered as long as they have the same length. The frequency response of all four filters my be expressed in terms of their zero phase response [99],

$$\begin{aligned} H_a(e^{j\omega}) &= e^{-jN_a\omega T/2}\bar{H}_a(\omega) \\ H_c(e^{j\omega}) &= e^{-jN_c\omega T/2}\bar{H}_c(\omega) \\ H_{Ma}(e^{j\omega}) &= e^{-jN_M\omega/2}\bar{H}_{Ma}(\omega) \\ H_{Mc}(e^{j\omega}) &= e^{-jN_M\omega/2}\bar{H}_{Mc}(\omega) \end{aligned} \tag{6.5}$$

Then the frequency response of the overall filter can be written as (6.6),

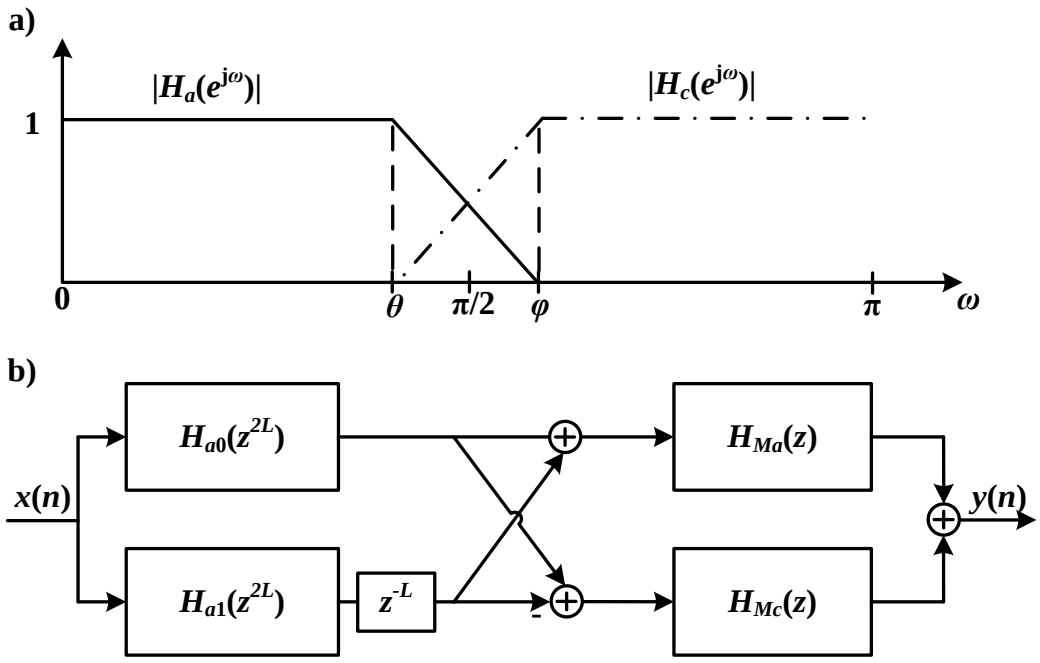

Figure 6.1 Special class of FRM, a)base and complementary filters frequency response, b) efficient polyphase implementation.

$$H(e^{j\omega}) = e^{-j(LN_a+N_M)\omega/2}U(\omega) \tag{6.6}$$

$$U(\omega) = \bar{H}_a(\omega)\bar{H}_{Ma}(\omega) + \bar{H}_c(\omega)\bar{H}_{Mc}(\omega) \tag{6.7}$$

According to [99], the condition for $H(z)$ to have linear phase is that $U(\omega T)$ must be a real function. From (6.7) it can be seen that this is achieved for traditional FRM.

In contrast with traditional FRM, for this special class of FRM the base and complementary filters are required to have odd order according to [208]. This means that if the base filter is designed as linear phase FIR filter with symmetric impulse response, the complementary filter obtained using (6.2) has an asymmetric impulse response. Consequently, when the frequency response of the complementary filter is expressed as in (6.5), it is altered as

$$H_c(e^{j\omega}) = je^{-jN_c\omega/2}\bar{H}_c(\omega) \tag{6.8}$$

This change is due to an extra π/2 phase rotation that appears in FIR filters with asymmetric impulse responses [99]. Applying (6.8) to the overall frequency response yields

$$H(e^{j\omega}) = e^{-j(LN_a+N_M)\omega/2}U(\omega) \tag{6.9}$$

$$U(\omega) = \bar{H}_a(\omega)\bar{H}_{Ma}(\omega) + j\bar{H}_c(\omega)\bar{H}_{Mc}(\omega) \tag{6.10}$$

where $U(\omega T)$ is now a complex function, and therefore $H(z)$ does not have linear phase response. However, when the special class of FRM is applied to the analysis and synthesis parts of filter banks connected in cascade, the resulting zero phase response is a real valued function which therefore presents a linear phase response [208]. However, this case does not find an application for the asymmetric base station use case where the analysis bank is used in isolation without cascading it with the synthesis bank.

The reason for choosing an odd filter order for the base filter in the special class of FRM is that base and complementary filters frequency response will be power complementary [114, 208]. If the masking filters are considered to approximate one and zero in their respective passbands and stopbands, when calculating the square magnitude response of the FRM structure, then

$$\left|H(e^{j\omega})\right|^2 = |U(\omega)|^2 = \left|\bar{H}_a(\omega)\right|^2 + \left|\bar{H}_c(\omega)\right|^2 \tag{6.11}$$

This means that the base and complementary filters are power complementary [112, 114]. This is important for achieving perfect reconstruction in symmetric filter bank applications where the analysis and synthesis filters are cascaded.

The power complementary relationship from (6.11) can not be achieved in the traditional FRM design with base and complementary filters having even orders. However, in this case the base and complementary filters can be designed to provide magnitude complementary frequency responses, however, since they are designed as half-band filters, they still posses the magnitude complementary property

$$\left|H(e^{j\omega})\right| = \left|\bar{H}_a(\omega)\right| + \left|\bar{H}_c(\omega)\right| \tag{6.12}$$

For the base station use case studied along this thesis, linear phase response is considered a requirement for the filters forming the base station channelizer. Due to the independent use of the analysis filter bank in the base station, which is not connected in cascade with the synthesis bank (asymmetric design), the special FRM base filter is designed with even order. Therefore, the linear phase response for the overall FRM frequency response is achieved according to (6.6).

6.3 FRM applied to uniform GDFT-FB (FRM GDFT-FB)

The capability of FRM capabilities to provide more efficient designs for sharp FIR filters has led to its applications in filter banks, specifically, QMFBs [209] and CMFBs [113, 202-206, 210]. In particular, much of the literature focuses on FRM for CMFBs.

However, FRM has not been applied to complex modulated filter banks. Its implementation to EMFB could be obvious from the CMFB case by just applying the same principle to the SMFB. Nevertheless, this has not been done by any author. In particular, the FRM application onto GDFT-FB presented in this section has not been attempted.

6.3.1 The FRM GDFT-FB (even stacked)

In this section, the application of the special FRM class to even-stacked GDFT-FB is addressed. As it was seen in Chapter 4, the even-stacked version of the GDFT-FB gets simplified to the DFT-FB implementation from Chapter 3. Therefore, FRM DFT-FBs, like classic DFT-FBs, provide an even-stacked sub-band allocation where the first channel is centred at DC.

As it was done for FRM CMFBs in [205-206, 210], the full FRM structure from Figure 3.10a is employed. In addition, as long as the transition band condition

established in Section 6.2 for the base filter is met, the structure in Figure 6.1b can be employed. Based on the application of the special FRM class to CMFB in [205-206], using (6.2)-(6.4), the GDFT-FB prototype filter $H(z)$ can be expressed as

$$\begin{aligned} H(z) &= H_{a0}(z^{2L})H_{Ma}(z) + z^{-L}H_{a1}(z^{2L})H_{Ma}(z) \\ &\quad + H_{a1}(z^{2L})H_{Mc}(z) - z^{-L}H_{a1}(z^{2L})H_{Mc}(z) \end{aligned} \tag{6.13}$$

Identifying the common components in (6.13), this can be rearranged as

$$\begin{aligned} A(z) &= H_{Ma}(z) + H_{Mc}(z) \\ B(z) &= H_{Ma}(z) - H_{Mc}(z) \end{aligned} \tag{6.14}$$

$$H(z) = H_{a0}(z^{2L})A(z) + z^{-L}H_{a1}(z^{2L})B(z) \tag{6.15}$$

To create the DFT-FB modulated bandpass filters from the lowpass prototype, the complex modulation of the prototype filter defined by (3.38) is applied

$$\begin{aligned} H_k(z) &= H_{a0}(z^{2L})A_k(z) + z^{-L}H_{a1}(z^{2L})B_k(z) \\ A_k(z) &= A(zW_K^k) \\ B_k(z) &= B(zW_K^k) \end{aligned} \tag{6.16}$$

The polyphase decomposition can be applied to the masking filters to yield

$$\begin{aligned} A(z) &= \sum_{i=0}^{K-1} z^{-i}E_{Ai}(z^K) \\ B(z) &= \sum_{i=0}^{K-1} z^{-i}E_{Bi}(z^K) \end{aligned} \tag{6.17}$$

Finally, then each of the modulated bandpass filters is given by

$$\begin{aligned} H_k(z) &= H_{a0}(z^{2L})\sum_{i=0}^{K-1} z^{-i}W_K^{-ki}E_{Ai}(z^K) \\ &\quad + (-1)^k z^{-L}H_{a1}(z^{2L})\sum_{i=0}^{K-1} z^{-i}W_K^{-ki}E_{Bi}(z^K) \end{aligned} \tag{6.18}$$

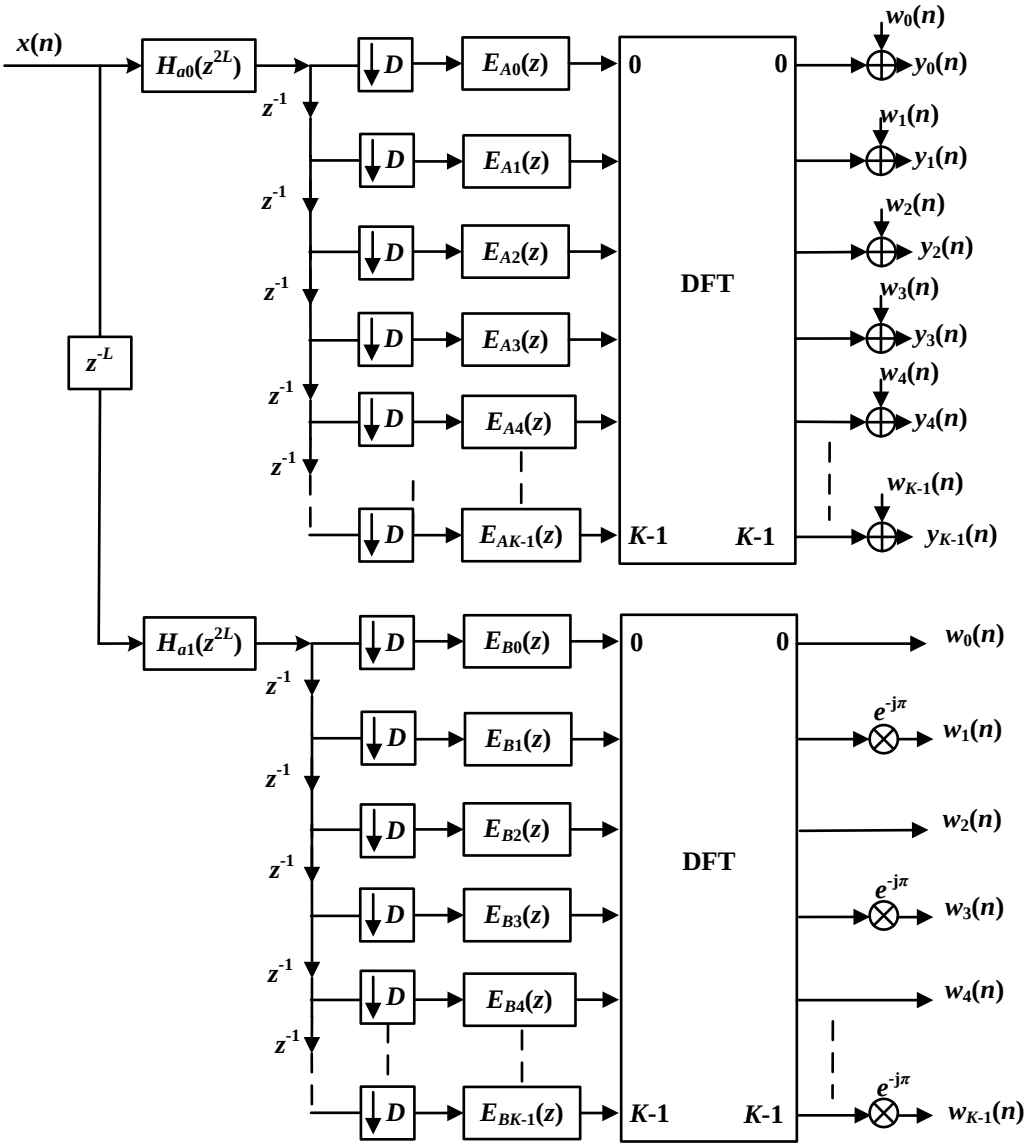

Figure 6.2 The GDFT-FB using full FRM.

For the outputs with odd indexes (k=1,2,…, K-1) there is a phase difference of π rad between the two polyphase components expressed in (6.18). Therefore, a phase rotation must be applied to the second component beforehand so that it can be added in phase with the first component in the filter bank outputs. The resulting FRM DFT-FB structure is shown in Figure 6.2.

To design the base and masking filters, the expressions in Table 3.2 are used. Given the desired passband and stopband cut-off for the prototype filter (ω_p and ω_s), the interpolation value must be selected in such a way that the transition band of the base filter (between θ and ϕ) includes the normalized frequency π/2

rad. Hence, the choice of the interpolation factor needs to comply with the following two cases

$$\begin{aligned} &\text{Case 1: } L = (4m+1)\frac{K}{2} \\ &\text{Case 2: } L = (4m-1)\frac{K}{2} \end{aligned} \tag{6.19}$$

where m is any integer equal or bigger than 1.

6.3.2 The narrowband FRM GDFT-FB (even-stacked)

Apart from the application of the full FRM structure to CMFBs, some research has been mainly focused on the application of only the narrowband FRM to CMFBs [113, 202-204]. In this work, the main reason for only applying the narrowband FRM is the objective of minimizing the CMFB filter orders and the amount of parameters to be optimized to achieve perfect reconstruction. Therefore, a reduction in the computational load is not achieved for all the cases. In addition, unlike the research on full FRM applied to CMFBs [205-206, 210], the special class of FRM is not applied to the narrowband FRM CMFB designs.

Unlike in [113, 202-204] for FRM CMFB, and following the design line from Section 6.3.1, in this section a novel application of narrowband FRM to even-stacked GDFT-FB is presented using the special class of FRM.

If only the positive branch is used, then (6.14) is simplified to

$$A(z) = B(z) = H_{Ma}(z) \tag{6.20}$$

Therefore, the prototype filter, the polyphase decomposition of the masking filter element and the modulated bandpass filters are given by

$$H(z) = H_{a0}(z^{2L})H_{Ma}(z) + z^{-L}H_{a1}(z^{2L})H_{Ma}(z) \tag{6.21}$$

$$H_{Ma}(z) = \sum_{i=0}^{K-1} z^{-i} E_{Mai}(z^K) \tag{6.22}$$

$$H_k(z) = H_{a0}(z^{2L})\sum_{i=0}^{K-1} z^{-i} W_K^{-ki} E_{Mai}(z^K) + (-1)^k z^{-L} H_{a1}(z^{2L})\sum_{i=0}^{K-1} z^{-i} W_K^{-ki} E_{Mai}(z^K) \quad (6.23)$$

As shown in Section 3.4.4, for narrowband FRM the transition band is purely given by the first image of the interpolated base filter frequency response. Therefore, there is only one possible value for the interpolation factor that complies with the constraint of including the π/2 rad frequency in the interpolated filter transition band imposed in Section 6.1.

$$L = \frac{K}{2} \quad (6.24)$$

Consequently, only the specifications for the base filter and one of the masking filters need to be calculated according using Table 3.2. Furthermore, from (6.23), it should be clear that filter bank must be implemented using the same basic structure as that for the full FRM case (Figure 6.2).

6.3.3 The odd-stacked FRM GDFT-FB

In Section 6.3.1 and Section 6.3.2 FRM and narrowband FRM were applied to an even-stacked GDFT-FB. Similar techniques can be applied to the GDFT-FB to achieve odd-stacked sub-band allocation (as in Figure 4.6). Previous research on FRM CMFBs does not look at the differences between even and odd sub-band configurations. However, the importance of distinguishing between even-stacked and odd-stacked is that the latter generally uses complex filters instead of real filters. Therefore, as it was seen from the computational load equations for the GDFT-FB structures in Chapter 4 and Chapter 5, odd-stacked designs require a larger number of operations than even-stacked ones.

Odd-stacked sub-band allocation in the FRM GDFT-FB is achieved by applying the modulation given by (4.13) to (6.16), yielding

$$\begin{aligned} A_k(z) &= A(zW_K^{(k+\frac{1}{2})}) \\ B_k(z) &= B(zW_K^{(k+\frac{1}{2})}) \end{aligned} \quad (6.25)$$

Similar to the masking filter, the base filter frequency response becomes odd staked by shifting its frequency response from DC to π/2. As a result, (6.18) is modified now for the odd stacked case

$$\begin{aligned} H_k(z) = H_{a0}(z^{2L}) e_K^{-j\frac{\pi}{2}} \sum_{i=0}^{K-1} z^{-i} W_K^{-\frac{1}{2}i} W_K^{-ki} E_{Ai}(z^K) \\ +(-1)^k z^{-L} H_{a1} e_K^{-j\frac{\pi}{2}} (z^{2L}) \sum_{i=0}^{K-1} z^{-i} W_K^{-\frac{1}{2}i} W_K^{-ki} E_{Bi}(z^K) \end{aligned} \tag{6.26}$$

Using the same approach the expression which represents the odd-stacked narrowband FRM GDFT-FB can be derived from (6.23), as

$$\begin{aligned} H_k(z) = H_{a0}(z^{2L} e^{-j\frac{\pi}{2}}) \sum_{i=0}^{K-1} z^{-i} W_K^{-ki} W_K^{-\frac{1}{2}i} E_{Mai}(z^K) \\ +(-1)^k z^{-L} H_{a1}(z^{2L} e^{-j\frac{\pi}{2}}) \sum_{i=0}^{K-1} z^{-i} W_K^{-ki} W_K^{-\frac{1}{2}i} E_{Mai}(z^K) \end{aligned} \tag{6.27}$$

The odd-stacked FRM GDFT-FB block diagram is the same as in Figure 6.2, with the difference that the DFT-FBs are replaced by the GDFT-FB structure in Figure 4.7 and the base filter is a complex filter instead of a real filter.

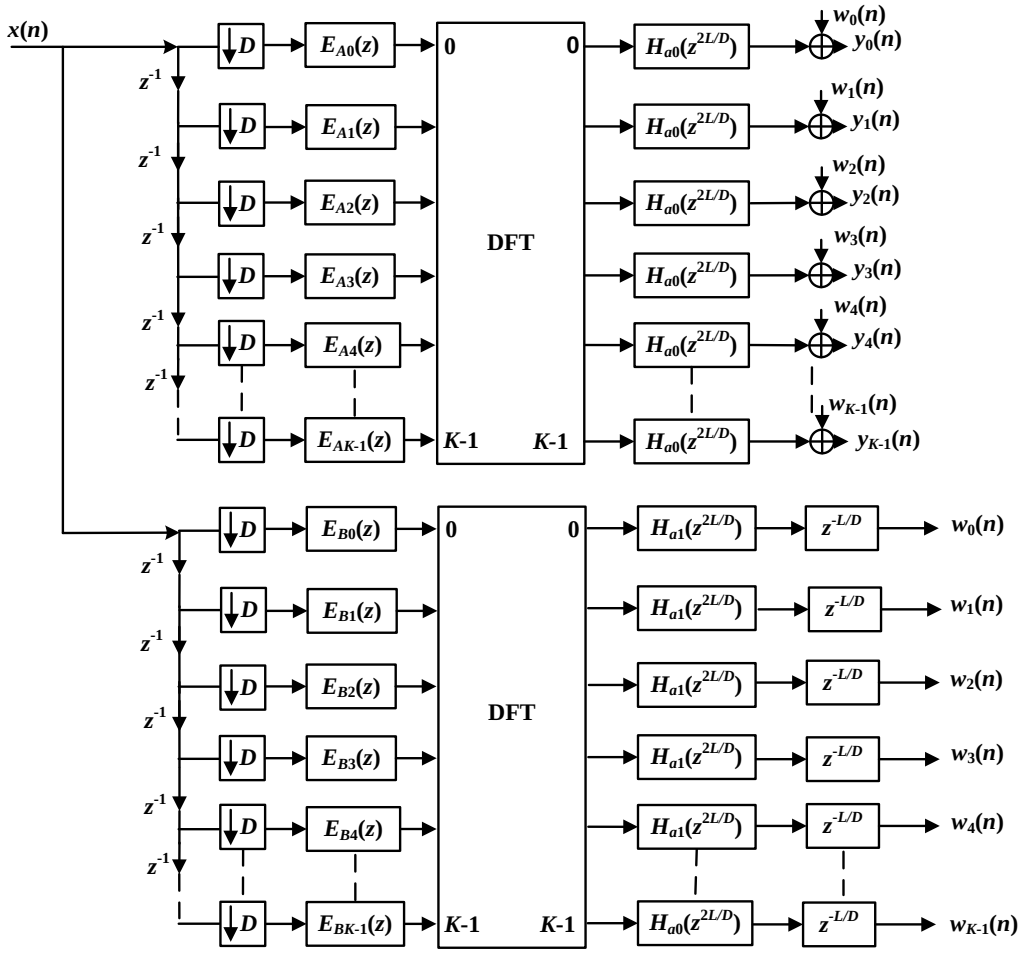

Figure 6.3 Alternative structure for oversampled FRM GDFT-FB.

6.3.4 Alternative structure for the oversampled FRM GDFT-FB

Probably the most attractive property of modulated filter banks is the ability to carry out the filtering operations at a lower sample rate than conventional filters. This is achieved by means of the polyphase decomposition and the noble identities [107]. In the basic FRM GDFT-FB (described in Section 6.3.1), the base filter is allocated before the modulated GDFT-FB structure. As a consequence, its filtering operations are carried out at a much higher rate than the masking filter operations. In addition, for a large number of channels K, the base filter interpolation factor, which must comply with (6.19), requires large zero padding and delay in the base filter polyphase components.

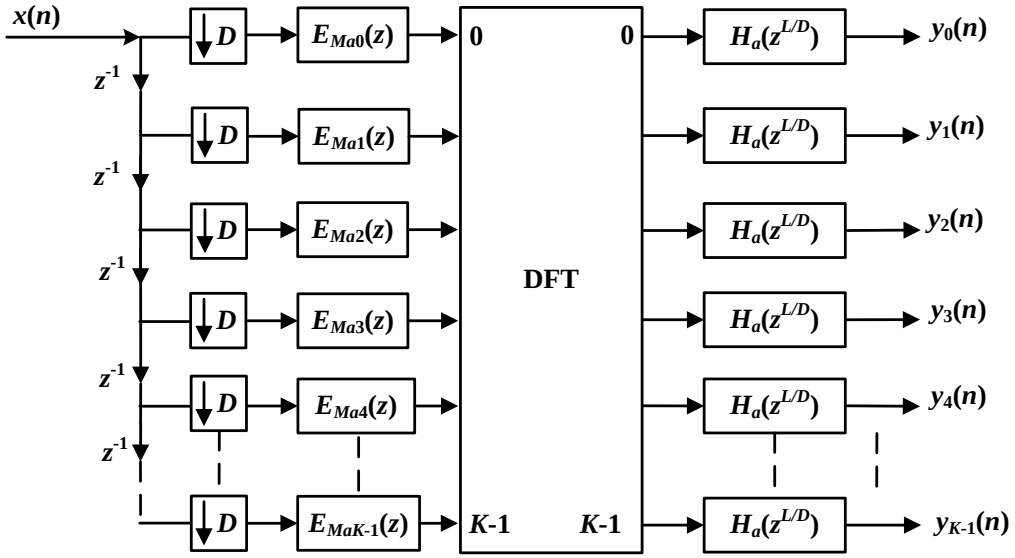

Figure 6.4 Efficient oversampled narrowband FRM GDFT-FB.

As an alternative to the basic FRM GDFT-FB structure the base filter can instead be commuted to the lower sample rate output side of the filter bank using the noble identities as shown in Figure 6.3. [205-206] use the same approach for FRM CMFBs. In addition to performing the base filter operations at the lowest sample rate, the interpolation factor applied to the base filter is reduced by a factor equal to the decimation, thereby reducing the zero padding and the system delay. Although more instances of the base filter are required to be applied to each GDFT-FB output, this has some benefits like the fact that these filters will be always real filters for both the even and odd-stacked configurations. This differs from the odd-stacked case in Section 6.3.3 where the base filter was required to be complex.

For the alternative FRM GDFT-FB to work, the filter bank must be oversampled ($K = L_{DFT}D$). Furthermore, the oversampling factor is constrained to be an even number.

If an oversampled filter bank configuration is considered ($K=L_{DFT}D$) an alternative structure can be proposed for the FRM DFT-FB and FRM GDFT-FB, as it is shown in Figure 6.3. For this special case, the oversampled factor is limited to have an even value, thus the base filter interpolation factor ($2L/D$) and the complementary the delays equal to L/D are integer numbers. The critically decimated case or odd oversampling factor values would lead to non-integer

interpolation factors for the base filter, which would not allow the structure in Figure 6.3.

For the narrowband FRM case, this structure can be simplified leading to a yet more efficient system as shown in Figure 6.4. In this variant, the polyphase decomposition of the base filter is avoided, so an interpolated version of the base filter can be used directly. In addition, since the base filter is not divided into polyphase components symmetry in its coefficients can be exploited to reduce the number of multiplications required.

6.4 Computational load analysis

For the basic FRM GDFT-FB (as depicted in Figure 6.2) the computational load is determined similarly to the GDFT-FB (see Section 4.3.3) by the same kind of expression than for the classic GDT-FB. The difference is that in this case the load is composed of a contribution which depends on the base filter order (N_A) combined with to GDFT-FB loads which depend on the masking filter order (N_{MA}) rather than the prototype filter order. Table 6.1 shows the resulting loads for both the full and narrowband FRM GDFT-FB in even and odd-stacked configurations.

Table 6.1 Number of real multiplications and real additions per input sample for FRM GDFT-FB (Figure 6.2).

	Sub-band stacking	Number of real multiplications and real additions
μ	Even	$(N_A+1)+\frac{L_{DFT}}{K}\left[4\left(N_{MA}+1\right)+3K\left(\log_2\left(K\right)-5\right)+16\right]$
	Odd	$2(N_A+1)+\frac{L_{DFT}}{K}\left[8\left(N_{MA}+1\right)+3K\left(\log_2\left(K\right)-5\right)+16+8K\right]$
α	Even	$(N_A-1)+\frac{L_{DFT}}{K}\left[4\left(N_{MA}+1-K\right)+7K(\log_2(K)-5)+16+2K\right]$
	Odd	$2N_A+\frac{L_{DFT}}{K}\left[8\left(N_{MA}+1-\frac{K}{2}\right)+7K(\log_2(K)-5)+16+6K\right]$

Table 6.2 Number of real multiplications and real additions per input sample for alternative full FRM GDFT-FB (Figure 6.3).

	Sub-band stacking	Number of real multiplications and real additions
μ	Even	$\frac{L_{DFT}}{K}\left[4\left(N_{MA}+1\right)+3K\left(\log_2\left(K\right)-5\right)+16+K(N_A+1)\right]$
	Odd	$\frac{L_{DFT}}{K}\left[8\left(N_{MA}+1\right)+3K\left(\log_2\left(K\right)-5\right)+16+4K+K(N_A+1)\right]$
α	Even	$\frac{L_{DFT}}{K}\left[4\left(N_{MA}+1-K\right)+7K(\log_2(K)-5)+16+KN_A\right]$
	Odd	$\frac{L_{DFT}}{K}\left[8\left(N_{MA}+1-\frac{K}{2}\right)+7K(\log_2(K)-5)+16+4K+KN_A\right]$

Table 6.3 Number of real multiplications and real additions per input sample for alternative narrowband FRM GDFT-FB (Figure 6.4).

	Sub-band stacking	Number of real multiplications and real additions
μ	Even	$\frac{L_{DFT}}{K}\left[2\left(N_{MA}+1\right)+\frac{3K}{2}\left(\log_2\left(K\right)-5\right)+8+K\frac{(N_A+1)}{2}\right]$
	Odd	$\frac{L_{DFT}}{K}\left[4\left(N_{MA}+1\right)+\frac{3K}{2}\left(\log_2\left(K\right)-5\right)+8+4K+K\frac{(N_A+1)}{2}\right]$
α	Even	$\frac{L_{DFT}}{K}\left[2\left(N_{MA}+1-K\right)+\frac{7K}{2}(\log_2(K)-5)+8+KN_A\right]$
	Odd	$\frac{L_{DFT}}{K}\left[4\left(N_{MA}+1-\frac{K}{2}\right)+\frac{7K}{2}(\log_2(K)-5)+8+2K+KN_A\right]$

For the alternative FRM GDFT-FB structure proposed for oversampled designs, the full and narrowband variants do not share the same expressions.

Table 6.2 shows the loads for the alternative full FRM GDFT-FB (Figure 6.3) and Table 6.3 shows the equivalent loads for the alternative narrowband FRM GDFT-FB (Figure 6.4).

The performance of the FRM GDFT-FBs case was evaluated using the TETRA V&D and TEDS use case 1 described in Section 4.4.3.1. Consequently the FRM GDFT-FB performance could be compared with those of the other methods evaluated in Chapters 4 and 5.

To implement the prototype filter for the FRM GDFT-FBs, the base and making filters need to be designed. In this case, the various filter specifications (and consequently the orders) depend on the chosen interpolation factor *L*. According to (6.19), for every value of the variable *m*, the interpolation factor *L* will get a different value depending on wether the prototype filter transition band will be implemented by the base or complementary filter and hence whether the FRM design follows the case 1 procedure or case 2 procedure respectively (see Section 3.4.4).

For every value of *L*, the filter specifications are determined by the expressions in Table 3.2. Some values of *m* (and consequently of *L*) can lead to non-real frequency specifications in the filter process design for either the base or complementary filters, and those values of *m* and *L* have to be discarded. This can be seen in Appendix C (Table C.1 to Table C.4) where the FRM GDFT-FB design frequencies for the different filters are presented for values of *m* between 1 and 5.

According to the base and masking filter specifications expressed in Table C.1-Table C.4 the filter orders were calculated. In general, if the value of *L* increases, the order of the masking filters also increases while the order of the base filter decreases. However, the increased rate of the masking filter order is much bigger than the decreased rate of the base filter order. Therefore a bigger computational load is required for bigger values of *L*. On the other hand, for a given value of *m*, design case 2 leads to smaller masking filters than case 1 and therefore lower computation. For example, for the TEDS 50 kHz 128 sub-bands channelizer required by the P-GDFT in use case 1 (see Table A.4), by using the case 2, the interpolation factor obtained is equal to $L = 192$ ($m=1$). Using the TEDS 50 kHz prototype channel specifications from Table 4.4, the passband and stopband cut-off frequencies can be calculated by applying the equations in Table 3.2. To calculate the order of the base and masking filters, Kaiser equation (3.8) was used to obtain an order equal to 20 for the base filter and an order equal to 971 for the masking filters [102].

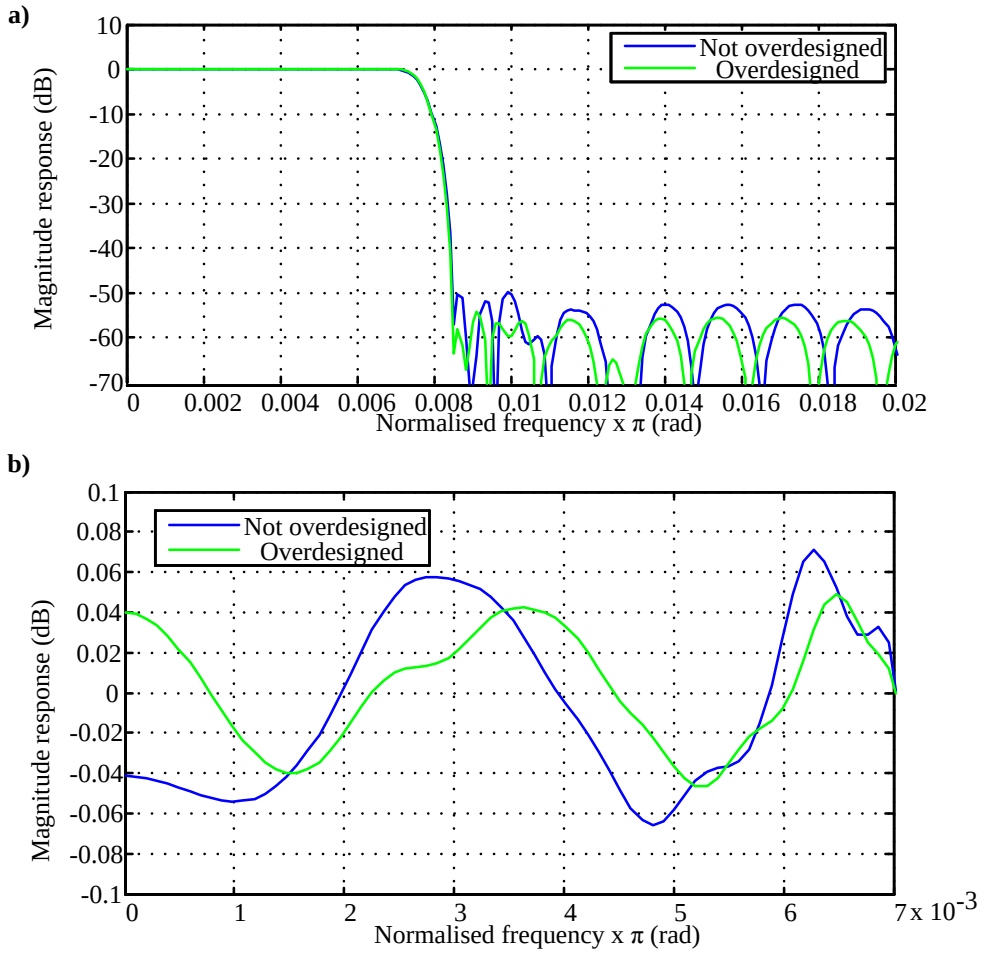

Figure 6.5 TEDS 50 kHz prototype filter for a 128 sub-bands channelizer implemented by an FRM GDFT-FB with both uncorrected and overdesigned specifications, a) complete magnitude response, b) passband magnitude response. designed using FRM GDFT-FB for a 128 channel channelizer both theoretical and with overdesigned methods.

In FRM designs, passband and stopband ripples from the individual base and masking filter frequency responses both contribute to the final composite frequency response. Because of this the passband and stopband specifications for the base and masking filters must be more stringent than the final filter. According to [150], a good approximation is to make the passband and stopband ripple specifications 20% more stringent for the base filter passband and stopband, and for the masking filter passband. For the masking, a 50% more stringent specification of the filter stopband specification is recommended. The difference between the theoretical values for the filter order with the normal specifications and increased specifications are shown in Figure 6.5 and Figure 6.6.

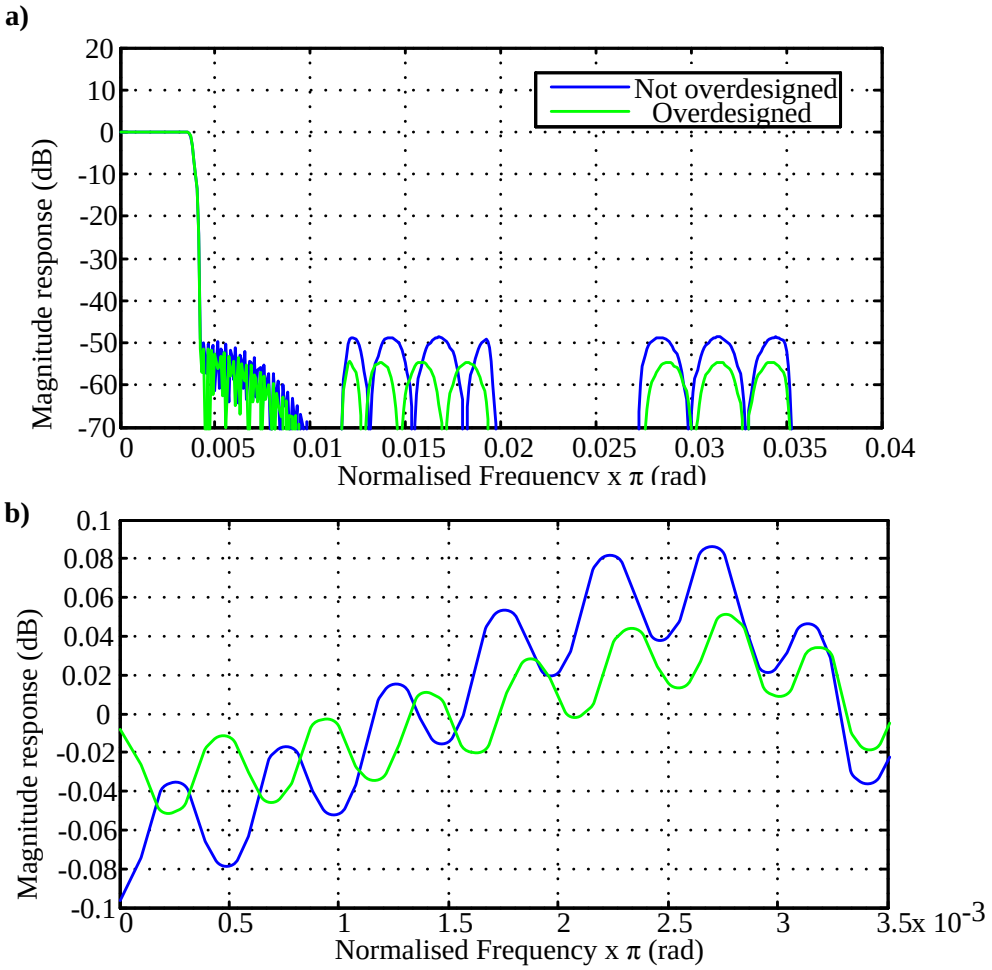

Figure 6.6 TETRA V&D 25 kHz prototype filter for a 256 sub-bands channelizer implemented by a narrowband FRM GDFT-FB with both uncorrected and overdesigned specifications. a) Complete magnitude response, b) passband magnitude response.

In both figures it can be seen that the δ_p = 0.1 dB and δ_s = 55 dB requirements previously established for the TETRA V&D and TEDS standards prototype filters are not met by the theoretical design. However, the overdesigned filters yield a composite response which complies with the passband and stopband ripple specifications. The TEDS 50 kHz prototype filter is implemented using the full FRM GDFT-FB structure. As it was seen in Chapter 5 for the multi-stage designs, in here also the cascading of the base and masking filters produces non-uniform ripples in the passband of the frequency response, even though the individual filters were designed using the FIR Remez equiripple algorithm.

Table 6.4 Filter orders calculated for the base and masking filters of FRM GDFT-FB applied to TETRA V&D and TEDS uniform channelizers.

		FRM GDFT-FB			
Standard	Number of sub-bands	GDFT-FB	Interpolation factor	Filter orders	Percentage of coefficients
TETRA V&D	K= 256	N=8085	L=384	N_A=24; N_{MA}=2043	50.83%
TEDS 50 kHz	K=128	N=3584	L=192	N_A=22; N_{MA}=1022	56.21%
TEDS 100 kHz	K=64	N=1444	L=96	N_A=16; N_{MA}=511	71.88%

Considering the parameters obtained in Appendix C (Table C.1-Table C.4) and the overdesign requirements, the filter orders and interpolation factors necessary for all the filters required for the use case 1 are summarized in Table 6.4. The last column refers to the number of non-zero coefficients that the FRM GDFT-FB requires compared to the GDFT-FB. This number is obtained considering that in this full FRM structure there is one base filter and two masking filters with the same order.

For the narrowband FRM GDFT-FB where only the positive branch of the FRM structure is used, there is only one possibility for the value of L which is given by (6.24). Again the base and masking filter specifications must be overdesigned in order to meet the specifications for the final composite response (as shown for the TETRA V&D 25 kHz example in Figure 6.6). Table 6.5 presents the interpolation factors and filter orders required for all configurations considering the overdesign requirements. Like Table 6.4, the number of non-zero coefficients in relation to the legacy GDFT-FB is shown. Comparing Table 6.4 and Table 6.5, it is clear that the narrowband FRM GDFT-FB requires significantly fewer filter coefficients than the full FRM GDFT-FB for the specific design cases considered here. This is relevant because lower filter orders mean filters that are easier to physically implement.

Table 6.5 Filter orders calculated for the base of masking filter of a narrowband FRM GDFT-FB applied to TETRA V&D and TEDS uniform channelizers.

		FRM GDFT-FB			
Standard	Number of sub-bands	GDFT-FB	Interpolation factor	Filter orders	Percentage of coefficients
TETRA V&D	K= 256	N=8085	L=128	N_A=68; N_{MA}=681	9.26%
TEDS 50 kHz	K=128	N=3584	L=64	N_A=62; N_{MA}=341	10.97%
TEDS 100 kHz	K=64	N=1444	L=32	N_A=48; N_{MA}=171	15.17%

When the number of operations is considered, the results depend on the interpolation factor employed in the filter bank (L_{DFT}) and the FRM GDFT-FB architecture applied. For the critically decimated FRM GDFT-FB (L_{DFT}=1) only the structure presented in Figure 6.2 can be applied. On the other hand, when the channelizer is oversampled (L_{DFT}>1) either the structure in Figure 6.2 or Figure 6.3 can be used. The particular case of oversampled and narrowband FRM GDFT-FB can benefit from the reduced structure in Figure 6.4.

Figure 6.7 shows the results for the computational load of the different FRM GDFT-FB structures employed as uniform channelizers for the standards used in use case 1. First, in Figure 6.7a, an odd-stacked critically decimated configuration is studied. From the results, it can be seen how the full FRM GDFT-FB requires slightly more operations than the direct GDFT-FB approach. However, the narrowband performance requires a more significant number of multiplications than the full FRM GDFT-FB and the GDFT-FB. The reason for this is the higher order of the base filter in the narrowband case with respect to the full FRM (even though the narrowband case requires significantly less overall coefficients as seen in Table 6.5). For the structure in Figure 6.2 the base filter performs at the highest sample rate whereas in the structures of Figure 6.3 and Figure 6.4 it performs at the same sample rate that the filter bank but several instances are required (one per filter bank sub-band output). Therefore, from experimental results, it was demonstrated that small increments in the base filter order represent considerable increments in the computational load.

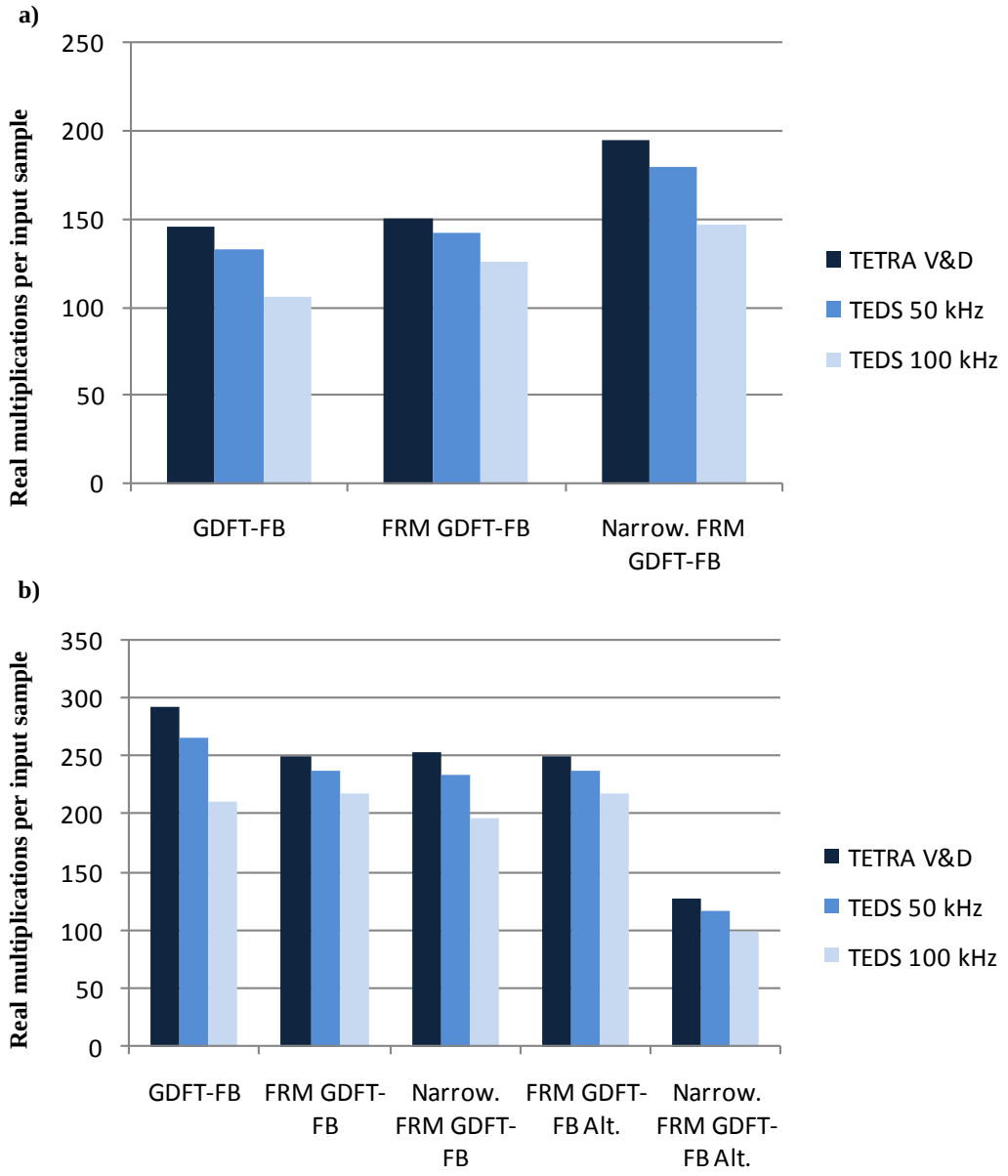

Figure 6.7 Computational load comparison between the different uniform odd-stacked FRM GDFT-FB channelizers for the standards included in use case 1, a) for critically decimated configuration, b) for oversampling

Second, in Figure 6.7b, the odd-stacked oversampled configuration is analysed. For this oversampled situation, it can be observed how all the uniform FRM GDFT-FB structures require fewer operations than the GDFT-FB. Especially, the efficient oversampled narrowband FRM GDFT-FB structure from Figure 6.4, which requires roughly 50% less multiplications than the GDFT-FB and the rest of FRM GDFT-FB designs. Even when compared with the critically

decimated case, the oversampled narrowband FRM GDFT-FB requires fewer multiplications than its critically decimated version, and even slightly less than the GDFT-FB. However, this last case might not always be true, as it can be seen in the tables Appendix C for the even-stacked case. The complete computational load study for the structures in Figure 6.4 can be found from Table C.5 to Table C.7 in Appendix C.

6.5 Recursive FRM GDFT-FB

Recursive FRM filtering structures have been also applied to FRM CMFB designs to further reduce the number of filter coefficients required [113]. The recursive structure consists of a second FRM structure applied to the base filter itself. However, the increased complexity of the design makes it tedious to implement for the full FRM GDFT-FB.

In the narrow band FRM GDFT-FB, for the Recursive FRM GDFT-FB (C-FRM GDFT) the FRM structure is modified by the addition of a second base filter as shown in Figure 6.8a.

The first base filter remains unchanged from the normal design since it will be responsible of the final frequency response transition band. The second base filter assists the masking filter to eliminate unwanted images created by interpolating the first base filter. The second base filter's interpolation factor, *L'*, is smaller than *L*. The resulting action of the first two filters is to relax the specification of the masking filter, thereby reducing its order. The three filtering stages are depicted in Figure 6.8b.

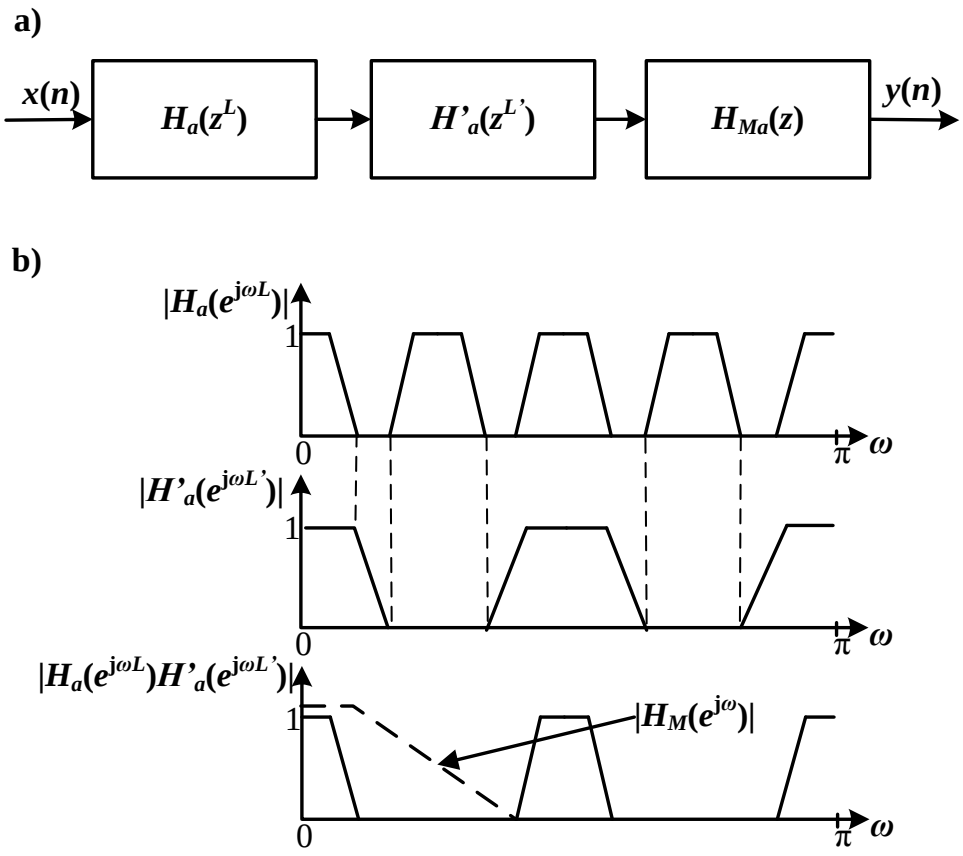

Figure 6.8 C-FRM GDFT, a) structure, b) filtering operations.

The design specifications for the three filters are given by:

$$\begin{aligned}
\theta &= \omega_p L \\
\phi &= \omega_s L \\
\theta' &= \omega_p L' \\
\phi' &= \left(\frac{2\pi}{L} - \omega_s\right) L' \\
\omega_{Mpa} &= \omega_p \\
\omega_{Msa} &= \frac{2\pi}{L'} - \left(\frac{2\pi}{L} - \omega_s\right)
\end{aligned} \tag{6.28}$$

This structure can be integrated into the basic and alternative narrowband FRM GDFT-FBs already described. By adding the second base filter, the models in Figure 6.2 and Figure 6.4 are modified to yield those in Figure 6.9 and Figure 6.10 for critically decimated and oversampled designs respectively.

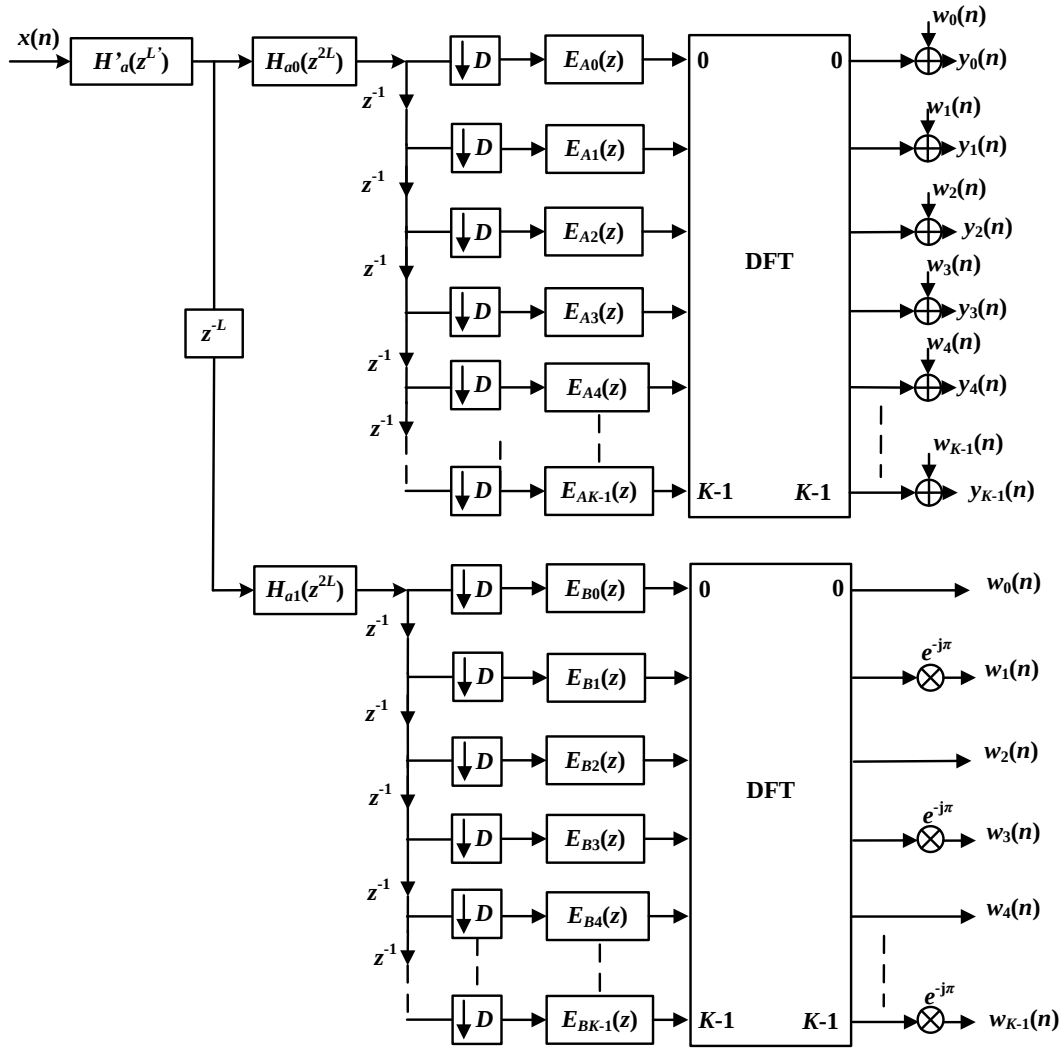

Figure 6.9 Critically decimated C-FRM GDFT.

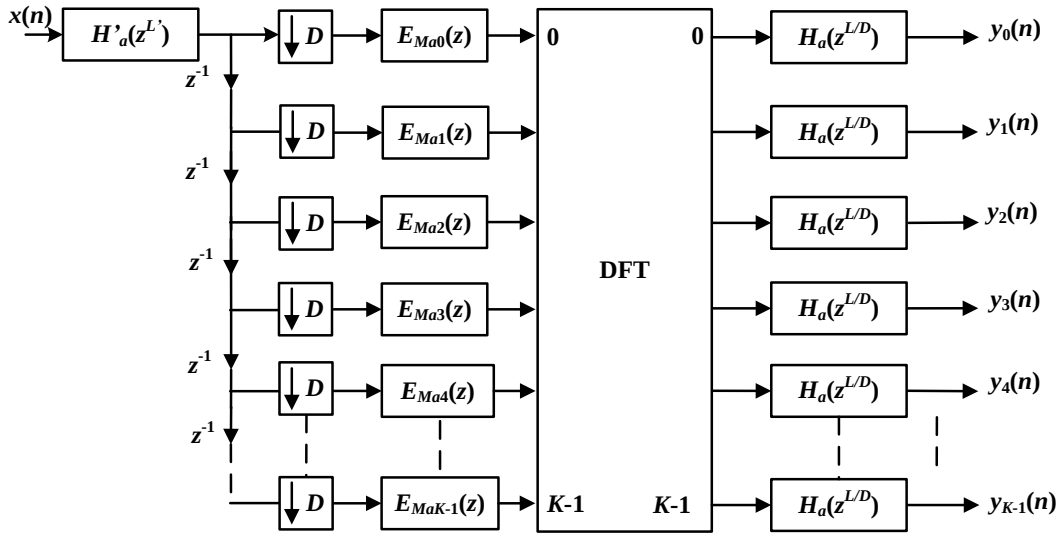

Figure 6.10 Oversampled C-FRM GDFT.

Table 6.6 Number of real multiplications and real additions per input sample for oversampled C-FRM GDFT (Figure 6.10).

	Sub-band stacking	Number of real multiplications and real additions
μ	Even	$(N'_A+1)+\frac{L_{DFT}}{K}\left[2\left(N_{MA}+1\right)+\frac{3K}{2}\left(\log_2\left(K\right)-5\right)+8+K\frac{(N_A+1)}{2}\right]$
	Odd	$2(N'_A+1)+\frac{L_{DFT}}{K}\left[4\left(N_{MA}+1\right)+\frac{3K}{2}\left(\log_2\left(K\right)-5\right)+8+4K+K\frac{(N_A+1)}{2}\right]$
α	Even	$2N'_A+\frac{L_{DFT}}{K}\left[2\left(N_{MA}+1-K\right)+\frac{7K}{2}(\log_2(K)-5)+8+KN_A\right]$
	Odd	$4(N'_A+\frac{1}{2})+\frac{L_{DFT}}{K}\left[4\left(N_{MA}+1-\frac{K}{2}\right)+\frac{7K}{2}(\log_2(K)-5)+8+2K+KN_A\right]$

Table 6.7 Design example of 256 sub-bands TETRA 25 kHz odd-stacked oversampled C-FRM GDFT.

Channelizer	Number of channels	Interpolation factor/s	Filters orders	Number of non-zero coefficients	μ
GDFT-FB	K= 256	-	N=8085	8085 (100%)	292.4 (100%)
FRM GDFT-FB	K=256	L=128	N_A=68 N_{MA}=681	749 (9.3%)	126.3 (43.2%)
	K=256	L=128 L'=16	N_A=68 N_A'=43 N_{MA}=49	130 (2 %)	214.31 (73.3%)
Recursive FRM GDFT-FB	K=256	L=128 L'=32	N_A=68 N_A'=22 N_{MA}=112	202 (2.5%)	154.5 (52.8%)
	K=256	L=128 L'=64	N_A=68 N_A'=12 N_{MA}=328	408 (5.1%)	141.28 (48.3%)

In the case of the alternative FRM GDFT-FB, it is worth noting that the second base filter can not be allocated after the analysis bank, because the interpolation factor L' is smaller than L, and therefore smaller than $2\times D$. As a consequence, the second base filter must run at the highest sample rate (as it does in the basic FRM GDFT-FB). Nevertheless, the structure of Figure 6.10 still has a lower computational load than the structure in Figure 6.9. The number of operations is obtained by adding the contribution of

the second base filter to the expressions in Table 6.1 and Table 6.3. Table 6.6 presents the resulting computational load for the most efficient design.

The recursive narrowband FRM GDFT-FB was applied to the design example of a TETRA 25 kHz channelizer and the results in Table 6.7 were obtained. From the third column it can be observed that the number of non-zero coefficients is reduced even further than in the single-stage FRM GDFT-FB and as much as almost 98 % relative to the GDFT-FB for this particular example.

For all the structures in Table 6.7 an odd-stacked oversampled scenario was considered, therefore the alternative narrowband FRM GDFT-FM (Figure 6.3) and alternative narrowband FRM GDFT-FB (Figure 6.10) structures were compared. Considering the number of real multiplications per input sample, the C-FRM GDFT still performs better than the GDFT-FB, but worse than the single-stage FRM GDFT-FB. This is a consequence of the bigger weight that the base filters have on the computational load compared to the masking filters. In the recursive case, the order of the masking filter is reduced dramatically, but the first base filter stays the same and a new base filter is added, which leads to a larger number of operations. Similar results are obtained in [203] when the recursive narrow band FRM is applied to CMFBs.

6.6 Multi-stage narrowband FRM GDFT-FB

Similar to the approach taken in Chapter 5, multi-stage filtering techniques can be used to reduce the order of the prototype filter, or in this case, the FRM implementation of the prototype filter in the FRM GDFT-FB. As in Chapter 5, the prototype filter specification is relaxed by increasing its transition band to include parts of the adjacent channels. Thereafter, a second stage comprising half-band filters at the filter bank output eliminates the extra undesired signal, leaving just the desired frequency band. Figure 6.11 shows this Multi-stage variant of the alternative FRM GDFT-FB (M-FRM GDFT). In Chapter 5 the necessity of the uniform channelizer to use an oversampled configuration ($L_{DFT} = 2$ more concretely) in order to be able to use the half-band filters at the outputs was explained. Then, since this also applies to the FRM GDFT-FB case,

the alternative narrowband FRM GDFT-FB represents the most efficient implementation by which to apply it.

Because the prototype filter passband includes parts of the adjacent channels the filter bank must be oversampled, as in [211]. The base and masking filters are designed in accordance with Table 3.2, but in this case the passband and stopband cut-off frequencies are chosen as $\omega_p = \pi/K$ and $\omega_s = 2\pi/K$. The contribution of the half-band filters (acting as shown in Figure 5.7) ensures that the final cut-off frequency and transition band of the composite response is as required. In terms of computational load, the operations required by the half-band filters have to be added to the FRM GDFT-FB. The number of real multiplications and additions per input sample for the M-FRM GDFT is given in Table 6.8 where N_B represents the half-band filter order.

To compare both C-FRM GDFT and M-FRM GDFT designs with the basic FRM GDFT-FB and GDFT-FB, the same TETRA V&D 25 kHz channels uniform channelizer from use case 1 (Section 4.4.3.1) was used. In all designs a K=256 analysis bank is necessary to extract the 200 possible TETRA 25 kHz channels from the 5 MHz frequency band. In the multi-stage FRM GDFT-FB, the fact that the number of occupied information channels is less than the number of filter bank sub-bands means that it is not necessary to add half-band filters to these outputs. This results in a computational saving which is not available in the other designs.

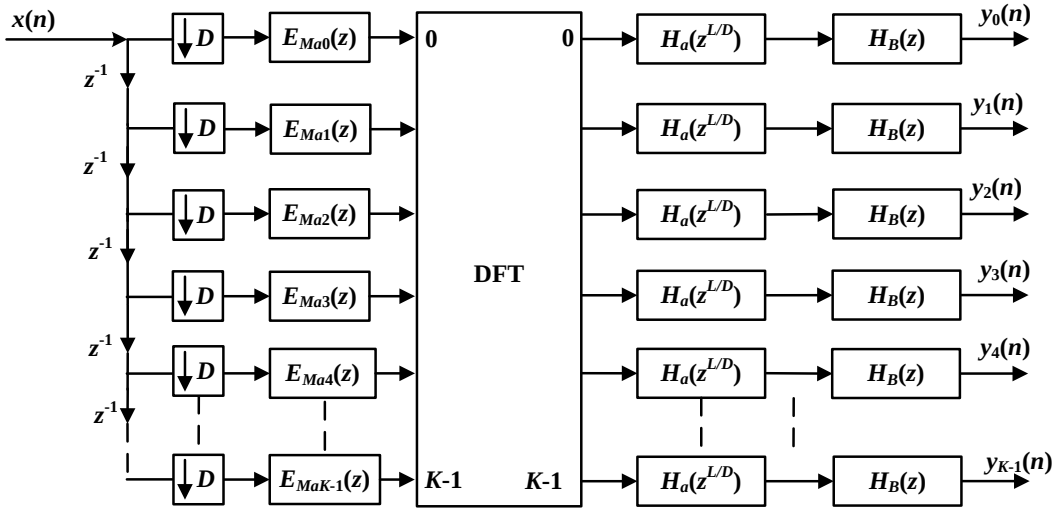

Figure 6.11 M-FRM GDFT channelizer with half-band filters.

Table 6.8 Comparison of uniform GDFT-FB designs for a K=256 channel TETRA 25 kHz channelizer.

Channelizer	Number of channels	Interpolation factor/s	Filters orders	Number of non-zero coefficients	μ
GDFT-FB	K= 256	-	N=8085	8085 (100%)	292.4 (100%)
FRM GDFT-FB	K=256	L=128	N_A=68 N_{MA}=681	749 (9.3%)	126.3 (43.2%)
C-FRM GDFT	K=256	L=128 L'=32	N_A=68 N_A'=22 N_{MA}=112	202 (2.5%)	154.5 (52.8%)
M-FRM GDFT	K=256	L=128	N_A=12 N_{MA}=1362 N_B=64	1438 (17.8%)	117 (40%)

As it was done in Section 6.5 for the recursive case, Table 6.8 compares the four different methods for an oversampled and odd-stacked configuration. It can be seen that the order of the M-FRM GDFT base filter was reduced relative to that of the other FRM GDFT-FB designs. These results from the relaxation of the base filter specifications in the multi-stage design. However, this increase in the base filter transition band implies that the images produced by interpolation are closer to each other than before. For this reason, the masking filter requires a sharper transition band to extract the lowpass image (while filtering out other images), and consequently must be of higher order. In total, the number of non-zero coefficients is still small compared to the GDFT-FB, but it is higher than the other FRM GDFT-FB methods.

Table 6.8 also shows that the M-FRM GDFT has the lowest number of multiplications per input sample. In the previous case for the C-FRM GDFT it was noted that the base filter order has a bigger influence on the channelizer computational load than that of the masking filter. In the multi-stage case the base filter order is reduced relative to the other FRM designs and this has a bigger influence on the computational load, despite the increase in the masking filter order and the addition of the half-band filters.

A combination of the two methods, recursive and multi-stage, could be also attempted for further reductions. For the particular design example used in Table 6.8, their combination has been experimentally proven not to lead to any further saving in the number of non-zero coefficients or the number of operations per input sample.

6.6.1 Recursive and multi-stage FRM GDFT-FB design example

The application of the recursive and multi-stage FRMGDFT-FB structures is demonstrated with an eight-channel example based on the TETRA V&D standard. Since an oversampled configuration ($L_{DFT} = 2$) is required for the multi-stage design, both recursive and multi-stage uniform channelizers are designed as oversampled to compare their output frequency responses.

For the recursive design, the filter orders are calculated in accordance with the FRM structure overdesign requirements in Section 6.4. The filter orders obtained are N_A=68, N'_A=12, and N_{MA}=22. In this case, the passband and stopband specifications (δ_p=0.1 dB and δ_s=55 dB) are met at the channelizer outputs.

The M-FRM GDFT design for the same prototype filter requires filter orders of N_A=12, N_{MA}=44, and N_B=64. In this case, the desired output filtering specifications are not achieved with these filter orders (similar to the multi-stage design in Chapter 5), and, therefore an increase in the half-band filter order to N_B=70 is necessary.

The frequency response of the sub-band outputs of both channelizers are shown in Figure 6.12. Both designs have a similar frequency response in the passband and transition band, but the multi-stage design provides more attenuation in the stopband due to the half-band filter at the FRM GDFT-FB outputs. It is clear that the passband ripple of both designs is within the maximum peak-to-peak ripple limit.

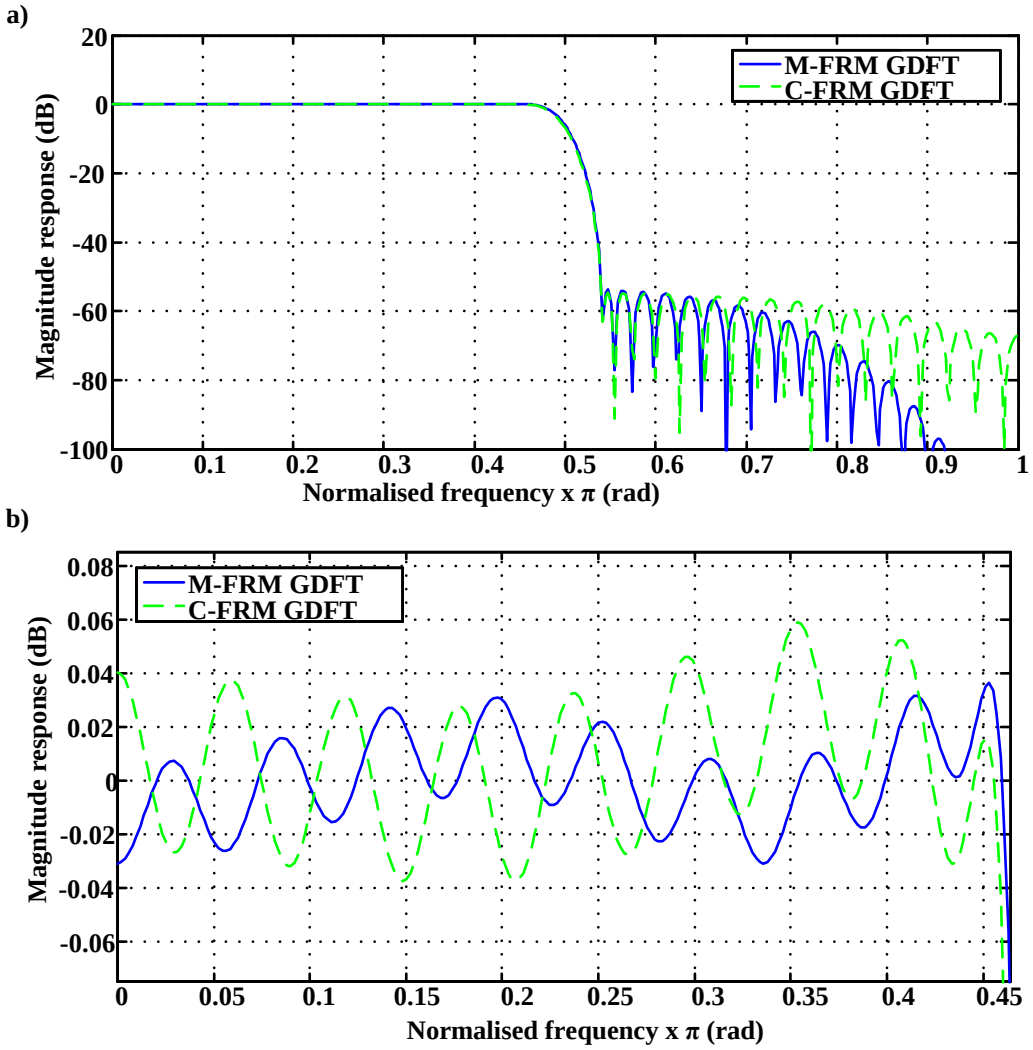

Figure 6.12 C-FRM GDFT and M-FRM GDFT output sub-bands for an oversampled 8-channel TETRA V&D channelizer, a) full magnitude response, b) pass band response.

6.7 Non-uniform channelization with FRM GDFT-FB designs

Like the multi-stage GDFT-FB techniques presented in Chapter 5, FRM GDFT-FBs, C-FRM GDFTs, and M-FRM GDFTs can be employed to implement non-uniform channelizers based on the P-GDFT-FB and R-GDFT-FB.

Table 6.9 Filter orders calculated for the P-GDFT and R-GDFT non-uniform channelizers using narrowband FRM GDFT-FB for use case 1.

		Uniform filter bank structure		
	Sub-band bandwidth	FRM GDFT-FB	C-FRM GDFT	M-FRM GDFT
P-GDFT	25 kHz	N_A= 68 N_{MA} = 681	N_A= 68 N_A' = 22 N_{MA} = 112	N_A=12 N_{MA} =1362 N_B=64
	50 kHz	N_A= 62 N_{MA} = 341	N_A= 62 N_A' = 22 N_{MA} = 56	N_A=22 N_{MA} =273 N_B=58
	100 kHz	N_A= 48 N_{MA} = 171	N_A= 48 N_A' = 22 N_{MA} = 28	N_A=44 N_{MA} =105 N_B=46
R-GDFT	25 kHz	N_A= 68 N_{MA} = 681	N_A= 68 N_A' = 22 N_{MA} = 112	N_A=12 N_{MA} =1362 N_B=64

Using the P-GDFT approach any of the FRM GDFT-FB designs could be connected in parallel, substituting for the GDFT-FB in the original P-GDFT design (see Figure 4.8). It is not strictly necessary that each of the uniform branches (connected in parallel) uses the same filter bank implementation and this allows the designer some freedom to choose the optimum filter bank for each uniform branch. The number of uniform branches depends on the number of standards to be supported by the non-uniform channelizer. The R-GDFT approach can also benefit from the use of FRM GDFT-FB structures instead of the basic GDFT-FB.

Analogously to Table 5.1 in Chapter 5 when the multi-stage GDFT-FB structures were applied to the P-GDFT and R-GDFT non-uniform channelizers, Table 6.9 presents the filter coefficient results for the P-GDFT and R-GDFT regarding narrowband FRM GDFT-FBs. This table also expands the information from Table 6.5, Table 6.7 and Table 6.8 for the C-FRM GDFT and M-FRM GDFT by providing the filter orders required for the TEDS standards.

Table 6.10 Number of coefficietns and computational load of the FRM GDFT-FB based non-uniform channelizers for use case 1 in comparison with the P-GDFT and R-GDFT.

Non-uniform channelizer	Number of coefficients (%)	μ (%)	α (%)
P-FRM GDFT (oversampled)	10.5	90.6	66.9
PC-FRM GDFT (oversampled)	5.5	113	82.7
PM-FRM GDFT (oversampled)	24.6	84.1	45
R-FRM GDFT (oversampled)	9.3	43.2	66.1
RC-FRM GDFT (oversampled)	2.5	40	81
RM-FRM GDFT (oversampled)	17.8	52.8	44.4

In addition, now analogously to Table 5.2 in Chapter 5, Table 6.10 shows the reductions achieved in the P-GDFT and R-GDFT implementations from the numbers in Table 6.9. From Table 6.10 it can be seen how the reduction in the number of non-zero coefficients is further decreased in comparison with the results in Table 5.2 for the multi-stage GDFT-FB designs, in particular when C-FRM GDFTs are employed. On the other hand, it also shows that the reductions in the number of multiplications are in general smaller than the best case in Table 5.2 (the M-GDFT) in comparison with the P-GDFT and R-GDFT. The only exception is the PC-FRM GDFT which requires more multiplications than the P-GDFT despite of the large reduction in the number of coefficients.

The overall computational load comparison between the P-GDFT and R-GDFT non-uniform channelizers employed in Chapter 4 for use case 1, and the more efficient structures presented in Chapters 5 and 6 can be seen in Figure 6.13.

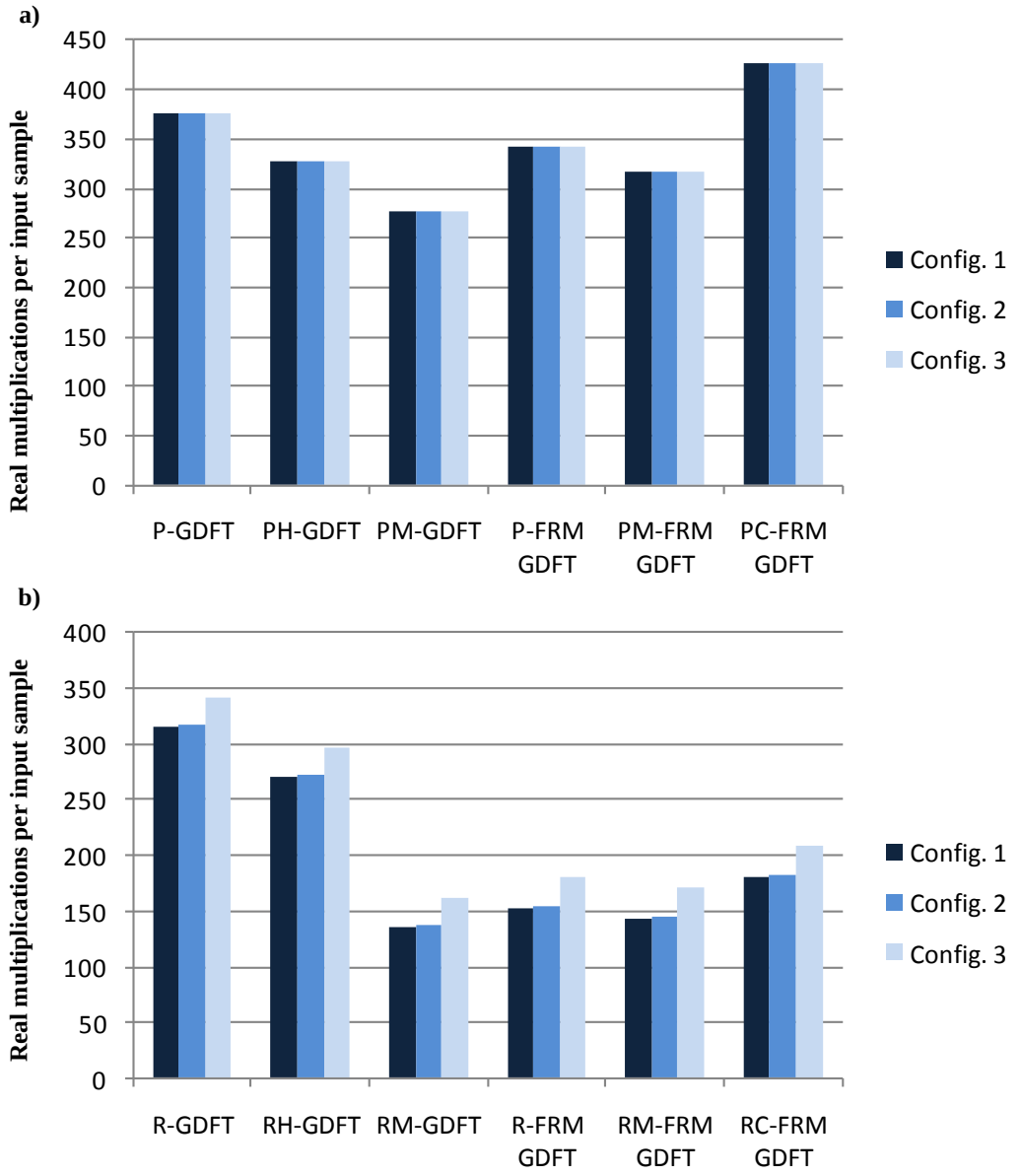

Figure 6.13 Overall non-uniform GDFT based non-uniform channelizers comparison for use case1, a) P-GDFT based, b) R-GDFT based.

From the overall comparison, it is seen how the uniform M-GDFT channelizers provide the best computational load efficiency when applied to the P-GDFT and R-GDFT channelizers. More in general, all the designs presented in Chapter 5 and 6 lead to lower computational loads than the direct implementation of the P-GDFT and R-GDFT from Chapter 4, with only the exception of the PC-FRM GDFT. However, for this particular case, the PC-FRM GDFT achieves over a 95% reduction in the number of non-zero coefficients with respect to the

direct P-GDFT. Also in general, all the structures presented in Chapter 5 and 6 provide dramatic reductions in the number of non-zero coefficients which facilitates the physical implementation of the channelizers, either uniform or non-uniform.

Regarding the recombination structure applied to the R-GDFT, no variations are required in comparison with previous cases except for the value of the phase shift applied to the recombined sub-bands. Similarly to Chapter 5, for the different structures presented in this chapter (FRM GDFT-FB, C-FRM GDFT, M-FRM GDFT) the sub-bands transition band is provided by a half-band filter. In the first two cases the base filter is a half-band filter due to the properties shown in Figure 6.1a, whereas for the last case a half-band filter is applied to every sub-band output. Therefore, in all the cases (as in Chapter 5) the magnitude complementary requirement for the recombined sub-bands is more optimized than when classic GDFT-FBs are used.

If the R-GDFT employed the FRM GDFT-FB structure, the phase shift would be given by

$$\varphi_r = -\left[M\left(\frac{LN_A + N_{MA}}{2D} \right) + \frac{N_M}{2} \right] \beta_r \quad \text{for } r = 0,...,R-1 \tag{6.29}$$

where N_M is the order of the interpolation filters at the recombination structure.

Optionally, if the C-FRM GDFT or M-FRM GDFT are used instead, the phase shifts are given respectively by

$$\varphi_r = -\left[M\left(\frac{LN_A + L'N'_A + N_{MA}}{2D} \right) + \frac{N_M}{2} \right] \beta_r \quad \text{for } r = 0,...,R-1 \tag{6.30}$$

and

$$\varphi_r = -\left[M\left(\frac{LN_A + N_{MA}}{2D} + \frac{N_B}{2} \right) + \frac{N_M}{2} \right] \beta_r \quad \text{for } r = 0,...,R-1 \tag{6.31}$$

where β is

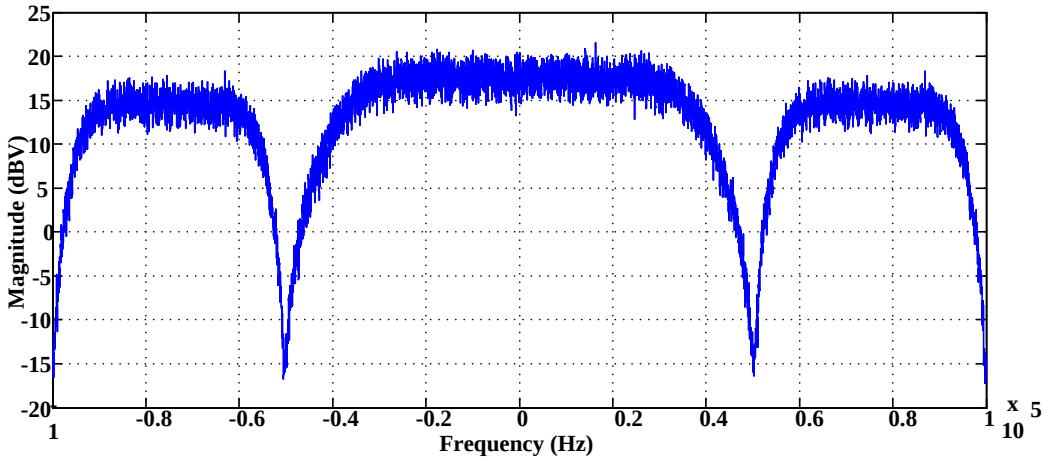

Figure 6.14 RM-FRM GDFT channelizer input signal.

$$\beta_r = \pi + \frac{\pi}{R}(2r+1) \quad \text{for } r = 0,...,R-1 \tag{6.32}$$

for all of them.

As an example, a multi-channel signal formed by TEDS 50 kHz and TEDS 100 kHz channels is fed to an RM-FRM GDFT which employs an 8-channel M-FRM GDFT from the example in Section 6.6.1. The input signal is shown in Figure 6.14. In contrast with the same type of example used in Section 5.5.3, in this case the multi-channel input signal is formed by two 50 kHz channels and one 100 kHz channels. Consequently, the two types of channels require the use of recombination structures to combine 2 and 4 sub-bands respectively

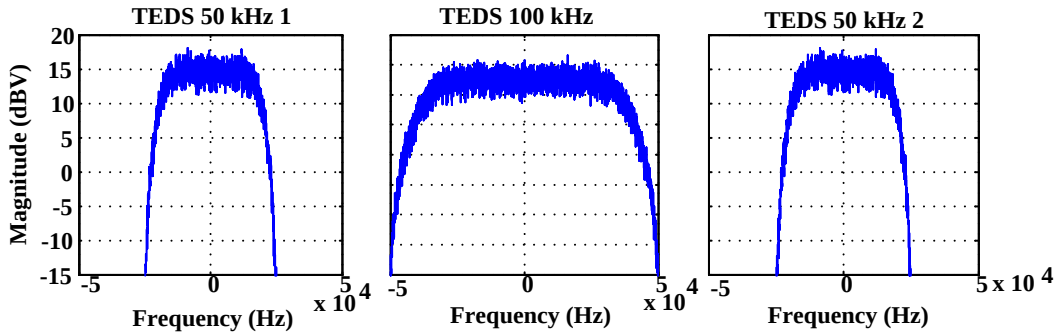

Figure 6.15 RM-FRM GDFT channel outputs.

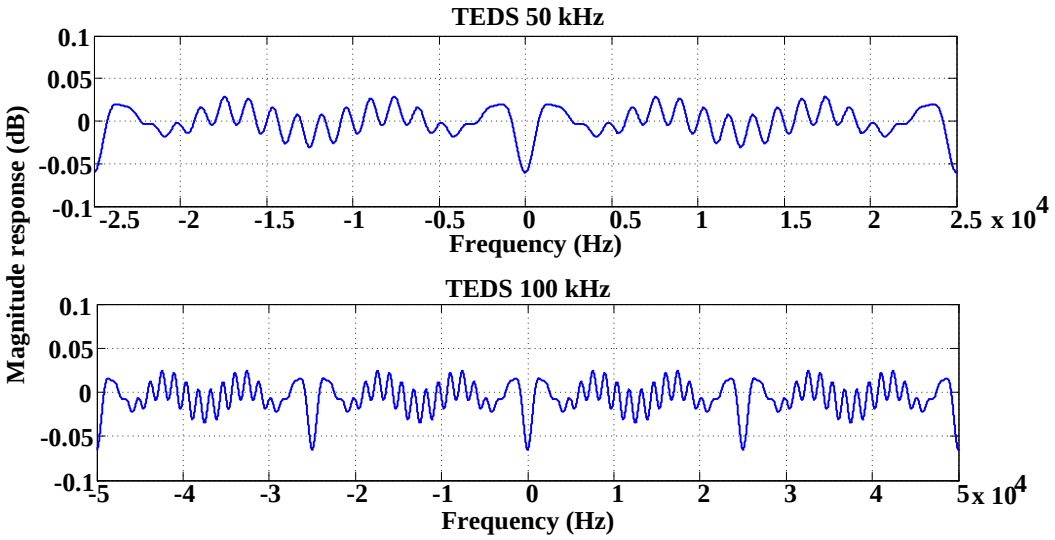

Figure 6.16 RM-FRM GDFT output magnitude responses.

The correct extraction of the three channels is shown in Figure 6.15. The frequency response of the recombined outputs is shown to provide passband ripples within the 0.1 dB limit as seen in Figure 6.16.

6.8 Chapter conclusions

The novel application of FRM for efficient prototype filter implementation in the GDFT-FB was presented in this chapter. The FRM GDFT-FB structure was analysed for different channel stacking configurations, oversampling factors, and type of FRM, full or narrowband. All of the structures showed a reduction in the number of non-zero coefficients compared to the GDFT-FB implementation. In contrast, when the number of operations was considered, the FRM GDFT-FB structures required more operations for critically decimated designs, but fewer operations for the oversampled designs. It was also shown that depending on the filter specifications, the oversampled narrowband FRM GDFT-FB can require even fewer multiplications per input sample than the critically decimated GDFT-FB.

In FRM related literature, a certain level of overdesign is suggested for the FRM filters design in order to meet the filtering specifications. In this chapter it was demonstrated that this overdesign is also required by FRM GDFT-FBs during

the design for their base and masking filter in order to meet the passband and stopband ripple specifications.

Recursive and multi-stage variants of the narrowband FRM GDFT-FBs were presented with the objective to further reduce the number of coefficients and computational load. On one hand, the C-FRM GDFT achieved further coefficient reduction with up to 95% of the filter orders in comparison with the GDFT-FB. However, its computational load was higher than the narrowband FRM GDFT-FB. On the other hand, the M-FRM GDFT required less operations than the C-FRM GDFT and narrowband FRM GDFT-FB, but a higher number of filter coefficients.

The application of these three narrowband structures (narrowband FRM GDFT-FB, C-FRM GDFT and M-FRM GDFT) to P-GDFT and R-GDFT channelizers was demonstrated within the use case 1, as an addition to the evaluation previously done in Chapter 5 with the same use case. From the overall comparison, it was concluded that all the novel techniques presented in Chapters 5 and 6 of this thesis yielded both reductions in the computational load and the filter orders of the GDFT-FB based non-uniform channelizers. The only exception was the PH-GDFT which required significant lower filter orders, but slightly higher computation. Concretely, the biggest reduction in the computational load was achieved by the PM-GDFT and RM-GDFT (Chapter 5).

For the R-GDFT using any type of FRM GDFT-FB, it was demonstrated that the magnitude complementary filter design is simplified with respect to the R-GDFT using GDFT-FB. This is a result, as in Chapter 5, of the utilization of half-band filters as base filters in the FRM and in the multi-stage designs.

Chapter 7

Channelization in Real-world Mobile Communication Systems

7.1 Introduction

This chapter presents a generalization of the non-uniform channelization structures evaluated in the thesis to a number of possible real world applications. In this thesis, the use case of a frequency band shared between TETRA V&D and TEDS channels has been used to evaluate the different channelization techniques. Here two more use cases are added: high data rate PMR (in which PMR standards are extended with 4G broadband communications) and so-called re-farming of the GSM 900 and 1800 MHz frequency bands (where 3G and 4G standards share the bands with existing GSM channels).

The second part of the chapter focuses on some physical implementation issues related to the GDFT-FB based non-uniform channelizers developed in this thesis. First, further coefficient reduction for the multi-stage GDFT-FB implementation is proposed by using half-band IIR filters with approximate linear phase response. These provide an alternative to FIR half-band filters in systems which can permit a small non-linearity in the phase response. Thereafter, the importance of coefficient reduction for FIR and IIR filters is analysed in terms of their physical implementation and fixed-point arithmetic. Finally, the relationship between the channelizer and the baseband signal processing of the independent channels is briefly examined from the perspective of overall receiver system optimization.

7.2 High data rate PMR: adding 4G to TETRA/TEDS

Even though the data rate limits of TETRA V&D were improved by the introduction of TEDS, these data rates remain insufficient for advanced PMR and PAMR applications such as remote patient monitoring, full-duplex video streaming, advanced telemetry, mobile robot control, 3D localization, and geographical information systems (GIS) [212]. As a possible solution to this data rate problem, the integration of the TETRA V&D and TEDS network with one of the 4G broadband wireless technologies, Worldwide Interoperability for Microwave Access (WiMAX) or LTE, has been proposed [30, 212-217]. Both are based on multicarrier OFDM techniques [218-219].

At the time of writing, WiMAX is one of the fastest growing broadband technologies offering a flexible and cheap solution for providing broadband access over the so-called last-mile [220-224]. Unlike TETRA, WiMAX is an IP-based technology more oriented towards data transmission services than voice services [214, 217]. At the physical layer, WiMAX is an OFDM based system. In its first specifications 802.16 and 802.16-2004 [220], known as fixed WiMAX or 802.16d, no end-user mobility was supported. For each user, a 3.5 MHz channel containing a set of 256 OFDM sub-carriers (including pilot sub-carriers) was allocated. Later, the 802.16e specification, known as mobile WiMAX, allowed end-user mobility and introduced new OFDM sizes of 128, 512, 1024 and 2048 sub-carriers corresponding to channel bandwidths from 1.25 MHz to 20 MHz. Another important addition over fixed WiMAX was Orthogonal Frequency Division Multiple Access (OFDMA) which allows the subcarriers within every channel to be divided between several users. (For example, the 1.25 MHz channel data sub-carriers can be shared between 2 or 3 users depending on the sub-channelization scheme.) Table 7.1 shows the OFDM parameters for the mobile WiMAX channels.

Table 7.1 Mobile WiMAX channel configurations.

	Mobile WiMAX scalable OFDMA physical layer			
Channel Bandwidth (MHz)	1.25	5	10	20
FFT Size	128	512	1024	2048
Data Sub-carriers	72	360	720	1440
Pilot Sub-carriers	12	60	120	240
Guardband Sub-carriers	44	92	184	368
Sub-carrier Spacing (kHz)	10.94			
Modulation Schemes	QPSK, 16-QAM, 64-QAM			

Competing with WiMAX, LTE represents the choice of the ETSI/3GPP for 4G packet-based commercial mobile communications. It was conceived as a "long term evolution" of UMTS with improvements such as higher data rates, lower latency, multi-antenna support (MIMO), reduced operating cost, bandwidth flexibility, and seamless implementation with legacy systems. Like WiMAX, LTE is based on multicarrier OFDM which allows it to provide a scalable physical layer with multiple channel bandwidths. In total it defines six possible channel bandwidths between 1.4 and 20 MHz, with a maximum data rate of 100 Mbps for the DL and 50 Mbps for the UL. In Table 7.2 the different LTE channel configurations are presented.

Unlike WiMAX, LTE employs OFDM only in the DL channel; in the UL channel single carrier Frequency Division Multiple Access (SC-FDMA) is employed. Using this scheme, the received UL signal is initially processed using OFDMA before a frequency-to-time domain conversion is applied to each group of sub-carriers corresponding to a single user, thereby making the resulting signals appear as single carrier signals [225].The main motivation for this scheme is that SC-FDMA requires less power than OFDM, which benefits mobile station battery life.

Both WiMAX and LTE can operate in time-division duplexing (TDD) and frequency-division duplexing (FDD) modes. TDD emulates a full duplex

communication over a half duplex communications link; both base station and mobile station transmit using the same carrier signal but at different time instants. On the other hand, FDD uses different frequencies for the DL and the UL channels and hence permits constant transmission in both directions. Although TETRA and TEDS use FDD, TDD is more commonly used in general because it provides better spectrum utilization when the DL and UL data rates are asymmetric.

To provide broadband communications channels to PMR applications, the introduction of WiMAX 1.25 MHz, LTE 1.4 MHz or LTE 3 MHz channels into the TETRA frequency band could be considered. For example, in the internationally reserved TETRA frequency band between 380 and 400 MHz up to 3 WiMAX 1.25 MHz or LTE 1.4 MHz channels could be allocated in a 5 MHz DL or UL band. These channels could be used on an as-needed basis for those services which require the highest data rates since their deployment in the 5 MHz DL or UL band would significantly reduce the TETRA/TEDS capacity.

Therefore, a trade-off between the TETRA and TEDS traffic capacity demanded at a certain instant and the number of broadband connections available is required.

Any update for broadband PMR base stations would in general have to maintain backward compatibility with legacy mobile stations at the same time as supporting new ones. For legacy mobile terminals, the allocation of TETRA and TEDS channels using FDD and TDM in the DL and UL signals must remain the same. Furthermore, their centre frequencies must remain compliant with the ECC specification for PMR systems [27].

Using the TDD mode of operation, a single WiMAX or LTE channel could be added to either the TETRA/TEDS DL or UL band. Because TETRA/TEDS uses FDD, however, any frequencies occupied in the DL band are automatically unavailable in the UL band and vice versa. Consequently, a better solution is to introduce two broadband channels, one in the UL and one in the DL, which can operate either independently in TDD mode or in conjunction in FDD mode.

Table 7.2 LTE channel configurations.

	LTE scalable OFDMA physical layer					
Channel Bandwidth (MHz)	1.4	3	5	10	15	20
FFT Size	128	256	512	1024	1536	2048
Occupied Sub-carriers (Data+Pilots)	72	180	300	600	900	1200
Guardband Sub-carriers	56	76	212	424	636	848
Sub-carrier Spacing (kHz)	15					
Modulation Schemes	BPSK, QPSK, 16-QAM, 64-QAM					

Using this solution (i.e. adding a broadband channel to the UL and DL bands), and focusing on the UL band, different approaches to dynamic spectrum allocation and channelization are considered in the following sections.

7.2.1 Dynamic contiguous spectrum allocation

The main motivation for the addition of broadband channels to PMR communications is to provide broadband services, such as live video streaming, which are not supported by the current TETRA and TEDS standards. Nevertheless, TETRA and TEDS must still provide robust communications channels for voice and enhanced data. In addition to maximize spectrum utilization all frequencies should be available for use. For this reason, unless broadband services are required, the entire UL and DL frequency bands should be available for TETRA and TEDS channel allocation.

For the TETRA and TEDS use cases described previously, DFSA was chosen as the most efficient way to share the frequency bands between the TETRA V&D 25 kHz, and TEDS 25, 50, 100 and 150 kHz channels. However, the large difference between the bandwidth of the WiMAX and LTE channels (1.25 MHz or 1.4 MHz respectively) and TETRA/TEDS channels complicates the channel allocation scheme. For example, if at a certain instant no broadband channel

were being used, occupied TETRA and TEDS channels could be distributed throughout the DL and UL bands such that there was no gap equal or bigger than 1.25 MHz (or 1.4 MHz) between them. Consequently it would not be possible to allocate a WiMAX (or LTE) channel until sufficient TETRA and TEDS channels were freed up (or reallocated elsewhere) to provide the required contiguous bandwidth.

Since the main use of the TETRA V&D and TEDS networks is for safety and security services, which must be robust in extreme situations such as natural disasters, the availability of high priority communication channels must be immediate when required. Therefore the question for the TETRA/TEDS operator to decide is which services have priority (voice, enhanced data, or broadband data). Once the priority has been decided users could be classified as primary or secondary based on the service they required. This is rather similar to the notion of primary and secondary users used by cognitive radio [11].

If it is decided that the broadband data service is primary, then the WiMAX/LTE channel bandwidth must be available on demand. When needed, any TETRA/TEDS channels occupying the WiMAX/LTE channel bandwidth must be immediately cleared or have their traffic reassigned to available channels outside the WiMAX/LTE channel bandwidth [10]. If, conversely, it was decided that voice or enhanced data should be primary then the WiMAX/LTE channel would need to be released immediately when additional TETRA/TEDS capacity was required. Even in this case, however, the policy of the resource allocation algorithm should always be to allocate and release TETRA/TEDS channels in such a way that a WiMAX/LTE channel bandwidth is available as much of the time as it is possible. Nevertheless, there is no perfect solution: no matter which services are primary or secondary, active communications on secondary channels would have to be stopped when the primary service is needed.

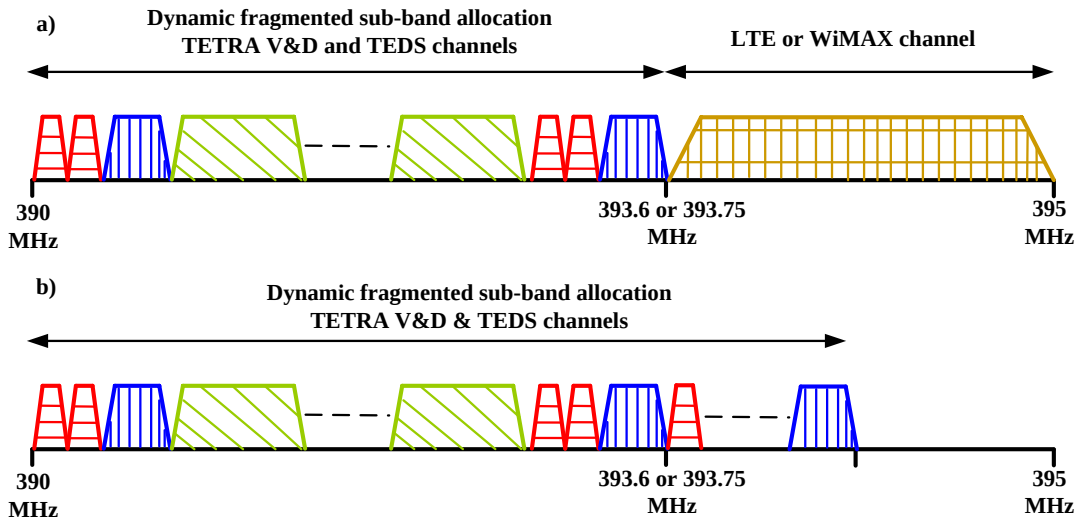

Figure 7.1 Dynamic continuous UL frequency band configuration for TETRA V&D, TEDS and broadband channels a) with broadband channel in use b) with broadband channel not in use and bandwidth occupied by TETRA/TEDS channels

The simplest dynamic spectrum allocation scheme to implement is that shown in Figure 7.1. The WiMAX/LTE channel is designated a fixed centre frequency. (In the figure, the WiMAX/LTE channel is shown adjacent to the overall band edge but that is not a required and it could just as easily be allocated in the middle of the range.) When the WiMAX/LTE channel is needed it is always allocated at the same frequency (see Figure 7.1a). TETRA/TEDS channels would be allocated in accordance with the DCSA or DFSA scheme—in practice there would be little difference between them in this situation. No matter which scheme was adopted, the resource allocation algorithm would need to implement the service priority scheme freeing up TETRA/TEDS channels or the WiMAX/LTE channel as needed. When the WiMAX/LTE channel is either not in use or has been cleared to make space for TETRA/TEDS channels, the spectrum may be allocated in the manner shown in Figure 7.1b.

7.2.2 Fixed spectrum allocation

The alternative to DSA is FSA (as in Figure 7.2). In this case, the broadband channel bandwidth is permanently reserved and no other channels can be allocated in its range. This is the simplest scheme to implement since it permits independent hardware or software circuits to be dedicated to each band. In

addition, the WiMAX/LTE channel is available immediately when needed. However in common with all FSA schemes, this scheme is spectrum inefficient. When no high data rate services are required, the WiMAX/LTE band will be unused and unavailable for other services. Therefore spectrum utilization will depend on how often (and for how long) high data rate services are required. Furthermore, the capacity for voice (and enhanced data) traffic is permanently reduced relative to the DSA approach.

Whichever channel allocation scheme is used, the non-uniform channelization technique employed must support the additional WiMAX/LTE channel. In the previous chapters the recombined GDFT-FB technique was shown to provide the best trade-off between flexibility and computational load. Applying the R-GDFT-FB to this scheme an appropriate granularity band could still be considered the 25 kHz of the TETRA V&D channels. If the R-GDFT-FB was applied to complete UL frequency band (including TETRA/TEDS and WiMAX/LTE bands), the reconstruction of an LTE or WiMAX channel could be done by recombining 56 or 50 sub-bands respectively.

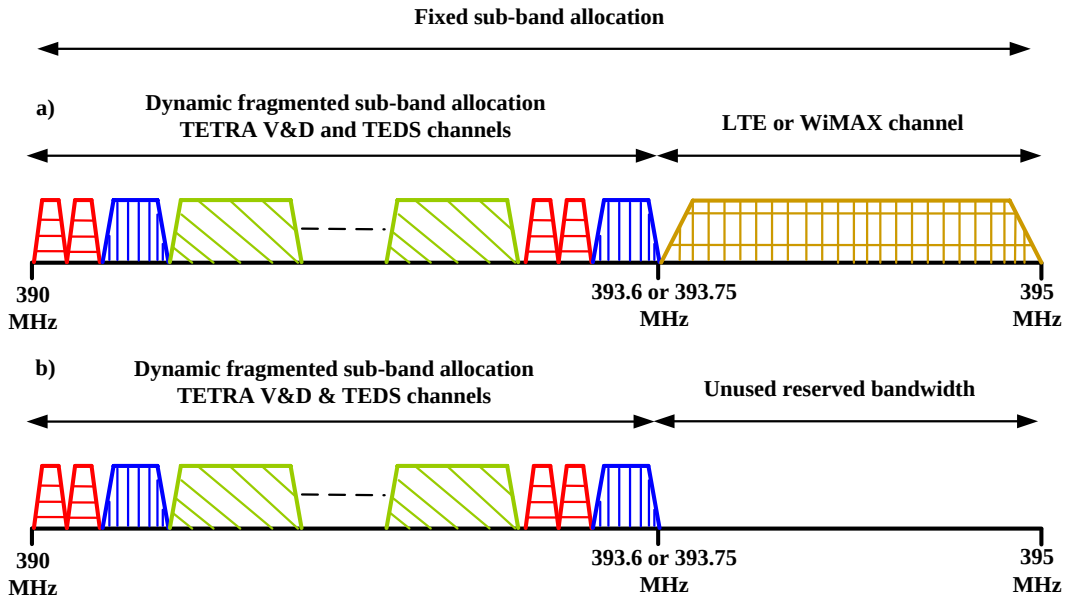

Figure 7.2 Fixed shared UL frequency band configuration for TETRA V&D, TEDS and broadband channels a) with broadband channel in use, b) with broadband channel not in use and extra bandwidth occupied by contiguous sub-band.

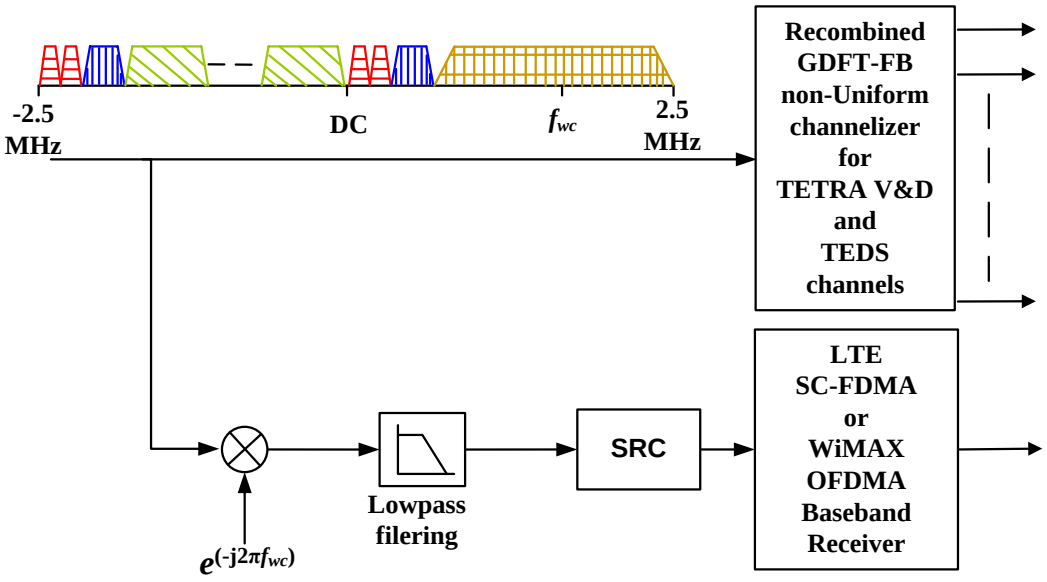

Figure 7.3 Parallel channelization structure formed by a non-uniform recombined GDFT-FB and an independent LTE or WiMAX receiver.

Nevertheless, this recombination operation is more computationally intensive than the ones required for TEDS 50, 100 and 150 kHz due to the much larger number of sub-bands involved. Observing the frequency allocation scheme presented in Figure 7.1 and Figure 7.2, it makes sense to consider a solution based on two different channelization structures, one for each of the contiguous sub-bands. Figure 7.3 presents a solution of this form. It is related to parallel channelizer structures such as the P-GDFT-FB but differs in two respects. First, the secondary channelizer does not channelize the whole frequency band but just one sub-band of it. Second, that sub-band must be independently shifted to DC for channelization.

The TETRA/TEDS band is channelized using an R-GDFT-FB. If using DSA this channelizer must cover the entire UL frequency band. On the contrary, for FSA the R-GDFT-FB only needs to cover the TETRA/TEDS sub-band.

In parallel the LTE or WiMAX channel is centred at DC, low-pass filtered, and sample rate adapted for demodulation. If the range of frequencies to which the broadband channel is allocated changes, only the mixer to centre the channel at DC needs to be adapted. If, when using the DSA, the broadband channel cannot

be used, the parallel channelizer is simply disabled and all the information channels are recovered from the non-uniform R-GDFT-FB.

7.2.3 Resource allocation and signalling

From a resource allocation point of view, TEDS was originally designed to use the same control channels as TETRA V&D to facilitate co-ordinated signalling and control in a shared frequency band implementation [1]. The base station informs mobile stations about the general access information of both standards using the broadcast control channel (BCCH). When a mobile station requires initiating a communication using TETRA V&D or TEDS, a request is issued to the base stations using a random access channel. If broadband services are implemented by adding a WiMAX/LTE channel, first, information related to this channel would need to be included in the broadcast information from the base station. Consequently, mobile stations capable of using this broadband channel can be made aware of its availability. Second, to request the use of the broadband channel, mobile stations would need to issue a request through the same control random access channels employed by TETRA V&D and TEDS.

7.3 Re-farming the 900 and 1800 MHz GSM bands for 3G and 4G commercial mobile communications

Commercial mobile communication standards generally advance more quickly than PMR standards. Unlike the first and second generation of mobile communications where every region of the world developed their own standards (for example, GSM in Europe, IS-95 CDMA and IS-54/136 in America, and PDC in Japan) third and fourth generation of communications have followed a reunification path [8]. This tendency to create more global mobile standards is a result of the creation of the International Mobile Telecommunications-2000 (IMT-2000) specification by the International Telecommunications Union (ITU). IMT-2000 was created as an effort to establish a common basis for not only mobile, but all third generation wireless systems [226].

For mobile standards, the telecommunications standards bodies which took part in the IMT-2000 specification united in two organizational partnerships: the 3G Partnership Project (3GPP) and 3G Partnership Project 2 (3GPP2) [227-228]. The 3GPP produces specifications based on the evolution of the GSM standard, including GPRS (2.5G), UMTS (3G), HSPA (3.5G) and LTE (4G). On the other hand 3GPP2 standards were based on the specifications of IS-95 and support CDMA2000 as their 3G standard option. Both 3G standard streams, UMTS (and HSPA) and CDMA2000, count with networks all around the world although UMTS/HSPA generally wider deployed in Europe whereas CDMA2000 is wider deployed in the United States. For 4G mobile communications, LTE (from the 3GPP) and WiMAX (from the Institute of Electrical and Electronic Engineers), represent the two main standards being developed.

So called re-farming of the GSM frequency bands has been studied as a possibility for providing additional spectrum with longer propagation distances to 3GPP 3G and 4G communications standards. Significant effort has been focused on the deployment of UMTS and HSPA channels in the GSM 900 MHz band (Band VIII in Table 7.3), an effort generally known as UMTS900 [229-230]. [230] also includes the re-farming of the GSM 1800 MHz band (3GPP band III). The main objective of re-farming the GSM900 frequency band is to bring broadband communications to rural areas with low population density. Because of having lower carrier frequencies than the general UMTS frequency band around 2.1 GHz (3GPP band I), lower path losses are experienced and cell sizes can be up to 2.5 times larger than UMTS2100 [231]. Consequently the number of base stations required to cover an area is reduced [2, 231-232].

LTE has generally been deployed using 3GPP frequency band VII around 2.6 GHz [233]. However, its deployment in the GSM1800 band has been also considered for the same reason as UMTS900. This alternative is generally known as LTE1800. The GSM1800 band (band III) provides a wider range of frequencies than GSM900 (band VIII) as shown in Table 7.3, therefore allowing the use of larger LTE channel bandwidths.

Table 7.3 3GPP frequency bands.

Operation band	Total spectrum	UL (MHz)	DL (MHz)
I	2 x 60 MHz	1920-1980	2110-2170
II	2 x 60 MHz	1850-1910	1930-1990
III	2 x 75 MHz	1710-1785	1805-1880
IV	2 x 45 MHz	1710-1755	2110-2155
V	2 x 25 MHz	824-849	869-894
VI	2 x 10 MHz	830-840	875-885
VII	2 x 70 MHz	2500-2570	2620-2690
VIII	2 x 35 MHz	880-915	925-960
IX	2 x 35 MHz	1749.9-1784.9	1844.9-1879.9
X	2 x 60 MHz	1710-1770	2110-2170

Interference between GSM and UMTS channels in the 900 MHz band has been studied to determine the adequate separation between both types of channels [231]. It was concluded that if the adjacent channels belong to the same mobile operator (coordinated GSM900 + UMTS900) GSM power control can permit UMTS channels of up to 4.2 MHz bandwidth with a channel spacing of 2.2 MHz. In contrast, if adjacent channels have different mobile operators (uncoordinated GSM900 + UMTS900) then UMTS channels have 5 MHz bandwidth and must be separated by 2.8 MHz. The author is not aware of similar studies having been published for LTE1800. Table 7.4 summarizes the channel bandwidths and channel spacings for the different 3GPP standards.

7.3.1 Spectrum allocation

When considering 3GPP standards, the evolution from GSM has promoted the continuation of a channel numbering system based on 200 kHz sub-bands. The required number of sub-bands for the UMTS and LTE channels is summarized in Table 7.5.

Table 7.4 Bandwidth and channel spacing for 3GPP standards under uncoordinated and coordinated conditions.

Standard	Bandwidth (kHz)	Channel spacing (kHz)
GSM	200	200
UMTS/HSPA	5000	5000
UMTS900/HSPA900	5000 (uncoordinated 4200 (coordinated	2800 (uncoordinated) 2200 (coordinated)
LTE	1400-20000	1400-20000
LTE1800	1400-20000	Undefined

Table 7.5 UMTS, HSPA and LTE number of granularity 200 kHz sub-bands.

Standard	Number of sub-bands
UMTS/HSPA	25
UMTS900/HSPA900	21
LTE	7, 15, 25, 50, 75 or 100

For the particular case of the 900 MHz band, a minimum of 7.5 MHz is the bandwidth estimated that a mobile operator must posses in order to use the GSM900 + UMTS900 implementation [231]. It is considered that, on average, a mobile operator generally owns 10 MHz of this band. Consequently, the deployment of a single UMTS or HSPA channel has been considered [232]. Some operators have also considered the deployment of LTE channels of 1.4, 3 or 5 MHz in this band [233].

From the channel allocation perspective, a similar approach to that used in the previous section to the PMR case could be applied here. Considering the 35 MHz bandwidth of the UL and DL (50 x 200 kHz bands), the single UMTS, HSPA or LTE carrier could be allocated a fixed or dynamic centre frequency. In the case of a dynamic centre frequency, it should at least be grid-constrained (see Section 2.2) to discrete multiples of the 200 kHz GSM band. Furthermore, in this case there is a difference between allocating the broadband channel at the edge of the operator frequency band or in the middle of it. As shown in Table 7.4 an uncoordinated UMTS900 channel (adjacent to another operator's bandwidth) requires a larger guard band than a coordinated channel (within a single

operator's bandwidth) [231]. For this reason, Figure 7.4 shows the third and fourth generation channels in the middle of a GSM900 operator band to minimize unusable guard bands and therefore maximize capacity within the band.

Mobile operators generally own larger bandwidths in the GSM 1800 MHz band due to the wider range of frequencies available (typically varying from 15 and 25 MHz depending on the country, the number of operators and the operator itself). The higher capacity of this band in comparison with the 900 MHz one is the main reason why it is preferred for LTE re-farming [2, 233]. Therefore a single LTE channel of up to 20 MHz could be allocated, or alternatively several 5MHz channels suitable for UMTS, HSPA, or LTE could be allocated.

As for PMR, spectrum may be allocated to GSM channels and broadband channels in accordance with FSA or DSA. As always, FSA is simplest to implement but generally under-utilizes the available spectrum. To implement DSA a priority scheme could be used (similar to that suggested for PMR in Section Multi-standard PMR base stations) or, since communication in a commercial system is not necessarily guaranteed, a best effort approach could be used. Using the best effort approach, channels would be allocated only if sufficient contiguous bandwidth was available.

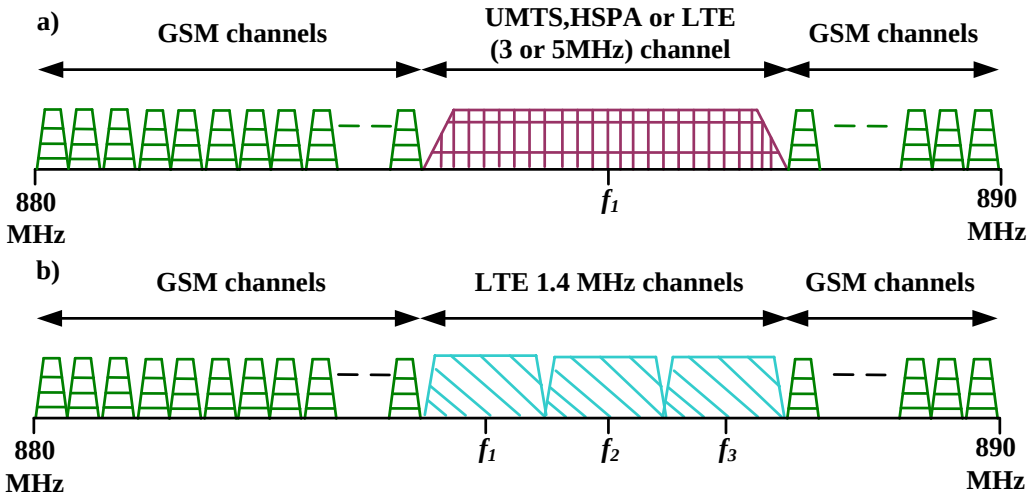

Figure 7.4 GSM 900 MHz multi-standard channel allocation a) with a single UMTS, HSPA or LTE (3 or 5 MHz) carrier, b) with three LTE 1.4 MHz carriers.

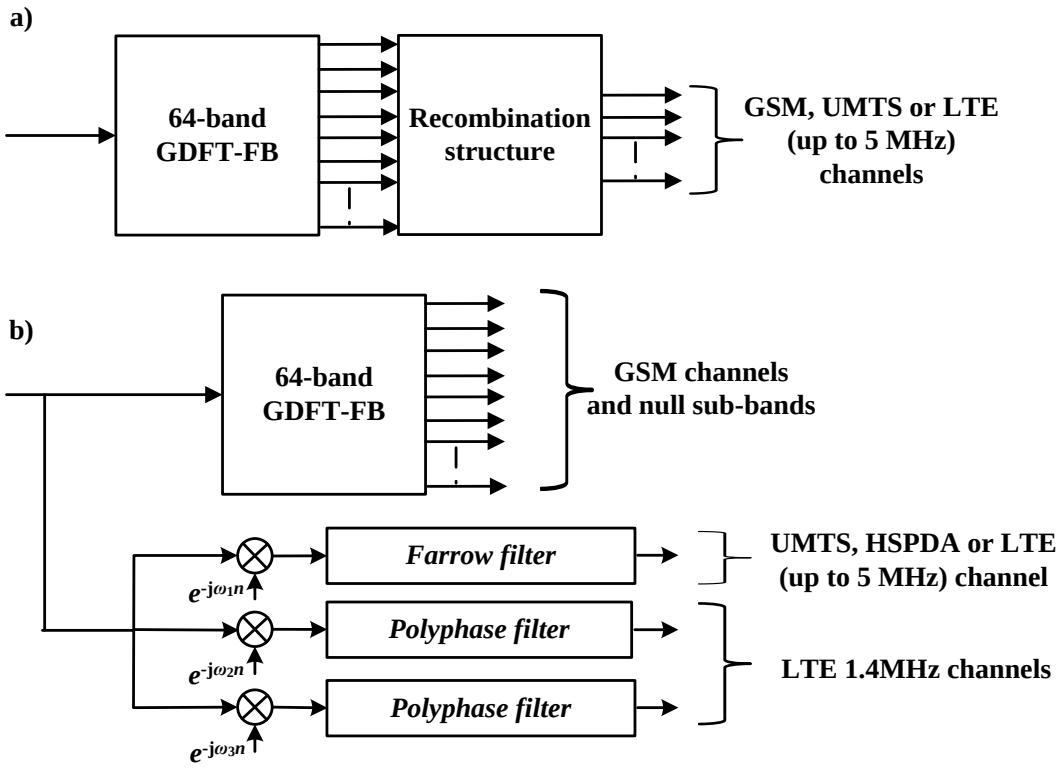

Figure 7.5 GSM 900 MHz band channelization structure, a) purely based on an R-GDFT, b) based on a parallel combination of a GDFT-FB and per-channel channelizers.

The appropriate DSA scheme to use in this case is DFSA. If DFSA were implemented in full, a broadband channel could be allocated at any (grid-constrained) centre frequency surrounded by sufficient contiguous available bandwidth and the frequencies f_1, f_2, and f_3 in Figure 7.4 need not have fixed values. Furthermore, in Figure 7.4b, the three LTE bands need not be adjacent to one another. However, if this level of flexibility were not required, the scheme could be simplified by fixing the frequencies at which broadband channels could be allocated. The scheme would still be dynamic because broadband channels would not be allocated when not needed and their bandwidth would be available for use by GSM channels. The scheme would still be fragmented because all GSM channels need not be contiguously allocated within the overall band.

7.3.2 Channelization

Two possible channelization structures are presented in Figure 7.5 for the channel allocation schemes described in the previous section. The first structure

(Figure 7.5a) is a R-GDFT non-uniform channelizer with granularity bands equal to a GSM channel bandwidth (200 kHz) covering the entire 10 MHz of a mobile operator GSM900 band. Broadband UMTS, HSPA or LTE channels are reconstructed from a number of uniform sub-bands (as specified in Table 7.5).

The second option (Figure 7.5b) is the parallel combination of a uniform GDFT modulated analysis bank with a per-channel channelizer with up to three branches. The uniform filter bank simply channelizes the GSM channels. For spectrum allocations based on a single 3 or 5 MHz channel, just one per-channel channelizer with one branch is required which can be implemented using an efficient polyphase decomposition. The Farrow channelizer provides flexibility to adapt the different bandwidths or sample rates that may be required. In contrast, for spectrum allocations based on several LTE channels, a channelizer composed of one Farrow filter (see Section 4.3.1) and two polyphase filters can be employed. The Farrow channelizer provides flexibility to adapt the different bandwidths or sample rates that may be required for the LTE bandwidths between 1.4 and 5 MHz. The other two polyphase filters are just used in case that two or three LTE 1.4 MHz channels are deployed.

Any of the channel allocation schemes described in Section 7.3.1 can be channelized by either of the channelization structures shown in Figure 7.5. For FSA, the recombination structure in Figure 7.5a need not be reconfigurable whereas for DSA reconfigurability is required. Similarly the mixers and Farrow channelizers in Figure 7.5b need not be reconfigurable to support FSA but should be in order to support DSA. The channelization structure is identical (although the size of the GDFT-FBs increases to 128 bands) for the re-farmed GSM1800 band.

To support re-farming as described, the GSM, UMTS, and LTE channels would need to share the same radio resource allocation mechanism. For GSM and UMTS networks the resource allocation management is performed by the Base Station Controller (BSC) and the Radio Network Controller (RNC) respectively. Their role is to control radio resources related with several base stations. One possible BSC implementation could be achieved by employing a network

architecture which encloses the two types of access networks both GSM and UMTS (and LTE), for example the 3GPP R99 network [234-235].

7.4 Channelizer implementation issues

There are differences between the theoretical design and analysis of a channelization structure on its own and its physical implementation as part of a processing chain. For example, components placed before the channelizer in the processing chain may affect the signal and need to be considered for the channelizer design. This is the main reason why Near Perfect Reconstruction (NPR) has recently drawn attention in filter bank design in contrast with Perfect Reconstruction (PR). Since other modules in the processing chain may alter the signal, it makes less sense to constrain the filter bank design to achieve PR. As long as the effects introduced by the channelizer are insignificant compared to the effects of other components NPR is perfectly reasonable. NPR designs have the benefit of requiring less optimization than PR designs. Similar reasoning can be applied to other aspects of channelizer design. For example, rather than requiring strictly linear phase response in the filters of the channelizer, a small amount of non-linearity in the phase response could often be acceptable.

7.4.1 Approximate linear phase using IIR filters

The channelizer is just one module in the receiver chain of the multi-channel UL signal in a base station. This thesis has focused on the implementation of non-uniform channelization structures using FIR filters because of their linear phase response. Although linear phase response is a desirable property, the channelizer generally inherits non-linear phase errors introduced in the receiver chain, such as from the low noise amplifier or ADC. Consequently, a small degree of non-linearity in the channelizer filters phase response could be allowed as long as it represents an insignificant contribution compared to the effects of other components.

Infinite Impulse Response (IIR) filters are an alternative to FIR designs which can be more efficient when a non-linear phase response is permitted [150]. As

seen in Chapter 4, FIR filters can require very high orders when sharp transition bands are needed. Specifically, for a given set of band ripples and sample rate, the FIR filter order is inversely proportional to the transition band width. IIR filters differ from FIR filters in that they add a feedback path. This feedback allows them to meet the same magnitude response specifications with a smaller order than FIR filters [100].

The high order of the prototype filter for GDFT-FB based channelizers was reduced in previous chapters using multi-stage techniques and the application of FRM. However, the order could be reduced even further by using IIR filters. Among the designs discussed in previous chapters, multi-stage GDFT-FBs employing half-band filters were shown to be efficient and useful because of two properties: the reduced order due to multi-stage filtering and the ease of design for complementary filters due to the use of half-band filters.

Similar to FIR designs, IIR half-band filters provide very attractive properties for their physical implementation [236-237]. As in the FIR case, IIR half-band filters have an impulse response in which every second coefficient is zero. However, unlike FIR, the impulse response of IIR half-band filters is not symmetrical. Among the different IIR half-band filter design methods, elliptic filters can be considered the IIR equivalent to equiripple FIR filters since they allow explicit specification of the passband and stopband ripples and they provide an optimal minimax solution to the specifications. Elliptic IIR half-band filters can be efficiently designed using a polyphase decomposition formed by two parallel all-pass filters [100, 238-241]. The two paths of the IIR polyphase structure depicted in Figure 7.6 can be designed in such a way that their frequency responses are in-phase and add constructively in the passband but are out of phase and add destructively in the stopband.

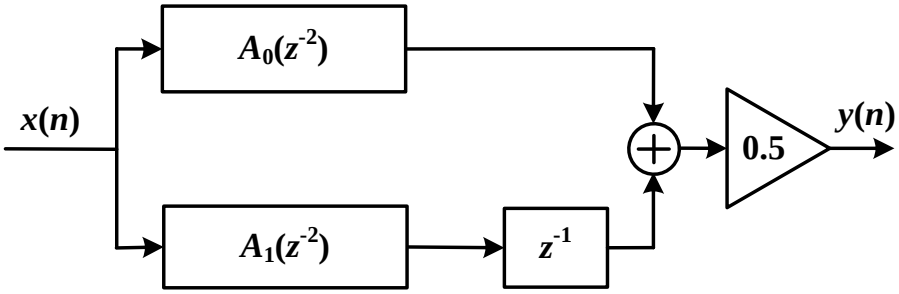

Figure 7.6 IIR polyphase half-band filter structure

In general, IIR half-band filters have smaller filter orders and passband ripple than FIR filters with the same magnitude specifications. If the phase response must be exactly linear then elliptic filters are not adequate. If a small degree of non-linearity can be tolerated, then an approximately linear phase response can be achieved using IIR filter designs. Approximate phase linearity can be achieved by designing the two all-pass filters to approximately cancel their non-linearity [242], by applying least-squares optimization [243], by compensating for the non-linearity with another all-pass section [244] or by substituting for one of the all-pass filters from the polyphase structure with a bulk delay [242, 244-245]. Among these options, the last one has proved to be particularly efficient and suitable for the fixed-point design and implementation of half-band filters [244]. The structure of the polyphase IIR filter with a bulk delay in parallel is shown in Figure 7.7.

In Chapter 4 and Chapter 5 it was shown that a multi-stage configuration of the GDFT-FB could reduce both the FIR filter orders and the computational load. In particular, the multi-stage combination of the GDFT-FB with output FIR half-band filters proved best considering filter orders, computational load, and ease of complementary designs (required for recombined filter banks). Where small phase non-linearity can be tolerated, lower order IIR half-band filters can be substituted for FIR half-band filters in the multi-stage GDFT-FB to further improve efficiency.

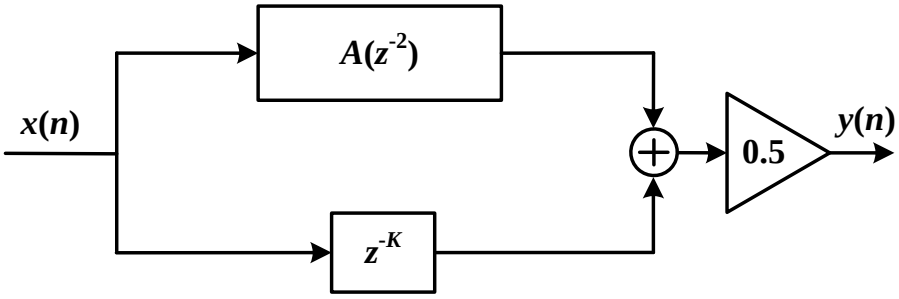

Figure 7.7 IIR approximate linear phase polyphase half-band filter structure.

To explore this further, IIR half-band filters were applied to the multi-stage designs in Figure 5.6 and Figure 6.11 for a TETRA V&D channelizer with 200 channels employing a 256-point FFT from use case 1 (see Section 4.4.3.1). The filters were designed in MATLAB using the *filterbuilder* tool using the previously established magnitude specifications. The design structure for the allpass filter was chosen to be a cascade of 2^{nd}-order minimum-multiply sections implemented using the Direct-form I [100, 150, 246]. (A combination of low order IIR filters in cascade or parallel have better fixed point arithmetic characteristics than a single higher order filter, a point which is explored further in section 7.4.2).

The total number of non-zero coefficients in the approximately linear phase IIR half-band filter was 15 (28 coefficients in total, half of them zero, plus 0.5 gain), compared to 33 (65 in total with half of them equal to zero and 16 symmetric) required by the FIR half-band filters from previous designs. Where non-linear phase is acceptable the total number of non-zero coefficients in the equivalent elliptic IIR half-band filter was found to be 6 (12 coefficients in total, half of them zero, plus 0.5 gain).

Table 7.6 compares the performance of the FIR based multi-stage GDFT-FB (Chapter 5) and multi-stage FRM GDFT-FB (Chapter 6) with modified designs using IIR filters.

The results show that when approximate linear phase is required, the number of operations required for the IIR implementation is not much less than the FIR implementation. Even though the IIR half-band filter order is decreased to less than half the equivalent FIR filter order, the lack of symmetry in the IIR

coefficients makes the FIR design perform almost as well. If non-linear phase is allowed, however, the elliptic IIR half-band design more significantly reduces the number of operations per input sample required.

Although the computation load may not be very different, IIR filters can provide other benefits over FIR filters: greater stopband attenuation, smaller passband ripples, and sharper transitions. Figure 7.8 shows the magnitude response of the three different half-band filters used in Table 7.6. All the filters were designed using MATLAB's *filterbuilder* tool.

Table 7.6 Design example of 256 channel TETRA 25 kHz odd-stacked oversampled channelizer using multi-stage implementations with FIR and IIR half-band filters.

Channelizer	Filters orders	Number of non-zero coefficients	Mults. per input sample (μ)
GDFT-FB	N=8085	8085 (100%)	292.4 (100%)
M-GDFT (FIR)	N=1294 N_B=64	1358 (16.8%)	101.9 (33.6%)
M-GDFT (FIR- approx. IIR)	N=1294 N_B=28	1322 (16.35 %)	98.4 (45.4%)
M-GDFT (FIR- elliptic IIR)	N=1294 N_B=12	1306 (16 %)	85.8 (29.3%)
M-FRM GDFT (FIR)	N_A=12 N_M=1362 N_B=64	1438 (17.8%)	117 (40%)
M-FRM GDFT (FIR-approx. IIR)	N_A=12 N_M=1362 N_B=28	1402 (17.3%)	113.5 (38.8%)
M-FRM GDFT (FIR-elliptic IIR)	N_A=12 N_M=1362 N_B=12	1386 (17.1%)	101 (34.5%)

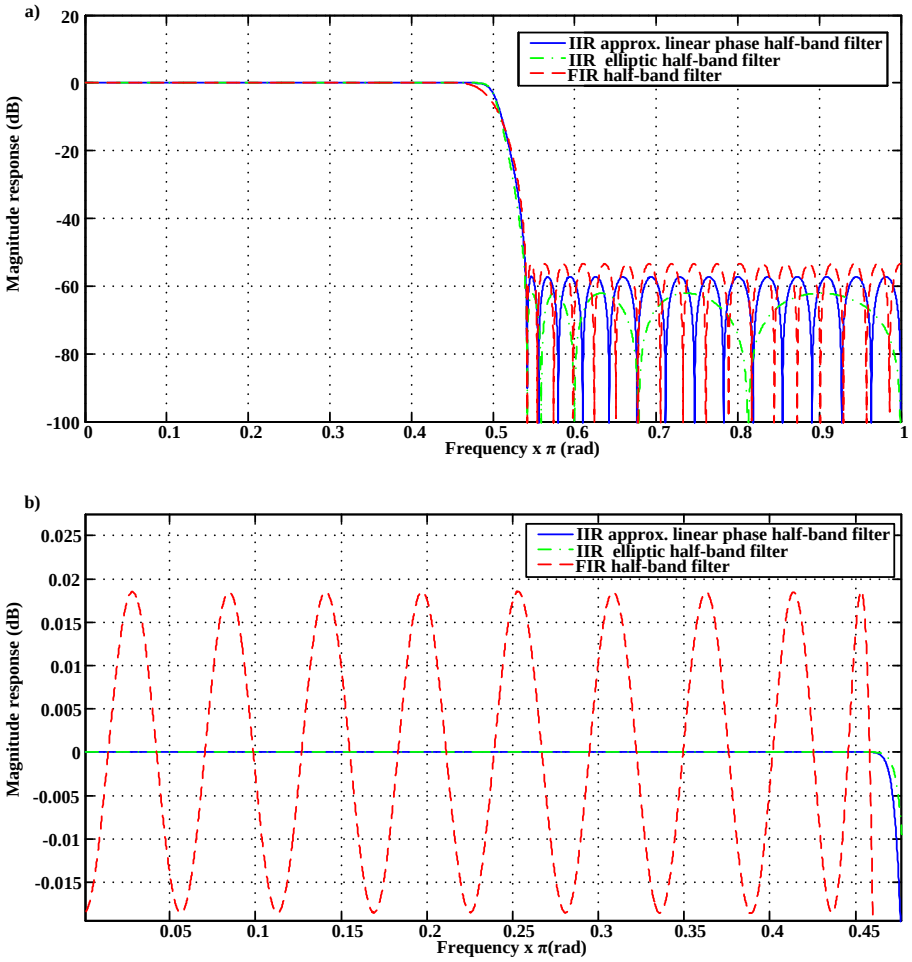

Figure 7.8 Magnitude response for half-band filters with FIR, approximately linear phase IIR, and elliptic IIR. a) Full magnitude response, b) passband ripple.

From Figure 7.8a it can be seen that the stopband attenuation of the two IIR designs is greater than that of the FIR filter. Figure 7.8b shows that the passband ripple of the IIR half-band designs appears almost flat compared to the FIR half-band filter passband ripple, in the order of micro dBs. Finally, it can be observed that the IIR designs exhibit a sharper transition than the FIR design. This occurs because the IIR designs have a magnitude of -3dB point at the frequency $\pi/2$ rad, whereas the FIR designs have a magnitude of -6 dB at the same frequency. In other words, the IIR half-band designs are power complementary instead of magnitude complementary [114].

7.4.2 Hardware platform and fixed-point implementation

The physical implementation of a channelizer in a programmable DSP device can be an important factor in its design. Run-time reconfigurability and processing speed are the two main desired characteristics of the hardware platform. FPGAs in particular have become more popular in recent years because they offer design flexibility, very high capacity parallel processing, and very fast on-chip communication. In addition, FPGA development tools have evolved and can provide assistance and optimisation of more complex designs.

The physical implementation of Parallel and Recombined GDFT-FB channelizers on FPGAs is specifically aided by the existence of efficient FIR design and FFT processing tool boxes, for example, the Xilinx LogiCORE FIR CompilerRuntime Reconfigurability [247] and the Xilinx LogiCORE Fast Fourier Transform [139] which can be used with Virtex and Spartans FPGAs. These toolboxes provide direct support for most of the component parts of the Parallel and Recombined GDFT-FB structures. Nevertheless, such toolboxes often have limitations: for example the FIR compiler limits filters to 1024 coefficients. With some minor filter optimisation, the multi-stage channelizers developed in previous chapters could be implemented with these toolboxes. However, the filter order limitation prevents these toolboxes being used to implement the single-stage channelizers because they require much higher filter orders. Single-stage implementations might still possible using a customized design but this requires longer development time.

Mobile communications systems generally employ modulation schemes based on I/Q signals. For these, complex signal processing represents a useful tool to simplify the signal operations and notation. Instead of considering the real-valued in-phase and quadrature input signals separately, they are mapped to complex input values as the real and imaginary parts respectively [95]. However, the physical implementation of the system must be carried out using real signal operations. Consequently, the real-valued in-phase and quadrature components are processed in two different physical paths. Operations such as filtering and frequency mixing have to be applied to both components separately.

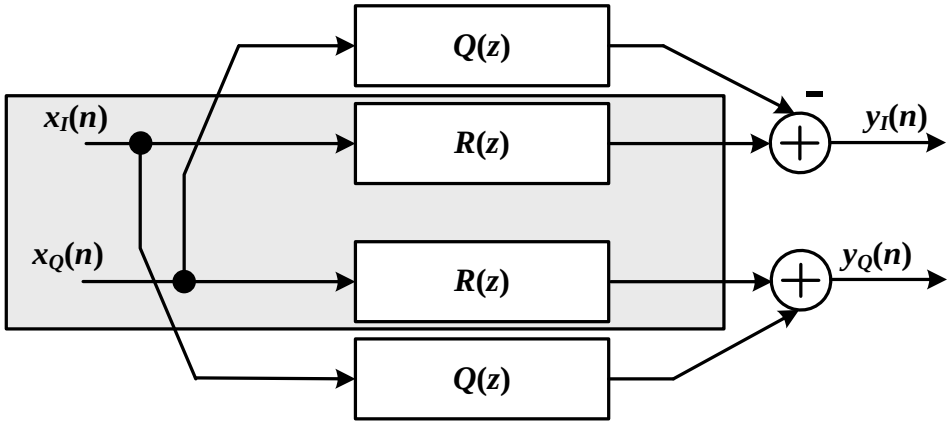

Figure 7.9 Physical implementation of a real digital filter (shaded) and complex digital filter applied to I/Q signals.

Focusing on filter implementation in particular, depending on whether the desired channel stacking configuration of the GDFT-FB is even or odd, the coefficients of the filter bank prototype filter will be either real or complex valued respectively. For real filters, the real-valued coefficients of the prototype filter $H(z)$ are applied independently to the two in-phase and quadrature signal components as depicted in Figure 7.9, where $R(z) = H(z)$ and $Q(z)=0$. In contrast, complex digital filter implementations require more computing resources since their complex coefficients need to be reduced to real values [95]. The two real value filter components, $R(z)$ and $Q(z)$, are obtained from the complex filter $H(z)$ as

$$R(z) = \frac{H(z) + H^*(z)}{2} \tag{7.1}$$

$$jQ(z) = \frac{H(z) - H^*(z)}{2} \tag{7.2}$$

Similar to real FIR filters, complex FIR filters have symmetric properties which can be exploited in the implementation of *R(z)* and *Q(z)* [248]. A complex filter requires twice the number of multipliers as a real digital filter of the same length; hence, the even stacked GDFT-FB with real value coefficients enables a more efficient physical implementation when applicable.

Fixed-point representation is another important factor in physical channelizer implementation. For the case of multirate filter banks, representing the coefficients and signals with fixed-point resolution produces errors such as analogue-to-digital input quantization noise, coefficient quantization errors, rounding errors, overflow errors, and sub-band quantization errors [249-250]. In FIR prototype filters, coefficient quantization errors do not affect the linear phase response characteristics but can affect the magnitude response. By using the multi-stage design with lower order filters, the zeros in the z-plane are further apart, and therefore the filter magnitude response is less sensitive to quantization error than for those with higher order single-stage designs [251].

In IIR filters, fixed-point arithmetic can affect the filter performance even more significantly than in the FIR case since both the magnitude and phase response are affected by the quantization and round-off effects [251]. These problems are worst when a direct implementation based on an N^{th}-order numerator and denominator is chosen. Consequently, parallel and cascade implementations using first or second order structures are preferred to reduce the sensitivity to coefficient quantization [100, 150, 252]. Both parallel and cascade designs have the advantage of a modular based design and, in addition, the second order sections can be designed to minimise the round-off noise and eliminate constant input limit cycles using state-space approaches [150, 251, 253].

Parallel designs like the filter polyphase decomposition, in particular, allow simultaneous processing in the parallel sub-filters. This is especially attractive for hardware platforms which allow parallel processing such as FPGAs. Unfortunately, however, parallel designs are sensitive to round-off noise produced by the positioning of the filter zeros. This sensitivity can be avoided in the cascaded structure since it allows more control over the position of poles and zeros in each second order section [251].

7.4.3 Optimization of the baseband processing chain

As discussed in Chapter 2, in an SDR base station, channelization can be considered to be the last front-end digital signal processing operations prior to independent baseband channel processing in the digital back-end. The back-end

digital processing comprises operations such as equalization, timing recovery, and symbol recovery or demapping to finally extract the information bits for every user [94].

As an example of how the channelizer and subsequent baseband processing can interact, consider the equalizer. Equalization plays a crucial role in mobile communication receivers because of the changing propagation properties of the wireless channel. These properties are hard to estimate in fast changing conditions, such as when the transmitter or receiver (or both) are moving. To eliminate the undesired effects of this time-varying channel, an adaptive cancelling operation must be performed by the equalizer. Adaptive equalizers can be subdivided into two main categories, linear and non-linear [254], and for each of these categories multiple structures and equalization algorithms exist. Here, linear equalizers are considered because of their possible sub-band implementation.

A linear equalizer is implemented as a FIR filter (also called transversal filter) with adjustable coefficients which may be adapted over time. Depending on the equalizer configuration, the high order of the FIR filter and the slow convergence of the adaption algorithm can produce large system delays and errors in the recovered signal. To combat this, a delayless equalizer configuration based on sub-band processing has been proposed [255-257]. This structure combines a fullband signal equalizer with a sub-band adaptive update of coefficients. The estimated sub-band coefficients are collectively transformed into an updated set of fullband filter coefficients. Furthermore, the updated coefficients are obtained at the same time that the current signal is being equalized, and it is for this reason that the approach is called delayless. Apart from the benefit of being delayless there are two further advantages: the computational load is approximately reduced by the number of sub-bands due to the coefficients being updated on a sub-band basis; and, convergence properties are improved because the spectral dynamic range is greatly reduced in every sub-band. This structure is shown in Figure 7.10.

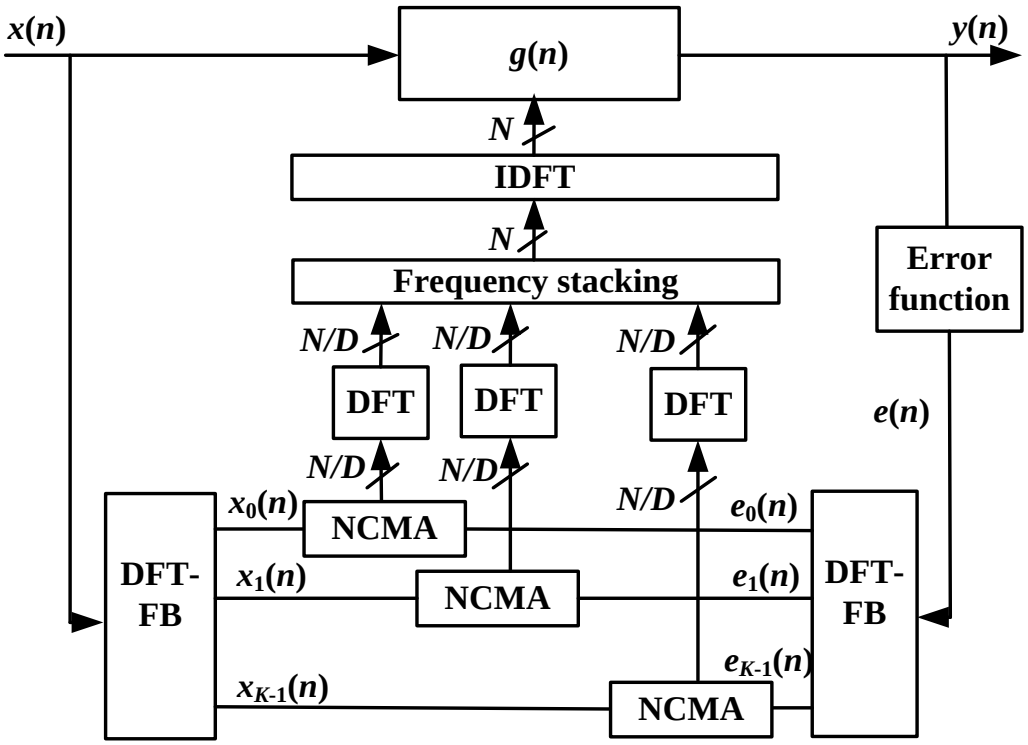

Figure 7.10 Adaptive sub-band equalizer structure with Normalized Constant Modulus Algorithm (NCMA).

The original received signal, $x(n)$, is filtered by the fullband equalizer, $g(n)$, to obtain the equalizer's output, $y(n)$. The received signal, $x(n)$, is fed at the same time to an analysis filter bank block. There, it is decimated by a factor D and divided into K sub-bands. This analysis bank is generally oversampled to reduce aliasing effects (relative to critically decimated alternative).

In an SDR base station using a recombined GDFT-FB channelizer there is an optimization that can be made to this equalizer as shown in Figure 7.11. The oversampled granularity sub-bands of the R-GDFT-FB could be directly used as the sub-band inputs to adaptive component of the equalizer, thereby eliminating the initial input analysis bank required in Figure 7.10. Recombination would be used as normal to re-create the single carrier signal from multiple granularity bands and it is this recombined signal that would provide the input to the full band equalizer, g.

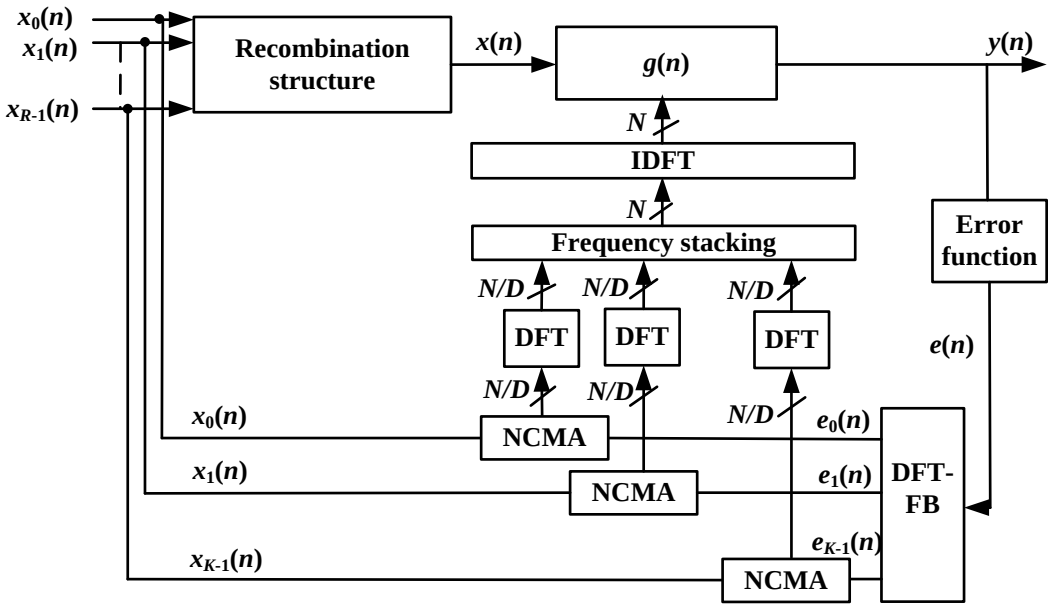

Figure 7.11 Reduced adaptive sub-band equalizer preceded by recombined GDFT-FB non-uniform channelizer.

Certain parameters of the non-uniform channelizer and the sub-band equalizer need to be jointly optimized so that the overall computational load of this subset of the processing chain can be minimized (while maintaining other desirable characteristics). These parameters are primarily the granularity band width, which determines the number of sub-bands to be recombined (R), and the number of sub-bands handled by the adaptive algorithm (K=R). Details of this optimization are outside the scope of the current work, but a study of the relationship between the equalizer order, the number of sub-bands, and the performance can be found in [255, 257].

In general, this example shows that metrics for the receiver processing chain such as the total computational load can be optimized by selection of components which complement each other (such as the R-GDFT-FB channelizer and sub-band equalizer) and by choosing the parameters that control those components carefully.

7.5 Chapter conclusions

In this chapter the non-uniform channelization techniques described in this thesis were applied to additional real world mobile use cases. Among the non-uniform channelization structures considered, recombined GDFT-FB channelizers proved to be the best option when there were a large number of channels of different bandwidths (usually from different standards) sharing the same frequency band. On the contrary, when the channel bandwidth differs dramatically (e.g. by an order of magnitude) between standards, or there are few standards, a parallel combination of different channelizers could be more effective.

It was shown that approximately linear phase IIR filters can reduce the overall number of filter coefficients required by a channelizer and its computational load. Nevertheless, when approximately linear phase IIR half-band filters were applied to the multi-stage GDFT-FB designs from previous chapters the computational load improvement was found to be rather small. It is possible that further reductions could be achieved by substituting approximately linear phase IIR designs for FIR designs in the prototype filter of the GDFT-FB.

The physical implementation of channelizers was also considered. In general, multi-stage techniques provide two valuable benefits for physical implementation. First, the order of individual filters can be reduced relative to single-stage designs. This is important because design tools available for reconfigurable hardware platforms such as FPGAs often limit the maximum filter order which can be handled—filters whose order is too high simply cannot be implemented. Second, the lower order filters of multi-stage and FRM GDT-FB designs are less sensitive to quantisation and round-off error effects in fixed point implementations.

Finally, it was shown that performance metrics for the receiver processing chain such as total computational load could be optimized by choosing complementary components. In particular it was shown that the recombined GDFT-FB channelizer could be designed in combination with adaptive sub-band

equalization techniques in order to reduce the complexity of the equalizer structure.

Chapter 8

Concluding Remarks

A variety of non-uniform channelization methods for SDR systems have been described in the literature [162-163, 165-167, 180, 187, 190]. In general, each method has been presented in isolation and from a theoretical point of view, mainly focusing on its reconfigurability since this is one of the key characteristics of SDR. Where method comparisons do exist, these have been limited to a subset of the methods and the comparisons have again focused mainly on method reconfigurability [166].

Focusing only on the reconfigurability of non-uniform channelizers is not enough to determine their suitability for a specific task or to evaluate differences in their overall performances. There are other factors such as the computational load or the channel allocation flexibility which play a crucial role in the channelizer performance for a specific application. Prior to this work, therefore, a faithful evaluation and comparison of the different types of non-uniform channelizers for a specific application remained an unresolved issue.

DSA, as a solution to inefficient spectrum utilisation, is a particularly interesting case for the application of non-uniform channelizers. By employing DSA and allocating their channels according to different schemes (i.e. DCSA or DFSA), multiple wireless standards may share the same UL frequency band. From the perspective of a base station, non-uniform channelizers are required to extract each one of the multi-standard communication channels from the common UL signal. Although the application of DSA to real-world PMR and commercial mobile communication standards has been discussed by different authors, prior to this work, a firm solution to the non-uniform channelization requirements of such applications had not been proposed.

8.1 Novel contributions to the state of the art

This thesis presented the evaluation and development of efficient non-uniform channelization techniques for real-world multi-standard SDR base stations. Unlike other comparative work, in this thesis it is shown that the definition of an application use case is essential to evaluating the performance of a specific non-uniform channelizer. Such use cases were developed in Chapter 2, Chapter 4 and Chapter 7.

The structure of a multi-standard base station compliant with DSA techniques was addressed in Chapter 2. The study of the DSA channel allocation requirements, mostly for DFSA, shows that advances over the classic hardware oriented base station designs are required. In particular for a hardware-based base station implementation, analysis of the required advances concludes that, especially for DFSA, this type of design is no longer an optimum and efficient solution. In contrast, SDR provides a compelling alternative that is able to offer a higher level of flexibility and reconfigurability than more traditional hardware-based systems. For an SDR implementation, it was concluded that the channelizer is the most important component for supporting DSA, but at the same time it is the component with the largest contribution to the receiver computational load. Therefore, if a generic reconfigurable hardware platform is used for the channelizer implementation (instead of highly optimized application specific circuits for a hardware-based implementation) an efficient design which minimizes its computational load must be employed.

In the channelization related literature, and in this thesis, two main design streams for non-uniform channelizers have been identified: the per-channel approach, which uses separate processing resources for each of the channels; and filter banks, which share resources between the processing operations of the different channels. In Chapter 3, these two streams were evaluated for uniform channelization designs (in which only one communication standard must be supported). Compared to other publications which evaluated filter banks as channelizers, a new perspective was taken based on the asymmetric relationship between base station and mobile stations. The comparative results showed that complex modulated filter banks clearly outperform per-channel designs,

particularly for designs with a large number of channels. Furthermore, among the complex modulated filter banks, DFT-FBs require fewer operations than EMFBs. Therefore, DFT-FBs were selected as the basis for non-uniform channelizers based on filter banks.

Using the TETRA V&D and TEDS application context set up in Chapter 2, a critical evaluation of non-uniform channelizers proposed by other researchers and novel non-uniform channelizers developed in this work (e.g. P-GDFT) was carried out in Chapter 4. It was concluded that the GDFT-FB based non-uniform channelizers, P-GDFT and R-GDFT, offer the lowest computational load and best trade-off between the non-uniform channelization capabilities (e.g. flexibility, reconfigurability, upgrade, SRC). Moreover, R-GDFT showed the smallest computational load in most of the configurations and the greatest flexibility for allocating the channel centre frequencies. Therefore, among the set of non-uniform channelizers, R-GDFTs are the most suitable solution for a multi-standard SDR base station, followed by the P-GDFT. Nevertheless, for all the methods considered the FIR filter designs were found to require very high filter orders (e.g. around 8000 coefficients for the theoretical TETRA V&D prototype filter). Such high orders make the physical implementation of these channelizers impractical with currently available hardware, no matter what their computational load or flexibility is.

For this reason two novel multi-stage GDFT-FB designs, H-GDFT and M-GDFT, were developed in Chapter 5 with the objective of reducing the required number of filter coefficients and computational load. When applied to parallel and recombined structures (PH-GDFT, RH-GDFT, PM-GDFT, RM-GDFT) the multi-stage techniques were shown to achieve better results, with up to 84% fewer filter coefficients and up to 65% lower computational load. In addition, the RH-GDFT and RM-GDFT offer a more straightforward means to achieving the required magnitude complementary property of the prototype filter than the single-stage R-GDFT version.

A different approach to achieving more efficient GDFT-FB implementations was taken in Chapter 6. In this case, previous work applying FRM to prototype filter design in real modulated filter banks (CMFB) was extended for complex

modulated GDFT-FBs. In addition this work unified previously separate research developments in full and narrowband FRM. An extensive analysis of the different FRM GDFT-FB structures for critically decimated and oversampled systems was carried out. It was demonstrated that full and narrowband FRM GDFT-FB designs reduce the order of the FIR filters by up to 90% in comparison with the basic GDFT-FB. This coefficient reduction is even better than that of the two multi-stage designs evaluated in Chapter 5. However, the computational load was reduced (relative to the GDFT-FB) only for the oversampled FRM GDFT-FB designs, and not for the critically decimated case. It was also shown that depending on the filter specifications, the oversampled narrowband FRM GDFT-FB can require even fewer multiplications per input sample than the critically decimated GDFT-FB.

Further optimization based on a combination of multi-stage techniques and the narrowband FRM GDFT-FB was also explored. Recursive FRM GDFT-FB (C-FRM GDFT) reduced the number of coefficients by up to 95% but it required slightly higher computational load than the narrowband FRM GDFT-FB. On the other hand, multi-stage FRM-GDFT-FB (M-FRM GDFT) reduced the number of multiplications per input sample relative to the narrowband FRM GDFT-FB, but only at the expense of an increase in the number of coefficients. In general, as with the designs in Chapter 5, all the FRM GDFT-FB designs in Chapter 6 provide a more straightforward method than the GDFT-FB to achieve magnitude complementary filter specifications due to the use of half-band filters.

The application of the three narrowband structures (narrowband FRM GDFT-FB, C-FRM GDFT and M-FRM GDFT) to P-GDFT and R-GDFT channelizers was explored with use case 1, as a complement to the evaluation previously done in Chapter 5 with the same use case. From the overall comparison, it was concluded that all the novel techniques presented in Chapters 5 and 6 of this thesis yielded reductions in both the computational load and filter orders over the GDFT-FB based non-uniform channelizers. The only exception was the PH-GDFT which required significantly lower filter orders, but slightly more computation. The biggest reduction in the computational load was achieved by the PM-GDFT and RM-GDFT (Chapter 5), with up to 26% and 85% less real multiplications per input sample respectively. For the number of

non-zero coefficients, the PC-FRM GDFT and RC-FRM GDFT (Chapter 6) achieved up to 96% less coefficients.

In Chapter 7 two additional real world use cases based on currently trending communications topics were introduced, specifically, the provision of 4G to PMR communications and the re-farming of the GSM 900 and 1800 MHz frequency bands with UMTS, HSPA and LTE channels. Literature related to these use cases published to date has only dealt with information theory issues, such as channel capacity, and network interoperation. The practical (and important) issues of channel allocation and channelization for these real world use cases had not been studied in detail. Therefore a number of channel allocation options were explored and the most appropriate channelization structures were identified as a consequence.

Also in Chapter 7, physical channelizer implementation was studied further. The use of approximately linear phase IIR filters was explored as yet another possible optimization of the channelizer filters. Using a straightforward substitution of IIR half band filters for FIR half band filters in multi-stage filter banks it was found that the number of coefficients was reduced but computational load was almost unchanged. Therefore it is not yet clear that approximately linear phase filters provide much benefit.

Chapter 7 also examined the practical issue of fixed point filter implementation. It was concluded that in general GDFT-FB structures having filters with smallest number of coefficients lead to implementations less sensitive to quantization and round-off noise effects. Specifically, this point favours the lower filter orders of multi-stage and FRM GDFT-FB designs which are less sensitive to quantisation and round-off error effects in fixed point implementations.

Finally, the concept of optimizing the performance of the receiver processing chain (according to some metric) by selecting components which naturally complement each other was proposed. As a specific example, combination of an R-GDFT structure and a sub-band linear equalizer was examined and it was shown using this type of non-uniform channelizer could save on the

computational load of the equalizer. This appears to be a promising concept for future optimization of practical receiver implementations.

8.2 Future work

As a result of the work described in this thesis a number of areas have been identified in which further work could be done. Primarily this future work is related to the optimized physical implementation of non-uniform channelizers.

1. The use of IIR filters with approximately linear phase response was only applied to the half-band filters of the multi-stage GDFT-FB in this work. The application of approximately linear phase IIR filters could be extended to other parts of the non-uniform channelizer, such as the GDFT-FB prototype filter. This could be expected to reduce the number of coefficients and computational load associated with the channelizer but the level of improvement would have to be characterized. Furthermore, additional exploration of the degree of non-linearity introduced and the maximum level of non-linearity that could be tolerated in various applications should be performed.

2. In this thesis an SDR receiver structure where a complex baseband signal is delivered to the channelizer has been considered. Therefore, complex modulated filter banks were used as the basis for many of the channelizers. If the radio front end used a superheterodyne architecture, the possibility of channelizing the wideband real-valued IF signal directly could be studied. Two benefits are envisaged for this alternative: first, the digital mixing after the ADC (see Figure 2.7) could be suppressed, and second, all the operations would be performed on real input samples instead of complex ones.

3. In Chapter 7 the consequences of using fixed-point implementation for the physical channelizer implementation were reviewed. Further work would need to be done in to simulate the performance of channelizers with finite word lengths. Such simulation would be required to progress

towards physical implementation of channelizers using fixed point arithmetic.

4. After simulation, the next logical step would be to create a physical implementation of the channelizers on a reconfigurable hardware platform such as an FPGA. As part of this effort, detailed implementation issues could be explored, such as, for example, the amount of various FPGA resources (including memory and multipliers) used by the channelizer.

5. The interaction of the channelizer with the rest of the baseband signal processing of the channels deserves further study. In Section 7.4.3 it was shown that using a specific channelizer type (based on the R-GDFT) could allow optimization of a following linear sub-band equalizer. How far could these ideas be extended and what gains might be made? It seems likely, for example, that appropriate oversampling in the channelizer could facilitate baseband processing such as timing recovery.

6. For non-uniform channelizers using complex modulated filter banks, the option of using EMFBs instead of GDFT-FBs could be studied. Unlike the asymmetric case between the base station and mobile station, using EMFBs would facilitate the perfect reconstruction conditions for applications using the same type symmetric transmitter-receiver structures (similar to OFDM). Non-uniform channelizers formed by EMFBs with perfect reconstruction could eliminate the aliasing effects on the filters frequency responses for these symmetric applications. Furthermore, the same multi-stage and FRM techniques applied in this thesis to GDFT-FBs could be also applied to EMFBs to achieve reductions in the number of coefficients and computational load.

7. Following the continuous evolution of the SDR software architectures (i.e. GNURadio, OSSIE, IRIS), in the future the implementation of the non-uniform channelizer using them could be considered. Therefore, both channelizer and digital baseband processing of the channels would

be integrated on the same device (e.g. FPGA, CPU, GPU) providing a higher flexibility of interaction, and common optimization.

8. Throughout the thesis, the Kaiser equation expressed in (3.8) has been used to estimate the orders of the different FIR filters for the different designs. This equation demonstrated a good level of accuracy between the theoretical order obtained and the filters' frequency responses using floating-point precision. However, the application of Kaiser's equation would need to be assessed for fixed-point implementations where coefficient quantization is applied.

8.3 Chapter conclusions

The main contribution of this work has been to bridge the gap between the theoretical DSP design of non-uniform channelizers to concrete real-world application such as SDR base stations for specific multi-standard use cases. Only by doing this were the capabilities and limitations of the different channelization techniques identified, and as a consequence, were improvements that provided more efficient and practical implementations reached.

In the end, a number of more efficient uniform and non-uniform channelization techniques were developed and evaluated in conjunction with previously described techniques. The result of this work is that the SDR designer now has a catalogue of channelizers (graded according to the most relevant metrics of computational load and DSA flexibility among others) from which the most suitable for a particular application can be selected.

While further work on the detailed optimization of physical implementations may be done in the future, the coefficient reductions and computational load reductions resulting from the work in this thesis have brought the prospect of a practical SDR implementing reconfigurable and flexible non-uniform channelization closer to reality.

Appendix A

Table A.1 Non-uniform methods number of real multiplications per input sample for odd-stacked sub-band allocation.

Non-uniform channelizer	Real multiplications per input sample (μ)
FPCC	$\sum_{j=1}^{J} X_j \left[(N_P + 1)(P + 2) + P + 7 \right]$
TQMFB	No supported
HTQMFB	$\frac{4(N_{DFT} + 1) + \frac{3K}{2}\left(\log_2(K) - 5\right) + 8 + 4K}{K} + \frac{N_{QMF} + 1}{4} T$
FRM-FB	$4\sum_{j=1}^{J}\left(\frac{N_{Aj} + 1}{2}\right) + 4\sum_{j=1}^{J}\left[X_j \frac{N_{Mj} + 1}{2} + 4X_j \right]$
CDFB	$4\sum_{j=1}^{J}\left(\frac{N_{Aj} + 1}{2X_j}\right) + 4\sum_{j=1}^{J}\left[X_j \frac{N_{Mj} + 1}{2} + 4X_j \right]$
P-GDFT	$\sum_{j=1}^{J} L_{DFTj} \left\lceil \frac{4\left(N_{DFTj} + 1\right) + \frac{3K_j}{2}\left(\log_2(K_j) - 5\right) + 8 + 4K_j}{K_j} \right\rceil$
R-GDFT (GDFT-FB part)	$L_{DFT} \left\lceil \frac{4\left(N_{DFT} + 1\right) + \frac{3K}{2}\left(\log_2(K) - 5\right) + 8 + 4K}{K} \right\rceil$
R-GDFT (Recomb. structure)	$\sum_{j=1}^{J} \frac{L_{DFT}}{K} \left\lceil X_j \left(M_j \times R_j \left(2\frac{N_{Ij} + 1}{2} + 4 + \frac{4}{M_j} \right) \right) \right\rceil$

Table A.2 Non-uniform methods number of real additions per input sample for even-stacked sub-band allocation.

Non-uniform channelizer	Real additions per input sample (α)
FPCC	$\sum_{j=0}^{J} X_j \left[2N_F(P+2)+P+2\right]$
TQMFB	$N_{QMF}T$
HTQMFB	$\frac{2\left(N_{DFT}+1-K\right)+\frac{7K}{2}(\log_2(K)-5)+8}{K}+N_{QMF}T$
FRM-FB	$2\sum_{j=1}^{J}\left[N_{Aj}+2N_{Mj}\left(X_j+1\right)\right]$
CDFB	$2\sum_{j=1}^{J}\left[\frac{N_{Aj}}{X_j}+2N_{Mj}\left(X_j+1\right)\right]$
P-GDFT	$\sum_{j=1}^{J} L_{DFTj}\left[\frac{2\left(N_{DFTj}+1-K_j\right)+\frac{7K_j}{2}(\log_2(K_j)-5)+8}{K_j}\right]$
R-GDFT (GDFT-FB)	$L_{DFT}\left[\frac{2\left(N_{DFTS}+1-K\right)+\frac{7K}{2}(\log_2(K)-5)+8}{K}\right]$
R-DFT (recombination)	$\sum_{j=1}^{J}\frac{L_{DFT}}{K}\left[M_j\left(2R_j\left(N_{Ij}+1+\frac{1}{M_j}\right)+2(R_j-1)\right)\right]$

Table A.3 Non-uniform methods number of real additions per input sample for odd-stacked sub-band allocation.

Non-uniform channelizer	Real additions per input sample (α)
FPCC	$\sum_{j=0}^{J} X_j \left[2N_F(P+2)+P+2\right]$
TQMFB	No supported
HTQMFB	$\frac{4\left(N_{DFT}+1-\frac{K}{2}\right)+\frac{7K}{2}(\log_2(K)-5)+8+2K}{K}+N_{QMF}T$
FRM-FB	$2\sum_{j=1}^{J}\left[2N_{Aj}+2N_{Mj}\left(X_j+1\right)+1\right]$
CDFB	$2\sum_{j=1}^{J}\left[2\frac{N_{Aj}}{X_j}+2N_{Mj}\left(X_j+1\right)+1\right]$
P-GDFT	$\sum_{j=1}^{J} L_{DFTj}\left[\frac{4\left(N_{DFTj}+1-\frac{K_j}{2}\right)+\frac{7K_j}{2}(\log_2(K_j)-5)+8+2K_j}{K_j}\right]$
R-GDFT (GDFT-FB)	$L_{DFT}\left[\frac{4\left(N_{DFTS}+1-\frac{K}{2}\right)+\frac{7K}{2}(\log_2(K)-5)+8+2K}{K}\right]$
R-DFT (recombination)	$\sum_{j=1}^{J}\frac{L_{DFT}}{K}\left[M_j\left(2R_j\left(N_{Ij}+1+\frac{1}{M_j}\right)+2(R_j-1)\right)\right]$

Table A.4 Use case 1 configuration parameters.

Non-uniform channelizer	Parameters
FPCC	$A_1 = 320, A_2 = A_3 = 100,\ B_1 = 9,\ B_2 = 6,\ B_3 = 12$ $P = 4,\ \ f_S = 6.4\text{MHz}, K_1 = X_1,\ K_2 = X_2, K_3 = X_3$
FRM-FB	$K_1 = 200, K_2 = 100, K_3 = 50,\ f_S = 5\text{MHz}$
CDFB	$D_{C1} = 200, D_{C2} = 100, D_{C3} = 50,\ f_S = 5\text{MHz}$
TQMFB	$T = 256,\ f_S = 6.4\text{MHz}$
HTQMFB	$T = 3, K = 64,\ f_S = 6.4\text{MHz}$
P-GDFT	$K_1 = 256, K_2 = 128, K_3 = 64$ $f_S = 6.4\text{MHz}$
R-GDFT	$K = 256, L_{DFT} = 2, R_1 = 1, R_2 = 2, M_2 = 1, N_{I2} = 0$ $R_3 = 4, M_3 = 2, N_{I3} = 28,\ f_S = 6.4\text{MHz}$ (X_1, X_2, X_3 depending on conf.)

Table A.5 Use case 2 configuration parameters.

Non-uniform channelizer	Parameters
FPC	$A_1 = 320, A_2 = A_3 = 100,\ B_1 = 9,\ B_2 = 6,\ B_3 = 18$ $P = 4,\ \ f_S = 6.4\text{MHz}, K_1 = X_1,\ K_2 = X_2, K_3 = X_3$
FRM-FB	$K_1 = 200, K_2 = 100, K_3 = 34$ $f_{S1} = f_{S2} = 5\text{MHz}, f_{S3} = 5.1\text{MHz}$
CDFB	$D_{C1} = 200, D_{C2} = 100, D_{C3} = 34$ $f_{S1} = f_{S2} = 5\text{MHz}, f_{S3} = 5.1\text{MHz}$
P-GDFT	$K_1 = 256, K_2 = 125, K_3 = 64$ $f_{S1} = f_{S2} = 6.4\text{MHz}, f_{S3} = 9.6\text{MHz}$
R-GDFT	$K = 256, L_{DFT} = 2, R_1 = 1, R_2 = 2, M_2 = 1, N_{I2} = 0$ $R_3 = 6, M_3 = 3, N_{I3} = 42,\ f_S = 6.4\text{MHz}$ (X_1, X_2, X_3 depending on conf.)

Appendix B

```
%FIR filter order calculation using Kaiser equation
%Example for TETRA V&D channels with 6.4 MHz input sample rate

%Sample rate (in Hz)
fs=6400000;

%Pass-band and stopband cut-off frequencies (in Hz)
wp=11500;
ws=13500;

%Passband and stopband ripples (in dB)
ap_db=0.1;
as_db=-55;

%Passband and stopband frequencies normalisation
wpn=wp/(fs/2);
wsn=ws/(fs/2);

%Passband and stopband ripples translation into times
ap=(10^(ap_db/40))-1;
as=10^(as_db/20);

%FIR filter order calculation
K=2*pi*((-20*log10(sqrt(ap*as))-13)/14.6);

Nprot=ceil(K/((wsn-wpn)*pi))
```

Appendix C

Table C.1 FRM GDFT-FB design example for TEDS 25 kHz filter bank with K=256. Shaded rows correspond to designs that lead to non-real frequencies and therefore can not be implemented.

Case	m	L	θ (rad)	φ (rad)	ω_{Mpa} (rad)	ω_{Msa} (rad)	ω_{Mpc} (rad)	ω_{Msc} (rad)	N_A	N_{MA}
1	1	640	0.3	0.7	0.00359	0.00516	0.00266	0.00422	14	3404
1	2	1152	0.14	0.86	0.00359	0.00446	0.00335	0.00422	8	6127
1	3	1664	-0.02	1.02	0.00359	0.00419	0.00362	0.00422	-	-
1	4	2176	-0.18	1.18	0.00359	0.00405	0.00376	0.00422	-	-
1	5	2688	-0.34	1.34	0.00359	0.00397	0.00385	0.00422	-	-
2	1	384	0.38	0.62	0.00161	0.0042	0.00359	0.00620	24	2043
2	2	896	0.22	0.78	0.00310	0.0042	0.00359	0.00471	10	4766
2	3	1408	0.06	0.94	0.00351	0.0042	0.00359	0.00430		
2	4	1920	-0.1	1.1	0.00370	0.0042	0.00359	0.00411	-	-
2	5	2432	-0.26	1.26	0.00381	0.0042	0.00359	0.004	-	-

Table C.2 FRM GDFT-FB design example for TEDS 50 kHz filter bank with K=128. Shaded rows correspond to designs that lead to non-real frequencies and therefore can not be implemented.

Case	m	L	θ (rad)	φ (rad)	ω_{Mpa} (rad)	ω_{Msa} (rad)	ω_{Mpc} (rad)	ω_{Msc} (rad)	N_A	N_{MA}
1	1	320	0.28	0.72	0.00713	0.01025	0.00537	0.0085	12	1617
1	2	576	0.104	0.896	0.00713	0.00886	0.00676	0.0085	7	2911
1	3	832	-0.072	1.072	0.00713	0.00833	0.00730	0.0085	-	-
1	4	1088	-0.248	1.248	0.00713	0.00804	0.00758	0.0085	-	-
1	5	1344	-0.424	1.424	0.00713	0.00787	0.00776	0.0085	-	-
2	1	192	0.0368	0.632	0.00329	0.0085	0.00713	0.01233	20	971
2	2	448	0.192	0.808	0.00627	0.0085	0.00713	0.00936	9	2264
2	3	704	0.016	0.984	0.00708	0.0085	0.00713	0.00855	6	3558
2	4	960	-0.16	1.16	0.00746	0.0085	0.00713	0.00817	-	-
2	5	1216	-0.336	1.336	0.00768	0.0085	0.00713	0.00795	-	-

Table C.3 FRM GDFT-FB design example for TEDS 100 kHz filter bank with K=64. Shaded rows correspond to designs that lead to non-real frequencies and therefore can not be implemented.

Case	m	L	θ (rad)	φ (rad)	ω_{Mpa} (rad)	ω_{Msa} (rad)	ω_{Mpc} (rad)	ω_{Msc} (rad)	N_A	N_{MA}
1	1	160	0.22	0.78	0.01388	0.02012	0.01112	0.01738	10	851
1	2	288	-0.004	1.004	0.01388	0.01735	0.0139	0.01738	-	-
1	3	416	-0.228	1.228	0.01388	0.01628	0.01497	0.01738	-	-
1	4	544	-0.452	1.45	0.01388	0.01571	0.01554	0.01738	-	-
1	5	672	-0.676	1.676	0.01388	0.01536	0.01589	0.01738	-	-
2	1	96	0.332	0.668	0.00696	0.01738	0.01388	0.02429	16	511
2	2	224	0.108	0.892	0.01291	0.01738	0.01388	0.01834	8	1192
2	3	352	-0.116	1.116	0.01453	0.01738	0.01388	0.01672	-	-
2	4	480	-0.34	1.34	0.01529	0.01738	0.01388	0.01596	-	-
2	5	608	-0.564	1.564	0.01573	0.01738	0.01388	0.01552	-	-

Table C.4 FRM GDFT-FB design example for TEDS 150 kHz filter bank with K=64. Shaded rows correspond to designs that lead to non-real frequencies and therefore can not be implemented.

Case	m	L	θ (rad)	φ (rad)	ω_{Mpa} (rad)	ω_{Msa} (rad)	ω_{Mpc} (rad)	ω_{Msc} (rad)	N_A	N_{MA}
1	1	160	0.35	0	0.1469	0.02146	0.01031	0.01604	26	786
1	2	288	0.23	0.5667	0.1469	0.01868	0.01309	0.01604	14	1332
1	3	416	0.11	0.62	0.1469	0.01761	0.01416	0.01604	10	1819
1	4	544	-0.01	0.6733	0.1469	0.01705	0.01472	0.01604	-	-
1	5	672	-0.13	0.7267	0.1469	0.0167	0.01507	0.01604	-	-
2	1	96	0.46	0.59	0.00615	0.01604	0.01469	0.02562	42	538
2	2	224	0.4067	0.71	0.0121	0.01604	0.01469	0.01967	18	1349
2	3	352	0.3533	0.83	0.01372	0.01604	0.01469	0.01805	12	2293
2	4	480	0.3	0.95	0.01448	0.01604	0.01469	0.01729	10	3404
2	5	608	0.2467	1.07	0.01492	0.01604	0.01469	0.01685	-	-

Table C.5 Computational load comparison between legacy GDFT-FB and FRM GDFT-FB TETRA 25 kHz channelizers for both even and odd channel stacking. Shaded rows represent the configurations where the FRM GDFT-FB requires fewer amount of operations than GDFT-FB.

Structure	L_{DFT}	μ	α	Overhead μ	Overhead α
GDFT-FB even stacked	1	78.1	83.1	100.0	100.0
GDFT-FB odd stacked	1	146.2	149.2	100.0	100.0
FRM GDFT-FB even stacked	1	84.9	94.9	108.7	114.2
FRM GDFT-FB odd stacked	1	149.9	155.9	102.5	104.5
Narrow FRM GDFT-FB even stacked	1	107.7	117.7	137.8	141.6
Narrow FRM GDFT-FB odd stacked	1	195.3	201.3	133.6	134.9
GDFT-FB even stacked	2	156.2	166.2	100.0	100.0
GDFT-FB odd stacked	2	292.4	298.4	100.0	100.0
FRM GDFT-FB even stacked	2	144.9	162.9	92.7	98.0
FRM GDFT-FB odd stacked	2	249.8	263.8	85.4	88.4
Narrow FRM GDFT-FB even stacked	2	146.3	164.3	93.7	98.9
Narrow FRM GDFT-FB odd stacked	2	252.6	266.6	86.4	89.3
Alternative FRM GDFT-FB even stacked	2	169.9	187.9	108.7	113.0
Alternative FRM GDFT-FB odd stacked	2	249.8	259.8	85.4	87.0
Alternative narrow FRM GDFT-FB even stacked	2	107.7	184.7	68.9	111.1
Alternative narrow FRM GDFT-FB odd stacked	2	126.3	197.3	43.2	66.1

Table C.6 Computational load comparison between legacy GDFT-FB and FRM GDFT-FB TEDS 50 kHz channelizers for both even and odd channel stacking. Shaded rows represent the configurations where the FRM GDFT-FB requires fewer amount of operations than GDFT-FB.

Structure	L_{DFT}	μ	α	Overhead μ	Overhead α
GDFT-FB even stacked	1	70.3	74.3	100.0	100.0
GDFT-FB odd stacked	1	132.6	134.6	100.0	100.0
FRM GDFT-FB even stacked	1	79.0	87.0	112.3	117.1
FRM GDFT-FB odd stacked	1	141.9	145.9	107.0	108.4
Narrow FRM GDFT-FB even stacked	1	97.7	105.7	139.0	142.3
Narrow FRM GDFT-FB odd stacked	1	179.4	183.4	135.3	136.2
GDFT-FB even stacked	2	140.6	148.6	100.0	100.0
GDFT-FB odd stacked	2	265.2	269.2	100.0	100.0
FRM GDFT-FB even stacked	2	134.9	148.9	96.0	100.2
FRM GDFT-FB odd stacked	2	237.9	247.9	89.7	92.1
Narrow FRM GDFT-FB even stacked	2	132.4	146.4	94.2	98.5
Narrow FRM GDFT-FB odd stacked	2	232.8	242.8	87.8	90.2
Alternative FRM GDFT-FB even stacked	2	157.9	171.9	112.3	115.7
Alternative FRM GDFT-FB odd stacked	2	237.9	243.9	89.7	90.6
Alternative narrow FRM GDFT-FB even stacked	2	97.7	166.7	69.5	112.2
Alternative narrow FRM GDFT-FB odd stacked	2	116.4	179.4	43.9	66.6

Table C.7 Computational load comparison between legacy GDFT-FB and FRM GDFT-FB TEDS 100 kHz channelizers for both even and odd channel stacking. Shaded rows represent the configurations where the FRM GDFT-FB requires fewer amount of operations than GDFT-FB.

Structure	L_{DFT}	μ	α	Overhead μ	Overhead α
GDFT-FB even stacked	1	55.8	58.8	100.0	100.0
GDFT-FB odd stacked	1	105.6	106.6	100.0	100.0
FRM GDFT-FB even stacked	1	69.0	75.0	123.6	127.5
FRM GDFT-FB odd stacked	1	126.0	128.0	119.3	120.0
Narrow FRM GDFT-FB even stacked	1	79.8	85.8	142.9	145.8
Narrow FRM GDFT-FB odd stacked	1	147.5	149.5	139.6	140.2
GDFT-FB even stacked	2	111.6	117.6	100.0	100.0
GDFT-FB odd stacked	2	211.3	213.3	100.0	100.0
FRM GDFT-FB even stacked	2	121.0	131.0	108.4	111.4
FRM GDFT-FB odd stacked	2	218.0	224.0	103.2	105.0
Narrow FRM GDFT-FB even stacked	2	110.5	120.5	99.0	102.4
Narrow FRM GDFT-FB odd stacked	2	197.0	203.0	93.3	95.2
Alternative FRM GDFT-FB even stacked	2	138.0	148.0	123.6	125.8
Alternative FRM GDFT-FB odd stacked	2	218.0	220.0	103.2	103.2
Alternative narrow FRM GDFT-FB even stacked	2	79.8	132.8	71.4	112.9
Alternative narrow FRM GDFT-FB odd stacked	2	98.5	145.5	46.6	68.2

References

[1] *Terrestrial Trunked Radio (TETRA); Feasibility Study into the Implications of Operating Public Safety Sector (PSS) TEDS using the proposed "Tuning Range" concept in the 410 MHz to 430 MHz and 450 MHz to 470 MHz frequency bands,* E. T. S. Institute ETSI TR 102 513 V1.1.1, 2006-12.

[2] R. D. Vieira, *et al.*, "GSM Evolution Importance in Re-Farming 900 MHz Band," in *Vehicular Technology Conference Fall (VTC 2010-Fall), 2010 IEEE 72nd*, 2010, pp. 1-5.

[3] P. Burns, *Software Defined Radio for 3G*: Artech House, Inc., 2003.

[4] S. Haykin, *Communication Systems*, 5th ed.: Wiley Publishing, 2009.

[5] ECP, "The European Table of Frequency Allocations and Utilisations Covering the Frequency Range 9 kHz to 275 GHz," ed, 2004.

[6] ITU. (2011, October). *International Telecommunications Union*. Available: www.itu.int

[7] V. H. MacDonald, "The cellular concept," *Bell Syst. Tech. J.*, vol. 58, pp. 15-41, Jan. 1979.

[8] L. D. Olavarrieta and A. A. Nava, "Wireless communications: a bird's eye view of an emerging technology," in *Communications and Information Technology, 2004. ISCIT 2004. IEEE International Symposium on*, 2004, pp. 541-546 vol.1.

[9] Motorola, "Long Term Evolution (LTE): Overview of LTE Air-Interface Technical White Paper," ed: Motorola, Inc., 2007.

[10] P. Leaves, *et al.*, "Dynamic spectrum allocation in composite reconfigurable wireless networks," *Communications Magazine, IEEE,* vol. 42, pp. 72-81, 2004.

[11] P. K. Bruce A. Fette, Pablo Robert, John Polson, Preston Marshall, , *Cognitive Radio Technology*: Newnes, 2006.

[12] S. Haykin, "Cognitive radio: brain-empowered wireless communications," *Selected Areas in Communications, IEEE Journal on,* vol. 23, pp. 201-220, 2005.

[13] C. Kiran, *et al.*, "Evolution of spectrum-agile cognitive radios: first wireless internet standard and beyond," in *Proceedings of the 2nd annual international workshop on Wireless internet*, Boston, Massachusetts, 2006.

[14] J. Mitola, III, "Cognitive radio for flexible mobile multimedia communications," in *Mobile Multimedia Communications, 1999. (MoMuC '99) 1999 IEEE International Workshop on*, 1999, pp. 3-10.

[15] J. Mitola, III and G. Q. Maguire, Jr., "Cognitive radio: making software radios more personal," *Personal Communications, IEEE [see also IEEE Wireless Communications]*, vol. 6, pp. 13-18, 1999.

[16] L. Bao and S. Liao, "Scheduling heterogeneous wireless systems for efficient spectrum access," *EURASIP J. Wirel. Commun. Netw.*, vol. 2010, pp. 1-14, 2010.

[17] ETSI, "Terrestrial Trunked Radio (TETRA);Voice plus Data (V+D);Part 2: Air Interface (AI)," vol. ETSI EN 300 392-2 V3.2.1, E. T. S. Institute, Ed., ed, 2007-09.

[18] *Terrestrial Trunked Radio (TETRA)Conformance testing specification;Part 1: Radio*, ETSI EN 300 394-1 V3.1.1, 2007-11.

[19] PSWN, "Comparison of conventional and trunked systems," Public Safety Wireless Networks, Homeland Security,1999.

[20] P. Stavroulakis, *TErrestrial Trunked RAdio - TETRA: A Global Security Tool*: Springer, 2010.

[21] T. Association. (2011, June). *TETRA Association Web Official Site*. Available: http://www.tetramou.com

[22] M. Nouri, *et al.*, "TEDS: A high speed digital mobile communication air interface for professional users," *Vehicular Technology Magazine, IEEE*, vol. 1, pp. 32-42, 2006.

[23] *Electromagnetic compatibility and Radio spectrum Matters (ERM); TETRA Enhanced Data Service (TEDS); System reference document*, ETSI TR 102 491 V1.2.1, 2006-05.

[24] *Terrestrial Trunked Radio (TETRA); Release 2; Designer's Guide; TETRA High-Speed Data (HSD); TETRA Enhanced Data Service (TEDS)*, E. T. S. Institute ETSI TR 102 580 V1.1.1, 2007-10.

[25] J. G. Proakis and M. Salehi, *Digital communications*: McGraw-Hill, 2008.

[26] *Terrestrial Trunked Radio (TETRA); Voice plus Data (V+D); Part 15: TETRA frequency bands, duplex spacings and channel numbering*, ETSI TS 100 392-15 V1.3.1, 2004.

[27] *Planning criteria and coordination of frequencies in the land mobile service in the range 29.7-921 MHz*, T/R 25-08, 2008.

[28] *Availability of frequency bands for the introduction of Wide Band Digital Land Mobile PMR/PAMR in the 400 MHz and 800/900 MHz bands*, Amended ECC/DEC/(04)06, June 2009.

[29] *Harmonisation of frequency bands for the implementation of digital Public Protection and Disaster Relief (PPDR) radio applications in bands within the 380-470 MHz range*, ECC/DEC/(08)05, June 2008.

[30] ECC, "Public protection and disaster relief spectrum requirements (ECC report 102)," HelsinkiJanuary 2007.

[31] Nokia. (2005, Enabling high speed data communications over TETRA. *Nokia Corporation White Paper*.

[32] WIF. (2011, October). *Wireless Innovation Forum*. Available: www.wirelessinnovation.org

[33] R. I. Lackey and D. W. Upmal, "Speakeasy: the military software radio," *Communications Magazine, IEEE,* vol. 33, pp. 56-61, 1995.

[34] W. Bonser, "SPEAKeasy military software defined radio (Presentation)," in *International Symposium on Advanced Radio Technologies*, 1998.

[35] J. Mitola, III, "Software Radios: Survey, Critical Evaluation and Future Directions," in *National Telesystems Conference (NTC-92),* 1992.

[36] W. Tuttlebee, *Software Defined Radio: Origins, Drivers and International Perspectives* vol. : John Wiley & Sons, LTD, 2002.

[37] P. Mackenzie, "Reconfigurable Software Radio Systems," Doctor in Philosophy Doctoral, Trinity College, Dublin, 2004.

[38] W. Lehr, *et al.*, "Software radio: implications for wireless services, industry structure, and public policy," in *The 30th Research Conference on Information, Communication, and Internet Policy, Telecommunications Policy Research Conference (TPRC),* 2002.

[39] S. P. Reichhart, *et al.*, "The software radio development system," *Personal Communications, IEEE [see also IEEE Wireless Communications],* vol. 6, pp. 20-24, 1999.

[40] W. Tuttlebee, *Software Defined Radio: Enabling Technologies*: John Wiley & Sons, LTD, 2002.

[41] U. Ramacher, "Software-Defined Radio Prospects for Multistandard Mobile Phones," *Computer,* vol. 40, pp. 62-69, 2007.

[42] B. Bing and N. Jayant, "A cellphone for all standards," *Spectrum, IEEE,* vol. 39, pp. 34-39, 2002.

[43] M. N. O. Sadiku and C. M. Akujuobi, "Software-defined radio: a brief overview," *Potentials, IEEE,* vol. 23, pp. 14-15, 2004.

[44] P. B. Kenington, *RF and Baseband Techniques for Software Defined Radio*: Artech House, Inc. Mobile Communication Series, 2005.

[45] A. Wiesler and F. K. Jondral, "A software radio for second- and third-generation mobile systems," *Vehicular Technology, IEEE Transactions on,* vol. 51, pp. 738-748, 2002.

[46] J. Mitola, "The software radio architecture," *Communications Magazine, IEEE,* vol. 33, pp. 26-38, 1995.

[47] T. Hentschel, *et al.*, "The digital front-end of software radio terminals," *Personal Communications, IEEE [see also IEEE Wireless Communications],* vol. 6, pp. 40-46, 1999.

[48] H. Yoshida, *et al.*, "Broadband RF front-end and software execution procedure in software-defined radio," in *Vehicular Technology Conference, 1999. VTC 1999 - Fall. IEEE VTS 50th*, 1999, pp. 2133-2137 vol.4.

[49] D. S. Dawoud and S. E. Phakathi, "Advanced filter bank based ADC for software defined radio applications," in *AFRICON, 2004. 7th AFRICON Conference in Africa*, 2004, pp. 61-66 Vol.1.

[50] M. Soudan and R. Farrell, "On time-interleaved analog-to-digital converter for wideband reconfigurable radios," in *Proceedings of the SDR'09 Technical Conference and Product Exposition*, 2009.

[51] K. El-Sankary and M. Sawan, "High resolution self-calibrated ADCs for software defined radios," in *Microelectronics, 2004. ICM 2004 Proceedings. The 16th International Conference on*, 2004, pp. 120-123.

[52] A. D. Jadhav, "Folding ADC Design for Software Defined GSM Radio-Mobile Station Receiver," *International Journal of Computer Science and Network Security (IJCSNS),* vol. 8, September 2008.

[53] T. Ching-Hsiang and C. Sun-Chung, "Direct downconversion of multiband RF signals using bandpass sampling," *Wireless Communications, IEEE Transactions on,* vol. 5, pp. 72-76, 2006.

[54] S. Rodriguez-Pareram, *et al.*, "Front-End ADC Requirements for Uniform Bandpass Sampling in SDR," in *Vehicular Technology Conference, 2007. VTC2007-Spring. IEEE 65th*, 2007, pp. 2170-2174.

[55] M. Patel and P. Lane, "Comparison of Downconversion Techniques for Software Radio," Department of Electrical Engineering, University College London.

[56] A. Ucar, *et al.*, "A Reconfigurable SDR Receiver for Multi-mode GNSS Applications," in *Proceedings of the SDR '08 Technical Conference and product Exposition*, Washington DC, 2008.

[57] D. M. Pham, *et al.*, "Efficient Sample Rate Conversion in Software Radio Employing Folding Number System," in *Communications, 2009. ICC '09. IEEE International Conference on*, 2009, pp. 1-5.

[58] N. Semiconductor. (2011, 2009). *Direct RF-Sampling ADCs*. Available: http://www.national.com/en/rf/rf_sampling_adc.html

[59] W. A. Abu-Al-Saud and G. L. Stuber, "Efficient sample rate conversion for software radio systems," *Signal Processing, IEEE Transactions on,* vol. 54, pp. 932-939, 2006.

[60] T. Hentschel and G. Fettweis, "Sample rate conversion for software radio," *Communications Magazine, IEEE,* vol. 38, pp. 142-150, 2000.

[61] L. Gao, *et al.*, "Opportunities and challenges for SDR in next generation TETRA systems," in *CISDR 2008 workshop*, Maynooth, Ireland, 2008.

[62] M. Carrick, *et al.*, "OSSIE 0.6.2 User Guide," Virginia TechDecember 2007 2007.

[63] GNURadio. (2008, January). *GNU Radio Web Page*. Available: http://gnuradio.org/trac

[64] T. C. Dublin, "IRIS: Implementing Radio in Software. Getting Starterd Guide.," June 2007 2007.

[65] C. R. C. Canada. (2001, October). *Scari Software Suite*. Available: http://www.crc.gc.ca/en/html/crc/home/research/satcom/rars/sdr/products/scari_suite/scari_suite

[66] Zeligsoft. (2001, 2009). *Spectra CX*. Available: http://www.zeligsoft.com/domains/sdr-sca

[67] G. Abgrall, *et al.*, "Predictibility of inter-component latency in a software communications architecture operating environment," in *Parallel & Distributed Processing, Workshops and Phd Forum (IPDPSW), 2010 IEEE International Symposium on*, 2010, pp. 1-8.

[68] C. Duyun, *et al.*, "OSSIE/GNU Radio Generic Component," in *Wireless Telecommunications Symposium (WTS), 2011*, 2011, pp. 1-5.

[69] C. R. A. Gonzalez, *et al.*, "Open-source SCA-based core framework and rapid development tools enable software-defined radio education and research," *Communications Magazine, IEEE*, vol. 47, pp. 48-55, 2009.

[70] E. Redding, *et al.*, "OSSIE-based GRA testbed," in *Military Communications Conference, 2009. MILCOM 2009. IEEE*, 2009, pp. 1-8.

[71] M. I. Taj, *et al.*, "Performance evaluation of SDR on embedded platform: The case of OSSIE," in *Computer, Control and Communication, 2009. IC4 2009. 2nd International Conference on*, 2009, pp. 1-5.

[72] J. Friedman, *et al.*, "Angle-of-arrival-assisted Relative Interferometric localization using Software Defined Radios," in *Military Communications Conference, 2009. MILCOM 2009. IEEE*, 2009, pp. 1-8.

[73] S. Heunis, *et al.*, "Passive radar using a software-defined radio platform and opensource software tools," in *Radar Conference (RADAR), 2011 IEEE*, 2011, pp. 879-884.

[74] V. Pejovic and E. M. Belding, "A context-aware approach to wireless transmission adaptation," in *Sensor, Mesh and Ad Hoc Communications and Networks (SECON), 2011 8th Annual IEEE Communications Society Conference on*, 2011, pp. 592-600.

[75] L. Williams and M. R. Inggs, "Low cost networked radar and sonar using open source hardware and software," in *Radar Systems, 2007 IET International Conference on*, 2007, pp. 1-5.

[76] A. Palomo Navarro, *et al.*, "Software Defined Radio Architectures Evaluation," in *Proceedings of the SDR '08 Technical Conference and product Exposition*, Washington DC, 2008.

[77] S. Valentin, *et al.*, "Evaluating the GNU Software Radio Platform for Wireless Testbed," Computer Network Group, University of Paderborn2006.

[78] F. Ge, *et al.*, "Software Defined Radio Execution Latency," in *Proceedings of the SDR '08 Technical Conference and product Exposition*, Washington DC, 2008.

[79] T. Tsou, *et al.*, "Latency Profiling for SCA Software Radio," in *Proceedings of the SDR'07 Technical Conference and Product Exposition*, Denver, Colorado, 2007.

[80] P. Balister, *et al.*, "Impact of the Use of CORBA for Inter-Component Communication in SCA Based Radio," in *Proceedings of the SDR'06 Technical Conference and Product Exposition*, Orlando, Florida, 2006.

[81] S. A. Fahmy, *et al.*, "Generic Software Framework for Adaptive Applications on FPGAs," in *Field Programmable Custom Computing Machines, 2009. FCCM '09. 17th IEEE Symposium on*, 2009, pp. 55-62.

[82] E. A. Blossom, "GCELL - An SPE Scheduler and Ashynchronous RPC Mechanism for the Cell Broadband Engine," in *Proceedings of the SDR '08 Technical Conference and product Exposition*, Washington DC, 2008.

[83] W. Plishker, *et al.*, "Applying graphics processor acceleration in a software defined radio prototyping environment," in *Rapid System Prototyping (RSP), 2011 22nd IEEE International Symposium on*, 2011, pp. 67-73.

[84] V. Bose, "Design and Implementation of Software Radios Using a General Purpose Processor," PhD Doctoral Thesis, Massachusetts Institute of Technology, 1999.

[85] JTRS, "Software Communications Architecture Specification," ed: Joint Tactical Radio System (JTRS) Joint Program Office, Version 2.2.2, 2006.

[86] Python. (2011, October). *Python Official Web Page*. Available: http://www.python.org

[87] W3C. (2011, 2009). *Extensible Markup Language (XML)*. Available: http://www.w3.org/XML/

[88] Z. Chen and L. Wang, "Green Base Station Solutions and Technology," *ZTE Comms. Journal. Special topic: Microwave/RF Technologies for Future Wireless Communications* vol. 9, 2011.

[89] K. C. Zangi and R. D. Koilpillai, "Software radio issues in cellular base stations," *Selected Areas in Communications, IEEE Journal on,* vol. 17, pp. 561-573, 1999.

[90] T. Turletti, *et al.*, "Toward the software realization of a GSM base station," *Selected Areas in Communications, IEEE Journal on,* vol. 17, pp. 603-612, 1999.

[91] T. Hentschel, "Channelization for software defined base stations," *Annales de Telecommunications,* May/June 2002.

[92] M. u. R. Awan and P. Koch, "Polyphase channelizer as bandpass filters in multi-standard Software Defined Radios," in *Cognitive Radio and Advanced Spectrum Management, 2009. CogART 2009. Second International Workshop on*, 2009, pp. 59-63.

[93] L. Pucker, "Channelization techniques for software defined radio," in *Proceedings of the SDR 2010 Technical Conference and product Exposition*, Washington DC, 2010.

[94] J. G. Proakis and D. G. Manolakis, *Digital Signal Processing*, 3rd ed., 1996.

[95] K. W. Martin, "Complex signal processing is not complex," *Circuits and Systems I: Regular Papers, IEEE Transactions on*, vol. 51, pp. 1823-1836, 2004.

[96] A. Viholainen, "Modulated filter bank design for communication signal processing," PhD, Tampere University of Technology, Tampere, 2004.

[97] R. E. Crochiere and L. R. Rabiner, *Multirate Digital Signal Processing*: Englewood Cliffs (NJ): Prentice Hall, 1983.

[98] F. J. Harris, *Multirate Signal Processing for Communication Systems*: Prentice Hall PTR, 2004.

[99] T. Saramäki, "Finite impulse response filter design," in *Handbook for Digital Signal Processing*, S. K. Mitra and J. F. Kaiser, Eds., ed New York , NY, USA: John Wiley & Sons, 1993, pp. 155-227.

[100] R. A. Losada. (2008). *Digital filters with MATLAB*.

[101] J. McClellan, *et al.*, "A computer program for designing optimum FIR linear phase digital filters," *Audio and Electroacoustics, IEEE Transactions on*, vol. 21, pp. 506-526, 1973.

[102] J. Kaiser, "Nonrecursive Digital Filter Design Using the IO-Sinh Window Function," in *IEEE International Symposium on Circuits and Systems*, 1974.

[103] A. Ray, "A survey of CORDIC algorithms for FPGA based computers," in *Proceedings of the 1998 ACM/SIGDA sixth international symposium on Field programmable gate arrays*, Monterey, California, United States, 1998.

[104] J. E. Volder, "The CORDIC trigonometric computing technique," *IRE Transactions on Electronic Computers*, vol. EC-8, pp. 330-334, Sept. 1959.

[105] M. Lohning and T. Hentschel, "Digital Down Conversion in Software Radio Terminals," in *Proceedings of the 10 European Signal Processing Conference (EUSIPCO)*, Tampere(Finland), 2000.

[106] Xilinx, "CORDIC v3.0 product specification," ed, 2005.

[107] P. P. Vaidyanathan, *Multirate Systems and Filter Banks*: Prentice Hall PTR, 1993.

[108] L. Yong, "Frequency-response masking approach for the synthesis of sharp linear phase digital filters," *Circuits and Systems, IEEE Transactions on,* vol. 33, pp. 357-364, 1986.

[109] R. C. S. Morling, *et al.*, "The design of a sigma-delta codec for mobile telephone applications," in *Advanced A-D and D-A Conversion Techniques and their Applications, 1994. Second International Conference on*, 1994, pp. 11-17.

[110] E. Hogenauer, "An economical class of digital filters for decimation and interpolation," *Acoustics, Speech and Signal Processing, IEEE Transactions on,* vol. 29, pp. 155-162, 1981.

[111] M. Bellanger, *et al.*, "Digital filtering by polyphase network:Application to sample-rate alteration and filter banks," *Acoustics, Speech and Signal Processing, IEEE Transactions on,* vol. 24, pp. 109-114, 1976.

[112] L. Milic, *Multirate Filtering for Digital Signal Processing*: Information Science Reference, 2009.

[113] L. C. R. de Barcellos, "Estruturas Eficientes de Transmultiplexadores e de Bancos de Filtros Modulados por Cossenos," PhD, Electronic Engineering, COPPE/UFRJ, Rio de Janeiro, 2006.

[114] S. Radhakrishnan Pillai and G. H. Allen, "Generalized magnitude and power complementary filters," in *Acoustics, Speech, and Signal Processing, 1994. ICASSP-94., 1994 IEEE International Conference on*, 1994, pp. III/585-III/588 vol.3.

[115] Y. Zhang and M. Zeytinoglu, "Block subband coding and time-varying filterbanks," in *Communications, Computers and Signal Processing, 1999 IEEE Pacific Rim Conference on*, 1999, pp. 483-486.

[116] M. R. Petraglia, *et al.*, "Performance comparison of adaptive subband structures applied to acoustic echo cancelling," in *Signals, Systems and Computers, 2001. Conference Record of the Thirty-Fifth Asilomar Conference on*, 2001, pp. 1535-1539 vol.2.

[117] G. Cherubini, *et al.*, "Filter bank modulation techniques for very high speed digital subscriber lines," *Communications Magazine, IEEE,* vol. 38, pp. 98-104, 2000.

[118] A. Viholainen, "Transmultiplexer design for VDSL modems," MsC, Department of Information Technology, Tampere University of Technology, 1998.

[119] A. N. Akansu, *et al.*, "Orthogonal transmultiplexers in communication: a review," *Signal Processing, IEEE Transactions on,* vol. 46, pp. 979-995, 1998.

[120] M. Vetterli, "Perfect transmultiplexers," in *Acoustics, Speech, and Signal Processing, IEEE International Conference on ICASSP '86.*, 1986, pp. 2567-2570.

[121] R. D. Koilpillai and P. P. Vaidyanathan, "Cosine-modulated FIR filter banks satisfying perfect reconstruction," *Signal Processing, IEEE Transactions on,* vol. 40, pp. 770-783, 1992.

[122] C.-R. Fernando, *et al.*, "Design of multi-channel near-perfect-reconstruction transmultiplexers using cosine-modulated filter banks," vol. 83, ed: Elsevier North-Holland, Inc., 2003, pp. 1079-1091.

[123] H. Bölcskei, "Oversampled Filter Banks and Predictive Subband Coders," Universität Wien, 1997.

[124] L. Yuan-Pei and P. P. Vaidyanathan, "Application of DFT filter banks and cosine modulated filter banks in filtering," in *Circuits and Systems, 1994. APCCAS '94., 1994 IEEE Asia-Pacific Conference on*, 1994, pp. 254-259.

[125] H. Bölcskei, *et al.*, "Oversampled FIR and IIR DFT filter banks and Weyl-Heisenberg frames," in *Acoustics, Speech, and Signal Processing, 1996. ICASSP-96. Conference Proceedings., 1996 IEEE International Conference on*, 1996, pp. 1391-1394 vol. 3.

[126] H. Bölcskei and F. Hlawatsch, "Oversampled cosine modulated filter banks with linear phase," in *Circuits and Systems, 1997. ISCAS '97., Proceedings of 1997 IEEE International Symposium on*, 1997, pp. 357-360 vol.1.

[127] H. Bolcskei and F. Hlawatsch, "Oversampled cosine modulated filter banks with perfect reconstruction," *Circuits and Systems II: Analog and Digital Signal Processing, IEEE Transactions on,* vol. 45, pp. 1057-1071, 1998.

[128] W. A. Abu-Al-Saud and G. L. Stuber, "Efficient wideband channelizer for software radio systems using modulated PR filterbanks," *Signal Processing, IEEE Transactions on,* vol. 52, pp. 2807-2820, 2004.

[129] M. U. R. Awan, *et al.*, "Design and implementation of an FPGA-based multi-standard software radio receiver," in *Norchip, 2007*, 2007, pp. 1-5.

[130] K. Chonghoon, *et al.*, "SDR-based digital channelizer/de-channelizer for multiple CDMA signals," in *Vehicular Technology Conference, 2000. IEEE VTS-Fall VTC 2000. 52nd*, 2000, pp. 2862-2869 vol.6.

[131] F. J. Harris, *et al.*, "Digital receivers and transmitters using polyphase filter banks for wireless communications," *Microwave Theory and Techniques, IEEE Transactions on,* vol. 51, pp. 1395-1412, 2003.

[132] S. M. Phoong, *et al.*, "DFT-modulated filterbank transceivers for multipath fading channels," *Signal Processing, IEEE Transactions on,* vol. 53, pp. 182-192, 2005.

[133] P. P. Vaidyanathan, "Filter banks in digital communications," *Circuits and Systems Magazine, IEEE*, vol. 1, pp. 4-25, 2001.

[134] D. S. Waldhauser, *et al.*, "Comparison of Filter Bank Based Multicarrier Systems with OFDM," in *Circuits and Systems, 2006. APCCAS 2006. IEEE Asia Pacific Conference on*, 2006, pp. 976-979.

[135] D. S. Waldhauser and J. A. Nossek, "Multicarrier systems and filter banks," *Adv. Radio Sci.*, vol. 4, pp. 165-169, 2006.

[136] J. Cooley and J. Tukey, "An Algorithm for the Machine Calculation of Complex Fourier Series," *Mathematics of Computation,* vol. 19, pp. 297-301, 1965.

[137] P. Duhamel and M. Vetterli, "Fast fourier transforms: a tutorial review and a state of the art," vol. 19, ed: Elsevier North-Holland, Inc., 1990, pp. 259-299.

[138] H. J. Nussbaumer, *Fast Fourier Transform and Convolution Algorithms*. Berlin: Springer, 1982.

[139] Xilinx, "LogiCORE IP Fast Fourier Transform v7.1 Product Specification," ed, 2010.

[140] N. J. Fliege, "Computational efficiency of modified DFT polyphase filter banks," in *Signals, Systems and Computers, 1993. 1993 Conference Record of The Twenty-Seventh Asilomar Conference on*, 1993, pp. 1296-1300 vol.2.

[141] P. N. Heller, *et al.*, "A general formulation of modulated filter banks," *Signal Processing, IEEE Transactions on,* vol. 47, pp. 986-1002, 1999.

[142] T. Karp and N. J. Fliege, "MDFT filter banks with perfect reconstruction," in *Circuits and Systems, 1995. ISCAS '95., 1995 IEEE International Symposium on*, 1995, pp. 744-747 vol.1.

[143] T. Karp and N. J. Fliege, "Computationally efficient realization of MDFT filter banks," in *Proceedings in the 8th European Signal Processing (EUSIPCO'96)*, 1996, pp. 336-365.

[144] T. Karp and N. J. Fliege, "Modified DFT filter banks with perfect reconstruction," *Circuits and Systems II: Analog and Digital Signal Processing, IEEE Transactions on,* vol. 46, pp. 1404-1414, 1999.

[145] C. S. Lee and K. Y. Yoo, "Polyphase filtered OFDM transmission system," *Electronics Letters,* vol. 40, pp. 687-688, 2004.

[146] J. Alhava and M. Renfors, "Exponentially-modulated filter bank-based transmultiplexer," in *Circuits and Systems, 2003. ISCAS '03. Proceedings of the 2003 International Symposium on*, 2003, pp. IV-233-IV-236 vol.4.

[147] J. Alhava, *et al.*, "Efficient implementation of complex exponentially-modulated filter banks," in *Circuits and Systems, 2003. ISCAS '03. Proceedings of the 2003 International Symposium on*, 2003, pp. IV-157-IV-160 vol.4.

[148] A. Viholainen, *et al.*, "Efficient implementation of complex modulated filter banks using cosine and sine modulated filter banks," *EURASIP Journal on Applied Signal Processing,* vol. 2006, p. 10 pages, 2006.

[149] A. Viholainen, *et al.*, "Complex modulated critically sampled filter banks based on cosine and sine modulation," in *Circuits and Systems, 2002. ISCAS 2002. IEEE International Symposium on*, 2002, pp. I-833-I-836 vol.1.

[150] P. S. R. Diniz, *et al.*, *Digital Signal Processing: System Analysis and Design*: Cambridge University Press, 2002.

[151] H. S. Malvar, "Extended lapped transforms: properties, applications, and fast algorithms," *IEEE Transactions on Signal Processing,* vol. 40, pp. 2703-2714, Nov 1992.

[152] T. Saramäki, "A generalized class of cosine-modulated filter banks," in *Proc. TICSP Workshop on transforms and filter banks*, Tampere, Finland, 1998, pp. 336-365.

[153] H. S. Malvar, *Signal Processing with Lapped Transforms*. Norwood, MA, USA: Artech House, Inc., 1992.

[154] S. Weiss, "Analysis and Fast Implementation of Oversampled Modulated Filter Banks," J. G. McWhirter and I. K. Proudler, Eds., ed: Oxford University Press, 2002, pp. 263-74.

[155] K. Eneman and M. Moonen, "DFT modulated filter bank design for oversampled subband systems," *Signal Processing,* vol. 81, pp. 1947-1973, 2001.

[156] S. Weiss and R. W. Stewart, "Fast implementation of oversampled modulated filter banks," *Electronics Letters,* vol. 36, pp. 1502-1503, 2000.

[157] Z. Cvetkovic and M. Vetterli, "Oversampled filter banks," *Signal Processing, IEEE Transactions on,* vol. 46, pp. 1245-1255, 1998.

[158] M. Vetterli and Z. Cvetkovic, "Oversampled FIR filter banks and frames in $l^2(Z)$," in *Acoustics, Speech, and Signal Processing, 1996. ICASSP-96. Conference Proceedings., 1996 IEEE International Conference on*, 1996, pp. 1530-1533 vol. 3.

[159] Z. Cvetkovic, "Oversampled modulated filter banks and tight Gabor frames in l²(Z)," in *Acoustics, Speech, and Signal Processing, 1995. ICASSP-95., 1995 International Conference on*, 1995, pp. 1456-1459 vol.2.

[160] A. Viholainen, *et al.*, "Implementation of parallel cosine and sine modulated filter banks for equalized transmultiplexer systems," in *Acoustics, Speech, and Signal Processing, 2001. Proceedings. (ICASSP '01). 2001 IEEE International Conference on*, 2001, pp. 3625-3628 vol.6.

[161] A. Palomo Navarro, *et al.*, "Non-uniform channelization methods for next generation SDR PMR base stations," in *Computers and Communications (ISCC), 2011 IEEE Symposium on*, 2011, pp. 620-625.

[162] A. P. Vinod, *et al.*, "A reconfigurable multi-standard channelizer using QMF trees for software radio receivers," in *Personal, Indoor and Mobile Radio Communications, 2003. PIMRC 2003. 14th IEEE Proceedings on*, 2003, pp. 119-123 Vol.1.

[163] R. Mahesh and A. P. Vinod, "Reconfigurable Frequency Response Masking Filters for Software Radio Channelization," *Circuits and Systems II: Express Briefs, IEEE Transactions on,* vol. 55, pp. 274-278, 2008.

[164] J. Lillington and S. Matthews, "Flexible architectures for wideband SDR channelisation," in *DSPenabledRadio, 2005. The 2nd IEE/EURASIP Conference on (Ref. No. 2005/11086)*, 2005, p. 7 pp.

[165] A. Eghbali, *et al.*, "A Farrow-structure-based multi-mode transmultiplexer," in *Circuits and Systems, 2008. ISCAS 2008. IEEE International Symposium on*, 2008, pp. 3114-3117.

[166] R. Mahesh, *et al.*, "Filter Bank Channelizers for Multi-Standard Software Defined Radio Receivers," *Journal of Signal Processing Systems, Springer New York*, 2008.

[167] J. Lillington, "Comparison of Wideband Channelisation Architectures," in *http://www.techonline.com/showArticle.jhtml?articleID=193102347&queryText=*, 2003.

[168] V. Valimaki and T. I. Laakso, "Principles of fractional delay filters," in *Acoustics, Speech, and Signal Processing, 2000. ICASSP '00. Proceedings. 2000 IEEE International Conference on*, 2000, pp. 3870-3873 vol.6.

[169] A. Eghbali, *et al.*, "An arbitrary-bandwidth transmultiplexer and its application to flexible frequency-band reallocation networks," in *Circuit Theory and Design, 2007. ECCTD 2007. 18th European Conference on*, 2007, pp. 248-251.

[170] A. Eghbali, *et al.*, "A Multimode Transmultiplexer Structure," *Circuits and Systems II: Express Briefs, IEEE Transactions on*, vol. 55, pp. 279-283, 2008.

[171] A. Eghbali, *et al.*, "On the filter design for a class of multimode transmultiplexers," in *Circuits and Systems, 2009. ISCAS 2009. IEEE International Symposium on*, 2009, pp. 89-92.

[172] C. W. Farrow, "A continuously variable digital delay element," in *Circuits and Systems, 1988., IEEE International Symposium on*, 1988, pp. 2641-2645 vol.3.

[173] B. Dordec, "Optimization of Polynomial-based Interpolation Filters Using Discrete-time Model," in *15th Telecommunications Forum TELFOR*, Belgrade, Serbia, 2007.

[174] T. I. Laakso, *et al.*, "Splitting the unit delay [FIR/all pass filters design]," *Signal Processing Magazine, IEEE*, vol. 13, pp. 30-60, 1996.

[175] J. Vesma and T. Saramaki, "Interpolation filters with arbitrary frequency response for all-digital receivers," in *Circuits and Systems, 1996. ISCAS '96., 'Connecting the World'., 1996 IEEE International Symposium on*, 1996, pp. 568-571 vol.2.

[176] D. Babic, *et al.*, "Discrete-time modeling of polynomial-based interpolation filters in rational sampling rate conversion," in *Circuits and Systems, 2003. ISCAS '03. Proceedings of the 2003 International Symposium on*, 2003, pp. IV-321-IV-324 vol.4.

[177] A. Mertins, *Signal Analysis: Wavelets, Filter Banks, Time-Frequency Transforms and Applications.*: John Wiley & Sons, 1999.

[178] F. J. Harris and E. Kjeldsen, "A Novel Interpolated Tree Orthogonal Multiplexing (ITOM) Scheme with Compact Time-Frequency Localization: an Introduction and Comparison to Wavelet Filter Bank and Polyphase Filter Banks," in *SDR 06 Technical Conference and Product Exposition*, 2006.

[179] D. Jaeger, *et al.*, "A Low-Complexity Architecture for Multicarrier Cognitive Radio," in *SDR 07 Technical Conference and Product Exposition*, 2007.

[180] C. Zhao, *et al.*, "Reconfigurable Architectures for Low Complexity Software Radio Channelizers using Hybrid Filter Banks," in *Communication systems, 2006. ICCS 2006. 10th IEEE Singapore International Conference on*, 2006, pp. 1-5.

[181] J. Lillington, "TPFT-Tuneable Pipeline Frequency Transform," ed. RF Engines Ltd, Technical Report. http://www.rfel.com/whipapdat.asp, 2002.

[182] J. Lillington, "The Pipeline Frequency Transform (PFT)," ed: RF Engines Ltd, Technical Report. http://www.rfel.com/whipapdat.asp, 2002.

[183] R. Mahesh, *et al.*, "A tree-structured non-uniform filter bank for multi-standard wireless receivers," in *Circuits and Systems, 2009. ISCAS 2009. IEEE International Symposium on*, 2009, pp. 213-216.

[184] Q.-G. Liu, *et al.*, "Simple design of oversampled uniform DFT filter banks with applications to subband acoustic echo cancellation," *Signal Processing*, vol. 80, pp. 831-847, 2000.

[185] F. J. Harris and R. Mc Gwier, "A receiver structure that performs simultaneous spectral analysis and time series channelization," in *SDR 09 Technical Conference and Product Exposition*, 2009.

[186] A. Palomo Navarro, *et al.*, "Overlapped polyphase DFT modulated filter banks applied to TETRA/TEDS SDR base station channelization," presented at the Royal Irish Academy Communication and Radio Science Colloquium, 2010.

[187] F. J. M. G. Harris, R., "A receiver structure that performs simultaneous spectral analysis and time series channelization," in *Proceedings of the SDR'09 Technical Conference and Product Exposition*, 2009.

[188] H. Johansson and P. Lowenborg, "Flexible frequency-band reallocation networks using variable oversampled complex-modulated filter banks," *EURASIP J. Appl. Signal Process.*, vol. 2007, pp. 143-143, 2007.

[189] A. Palomo Navarro, *et al.*, "Practical Non-Uniform Channelization for Multi-standard Base Stations," *ZTE Comms. Journal. Special topic: Digital Front-End and Software Radio Frequency in Wireless Communication and Broadcasting*, vol. 9, December 2011.

[190] A. Eghbali, *et al.*, "Reconfigurable Nonuniform Transmultiplexers Using Uniform Modulated Filter Banks," *Circuits and Systems I: Regular Papers, IEEE Transactions on*, vol. PP, pp. 1-1, 2010.

[191] A. Palomo Navarro, *et al.*, "Non-Uniform Channelization Methods for Next Generation SDR PMR Base Stations," in *IEEE Symposium in Computers and Communications (ISCC 2011)*, 2011.

[192] R. Mahesh and A. P. Vinod, "A new low complexity reconfigurable filter bank architecture for software radio receivers based on interpolation and masking technique," in *Information, Communications & Signal Processing, 2007 6th International Conference on*, 2007, pp. 1-5.

[193] R. Mahesh and A. P. Vinod, "Frequency Response Masking based Reconfigurable Channel Filters for Software Radio Receivers," in *Circuits and Systems, 2007. ISCAS 2007. IEEE International Symposium on*, 2007, pp. 2518-2521.

[194] R. Mahesh and A. P. Vinod, "An Architecture For Integrating Low Complexity and Reconfigurability for Channel filters in Software Defined Radio Receivers," in *Circuits and Systems, 2007. ISCAS 2007. IEEE International Symposium on*, 2007, pp. 2514-2517.

[195] R. Mahesh and A. P. Vinod, "Coefficient decimation approach for realizing reconfigurable finite impulse response filters," in *Circuits and Systems, 2008. ISCAS 2008. IEEE International Symposium on*, 2008, pp. 81-84.

[196] R. Mahesh, *et al.*, "Filter Bank Channelizers for Multi-Standard Software Defined Radio Receivers," *Journal of Signal Processing Systems, Springer New York*, 2009.

[197] ECC, "Planning criteria and coordination of frequencies in the land mobile service in the range 29.7-921 MHz," vol. T/R 25-08, ed, 2008.

[198] C. Y. Fung and S. C. Chan, "A multistage filterbank-based channelizer and its multiplier-less realization," in *Circuits and Systems, 2002. ISCAS 2002. IEEE International Symposium on*, 2002, pp. III-429-III-432 vol.3.

[199] A. V. Oppenheim, *et al.*, *Discrete-time signal processing*: Prentice Hall, 1999.

[200] K. F. C. Yiu, *et al.*, "Multicriteria design of oversampled uniform DFT filter banks," *Signal Processing Letters, IEEE*, vol. 11, pp. 541-544, 2004.

[201] L. C. R. de Barcellos, *et al.*, "A Generalized Oversampled Structure for Cosine-Modulated Transmultiplexers and Filter Banks," *Circuits, Systems, and Signal Processing*, vol. 25, pp. 131-151, 2006.

[202] P. S. R. Diniz, *et al.*, "Design of cosine-modulated filter bank prototype filters using the frequency-response masking approach," in *Acoustics, Speech, and Signal Processing, 2001. Proceedings. (ICASSP '01). 2001 IEEE International Conference on*, 2001, pp. 3621-3624 vol.6.

[203] P. S. R. Diniz, *et al.*, "Design of high-resolution cosine-modulated transmultiplexers with sharp transition band," *Signal Processing, IEEE Transactions on,* vol. 52, pp. 1278-1288, 2004.

[204] S. L. Netto, *et al.*, "Efficient implementation for cosine-modulated filter banks using the frequency response masking approach," in *Circuits and Systems, 2002. ISCAS 2002. IEEE International Symposium on*, 2002, pp. III-229-III-232 vol.3.

[205] L. Rosenbaum, "On low-complexity frequency selective digital filters and filter banks," PhD, Department of Electrical Engineering, University of Linköping, Institute of Technology, Linköping, 2007.

[206] L. Rosenbaum, *et al.*, "An approach for synthesis of modulated M-channel FIR filter banks utilizing the frequency-response masking technique," *EURASIP J. Appl. Signal Process.,* vol. 2007, pp. 144-144, 2007.

[207] M. B. Furtado, Jr., *et al.*, "On the design of high-complexity cosine-modulated transmultiplexers based on the frequency-response masking approach," *Circuits and Systems I: Regular Papers, IEEE Transactions on,* vol. 52, pp. 2413-2426, 2005.

[208] H. Johansson, "New classes of frequency-response masking FIR filters," in *Circuits and Systems, 2000. Proceedings. ISCAS 2000 Geneva. The 2000 IEEE International Symposium on*, 2000, pp. 81-84 vol.3.

[209] H. Johansson and T. Saramäki, *Two-channel FIR filter banks utilizing the FRM approach*. Heidelberg, ALLEMAGNE: Springer, 2003.

[210] L. Rosenbaum, "Oversampled Complex-Modulated Causal IIR Filter Banks for Flexible Frequency-Band Reallocation Networks," in *Proc. XIV European Signal Processing Conf.*, Florence, Italy, 2006.

[211] A. Palomo Navarro, *et al.*, "Practical Non-Uniform Channelization for Multi-standard Base Stations," *ZTE Comms. Journal in Digital Front-End and Software Radio Frequency in Wireless Communication and Broadcasting [Unpublished work],* 2011.

[212] A. Civardi, "PSDR Mobile Integration Solution," in *IEEE Wireless Rural and Emergency Commun.*, 2007.

[213] S. Communications, "WiMAX and its applications," ed: Selex Communications, White paper, http://www.selex-comms.com/internet/media/docs/WhitepaperWiMAX-EnglishV1.pdf.

[214] A. Durantini and M. Petracca, "Performance comparison of vertical handover strategies for psdr heterogeneous networks," *Wireless Communications, IEEE,* vol. 15, pp. 54-59, 2008.

[215] A. Durantini, *et al.*, "Integration of Broadband Wireless Technologies and PMR Systems for Professional Communications," in *Networking and Services, 2008. ICNS 2008. Fourth International Conference on*, 2008, pp. 84-89.

[216] L. Gao and R. Farrell, "RF SDR for Wideband PMR," *Procededings of the China-Ireland Information and Communications Technologies Conference (CIICT),* 2009.

[217] M. Morresi and E. Donnini, "TETRA and WiMAX: Complementing or competing?," ed: TETRA MoU White Paper, http://www.tetramou.com/tetramou.aspx?id=5336#.

[218] U. S. Jha and R. Prasad, *OFDM Towards Fixed and Mobile Broadband Wireless Access*: Artech House, Inc., 2007.

[219] J. G. Andrews, *et al.*, *Fundamentals of WiMAX: Understanding Broadband Wireless Networking (Prentice Hall Communications Engineering and Emerging Technologies Series)*: Prentice Hall PTR, 2007.

[220] IEEE802.16, "IEEE Standard for Local and Metropolitan Area Networks, Part 16: Air Interface for Fixed Broadband Wireless Access Systems," ed, Mar 2004.

[221] IEEE802.16e, "IEEE Standard for Local and Metropolitan Area Networks, Part 16: Air Interface for Fixed and Mobile Broadband Wireless Access Systems Amendment 2: Physical and Medium Access Control Layers for Combined Fixed and Mobile Operation in Licensed Bands," ed, Feb 2006.

[222] K. Etemad and M. Lai, "Mobile WiMAX [Guest Editorial]," *Communications Magazine, IEEE,* vol. 47, pp. 82-83, 2009.

[223] W. Fan, *et al.*, "Mobile WiMAX systems: performance and evolution," *Communications Magazine, IEEE,* vol. 46, pp. 41-49, 2008.

[224] K. Etemad, "Overview of mobile WiMAX technology and evolution," *Communications Magazine, IEEE,* vol. 46, pp. 31-40, 2008.

[225] *LTE; Evolved Universal Terrestrial Radio Access (E-UTRA); Physical channels and modulation* 3GPP TS 36.211 version 10.2.0 Release 10, 2011.

[226] ITU. (2002, October). *What is IMT-2000?* Available: http://www.itu.int/osg/imt-project/docs/What_is_IMT2000-2.pdf

[227] 3GPP. (2011, October). *3G Partnership Project Official Web Site*. Available: http://www.3gpp.org/

[228] 3GPP2. (2001, October). *3G Partnership Project 2 Official Web Site*. Available: http://www.3gpp2.org/

[229] GSA, "UMTS900 Global Status," Global mobile Suppliers Association2011.

[230] *ECC Decision of 1 December 2006 on the designation of the bands 880-915 MHz, 925-960 MHz, 1710-1785 MHz and 1805-1880 MHz for terrestrial IMT-2000/UMTS systems,* (ECC/DEC/(06)13, 2006.

[231] H. Holma, *et al.*, "UMTS900 Co-Existence with GSM900," in *Vehicular Technology Conference, 2007. VTC2007-Spring. IEEE 65th*, 2007, pp. 778-782.

[232] A. Moral, *et al.*, "Assessment of the benefits of introducing a HSDPA carrier at 900MHz," in *GLOBECOM Workshops (GC Wkshps), 2010 IEEE*, 2010, pp. 834-838.

[233] GSA, "Evolution to LTE Report," Global mobile Suppliers Association2011.

[234] R. Herradón Diez, *Comunicaciones moviles digitales*. Madrid: Departamento de Ingeniería Audiovisual y Comunicaciones, E.U.I.T. de Telecomunicaciones, UPM, 2005.

[235] D. Kumar, *et al.*, "Availability Modelling of 3GPP R99 Telecommunication networks," pp. Vol 1, pages: 977-984, 2003.

[236] H. W. Schüßler and P. Steffen, "Recursive Halfband-Filters," *AEU - International Journal of Electronics and Communications*, vol. 55, pp. 377-388, 2001.

[237] R. A. Losada and V. Pellisier, "Designing IIR filters with a given 3-dB point," *Signal Processing Magazine, IEEE*, vol. 22, pp. 95-98, 2005.

[238] A. Krukowski, *et al.*, "The design of polyphase-based IIR multiband filters," in *Acoustics, Speech, and Signal Processing, 1997. ICASSP-97., 1997 IEEE International Conference on*, 1997, pp. 2213-2216 vol.3.

[239] F. J. Harris, "On the Design and Performance of efficient and Novel Filter Structures Using Recursive Allpass Filters," in *IEEE 3rd International Symposium on Signal Processing and its Applications (ISSPA'92)*, Gold Coast, Queensland, Australia, 1992, pp. 1-5.

[240] P. A. Regalia, *et al.*, "The digital all-pass filter: a versatile signal processing building block," *Proceedings of the IEEE*, vol. 76, pp. 19-37, 1988.

[241] I. Kale, *et al.*, "A high fidelity decimation filter for sigma-delta converters," in *Advanced A-D and D-A Conversion Techniques and their Applications, 1994. Second International Conference on*, 1994, pp. 30-35.

[242] S. S. Lawson, "On design techniques for approximately linear phase recursive digital filters," in *Circuits and Systems, 1997. ISCAS '97., Proceedings of 1997 IEEE International Symposium on*, 1997, pp. 2212-2215 vol.4.

[243] W. S. Lu, "Design of stable IIR digital filters with equiripple passbands and peak-constrained least-squares stopbands," *Circuits and Systems II: Analog and Digital Signal Processing, IEEE Transactions on*, vol. 46, pp. 1421-1426, 1999.

[244] A. Krukowski and I. Kale, "Polyphase Filter Design with Reduced Phase Non-Linearity," ed. Applied DSP and VLSI Researh Group, University of Westminster, London, 2001.

[245] A. Krukowski and I. Kale, "Almost linear-phase polyphase IIR lowpass/highpass filter approach," in *Signal Processing and Its Applications, 1999. ISSPA '99. Proceedings of the Fifth International Symposium on*, 1999, pp. 969-972 vol.2.

[246] A. Krukowski and I. Kale, *DSP System Design, Complexity Reduced IIR Filter Implementation for Practical Applications*: Kluwer Academics Publishers, 2003.

[247] Xilinx, "IP LogiCORE FIR Compiler v5.0 Product Specification," ed, 2011.

[248] F. Bruekers, "Symmetry and Efficiency in Complex FIR Filters," Philips Research Laboratories, Eindhoven, 2009.

[249] M. Abo-Zahhad, "Current state and future directions of multirate filter banks and their applications," *Digital Signal Processing,* vol. 13, pp. 495-518, 2003.

[250] T. Karp and A. Mertins, "Implementation of biorthogonal cosine-modulated filter banks with fixed-point arithmetic," in *Circuits and Systems, 2001. ISCAS 2001. The 2001 IEEE International Symposium on*, 2001, pp. 469-472 vol. 2.

[251] J. G. Proakis and D. G. Manolakis, *Digital signal processing: Principles, Algorithms and Applications*: Pearson Prentice Hall, 2007.

[252] A. Krukowski, *et al.*, "Decomposition of IIR Transfer Functions Into Parallel Arbitrary-Order IIR Subfilters," in *Nordic Signal Processing Symposium (NORSIG´96)*, Espoo, Finland, 1996.

[253] C. Mullis and R. Roberts, "Roundoff noise in digital filters: Frequency transformations and invariants," *Acoustics, Speech and Signal Processing, IEEE Transactions on,* vol. 24, pp. 538-550, 1976.

[254] J. G. Proakis, "Adaptive equalization techniques for acoustic telemetry channels," *Oceanic Engineering, IEEE Journal of,* vol. 16, pp. 21-31, 1991.

[255] A. Palomo Navarro, "Adaptive Subband Equalization in Wireless Systems," Department of Signal Processing, Blekinge Institute of Technology, Ronneby, 2006.

[256] H. H. Dam, *et al.*, "Non-causal delayless subband adaptive equalizer," in *Acoustics, Speech, and Signal Processing (ICASSP), 2002 IEEE International Conference on*, 2002, pp. III-2649-III-2652.

[257] J. Nordberg, "Blind subband adaptive equalization, Research Report 2002:11 , ISSN: 1103–1581," Blekinge Institute of Technology, Ronneby, Sweden2002.